

INFORMATION TO USERS

This manuscript has been reproduced from the microfilm master. UMI films the text directly from the original or copy submitted. Thus, some thesis and dissertation copies are in typewriter face, while others may be from any type of computer printer.

The quality of this reproduction is dependent upon the quality of the copy submitted. Broken or indistinct print, colored or poor quality illustrations and photographs, print bleedthrough, substandard margins, and improper alignment can adversely affect reproduction.

In the unlikely event that the author did not send UMI a complete manuscript and there are missing pages, these will be noted. Also, if unauthorized copyright material had to be removed, a note will indicate the deletion.

Oversize materials (e.g., maps, drawings, charts) are reproduced by sectioning the original, beginning at the upper left-hand corner and continuing from left to right in equal sections with small overlaps. Each original is also photographed in one exposure and is included in reduced form at the back of the book.

Photographs included in the original manuscript have been reproduced xerographically in this copy. Higher quality 6" x 9" black and white photographic prints are available for any photographs or illustrations appearing in this copy for an additional charge. Contact UMI directly to order.

UMI

A Bell & Howell Information Company
300 North Zeeb Road, Ann Arbor, MI 48106-1346 USA
313/761-4700 800/521-0600

**THE FEASIBILITY OF A NOVEL METHOD OF SOLUTION
RECOVERY OF COBALT-RICH FERROMANGANESE CRUSTS
FROM SEAMOUNTS**

**A DISSERTATION SUBMITTED TO THE GRADUATE DIVISION OF THE
UNIVERSITY OF HAWAII IN PARTIAL FULFILLMENT OF THE
REQUIREMENTS FOR THE DEGREE OF**

DOCTOR OF PHILOSOPHY

IN

OCEANOGRAPHY

AUGUST 1995

By

Kimo K. Zaiger

Dissertation Committee:

**Alexander Malahoff, Chairperson
Michael J. Cruickshank
Lorenz Magaard
Gary McMurtry
John C. Wiltshire**

UMI Number: 9604190

UMI Microform 9604190

Copyright 1995, by UMI Company. All rights reserved.

This microform edition is protected against unauthorized
copying under Title 17, United States Code.

UMI

300 North Zeeb Road
Ann Arbor, MI 48103

ACKNOWLEDGEMENTS

I wish to express my sincere gratitude to Dr. Alexander Malahoff for providing research assistantships, unique scientific opportunities, and other significant support during this lengthy research project. Dr. John Wiltshire also ranks high on my list for providing me with continual encouragement and by acting as an advocate on my behalf, introducing my ideas to various industry contacts. I would also like to acknowledge the illuminating discussions during the early phase of the project provided by Drs. Eric De Carlo and Daniel Schein at the *University of Hawaii*, and Dr. Diane Marozas at the *U.S. Bureau of Mines, Twin Cities Research Center* on pertinent aspects of applied geochemistry. Dr. Hans-Jurgen Krock also provided early support in providing use of Ocean Engineering facilities and equipment at the *Look Laboratory*. Drs. Mike Cruickshank and Charles Morgan at the *Marine Minerals Technology Center, Ocean Basins Division* always provided sage counsel and sponsored my attendance at the *25th Annual Underwater Mining Institute* in Monterey, California. Thanks also to Dr. George Luther III, *University of Delaware* for his informal lecture series and discussions pertaining to frontier molecular orbital theory and to Dr. Thomas Loudat for his important collaboration on the economic aspects of my project. Dr. Jim Cowan graciously loaned me components for the high pressure bomb apparatus, Dr. Chris Winn provided temporary use of a recirculating chiller unit, and Dr. Jane Tribble and the *SOEST Core Lab* curatorial staff provided me with the long term use of analytical laboratory equipment and the ferromanganese crust samples used in this research. Charles Fraley at the *SOEST Atomic Spectroscopy Laboratory* performed the atomic emission spectrophotometric

analyses. Brian Daniel at the *Hawaii Undersea Research Laboratory* provided technical assistance on numerous occasions. Finally, special thanks goes to my wife Shari, for her encouragement, love and unwavering support throughout the duration of the project and to my father, Dolliver Zaiger who instilled in me my interest in science.

Funding for this project was provided in part by the *State of Hawaii Department of Business and Economic Development*, by the *University of Hawaii Sea Grant College Program* under an Institutional grant from the *National Oceanic and Atmospheric Administration*, and by the *Hawaii Undersea Research Laboratory*.

ABSTRACT

Significant deposits of cobalt-rich ferromanganese crust are found on seamounts in the Exclusive Economic Zones (EEZ) of many Pacific nations. The United States crust bearing EEZs encompass the Hawaiian and Johnston Island archipelagos and have a cumulative crust permissive area of nearly 27,000 km², averaging 40 percent crust coverage. EEZ mean crust thickness is 2.5 cm with an average grade of 0.87% cobalt. These deposits present significant high value mineral potential, for cobalt, nickel, and manganese metals with an estimated ore value of \$449 per metric ton (1993 dollars).

A novel *in situ* solution mining method is introduced. This patented mining system (assigned to the University of Hawaii) uses a *Containment and Regulation Cover* that in effect creates a semi-batch reactor sealed to the sea floor and adapts terrestrial *in situ* leach mining methods to the deep ocean. The crust mining potential of the solution mining method is assessed and compared with other ocean mining technologies. This new mining system is expected to cause much less environmental damage than the environmental disruption projected from sediment plumes caused by mining crusts by mechanical methods. Also, the innovative and low cost technology of solution mining favorably alters the economic viability of the crust mining equation. A preliminary economic analysis yields an Internal Rate of Return (IRR) on investment of 33.5 percent for the crust solution mining base case scenario. If a selective high cobalt grade (1.25%) mining scenario is considered, an IRR of 47.5 percent and very short pay back periods on capital can be attained. This makes the solution mining system for crusts highly attractive.

In order for an *in situ* solution mining system to be viable, the leach kinetics and physicochemical hydrodynamics must be favorable at *in situ* conditions. Results from extensive laboratory bench and refrigerated pressure bomb experiments show rapid crust dissolution rates with greater than 90% extraction of Co, Cu, Mn, and Ni using a sulphurous/dithionate lixiviant. Experiments on intact crust fragments show that the problem of *surface layer product* formation can be mitigated by controlling the leach chemistry.

TABLE OF CONTENTS

	Page
ACKNOWLEDGEMENTS	iii
ABSTRACT	v
LIST OF TABLES	x
LIST OF FIGURES	xi
CHAPTER 1 INTRODUCTION	1
1.1 The Utility of Cobalt	1
1.2 Resource Potential of Fe-Mn Cobalt-Rich Crusts from Seamounts	1
1.2.1 <i>Resource Area in the EEZ Adjacent to Hawaii and Johnston Island</i>	2
1.3 Summary of Open Ocean Ferromanganese Crust Properties	3
1.3.1 <i>Physical Characteristics of Ferromanganese Crust</i>	3
1.3.2 <i>Mineralogy and Structure of Ferromanganese Crust</i>	6
1.3.3 <i>Chemistry of Ferromanganese Crust</i>	7
1.4 Historical Metal Prices of Cobalt, Nickel and Manganese	10
1.5 A Novel Method of Crust Mining by Solution Recovery	10
1.6 Value of Cobalt-Rich Ferromanganese Crusts	12
1.7 Potential Crust Mining Sites in the Johnston Island EEZ	12
1.8 Objectives of this Research	14
CHAPTER 2 POTENTIAL CRUST MINING TECHNOLOGIES	16
2.1 Robotic Miner System	16
2.2 Continuous Line Bucket System	19

2.3	Novel <i>In Situ</i> Batch Reactor System	23
2.3.1	<i>CRC System</i>	25
2.3.2	<i>CRC Sealing and Maintenance</i>	26
2.3.3	<i>CRC Deployment and Relocation</i>	27
2.3.4	<i>Effect of Tidal Currents</i>	30
2.3.5	<i>Solution Dynamics in Crust Substrate</i>	31
2.3.6	<i>At Sea Processing</i>	32
2.3.7	<i>Environmental Impact of the In Situ Batch Reactor System</i>	34
2.4	Comparison of Crust Mining Systems	38
CHAPTER 3 LIXIVIANT SELECTION AND CHEMISTRY REVIEW		40
3.1	Lixiviant Selection	42
3.2	The Sulfurous Acid System	44
3.3	Review of Chemical Bonding	45
3.4	Ligand Field Theory	49
3.5	Frontier Molecular Orbital Theory	51
3.6	Proposed Mechanism of Reductive Dissolution by SO ₂	57
3.7	Thermodynamic Evaluation of SO ₂ Reactivity	58
3.8	Kinetic Evaluation of SO ₂ Reactivity	59
3.9	Previous Research on the Dissolution of Selected Oxides with SO ₂	61
CHAPTER 4 RESEARCH GOALS AND METHODS		66
4.1	Experimental Research Goals	66
4.1.1	<i>Effect of Temperature</i>	67

4.1.2	<i>Effect of Pressure</i>	68
4.2	Experimental Methods	71
4.2.1	<i>Batch Leach Experiments</i>	71
4.2.2	<i>Semi-Batch Intact Crust Experiments</i>	75
CHAPTER 5 RESULTS AND DISCUSSION		79
5.1	Effect of Temperature on Batch Leach Experiments	79
5.2	Effect of Pressure on Batch Leach Experiments	99
5.3	Effect of pH on Batch Leach Experiments	113
5.4	Effect of Leach Duration on Batch Leach Experiments	124
5.5	Semi-Batch Intact Crust Leach Experiment Results	138
5.6	Discussion	147
CHAPTER 6 ECONOMIC ASSESSMENT		150
6.1	Basic Assumptions	150
6.2	System Costs	151
6.3	Cost Summaries	158
6.4	Economic Analysis	159
6.5	Analysis Results	161
CHAPTER 7 SUMMARY AND CONCLUSIONS		165
APPENDIX: EXPERIMENTAL DATA; GROUND CRUST		168
REFERENCES		170

LIST OF TABLES

<u>Table</u>	<u>Page</u>
1.1 Physical Properties and Values of Hawaii and Johnston Island EEZ Crust Resource	5
1.2 Bulk Chemistry of Pacific Ocean Ferromanganese Crusts	9
1.3 Metal Historical Price Statistical Summary	11
1.4 Cobalt-Rich Ferromanganese Crust Per Ton Value by the Novel Solution Mining Method	12
3.1 Thermodynamic Evaluation of Mineral Leaching in Ferromanganese Crust	59
6.1 CRC Subsystem Capital Costs (1993 dollars)	153
6.2 Processing Subsystem Capital Cost (millions of 1993 dollars)	154
6.3 Processing Subsystem Operating Costs (millions of 1993 dollars)	156
6.4 Total Solution Mining System Capital Cost Summary (millions of 1993 dollars)	159
6.5 Total Solution Mining System Operating Cost Summary (millions of 1993 dollars)	160
6.6 Solution Mining Crust per Ton Value (1993 dollars)	161
6.7 Solution Mining System Base Case Scenario Results	162
6.8 Impact of Changing Cobalt Grade on Solution Mining IRR	162
6.9 Impact of Changing Cobalt Price on Solution Mining IRR	163
6.10 Solution Mining System High Grade Selective Mining Scenario Results (1.25% Co, 0.87% Ni, 30.19% Mn, \$16.70/lb Cobalt Market Value)	164

LIST OF FIGURES

<u>Figure</u>	<u>Page</u>
1.1 Potential Marine Mining Lease Tracts in the EEZ Adjacent to Hawaii and Johnston Island	4
2.1 Robotic Bottom Miner System for Ferromanganese Crusts	17
2.2 Continuous Line Bucket System Design Configurations	21
2.3 <i>In Situ</i> Batch Reactor Submarine Solution Mining System	24
2.4 Cross Section of Edge Sealing Tube System	27
2.5 CRC Deployment Scheme	29
2.6 Crust <i>In Situ</i> Solution Extraction Process Flow Diagram	33
2.7 Schematic Cross Section of Cross Seamount illustrating the truncated summit, The distribution and relative thickness of cobalt-rich ferromanganese crusts and biotic zonation	35
3.1 Eh - pH Diagram for the Fe - H ₂ O, Mn - H ₂ O, Cu - H ₂ O, Ni - H ₂ O, and Co - H ₂ O Systems at 25°C	41
3.2 The Effect of Solution pH on the Recovery of Metals During a 10 minute Leach of 20 gm of Ground (-100 mesh) Ferromanganese Nodule Material at 25°C, one atm;	43
3.3 Distribution of the Sulfurous Acid System with pH, at 1 bar and 25°C	45
3.4 Energy Level Diagram Showing the Splitting of a Set of Metal Atom (ion) d Orbitals by Octahedral and Tetrahedral Electrostatic Ligand Fields	50
3.5 Molecular Orbital Theory Energy Diagram for σ -Bonding in an Octahedral Transition-Metal--Ligand Complex (ML ₆) which has No Ligand π -Bonding	53
3.6 Qualitative Molecular Orbital Theory Energy Diagram for SO ₂ . The x-axis is Perpendicular to the Page. “*” Denotes Antibonding and “N” Denotes Non-Bonding Orbitals	54

3.7	Molecular Orbital Diagram Demonstrating the Two-Electron Reduction of Mn^{4+} by SO_2 . Electron Transfer Occurs from SO_2 $4a_1$ Orbital to Each of the Degenerate $3e_g$ Orbitals on Mn^{4+}	56
3.8	Reductive Dissolution Mechanism of Mn Oxide by $SO_{2(aq)}$	58
3.9	Leaching Curves (10 minutes) for Several Metal Values from 20 Grams of -200 Mesh Ferromanganese Nodule Particles in Water Containing Various Quantities of SO_2	64
4.1	Relationship Between $k_p / k_{1 atm}$ and Volume of Activation, Δ^*V° , for Average <i>In Situ</i> Ferromanganese Crust Conditions	70
4.2	Semi-Batch Whole Crust Reactor Flask Apparatus for $SO_{2(aq)}$ Leaching of Intact Ferromanganese Crust Fragments	77
5.1.1	Effect of Temperature on Metal Recovery of Ferromanganese Crust in 1% Sulfurous Acid Batch Leach, <u>5 Minute Leach Time</u> , pH = 1.0, Pressure = 1 atm, 400 rpm Stir Rate	81
5.1.2	Effect of Temperature on Metal Recovery of Ferromanganese Crust in 1% Sulfurous Acid Batch Leach, <u>5 Minute Leach Time</u> , pH = 2.0, Pressure = 1 atm, 400 rpm Stir Rate	82
5.1.3	Effect of Temperature on Metal Recovery of Ferromanganese Crust in 1% Sulfurous Acid Batch Leach, <u>15 Minute Leach Time</u> , pH = 1.0, Pressure = 1 atm, 400 rpm Stir Rate	83
5.1.4	Effect of Temperature on Metal Recovery of Ferromanganese Crust in 1% Sulfurous Acid Batch Leach, <u>15 Minute Leach Time</u> , pH = 1.0, <u>Pressure = 100 atm</u> , 400 rpm Stir Rate	84
5.1.5	Effect of Temperature on Metal Recovery of Ferromanganese Crust in 1% Sulfurous Acid Batch Leach, <u>15 Minute Leach Time</u> , pH = 1.0, <u>Pressure = 200 atm</u> , 400 rpm Stir Rate	85
5.1.6	Effect of Temperature on Metal Recovery of Ferromanganese Crust in 1% Sulfurous Acid Batch Leach, <u>15 Minute Leach Time</u> , pH = 2.0, Pressure = 1 atm, 400 rpm Stir Rate	86
5.1.7	Effect of Temperature on Metal Recovery of Ferromanganese Crust in 1% Sulfurous Acid Batch Leach, <u>15 Minute Leach Time</u> , pH = 2.0, <u>Pressure = 100 atm</u> , 400 rpm Stir Rate	87

5.1.8 Effect of Temperature on Metal Recovery of Ferromanganese Crust in 1% Sulfurous Acid Batch Leach, 5 Minute Leach Time, pH = 2.0, <u>Pressure = 200 atm</u> , 400 rpm Stir Rate	88
5.1.9 Effect of Temperature on Metal Recovery of Ferromanganese Crust in 1% Sulfurous Acid Batch Leach, 15 Minute Leach Time, <u>pH = 3.0</u> , Pressure = 1 atm, 400 rpm Stir Rate	89
5.1.10 Effect of Temperature on Metal Recovery of Ferromanganese Crust in 1% Sulfurous Acid Batch Leach, 5 Minute Leach Time, pH = 3.0, <u>Pressure = 100 atm</u> , 400 rpm Stir Rate	90
5.1.11 Effect of Temperature on Metal Recovery of Ferromanganese Crust in 1% Sulfurous Acid Batch Leach, 15 Minute Leach Time, pH = 3.0, <u>Pressure = 200 atm</u> , 400 rpm Stir Rate	91
5.1.12 Effect of Temperature on Metal Recovery of Ferromanganese Crust in 1% Sulfurous Acid Batch Leach, 15 Minute Leach Time, <u>pH = 5.0</u> , Pressure = 100 atm, 400 rpm Stir Rate	92
5.1.13 Effect of Temperature on Metal Recovery of Ferromanganese Crust in 1% Sulfurous Acid Batch Leach, 15 Minute Leach Time, pH = 5.0, <u>Pressure = 200 atm</u> , 400 rpm Stir Rate	93
5.1.14 Effect of Temperature on Metal Recovery of Ferromanganese Crust in 1% Sulfurous Acid Batch Leach, <u>30 Minute Leach Time</u> , pH = 1.0, Pressure = 1 atm, 400 rpm Stir Rate	94
5.1.15 Effect of Temperature on Metal Recovery of Ferromanganese Crust in 1% Sulfurous Acid Batch Leach, 30 Minute Leach Time, pH = 1.0, <u>Pressure = 100 atm</u> , 400 rpm Stir Rate	95
5.1.16 Effect of Temperature on Metal Recovery of Ferromanganese Crust in 1% Sulfurous Acid Batch Leach, 30 Minute Leach Time, pH = 1.0, <u>Pressure = 200 atm</u> , 400 rpm Stir Rate	96
5.1.17 Effect of Temperature on Metal Recovery of Ferromanganese Crust in 1% Sulfurous Acid Batch Leach, 30 Minute Leach Time, <u>pH = 2.0</u> , Pressure = 1 atm, 400 rpm Stir Rate	97
5.1.18 Effect of Temperature on Metal Recovery of Ferromanganese Crust in 1% Sulfurous Acid Batch Leach, 30 Minute Leach Time, pH = 2.0, <u>Pressure = 100 atm</u> , 400 rpm Stir Rate	98

5.2.1 Effect of Pressure on Metal Recovery of Ferromanganese Crust in 1% Sulfurous Acid Batch Leach, <u>5 Minute Leach Time</u> , pH = 1.0, Temperature = 15°C, 400 rpm Stir Rate	100
5.2.2 Effect of Pressure on Metal Recovery of Ferromanganese Crust in 1% Sulfurous Acid Batch Leach, 5 Minute Leach Time, <u>pH = 2.0</u> , Temperature = 15°C, 400 rpm Stir Rate	101
5.2.3 Effect of Pressure on Metal Recovery of Ferromanganese Crust in 1% Sulfurous Acid Batch Leach, <u>15 Minute Leach Time</u> , pH = 1.0, <u>Temperature = 5°C</u> , 400 rpm Stir Rate	102
5.2.4 Effect of Pressure on Metal Recovery of Ferromanganese Crust in 1% Sulfurous Acid Batch Leach, 15 Minute Leach Time, pH = 1.0, <u>Temperature = 15°C</u> , 400 rpm Stir Rate	103
5.2.5 Effect of Pressure on Metal Recovery of Ferromanganese Crust in 1% Sulfurous Acid Batch Leach, 15 Minute Leach Time, <u>pH = 2.0</u> , <u>Temperature = 5°C</u> , 400 rpm Stir Rate	104
5.2.6 Effect of Pressure on Metal Recovery of Ferromanganese Crust in 1% Sulfurous Acid Batch Leach, 15 Minute Leach Time, pH = 2.0, <u>Temperature = 15°C</u> , 400 rpm Stir Rate	105
5.2.7 Effect of Pressure on Metal Recovery of Ferromanganese Crust in 1% Sulfurous Acid Batch Leach, 15 Minute Leach Time, <u>pH = 3.0</u> , <u>Temperature = 5°C</u> , 400 rpm Stir Rate	106
5.2.8 Effect of Pressure on Metal Recovery of Ferromanganese Crust in 1% Sulfurous Acid Batch Leach, 15 Minute Leach Time, pH = 3.0, <u>Temperature = 15°C</u> , 400 rpm Stir Rate	107
5.2.9 Effect of Pressure on Metal Recovery of Ferromanganese Crust in 1% Sulfurous Acid Batch Leach, 15 Minute Leach Time, <u>pH = 5.0</u> , <u>Temperature = 5°C</u> , 400 rpm Stir Rate	108
5.2.10 Effect of Pressure on Metal Recovery of Ferromanganese Crust in 1% Sulfurous Acid Batch Leach, 15 Minute Leach Time, pH = 5.0, <u>Temperature = 15°C</u> , 400 rpm Stir Rate	109
5.2.11 Effect of Pressure on Metal Recovery of Ferromanganese Crust in 1% Sulfurous Acid Batch Leach, <u>30 Minute Leach Time</u> , pH = 1.0, Temperature = 5°C, 400 rpm Stir Rate	110

5.2.12 Effect of Pressure on Metal Recovery of Ferromanganese Crust in 1% Sulfurous Acid Batch Leach, 30 Minute Leach Time, pH = 1.0, <u>Temperature = 15°C</u> , 400 rpm Stir Rate	111
5.2.13 Eh-pH Diagram for the Simple Cu-O-H Geochemical System	112
5.3.1 Effect of pH on Metal Recovery of Ferromanganese Crust in 1% Sulfurous Acid Batch Leach, <u>Leach Time = 5 Minutes</u> , <u>Temperature = 0.1°C</u> , Pressure = 1 atm, 400 rpm Stir Rate	114
5.3.2 Effect of pH on Metal Recovery of Ferromanganese Crust in 1% Sulfurous Acid Batch Leach, Leach Time = 5 Minutes, <u>Temperature = 15°C</u> , Pressure = 1 atm, 400 rpm Stir Rate	115
5.3.3 Effect of pH on Metal Recovery of Ferromanganese Crust in 1% Sulfurous Acid Batch Leach, <u>Leach Time = 15 Minutes</u> , <u>Temperature = 0.1°C</u> , Pressure = 1 atm, 400 rpm Stir Rate	116
5.3.4 Effect of pH on Metal Recovery of Ferromanganese Crust in 1% Sulfurous Acid Batch Leach, Leach Time = 15 Minutes, <u>Temperature = 5°C</u> , Pressure = 1 atm, 400 rpm Stir Rate	117
5.3.5 Effect of pH on Metal Recovery of Ferromanganese Crust in 1% Sulfurous Acid Batch Leach, Leach Time = 15 Minutes, Temperature = 5°C, <u>Pressure = 100 atm</u> , 400 rpm Stir Rate	118
5.3.6 Effect of pH on Metal Recovery of Ferromanganese Crust in 1% Sulfurous Acid Batch Leach, Leach Time = 15 Minutes, Temperature = 5°C, <u>Pressure = 200 atm</u> , 400 rpm Stir Rate	119
5.3.7 Effect of pH on Metal Recovery of Ferromanganese Crust in 1% Sulfurous Acid Batch Leach, Leach Time = 15 Minutes, <u>Temperature = 15°C</u> , <u>Pressure = 1 atm</u> , 400 rpm Stir Rate	120
5.3.8 Effect of pH on Metal Recovery of Ferromanganese Crust in 1% Sulfurous Acid Batch Leach, Leach Time = 15 Minutes, Temperature = 15°C, <u>Pressure = 100 atm</u> , 400 rpm Stir Rate	121
5.3.9 Effect of pH on Metal Recovery of Ferromanganese Crust in 1% Sulfurous Acid Batch Leach, Leach Time = 15 Minutes, Temperature = 15°C, <u>Pressure = 200 atm</u> , 400 rpm Stir Rate	122

5.3.10 Effect of pH on Metal Recovery of Ferromanganese Crust in 1% Sulfurous Acid Batch Leach, Leach Time = <u>30 Minutes</u> , Temperature = 15°C, Pressure = 1 atm, 400 rpm Stir Rate	123
5.4.1 Effect of Leach Time on Metal Recovery of Ferromanganese Crust in 1% Sulfurous Acid Batch Leach, pH = 1.0, <u>Temperature = 0.1°C</u> , Pressure = 1 atm, 400 rpm Stir Rate	125
5.4.2 Effect of Leach Time on Metal Recovery of Ferromanganese Crust in 1% Sulfurous Acid Batch Leach, pH = 1.0, <u>Temperature = 5°C</u> , Pressure = 1 atm, 400 rpm Stir Rate	126
5.4.3 Effect of Leach Time on Metal Recovery of Ferromanganese Crust in 1% Sulfurous Acid Batch Leach, pH = 1.0, <u>Temperature = 15°C</u> , Pressure = 1 atm, 400 rpm Stir Rate	127
5.4.4 Effect of Leach Time on Metal Recovery of Ferromanganese Crust in 1% Sulfurous Acid Batch Leach, pH = 1.0, Temperature = 15°C, <u>Pressure = 100 atm</u> , 400 rpm Stir Rate	128
5.4.5 Effect of Leach Time on Metal Recovery of Ferromanganese Crust in 1% Sulfurous Acid Batch Leach, pH = 1.0, Temperature = 15°C, <u>Pressure = 200 atm</u> , 400 rpm Stir Rate	129
5.4.6 Effect of Leach Time on Metal Recovery of Ferromanganese Crust in 1% Sulfurous Acid Batch Leach, <u>pH = 2.0</u> , <u>Temperature = 0.1°C</u> , Pressure = 1 atm, 400 rpm Stir Rate	130
5.4.7 Effect of Leach Time on Metal Recovery of Ferromanganese Crust in 1% Sulfurous Acid Batch Leach, pH = 2.0, <u>Temperature = 5°C</u> , Pressure = 1 atm, 400 rpm Stir Rate	131
5.4.8 Effect of Leach Time on Metal Recovery of Ferromanganese Crust in 1% Sulfurous Acid Batch Leach, pH = 2.0, Temperature = 5°C, <u>Pressure = 100 atm</u> , 400 rpm Stir Rate	132
5.4.9 Effect of Leach Time on Metal Recovery of Ferromanganese Crust in 1% Sulfurous Acid Batch Leach, pH = 2.0, Temperature = 5°C, <u>Pressure = 200 atm</u> , 400 rpm Stir Rate	133
5.4.10 Effect of Leach Time on Metal Recovery of Ferromanganese Crust in 1% Sulfurous Acid Batch Leach, pH = 2.0, <u>Temperature = 15°C</u> , Pressure = 1 atm, 400 rpm Stir Rate	134

5.4.11 Effect of Leach Time on Metal Recovery of Ferromanganese Crust in 1% Sulfurous Acid Batch Leach, pH = 2.0, Temperature = 15°C, Pressure = 100 atm, 400 rpm Stir Rate	135
5.4.12 Effect of Leach Time on Metal Recovery of Ferromanganese Crust in 1% Sulfurous Acid Batch Leach, pH = 3.0, Temperature = 15°C, Pressure = 1 atm, 400 rpm Stir Rate	136
5.4.13 Effect of Leach Time on Metal Recovery of Ferromanganese Crust in 1% Sulfurous Acid Batch Leach, pH = 5.0, Temperature = 15°C, Pressure = 1 atm, 400 rpm Stir Rate	137
5.5.1 Semi-Batch Intact Crust Leach Experiment: Hancock Seamount Crust in 9% Sulfurous Acid Batch Leach, Temperature = 4°C, pH = 1.0, Pressure = 1 atm, 400 rpm Stir Rate	139
5.5.2 Semi-Batch Intact Crust Leach Experiment: Karin Seamount Range Crust in 9% Sulfurous Acid Batch Leach, Temperature = 4°C, pH = 1.0, Pressure = 1 atm, 400 rpm Stir Rate	140
5.5.3 X-ray Powder Diffractometer Record of Hancock Seamount Crust Leached Surface Product	142
5.5.4 Scanning Electron Micrograph Showing Texture of Hancock Seamount Leached Crust Surface Product	144
5.5.5 Energy Dispersive X-ray Fluorescence Spectrometer Record Showing Apparent Elemental Concentration Peaks of Hancock Seamount Crust Leached Surface Product Layer Material	145

CHAPTER 1 INTRODUCTION

1.1 The Utility of Cobalt

The United States is the world's largest consumer of cobalt. In 1989, the United States consumed 7,164 mt (metric tons) nearly 30% of the estimated world production of 26,237 mt (Shedd, 1991). There is no domestic production, so demand is met primarily from imports, with the exception of about 17% from secondary sources (recycling of superalloy and other forms of scrap). World cobalt demand is growing at a rate of 3-4% a year in spite of the current world-wide economic recession (Johnson, 1992). According to Loudat and others (1994), it is unlikely that terrestrial sources of cobalt can sustain long term growth at these rates. The increase in cobalt demand is driven by new uses, particularly in computer memory storage media (hard disks), magnets, superalloys, and specialty composites such as cobalt-tungsten carbide ceramics. Cobalt is an indispensable element in a variety of critical and strategic applications and has few viable substitutes in most of its major end uses. Due to its extensive use in the aerospace and manufacturing industries, cobalt is considered to be a "strategic material", defined as a commodity whose lack of availability would seriously affect the economic, industrial and defensive capability of the United States, and a national defense stockpile (24,088 mt reported by the Defense Logistics Agency in 1990) is maintained by the federal government at several locations in the United States (Shedd, 1991).

1.2 Resource Potential of Cobalt-Rich Ferromanganese Crusts from Seamounts

During the past ten years, numerous studies of the resource potential of cobalt-rich ferromanganese crust deposits on central Pacific seamounts have been conducted (Halbach

and Manheim, 1984; Manheim, 1986; Ritchey et al., 1986; Johnson et al., 1987; Ritchey, 1987). Significant deposits of cobalt-rich ferromanganese crust are found in the Exclusive Economic Zones of many Pacific nations, including, for the United States, zones adjacent to Hawaii and Johnston Island. The exact resource potential of these deposits is not known due to limited coverage by high-resolution survey data, but is projected in the hundreds of millions of tons--a significant mineral potential, given the appropriate mining technology. The U.S. Department of Interior's Minerals Management Service (MMS) and U.S. Bureau of Mines (USBM) has worked closely with the State of Hawaii's Department of Business, Economic Development, and Tourism to promulgate future exploitation of the ferromanganese crust resource in the Exclusive Economic Zone (EEZ) adjacent to Hawaii and Johnston Island, by funding and overseeing important research work, culminating with (after seven years in preparation) the release of a final environmental impact statement (U.S. Minerals Management Service and State of Hawaii Dept. of Business and Economic Development, 1990 (hereafter referred to as: EIS, 1990)) and the formation of a joint federal/state task force, "The Hawaii Joint Planning Arrangement," to promote lease sales for crusts in the Hawaiian and Johnston Islands' EEZ.

1.2.1 Resource Area in the EEZ Adjacent to Hawaii and Johnston Island.

For the purposes of feasibility analysis in this research work, the crust resource area considered corresponds to the permissive areas in the EEZ adjacent to Hawaii and Johnston Island. The Hawaii and Johnston Island EEZ (EIS, 1990) encompasses approximately 2.2 million square kilometers (km²) stretching 3,300 km from southeast of the island of Hawaii

to northeast of Kure Atoll and 370 km (200 nautical miles) to either side of the Hawaiian archipelago and 370 km around Johnston Island, excluding designated areas around populated islands, wildlife preserves, and military use zones (see Figure 1.1) For prospective leasing, the seafloor in the EEZ has been subdivided into ten tentative lease tracts, four in the Hawaii area (labeled A, B, CG, and HI) and six in the Johnston Island area (labeled K, L, M, N, O, and P). Prospective crust mining sites are located on portions of flanks and summits of about 126 seamounts and island slope areas between water depths of 800 and 2,400 meters (*ibid.*). The total crust mining permissive area is therefore less than 1% of the EEZ, about 10,660 km² in the Hawaii area and about 16,250 km² in the Johnston Island area.

1.3 Summary of Open Ocean Ferromanganese Crust Properties

1.3.1 *Physical Characteristics of Ferromanganese Crust*

Open ocean ferromanganese crusts are oxide encrustations which form on hard substrates in raised areas such as seamounts and ridges that are kept free from detrital sedimentation by periodic currents and steep slopes. Crusts tend to occur in a highly localized manner on and around seamounts and ocean ridges, on current-swept terraces and plateaus, and on some steep island slopes (Manheim, 1989). Crust thickness ranges from a mere patina, or oxide staining of substrate to encrustations as much as 15 cm thick (Hein et al., 1990). The substrate on which crusts are formed tends to be rough, irregular, and difficult to sample. Table 1.1 lists physical variables and values for crusts in the Hawaii and Johnston Island EEZ resource areas. Crusts generally adhere to underlying substrate making it difficult to mechanically separate the ore material during the recovery process without

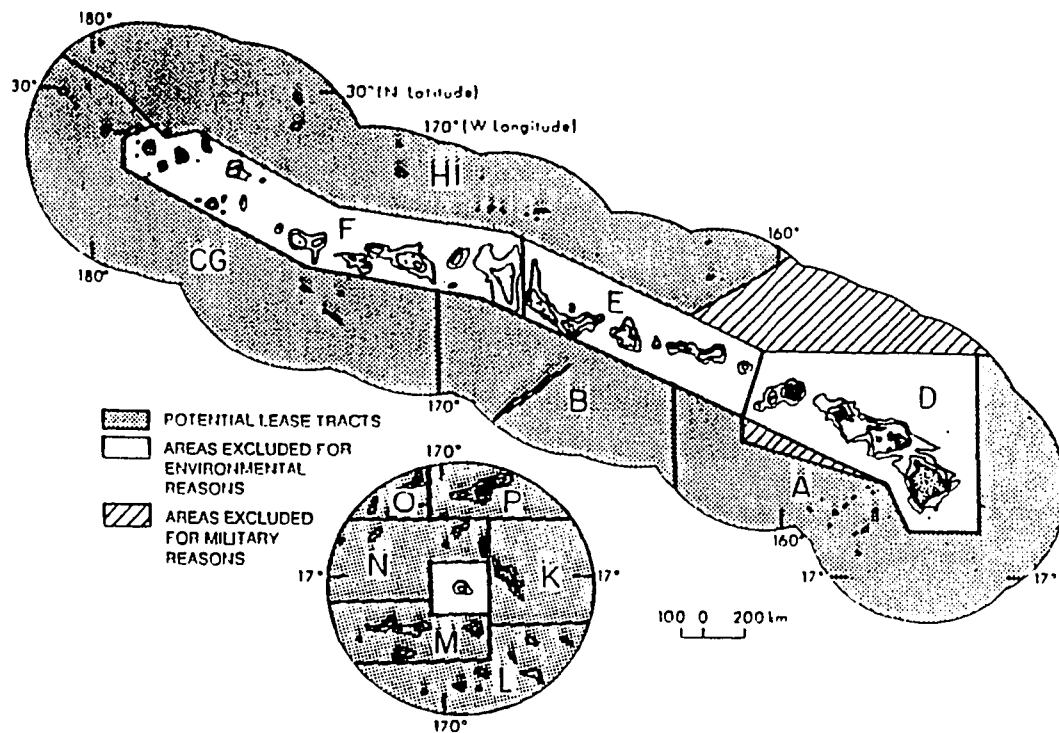


Figure 1.1 *Potential Marine Mining Lease Tracts in the EEZ Adjacent to Hawaii and Johnston Island (U.S. Minerals Management Service and State of Hawaii Dept. of Business and Economic Development, 1990).*

Table 1.1 Physical Properties and Values of Hawaii and Johnston Island EEZ Crust Resource. Mechanical Properties for Brine (1.02 g/cm³) Saturated Crust from the Hawaii EEZ Area (data from Cruickshank and Paul, 1986; Larson et al., 1987; and EIS, 1990).

Crust Variables	Mean	Range	S.D. (δ)
Thickness (cm)	2.5	0.1 - 15.0	1.78
Coverage (% area)	40 %	0 - 100 %	16.7 %
Specific Weight (wet; g/cm ³)	1.86	1.82 - 1.89	0.02
Porosity (%)	55 %	52.3 - 66.4 %	6.85 %
Void Ratio	1.22	-	-
Shore Hardness	13	9 - 18	5.32
Compressive Strength (MPa)	7.16	5.39 - 8.92	2.08
Tensile Strength (MPa)	0.45	-	-
Cohesive Strength (MPa)	1.49	-	-
Young's Modulus (GPa)	3.68	3.11 - 4.25	0.67
Poisson's ratio, dynamic	0.26	0.11 - 0.34	0.14
Angle of Internal Friction (ϕ)	76°	-	-

reducing the ore grade by diluting the ore material with worthless substrate (Morgan, 1989).

Crust "pavements" are generally comparable to medium hard coal in strength and in their resistance to mechanical cutting (Cruickshank and Paul, 1986).

The coverage of ferromanganese crust on seamounts within the Hawaii and Johnston Island EEZ varies from no deposit (in areas with thick sediment layers) to 100% coverage. The amount of coverage for a site is estimated primarily by analysis of bottom photographs from camera tow tracks. Preliminary work has also been made to refine the knowledge of the spatial distribution of crust deposits using stereo photogrammetric techniques to produce

high resolution microtopographic models of surface roughness (Morgan et al., 1988). Average crust coverage for the Hawaii and Johnston Island EEZ resource areas has been estimated at 25% in areas D, E, and F and 40% in the ten potential lease tract areas: A, B, CG, HI, K, L, M, N, O, and P depicted in Figure 1.1 (Halbach and Manheim, 1984; EIS, 1990). Rankings by Hein and others (1986) of estimated resource potential of Pacific Area crust deposits lists the Johnston Island area as having *High Potential*, with a relative ranking of #3, behind the Kiribati Islands and the Marshall Islands resource areas. The Hawaii area was afforded *Medium Potential* (ibid.) with a relative ranking of #7. In a similar comparison, the Johnston Island area was ranked #5 out of the ten prospective resource areas considered by Clark and Johnson (1986) to have potential economic viability. The values estimated for the Johnston Island area will be assumed in the economic analysis of the crust mining scenario presented in Chapter 6.

1.3.2 Mineralogy and Structure of Ferromanganese Crust

Bulk (i.e., total thickness) crust mineralogy in the Hawaii and Johnston Island EEZ resource areas are typically composed of over 90% δ -MnO₂ (vernadite) of hydrogenitic origin with the Fe phase(s) epitaxially intergrown as amorphous Fe oxyhydroxide with occasionally goethite in the inner layers of some crusts (De Carlo et al., 1987; Hein et al., 1990; De Carlo, 1991). Rarely, Mn phase minerals, todorokite and birnessite occur in the innermost layers and may represent a change in deposition redox conditions (Hein et al., 1990; 1992). Carbonate fluorapatite can be abundant (up to 36%) in the inner layers of many crusts (Hein et al., 1986; 1990). Other minor minerals include plagioclase, quartz, barite, K-feldspar, calcite,

manjiroite, zeolite, and clay minerals. The quartz and some of the plagioclase are eolian in origin. The rest of the plagioclase and the pyroxene, K-feldspar, zeolite, and others are derived from substrate material, primarily by means of suspension and settling of substrate detritus. Calcite and phosphorite are derived from surface water biological production (*ibid.*).

Four types of internal growth structures have been identified in crusts by Ingram and others (1990) as botryoidal, columnar, compact (massive), and mottled (also referred to as micronodule texture by VonderHaar (1990)). Hein and collaborators (1992) suggest that the compact and mottled structures indicate relatively fast growth under quiescent flow conditions whereas the botryoidal and columnar structures indicate relatively slow growth under higher flow regimes.

1.3.3 Chemistry of Ferromanganese Crust

The chemical composition of crusts can be generally characterized by assigning the elements to four major genetic groups by interrelation associations derived from factor analysis (Wen, 1995). These are represented by a hydrogenetic group (Mn, Co, Ni, Zn, Cu, Ce and Ce anomaly), a biogenetic group (Ba, Zn, Cu, Pt, Fe and Ce anomaly), a detrital group (Si, Al and Fe) and a carbonate fluorapatite group (Ca, P and rare earth elements). The hydrogenetic and detrital groups demonstrate strong inverse correlation, and the biogenetic group exhibit environment dependence (*ibid.*). Although chemical composition can be highly variable between individual samples, the average abundances of metals are remarkably similar for large areas of the central Pacific (Hein et al., 1986). Table 1.2 lists the abundance statistics for the total Pacific, albeit with a heavy bias in the Hawaii and Johnston Island EEZ

areas (397 of 834 samples). In general, for the five metals of interest analyzed in this research for prospective mining within the Hawaii and Johnston Island EEZ areas, values range between 20 - 30% Mn, 15 - 20% Fe, 0.5 - 1.1% Co, 0.3 - 0.7% Ni, and 0.05 - 0.15% Cu.

Cobalt is commonly enriched in the younger outer layers of the crusts, whereas Pt enrichment is found in the older inner layers (Halbach et al., 1989). Thinner crusts are chemically equivalent to the outer parts of thicker crusts (yielding a relatively higher bulk grade of Co in thinner crusts). Hein and collaborators (1990) attribute this chemical equivalence to the erosion of old crust layers at sites where thinner crusts are found, prior to the ubiquitous deposition in crust permissive areas of the younger crust layers enriched in cobalt. The increase in cobalt concentration in the younger crust layers is postulated to be an effect of slower crust growth rate, as a slow-growth rate is conducive to a greater degree of cobalt scavenging by δ -MnO₂ (Halbach et al., 1983; Hein et al., 1986). Confirmation of slower growth rate of the younger crust layers relative to older inner layers since about the Middle Miocene has been accomplished by stratigraphic radiometric age dating and collaborating microfossil and Co chronometer evidence (Segl et al., 1984; Manheim and Lane-Bostwick 1988; Segl et al., 1989; Cowen, et al., 1993; McMurtry et al., 1994).

Cobalt and Ni concentrations are positively correlated with Mn content whereas Cu concentration usually is positively correlated with Fe (Halbach and Manheim, 1984; Aplin and Cronan, 1985; Hein et al., 1986; De Carlo et al., 1987; Halbach et al., 1989; De Carlo et al., 1991). Correlations are also evident between various elements and water depth. Abundance of Cu and Fe increase with increasing water depth, whereas Mn, Co, and Ni increase with decreasing water depth (Aplin and Cronan, 1985; Hein et al., 1986; De Carlo et al., 1987).

Table 1.2 Bulk Chemical Composition of Pacific Ocean Ferromanganese Crusts (note, mean is biased by a large population (397 samples) in the Hawaii and Johnston Island EEZ areas). Values in percent moisture-free material, except Pt (ppm). After Manheim and Lane-Bostwick (1989).

Variable	No. Samples	Mean	Range	S.D. (δ)
Depth (m)	819	2012	598 - 6890	721
Mn	773	25.02	15.10 - 38.79	4.14
Fe	802	16.89	5.98 - 22.95	2.93
Co	805	0.87	0.03 - 3.02	0.37
Ni	773	0.46	0.12 - 1.54	0.17
Cu	603	0.08	0.01 - 0.55	0.05
Mg	632	1.16	0.71 - 2.39	0.20
Ca	655	2.83	1.41 - 5.97	0.78
Al	746	0.95	0.06 - 2.50	0.51
Ti	675	1.12	0.10 - 2.46	0.28
K	443	0.54	0.06 - 1.01	0.10
P	653	0.51	0.03 - 1.88	0.25
Si	542	3.42	0.61 - 6.99	1.64
Na	293	1.74	0.21 - 3.32	0.48
Ba	401	0.185	0.084 - 0.430	0.060
Mo	399	0.057	0.017 - 0.149	0.021
Pb	476	0.192	0.015 - 0.370	0.056
Sr	444	0.167	0.083 - 0.245	0.023
V	399	0.070	0.025 - 0.160	0.013
Zn	460	0.073	0.010 - 0.671	0.039
Y	264	0.019	0.008 - 0.050	0.004
Ce	264	0.123	0.006 - 0.285	0.037
As	265	0.029	0.014 - 0.343	0.022
Cd	271	0.0004	<0.0001 - 0.0014	0.0002
Pt (ppm)	8	0.484	0.164 - 1.294	0.393

These relations are considered to reflect the differing scavenging behavior of Mn and Fe oxides in the water column and change in crust Mn/Fe ratio with depth due to a increase in Mn flux in the water column above ~ 2 km depth, derived from horizontal advection from continental sources and/or from diffusion out of the oxygen minimum zone (Aplin and Cronan, 1985; De Carlo et al., 1987).

1.4 Historical Metal Prices of Cobalt, Nickel and Manganese

Table 1.3 shows metal historical price summary statistics for cobalt, nickel and manganese, used to value potential crust ore. The mean prices are used to value the ore and the 95% confidence interval prices are used for the economic study and sensitivity analyses in Chapter 6. As shown in Table 1.3, the coefficient of variation indicates that cobalt prices are more than twice as volatile as other metal prices. This volatility of the cobalt price will be a major point of concern for future crust mining (Loudat et al., 1994). The mean historical prices used in the economic study (presented in Chapter 6) are considered conservative, understating the average expected future cobalt price, due to rising demand and expected future shortfalls in cobalt supply.

1.5 A Novel Method of Crust Mining by Solution Recovery

A preliminary design for a method with potential for mining cobalt-rich crusts on seamounts was developed at the University of Hawaii (Zaiger, 1993; 1994; 1995). This patented invention (entire right, title and interest has been assigned to the University of Hawaii) forms in effect, an *in situ* batch reactor upon a crust site and adapts terrestrial *in situ* leach mining methods to the deep ocean floor. The proposed processing method of this

Table 1.3 Metal Historical Price Statistical Summary (all values expressed in 1993 dollars). Source of data; USBM Annual Reports and Mineral Industry Surveys 1970-1993 (after Loudat, Zaiger and Wiltshire, 1994).

Item	Cobalt (\$/lb)	Nickel (\$/lb)	Manganese (\$/mt)
# of Observations	24	34	24
Minimum	\$7.76	\$2.26	\$252.60
Maximum	\$47.40	\$7.47	\$653.29
Arithmetic Mean (μ)	\$16.70	\$4.01	\$445.41
Standard Deviation (δ)	\$11.57	\$1.16	\$129.02
Coefficient of Variation (δ/μ)	0.69	0.29	0.29
<u>95 % Confidence Interval</u>			
Lower Bound	\$11.78	\$3.62	\$390.47
Upper Bound	\$21.63	\$4.40	\$500.35

system is a variant of the successful solvent extraction and electronwinning (SX-EW) process developed for heap leached copper ore solutions. The SX-EW process made its initial appearance in the copper industry in 1968 and now produces approximately 11% of the world copper supply (Carter, 1991). U.S. Bureau of Mines research and pilot plant studies (Jeffers, 1985; Jeffers and Harvey, 1985, Gritton and Jeffers, 1987; Jordon, 1988) have developed a number of SX-EW procedures which appear suitable for the production of metallic cobalt from dilute crust leach solutions. The innovative and low cost technology of solution mining may favorably alter the economic equation leading to more timely commercial marine mining ventures.

1.6 Value of Cobalt-Rich Ferromanganese Crusts

The value per ton of cobalt-rich ferromanganese crust is derived from the estimated metal recoveries per ton of crust ore/substrate and the mean metal prices (Table 1.3). Table 1.4 shows the value per ton of crust ore based on the novel *in situ* solution mining system described in detail in Chapter 2 and the base case assumptions described in Chapter 5. Clearly, the largest revenue producer is cobalt comprising 67.8% of total annual revenues under the base case scenario. Manganese is the second largest revenue producer with 23.6% of the total mining venture revenues.

1.7 Potential Crust Mining Sites in the Johnston Island EEZ

The *in situ* solution mining system (described in section 2.3) requires mine site areas that are relatively flat with relatively smooth topography to allow proper sealing of the batch reactor to the crust bearing surface. Numerous very nearly flat areas have been identified

Table 1.4 Cobalt-Rich Ferromanganese Crust Per Ton Value (1993 dollars) by the Novel Solution Mining Method. Assumes 50% Crust Extraction Efficiency and 95% Metals Recovery from Lixiviant. After Loudat, Zaiger, and Wiltshire, 1994.

Metal Product	Recovery Per Ton of Ore Processed	Annual Metal Weight Recovered	Base Case Metal Price	Annual Revenue (mil. \$)	% of Total Revenues
Cathode Co (lbs)	0.83%	5,502,809	\$16.70	\$91.90	67.80%
Cathode Ni (lbs)	0.44%	2,909,531	\$4.01	\$11.67	8.61%
Mn (Metric tons)	23.77%	71,782	\$445.41	\$31.97	23.59%
Total Annual Revenue				\$135.55	(mil. \$)
Dry Tons of Crust Processed				302,000	(per year)
Processed Crust Ore Value				\$448.84	(per ton)

on specific seamounts targeted for potential crust mining. Good examples are located north of Johnston Atoll on Horizon Guyot (19°30'N 168°45'W). Horizon Guyot is the most extensively studied seamount within the Johnston Island EEZ. Since 1956, numerous sampling and surveying expeditions have been carried out at Horizon Guyot, including cores from Deep Sea Drilling Project (DSDP) Leg VI Site 44 and Leg XXXIII Site 171 (Heezen et al., 1971; Natland, 1976), and six major expeditions by the Scripps Institute of Oceanography (Lonsdale et al., 1972). On the northern flank of Horizon Guyot, 15 nearly flat terraces have been identified each extending up to 10 km in length with an average width of 3 km. These terraces are probably constructional volcanic features, either dammed hyaloclastite flows (Lonsdale et al., 1972) or individual volcanic breccia flow units (Natland, 1976) and are found at depths between 1,730 - 2,010 m. The terraces are remarkably flat with regional outward slopes of less than 1 in 150 (0.38°) and are separated by distal scarps (inferred flow fronts) with slopes of about 20° and heights up to 100 meters. Micro-topography surveys by the *Scripps Deep Tow Sidescan-SONAR and narrow-beam echo sounder* instrument package (Spiess and Mudie, 1970) determined a small-scale topography of 5-10 meters on and near the escarpments and very low topographic relief (<< 1 meter) and uniform acoustic roughness (texture) on the terraces. Dredge hauls on the terraces collected samples of breccia and altered hyaloclastite fragments encrusted with ferromanganese oxide. The average crust coverage on these terraces is estimated from camera tows to be 52%, however this figure includes the upper terraces which are partly buried with sediments derived from the pelagic sediment cap of the guyot. Deeper terraces were relatively sediment free with maximum coverage on a single terrace estimated to be 93%. The average crust

thickness from dredge sampling was 1.5 cm with a maximum recovered sample thickness of 5.0 cm (Lonsdale et al., 1972). Other nearly continuous flat crust fields greater than 10 km in size have been documented in the Johnston Island EEZ, south of Johnston Atoll (Halbach and Puteanus, 1985; Wiltshire, 1993). Three seamounts surveyed by Seabeam™ Bathymetric mapping and television tows during German expeditions in the 1980s identified broad relatively flat plateau areas with considerable mine site potential. Nearly flat sites such as the seamount terrace and plateau areas described above are considered excellent prospects for crust mining.

1.8 Objectives of this Research

In order for a deep ocean *in situ* solution extraction crust mining system to be viable, an important hypothesis must be proved: *The leach kinetics and physicochemical hydrodynamics at in situ conditions will be favorable for the economically viable recovery of metal cations in crusts.* To accomplish this, a number of research goals must be attained:

1. To determine the reaction rates of candidate leach methods as a function of temperature, pressure, and concentration of reactants at simulated *in situ* crust conditions (using homogeneous ground crust samples.)
2. To determine the efficiency of recovery of economic metals from crust samples by the selected leach method at simulated *in situ* solution mining conditions.
3. To study the physicochemical nature of the selected leach method on intact crust.
4. To determine whether leach reaction is limited by the reaction rate or by surface layer diffusion at the reactant surface.

If the viability hypothesis seems to be validated by laboratory work, then the feasibility of the crust mining method can be assessed by the additional research goals:

5. To prepare a base case scenario specifying all the requisite systems for a hypothetical first generation *in situ* solution-extraction crust mining system.
6. To perform an economic analysis of the *in situ* mining system scenario.
7. To perform an economic comparison between the *in situ* mining system and a prospective competing crust mining system based on an alternate technology.

Achieving these objectives allows an evaluation of the feasibility of the new mining system and insight in developing kinetic and transport models for further design work.

CHAPTER 2

POTENTIAL CRUST MINING TECHNOLOGIES

A number of creative approaches have been proposed to mine ferromanganese crusts. Some of these, such as the *hydraulic jet crust ablation system* (Werjefelt et al., 1989) have quickly faded into obscurity. However, three systems have persevered at least through preliminary feasibility studies and economic analyses. These are the *Robotic Bottom Miner System* and the *Continuous Line Bucket System*, summarized in Sections 2.1 and 2.2, and the subject of this research, the solution recovery based *In Situ Batch Reactor System* described in detail in Section 2.3.

2.1 Robotic Bottom Miner System

The *Robotic Bottom Miner System* (Halkyard and Felix, 1987) depicted in Figure 2.1, has been the conceptual mining method used in a number of preliminary feasibility analyses of potential ferromanganese crust mining. In particular, the *Robotic Bottom Miner System* was used to develop the mining scenario for the EIS (1990) for the Hawaii and Johnston Island EEZ, and by Loudat and others (1994). The *Robotic Bottom Miner* consists of a conceptual 100 mt self-propelled, bottom crawling (approximate speed of 20 cm/sec) tracked vehicle. Dimensions of the bottom miner would be approximately eight meters wide by 13 meters long and six meters high. The miner fragments crust ore at a rate of 125 kg/sec as it moves along the ocean floor of the mine site (EIS, 1990). Rotating cutter drums on articulated arms allows the miner to adjust depth and angle of cut to correspond to the thickness of the crust as it is mined to maximize efficiency of crust recovery while limiting the take of worthless substrates. Hypothetical “first order” modeling of cutter head efficiency by

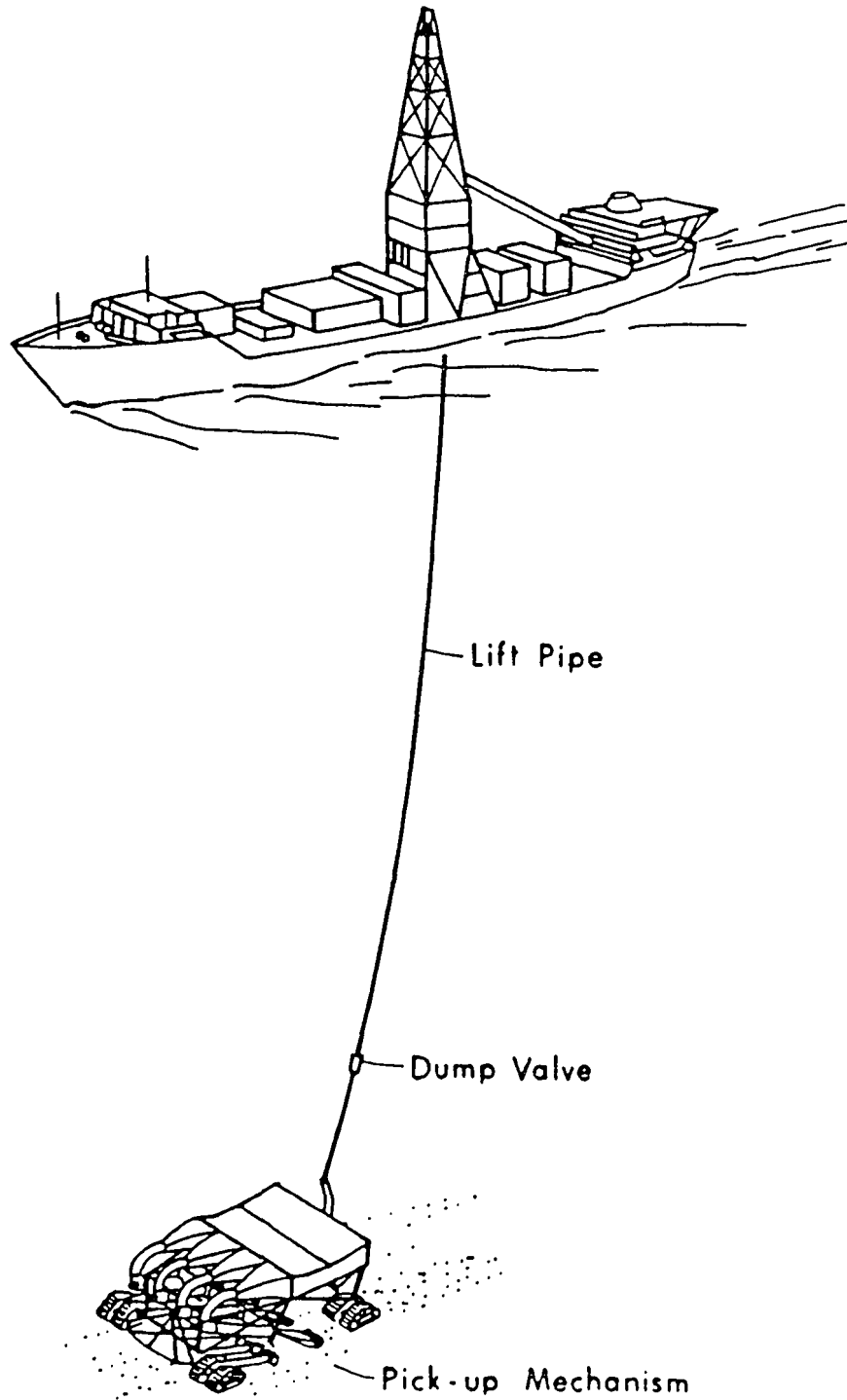


Figure 2.1 *Robotic Bottom Miner System for Ferromanganese Crusts (Halkyard and Felix, 1987).*

Morgan (1989) predicated a maximum attainable crust recovery efficiency of 80% with a 25%-50% dilution of the crust material with the substrate, based on microtopographic data of crust deposits derived from stereo bottom photos and dredged samples. Approximately 95% of the fragmented crust/substrate material would be picked up by hydraulic suction, fed through diffusers and sized through a mechanical screen prior to transport as a slurry through a 27-cm diameter lift pipe to the *Mine Ship* by means of a compressed air-hydraulic lift system (EIS, 1990). This technology is essentially the hybrid of cutting equipment used in underground coal mining with that originally proposed for manganese nodule mining in the 1960s and 1970s (Wiltshire, 1993). The 75,000 dwt *Mine Ship* provides “command and control” input to the *Robotic Bottom Miner*, and is connected to the bottom miner by a rigid hydraulic lift pipe string and electrical umbilical. The *Mine Ship* has onboard high capacity-high pressure pumps to provide the airlift of the crust slurry to the surface via the lift pipe and also launches and retrieves the bottom miner and lift pipe system through a “moon pool.” It uses highly specialized heavy lift equipment similar to that developed for the *Ocean Minerals Company’s Glomar Explorer* (Welling, 1985) or *Deep Sea Drilling Program* ships. The crust slurry is stored and dewatered by decantation aboard the *Mine Ship* prior to loading on a bulk transport vessel for delivery to a land-based processing plant.

The *Robotic Bottom Miner* will follow predetermined tracks using precision satellite navigation, coordinated with long baseline bottom transponder grids. Mine tracks will be laid based on detailed site surveys and selected to favor areas of higher ore grade, avoiding rough topography and other obstacles, and parallel bathymetric contour lines as much as possible to minimize changing the length of the lift pipe string. SONAR mounted on the bottom miner

will aid in obstacle recognition, tracking navigation benchmarks and previous mine swaths.

The *Robotic Bottom Miner* was designed for a hypothetical recovery of one million dry tons of crust per year based on two hundred and twenty-six 24-hour days of mining (EIS, 1990). Primary downtime for a bottom miner regular overhaul would be scheduled during the August to September time frame, to coincide with the peak hurricane season in the resource area. Other downtime will occur as necessary for repair and maintenance. The EIS (1990) projects a 4-day maintenance period every 20-50 days to change out cutter drums.

Development of the *Robotic Bottom Miner* system has not progressed past the preliminary development stage. Also, no model testing of components has been completed. Nevertheless, this mining system is an excellent representative as a probable “high end” standard for comparison studies with other mine system candidates.

2.2 Continuous Line Bucket System

The *Continuous Line Bucket* (CLB) system developed by Yoshio Masuda (Masuda et al., 1971) is the only system actually tested at sea. The CLB system consists essentially of a long rope loop (85-200 mm braided polypropylene line) suspended from a surface vessel (mine ship) to the seabed (Figure 2.2), to which dredging buckets are attached at regular intervals. The motive force on the rope loop is provided by a series of paired ball roller traction devices on board the mine ship (Masuda and Cruickshank, 1991; Masuda et al., 1993). The rate and bottom contact time of each bucket is a factor of the rope speed, the rope slack on the bottom, and the drift over ground of the mine ship. Buckets filled with seabed material are continuously raised to the surface, emptied on board the mine ship and

returned to the seabed on the downward passage of the rope. The production rate is determined by bottom contact time (affects bucket filling efficiency), rope speed and the spacing of the buckets on the line.

Since 1968, numerous small scale pilot tests of the CLB systems have been conducted in depths to five thousand meters (Masuda, 1985; Masuda et al., 1991; Masuda and Cruickshank, 1991; Masuda et al., 1993). Several problems were encountered, resulting in system design evolution through four different configurations.

The original configuration (Figure 2.2 A.) separated the upward tending line from the downward tending line by the ship's length in order to maintain suitable separation for adequate bottom contact time and to avoid entanglements. The mine ship is required to move sideways using thrusters and by drifting broadside to prevailing winds and current. Control of the mine ship's sideways speed over ground is critical as it affects the catenary of the line loop (optimum CLB rope length is about 2.4 times the water depth). If speed over ground is too fast, the buckets will have little or no bottom contact time, too slow and the buckets on the downward tending line pile up and get entangled. The optimum sideways speed over ground for a 1972 CLB test near Hawaii was determined to be 0.78 kts (0.4 m/s) for a 100-meter line separation in 4,900 m water depths. This optimum sideways speed was only achieved during brief periods in the 1972 test during low wind conditions (Masuda, 1985). The prevailing trade winds typically induced too much speed over ground for effective CLB dredging.

Because of the wind drift induced problems experienced by the original CLB, a two-ship CLB configuration (Figure 2.2 B.) was developed and studied by the French *Center for*

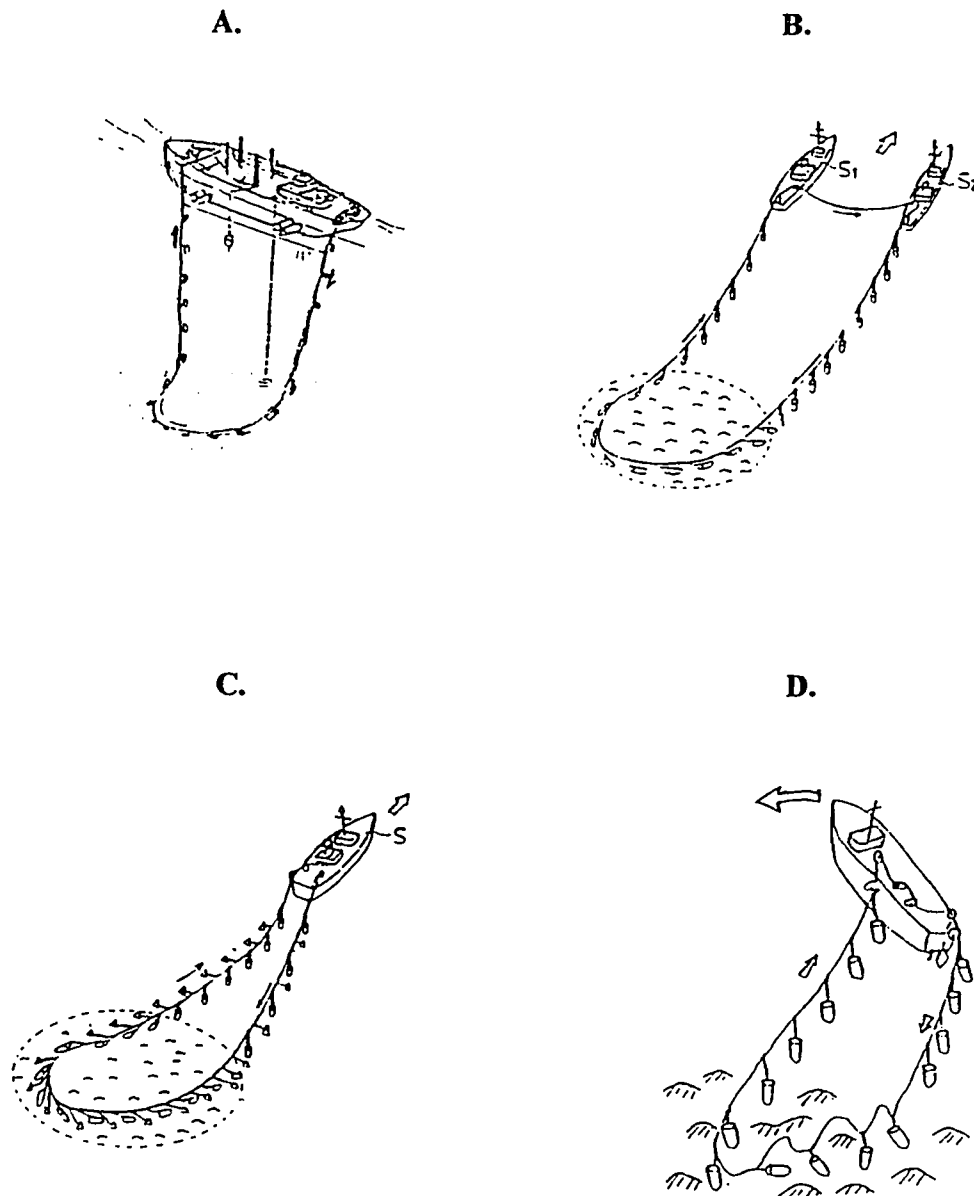


Figure 2.2 *Continuous Line Bucket System Design Configurations:*
A. Original CLB; B. Two Ship CLB; C. Hydro-Dynamic Separator CLB;
D. Turning CLB. After Masuda and Cruickshank, 1991.

Exploration of the Ocean (CNEXO). Development work was completed on the bucket, rope, and traction systems (Masuda and Cruickshank, 1991) and model testing was conducted in a deep tank and in a lake during the 1974-1976 period. Further pilot studies were not undertaken, but it is apparent that even though ship control during operations is much improved (as wind drift can be minimized by heading into the wind), it is still not ideal. Because the optimum speed over ground for the CLB dredge operation is slow, positive steering control can not be provided by rudders and most of the positioning effort will fall on the thrusters. Because the paired mine ships will have very different line tensions, maintaining safe separation between the ships during dredging operations in moderately heavy seas could prove challenging. The guide ship, (the line uphaul ship in the *two ship* CLB case) must be able to maintain “rock steady” course and speed, such that the maneuvering ship can accurately predict and make timely course and speed corrections to keep on station. As thrusters generally provide relatively slow response, this may be difficult to achieve, resulting in limiting effective CLB mining to fairly calm sea states.

At the same time, an alternate configuration (Figure 2.2 C.) based on hydrodynamic separation was under development by Japanese co-operators (Masuda and Cruickshank, 1991). Separator plates, similar to trawl net “otter boards” or specially configured buckets are used to separate the rope lines using natural hydrodynamic forces. Successful small scale tests were carried out in 4000 m water depth near Japan during 1975. Although the *hydrodynamic separation* CLB configuration resolves the high sea state safety issue of the *two ship* configuration, the separator plates result in increased tension load on the lines and increased complexity in handling the buckets on board during operations.

The latest configuration currently favored by Masuda (Masuda and Cruickshank, 1991; Masuda et al., 1993) is the *turning* CLB (Figure 2.2 D.). In this configuration, the mine ship proceeds along a circular track around the locus of the bucket bottom contact point on the crust mine site. Good separation of the lines is achieved by trailing the empty buckets over the stern and bringing up the loaded bucket amidships from the inside of the turn arc track. Proper flare (catenary) of the down trending line can be maintained to preclude entanglements by adjusting the mining ship's stern twist away from the line. As the mine ship is turning about a long radius from the locus of the bucket bottom contact point, adequate way on (3-5 kts) is achieved for positive rudder steerage (the most rapid and responsive maneuvering control). This configuration is considered superior to its predecessors as it provides the simplest control of line separation and better system control under a wider range of sea states. The circuitous track of the mine ship in the *turning* CLB configuration may be constrained by the bathymetry of some potential crust mine sites, but it appears that it may be well suited to many seamount slope geometries. Currently, Masuda is proposing a small scale test (40 mt/day production) of this latest CLB configuration out of Majuro in the Republic of the Marshall Islands (Masuda et al., 1993).

2.3 *In Situ* Batch Reactor System

The deep-sea mining method developed at the University of Hawaii (Zaiger 1993; 1994; 1995) adapts terrestrial *in situ* leach mining methods to the deep ocean floor. The mining method uses a dedicated hydrometallurgical processing ship (Figure 2.3) or large floating platform and two or more "containment and regulation covers" (CRCs).

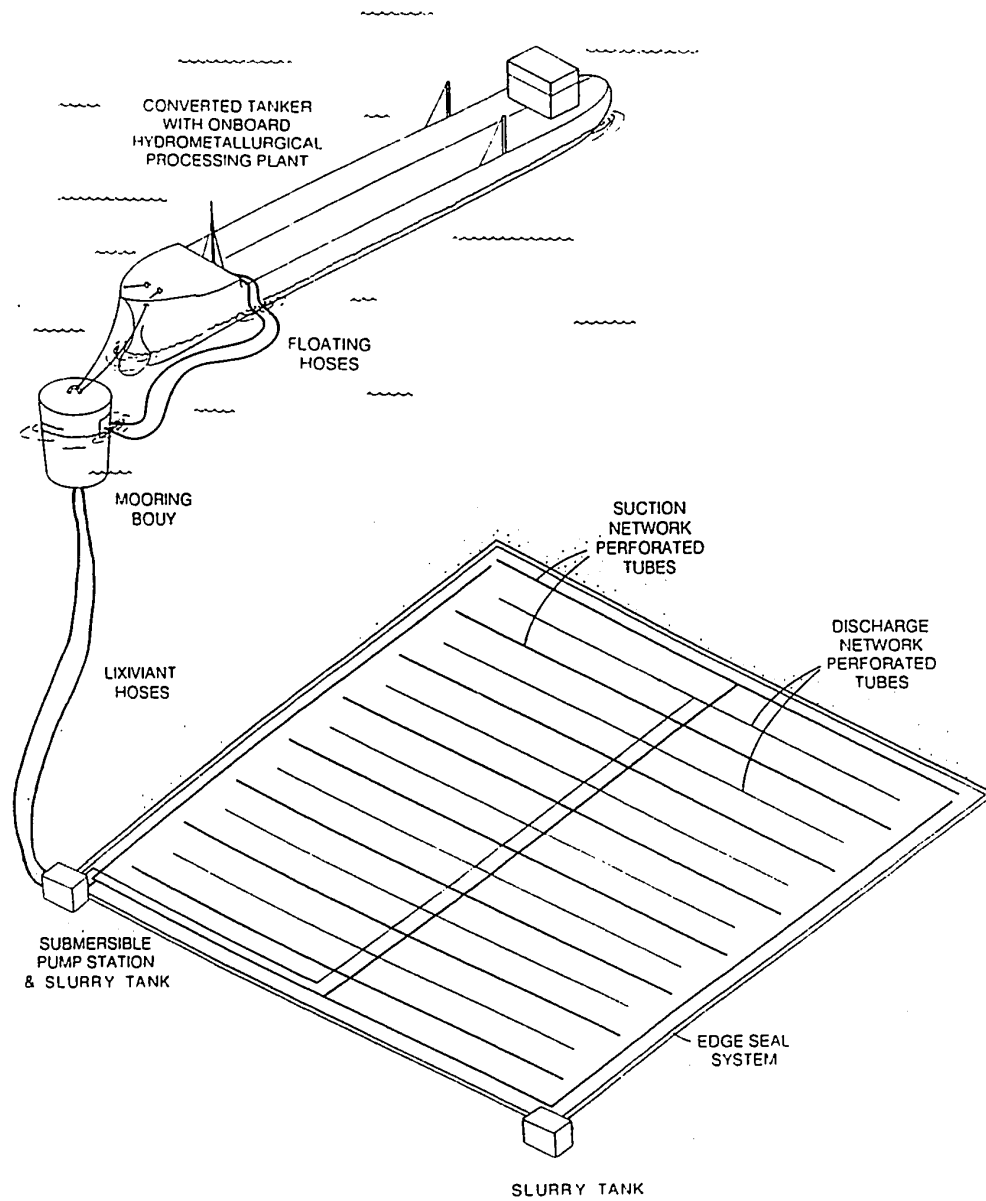


Figure 2.3 In Situ Batch Reactor Submarine Solution Mining System.

2.3.1 CRC System

The containment and regulation cover (CRC) is designed to deliver and confine lixiviant (recycling leach solution) to the ore stratum at a mining site and retrieve pregnant (metal containing) solution for processing onboard the mining ship (or floating platform). A CRC placed and sealed on a crust mine site is essentially a semi-batch chemical reactor in that the inlet feed stream and internal volume are constant but composition and product (outlet) changes. Any leach solution (weakly acidic) escaping the CRC would be quickly neutralized by the alkalinity of the seawater. The amount of leach solution lost is anticipated to be minimal, probably negligible. Multiple CRCs are used in this mining system in order to keep mining ship processing "down time" to a minimum. When leaching is complete at a mine site, the mining ship would detach hoses and quickly move to an alternate CRC which has been prepositioned on a new site within the mine area. While leaching commences at the new site, residual lixiviant at the old site is neutralized with a wash of weak lime [CaO] solution followed by flushing with sea water prior to CRC removal. This site neutralization process would be provided through the CRC surface hose hookups.

The CRC is constructed of a tough flexible membrane, similar to the synthetic geoliners used terrestrially for reservoirs and environmental containment, which covers and supports perforated tubing distribution and expanded-net leachate collection networks for lixiviant control. The CRC membrane is laminated over a *wire rope* grid which provides the tensile strength needed to allow recovery and relocation of the CRC to other mine area sites.

2.3.2 CRC Sealing and Maintenance

The CRC is sealed to the substrate by weighing down the edges with perimeter dike-tubes filled after deployment with a heavy fluid such as barite drilling mud (the density of BaSO_4 is $4.48 \text{ g}\cdot\text{cm}^{-3}$) and maintaining negative pressure inboard of the dike-tubes under the membrane using perforated suction tubes (Figure 2.4). Approximately 340 mt of heavy fluid will be used per CRC distributed between two pump/weighting slurry tank stations located at two adjacent corners of the CRC (the bottom edge during site-to-site transport). Inflation/deflation of the CRC edge sealing dike-tubes with heavy fluid from/to the weighting slurry tanks will be effected using heavy-duty electric slurry pumps modified for submarine use.

The leakage of sea water into the leach circuit by migration through the crust stratum under the seals can be controlled by reducing the hydraulic gradient. This is accomplished by increasing the length of the seepage path, by the use of CRC edge weighting tubes in series acting as a blanket and by reducing pressure head by operating at as low a negative system pressure as practicable. The permeable stratum is the crust itself, and average thickness of this stratum is only a few centimeters. Although transmissivity may be relatively high in crusts, the small cross sectional area will greatly limit flow volume. To ensure that CRC edge sealing is adequately maintaining a low hydraulic gradient, continuous monitoring of a perimeter grid of pressure transducer piezometers will be conducted during operations.

Since the system operates with negative pressure within the CRC, any perforation of the membrane that may occur would result in dilution of the leach circuit and additional sea water being pumped up to the ship. Minor membrane tears could be repaired in place or

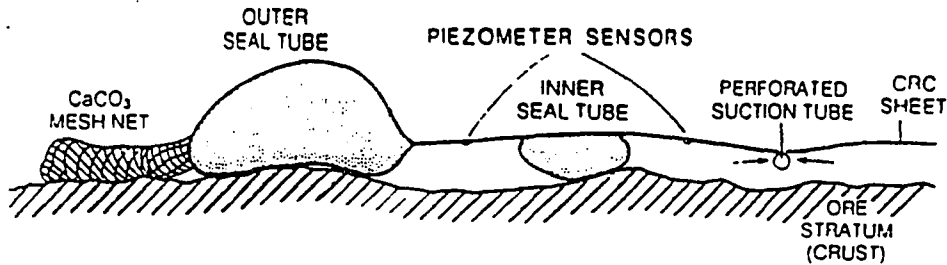


Figure 2.4 Cross Section of Edge Sealing Tube System.

during the relocation phase by using *Remotely Operated Vehicles (ROVs)* equipped with adhesive patches and an electrical plastic extrusion/welding tool. *ROVs* would also perform CRC edge seal inspections during pre-mining "draw-down" tests and could repair minor seal breaches.

2.3.3 CRC Deployment and Relocation

A CRC is initially towed on the ocean surface to the mine area in a roll configuration with an empty pump/weighting slurry tank station at each end. Flotation on the surface is provided by pontoons detached prior to lowering the CRC to the mine site (not shown in figures). The roll configuration provides a shape amenable for surface towing and rapid lowering onto a seamount mine site. Deployment of the CRC upon arriving at the mine site area would be made by filling the slurry tanks with BaSO_4 weighting fluid, then lowering the roll configuration to the surface of the crust mine site. The two pump/slurry tanks are the primary anchor/lift points and are navigated to predesignated "set-down" locations using long-baseline bottom transponder grids. The CRC roll is unrolled on the bottom using ocean

tugs equipped with powerful trawler-type winches (Figure 2.5). Spreading on the bottom is also assisted by inflating spreading tubes located on the CRC (not shown in figures). It is estimated that CRCs up to 200 m in linear dimension can be deployed and retrieved to depths of two kilometers, based on the design constraints of available commercial deck gear.

Relocation of the CRC to another site in the mine area is effected by first evacuating the weighting fluid from the perimeter edge sealing tubes by pumping the heavy fluid to the weighting slurry tanks at the corners of the CRC "bottom edge", then lifting by tug winches the CRC "top edge" corners opposite the pump stations, until the CRC is suspended vertically with just the pump/weight slurry tank stations and CRC "bottom edge" still anchored to the bottom (total static load of 360 mt). Next the heavy pump/weight slurry tank stations with CRC "bottom edge" suspended between them are carefully hoisted by tug winch to safely clear any bottom obstruction. Placement of this "bottom edge" controls the positioning of the CRC on the next site. The "bottom edge" is carefully navigated to the next location 200 meters or more away, using the long-baseline acoustic bottom transponder system, and lowered into the next "set-down" position. "Set-down" is followed by the draping of the CRC over the new site. To avoid shearing damage to the CRC membrane, the up haul angles on the "top edge" corners must initially be inclined slightly towards the weighted "pump station" edge and slightly outward from each other in the plane of the sheet (analogous to lifting a blanket off a bed by its corners without dragging it).

Variable (and sealable) orifices on the CRC (not shown in figures) would reduce sheet drag during transport and provide some control of settling velocity while draping the CRC on a new mine site. This process is also aided by the re-inflation of the spreading tubes with

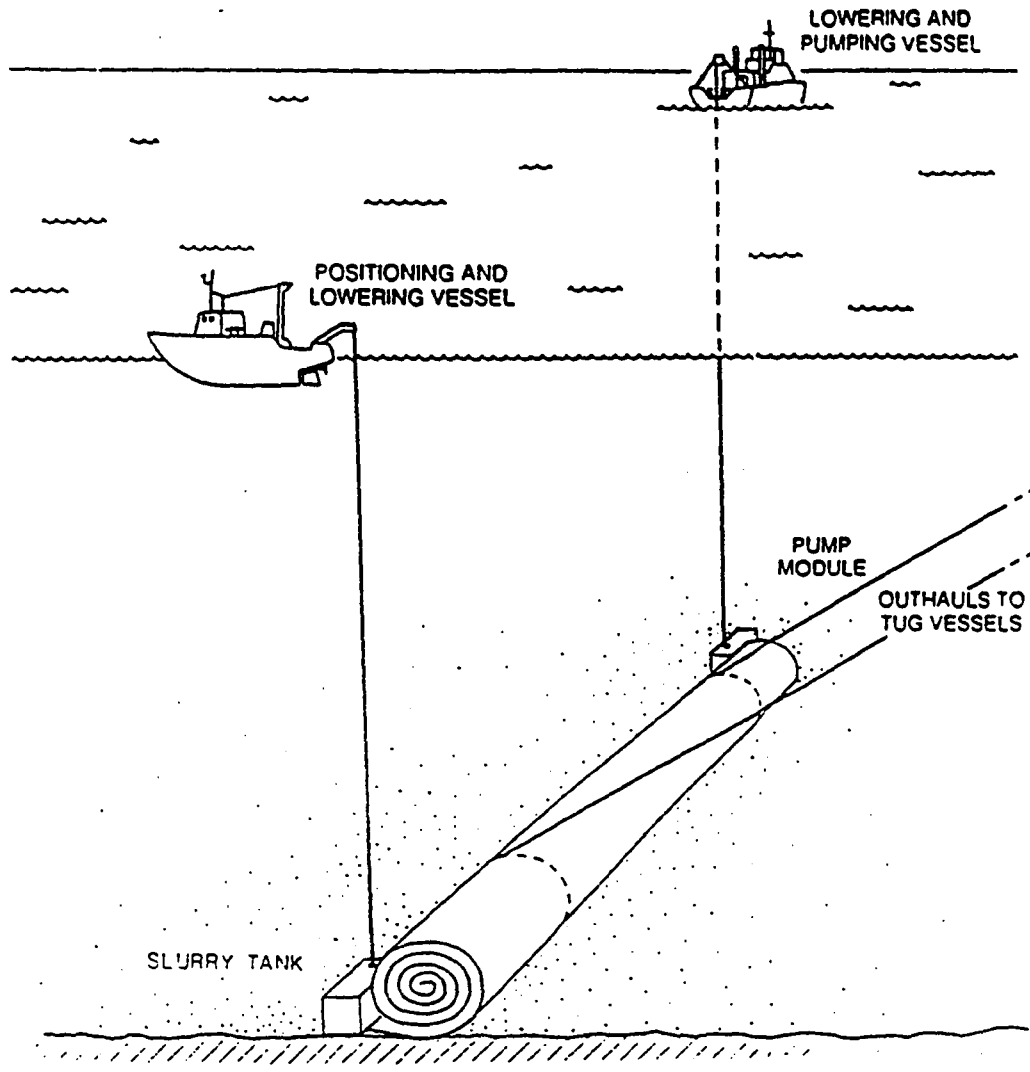


Figure 2.5 *CRC Deployment Scheme.*

sea water and the perimeter edge sealing tubes with weighting fluid. As mentioned below (Section 2.3.4), bottom currents at potential seamount mine sites are predominantly tidal. Thus, it is important to time the hoisting and draping phases of CRC relocation to coincide with periods of *slack water* and transport to parallel the direction of tidal flow whenever possible. Hauling the CRC up to the surface would be necessary only in the event of major (not repairable by *ROV*) structural damage or cessation of mining in the area. When a CRC is no longer usable, it would be hauled to the surface, separated into smaller sections and transported back to shore for recycling or proper disposal.

Although relatively cumbersome, the process of relocating a CRC from mine site to mine site is within the technological and seamanship capabilities demonstrated regularly by commercial trawlers and purse seiners working with nets an order of magnitude larger in size.

2.3.4 Effect of Tidal Currents

A moored current meter was deployed 180 m above the summit of Horizon Guyot (19°26.9'N 168°48.9'W) in the Johnston Island EEZ (Hein et al., 1985) at a depth of 1,635 meters. Over a 10 month period it recorded a current pattern which exhibited strong tidal influence with lesser influences from internal waves and thermohaline flow. The current pattern exhibited mean easterly velocity of $1.34 \text{ cm}\cdot\text{s}^{-1}$ with a variance of $35.33 \text{ cm}\cdot\text{s}^{-1}$ and mean southerly velocity of $0.86 \text{ cm}\cdot\text{s}^{-1}$ with a variance of $54.20 \text{ cm}\cdot\text{s}^{-1}$. The maximum current velocity measured was $30 \text{ cm}\cdot\text{s}^{-1}$ (about 0.6 knots). It is feasible to design the mining system with anchoring and sealing capabilities to safely operate in this and similar flow regimes.

Tidal currents can be locally amplified due to impinging interaction with seamount topography. Also, vortex-wake eddies may form in the lee of seamounts where topography acts as a barrier to incident current flow (Roden, 1987). These influences are site specific and their influence on the current pattern at each potential mine site needs to be determined during the site selection process. However, it is likely that these local effects will not be critical at many prospective mine sites.

2.3.5 Solution Dynamics in Crust Substrate

Common crust substrates include altered basalt, indurated hyaloclastite, cemented volcanic breccia and phosphatized limestone. Hydrologic properties have been measured for terrestrial analogues (Columbia River Plateau, Yakima Basalt Flows and interbeds) of these rock types and yield ranges of *hydraulic conductivity* (K) of 10^{-11} to 10^{-8} ms^{-1} for basalt and 10^{-9} to 10^{-5} ms^{-1} for fractured, highly weathered, or brecciated basalt (Freeze and Cherry, 1979). The wide variation in quantitative values of hydraulic conductivity in basaltic rock is due to differences in fracture densities, vesicle size and distribution and interconnections between vesicles and fractures. It is expected that the substrate which underlies crust will also exhibit variation in hydraulic conductivity of a similar scale.

Due to the deep ocean location, pore space in crust and underlying rock substrate is fully saturated and under hydrostatic conditions. Mining fluid (leachate) migration into the substrate will not be percolation or "trickle down seepage" but instead will be a miscible displacement in which molecular diffusion dominates over mechanical dispersion (turbulent mixing).

The density of the leach solution will be about $1,110 \text{ kg}\cdot\text{m}^{-3}$ an increase of 7.5% over *in situ* sea water. However, as the leach solution is confined to just a shallow layer (~10 cm) above the crust, the effective hydraulic head at the rock face and resultant hydraulic gradient into the substrate will be very small. With the exception of highly fractured crust substrate, diffusion will be the dominant dispersive process transporting leach solution into the substrate underlying crust and fluid migration rates would be on the order of centimeters per year. It is likely that numerous potential crust mine sites will be found with virtually impermeable ($K < 10^{-9}$) substrate.

2.3.6 At Sea Processing

The *in situ* batch reactor solution mining system uses a 40,000 dwt ship (surplus tanker) converted into a dedicated hydrometallurgical processing ship. The favored shipboard process method is an adaptation of the U.S. Bureau of Mines process developed to recover cobalt from dilute copper leach solutions (Jeffers 1985, Jeffers and Harvey 1985, Gritton and Jeffers 1987, Jordan 1988). This ion exchange/solvent extraction/electrowinning process uses feed material currently produced on a large scale and readily available industrial equipment (modified for shipboard use). All process streams are recycled or used for product recovery, minimizing the potential for environmental damage (Shedd 1991). Continuous operation is achieved by using parallel banks of multi-compartment ion exchange units in conjunction with highly effective resin stripping Pachuca reactors (Bennett and Jeffers 1988) and using a solvent extraction step to separate the cobalt from the cobalt-nickel bearing raffinate prior to electrowinning (Figure 2.6).

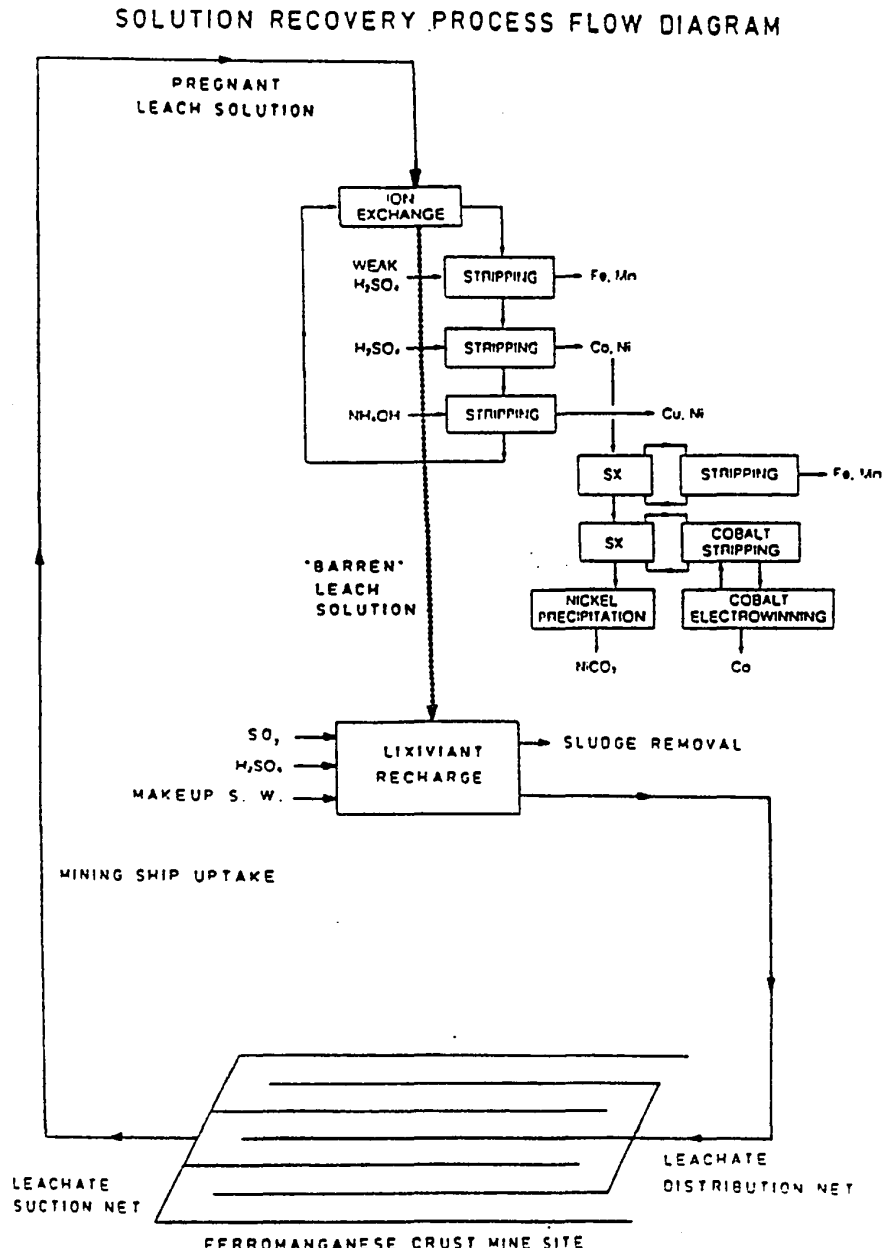


Figure 2.6 Crust In Situ Solution Extraction Process Flow Diagram
 (SX = solution extraction; S. W. = seawater).

2.3.7 *Environmental Impact of the In Situ Batch Reactor System*

In general, bathyal megafauna (predominantly sessile) and bottom fish are extremely low in diversity and abundance on seamounts in the "crust zones." This low biomass density reflects the restricted food supply, derived as residues of photic zone production from above or from *in situ* production. Little is known about the geographical range of each species and special interdependence in the bathyal assemblage, but due to the rigor of the deep-sea environment, benthic species are most likely ubiquitous and distributed over large geographic areas. As benthic species are not likely to exist in concentrated pockets, the demise of fauna in a mine area will not result in species extinctions. Species abundance is particularly low on seamounts in crust areas, possibly a result of larval avoidance. A comprehensive photo reconnaissance by Grigg and others (1987) of Cross Seamount (18°40'N 158° 17'W) counted 61 species with an average density of 0.14 organisms per m² with 81% of the organisms found in the areas of low crust abundance (Figure 2.7).

It is well known that some seamounts are the sites of economic fishing grounds. A number of the southern Emperor-northern Hawaiian ridge seamounts have been commercially exploited since 1967 for groundfish (primarily alfoncin, *Beryx splendens*, and pelagic armorhead, *Pseudo-pentaceros wheeleri*, and to a lesser extent, squid, *Ommastrephes bartramii*) by the Japanese, Koreans and former Soviets (Uchida and Tagami, 1984; Sasaki, 1986; Uchida et al., 1986). Other northern Emperor ridge seamounts are known to aggregate schools of migratory tuna (bluefin tuna, *Thunnus thynnus*) at depths down to 400 meters over the seamount slopes (Yamanaka, 1986). The relationship between seamounts and fish aggregation has been suggested to be a result of complex flow-topography interactions

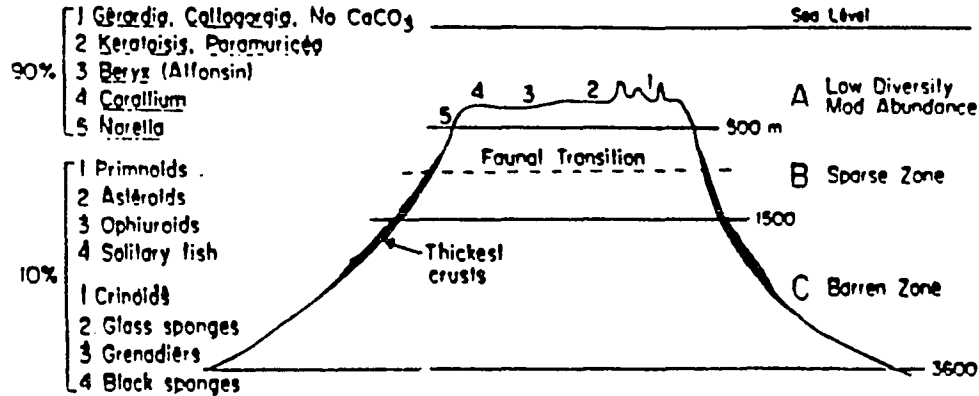


Figure 2.7 Schematic cross section of Cross Seamount illustrating the truncated summit, the distribution and relative thickness of cobalt-rich ferromanganese crusts and biotic zonation. Eighty-one percent (2545 organisms) of the fauna was observed at depths shallower than 500 meters (Zone A), fifteen percent (463 organisms) was observed between 501 and 1500 meters (Zone B), and four percent (116 organisms) was observed below 1501 meters (Zone C). After Grigg et al., 1987.

generating local nutrient upwelling and eddy formation (Boehlert and Genin, 1987). Evidence of upwelling associated with Taylor columns and strong mesoscale eddies in the vicinity of the Emperor Seamounts have been identified indirectly based on the observation of the dome shaped uplift of thermohaline isolines up to the seasonal pycnocline below the mixed surface layer (Roden and Taft, 1985). However Roden (1987) emphasizes that the dynamics of flow-topography interactions are poorly understood for nonuniform, time-varying flow, and the current theoretical models need to be verified by suitable field observations. Only one assessment of seamount related fishing grounds is discussed in the literature for the Johnston Island EEZ area. The Japan Fisheries Agency surveyed the Mid-Pacific seamounts for potential fisheries development in 1972 (Nasu and Sasaki, 1973). The objective was to locate additional open ocean groundfish resources similar to those exploited on seamounts of the

southern Emperor-northern Hawaiian ridge. Eleven flat topped seamounts were studied (locations were not disclosed) and dredge hauls were made on the five most promising prospects. The catches were extremely poor, ranging from 1-47 kg and totaling only 168 kg in nine tows. Fifty-three species of fauna were taken, but none were considered to have any commercial potential.

Any leakage or spill of leach solution into sea water is unlikely to cause lasting detriment. Sea water is alkaline so leaked leach solution would be quickly neutralized by the buffering effect of sea water (total alkalinity $\sim 2 \times 10^{-3}$ eq/l). Ocean primary production "food chains" will not be directly affected by leakage at a crust mine site as there is no chance of advection of leach solution into the euphotic zone, due to the stable layered thermohaline structure of the water column. Seamount mining sites are substantially deeper than the thermocline/pycnocline depths. Higher order species in the local "food chain" are not at risk because the metals (Fe, Mn, Cu, Ni, Co) released from crust are not known to bioaccumulate. In fact, biological productivity may be enhanced, as evidence suggests that Mn is a limiting nutrient in normal sea water whose aquatic fate appears to be dominated by microbial mediation (Cowen et al., 1990; Cowen and Li, 1991). Recent biogeochemical data from hydrothermal plume waters along the Southern Juan de Fuca Ridge (*ibid.*), indicates a positive correlation of total marine bacterial biomass in the water column to increasing concentration of (dissolved) Mn from hydrothermal plumes, and strongly supports a particulate Mn formation (scavenging) mechanism with increasing plume "age" dependent upon the local microbial population.

Although the acidity and leach products of the leach solution would cause the demise of sessile organisms at the crust mine site and immediate vicinity (in event of fugitive leakage) the impact would be temporary. It is expected that following cessation of mining and site neutralization, recolonization would rapidly return the species assemblage to its premining balance.

In some respects, one can consider the loss of crust mining leach solution as an analogue to deep sea hydrothermal emissions. Both are acidic and enriched in dissolved metals. One can speculate that like hydrothermal vent emissions, by-products of leach solutions may temporarily support communities of species based on the production of autocatalytic bacteria. The major differences are fluid density (hydrothermal solutions are buoyant and form mid-water plumes), and the concentrations of dissolved species. However, the physicochemical characteristics of each are quickly neutralized upon dilution with sea water and it would be hard to discern temporal effects on the environment within 100 meters of their respective emission points. One major difference is mass flux. Even in the worst case scenario, e.g. the loss of the full inventory of metal-laden leachate, the overall effect on the ocean environment would be insignificant compared to the ongoing mass flux from submarine hydrothermal emissions.

During the "scoping" process in the drafting of the Environmental Impact Statement for the *Proposed Marine Mineral Lease Sale: Exclusive Economic Zone Adjacent to Hawaii and Johnston Island* (EIS, 1990), it was apparent during open public symposia that considerable negative feelings exist concerning the notion of marine mining. Many concerns were raised by spokespersons for environmental protection special interest groups and

individual community activists. Hopefully, "environmental backlash" can be avoided by educating the general public, as deep ocean crust mining has the least amount of impact on the overall environment when compared to any existing or potential terrestrial mine producing the same commodities. The benthic population density of a seamount is approximately one organism per 7 m². In striking contrast, the population density of a rain forest is approximately 100,000 organisms per 1 m².

2.4 Comparison of Crust Mining Systems

The batch reactor crust mining system based on *in situ* hydrometallurgical leach processing has a number of advantages over the mechanical based mining systems under development. These include:

1. **Simpler technology:** motive ability on irregular seamount topography, mechanical comminution and handling of crust material, obstacle avoidance, and critically precise navigation during the mining operation are unnecessary.
2. **Greater energy efficiency in ore extraction:** material transport between the mine site and ocean surface is single phase (liquid only) instead of mixed phase, also, energy is saved because crust comminution is eliminated.
3. **On site processing eliminates the need for land based infra-structure and reduces transportation distances.**
4. **Less environmental disruption is caused due to the elimination of mining and dewatering sediment plumes.**

Limitations of the University of Hawaii deep-sea mining method include:

1. Design constraints of CRC edge sealing which limit potential mine sites to fairly flat seamount areas without excessive roughness or substrate(s) of high permeability.
2. Leach chemistry considerations which limit potential mine sites to those with refractory (non-reactive, e.g. basalt and hyaloclastite) underlying substrate(s) to avoid excessive lixiviant consumption.

CHAPTER 3

LIXIVIANT SELECTION AND CHEMISTRY REVIEW

The major objective of this research project is to evaluate the verity of cobalt-rich ferromanganese crust mining by the *in situ* solution extraction batch reactor system described in Chapter 2. This requires testing the hypothesis stated in Section 1.8, i.e., *the leach kinetics and physicochemical hydrodynamics at in situ conditions will be favorable for the economically viable recovery of metal cations in crusts.*

The primary issue in testing the above hypothesis is to select a suitable lixiviant (recycling leach solution). Figure 3.1 shows the Eh - pH diagram at 25°C and ion unit activity for Cu, Ni, Co, Fe, and Mn (Fuerstenau and Han, 1977). Only the stable dissolved species regions for each metal are shown. To be successful, the potential *in situ* leach system must solubilize crust metals rapidly and have Eh - pH characteristics corresponding to area "C" in Figure 3.1 for maximum extraction of crust material. This differs from the criteria of most of the hydrometallurgical leach studies in the literature (Mero, 1962; Han, 1972; Kane and Cardwell, 1975; Lee, 1979; Khalafalla and Pahlman, 1981; Schein, 1986) which have been concerned with the selective recovery of the minor elements, such as Ni, Cu, and Co from ferromanganese nodules and crusts (Eh - pH characteristics corresponding to areas "A" and "B" in Figure 3.1). Selective extraction of just the high value elements ($\leq 2\%$ of the crust weight) makes very good economic sense if the crust ore material is comminuted and delivered to a land-based processing plant. However, in crust mining by the *in situ* solution-extraction system, it is expected that the more costly metal processing would be offset by the advantages of simpler technology, and less energy requirements in ore recovery.

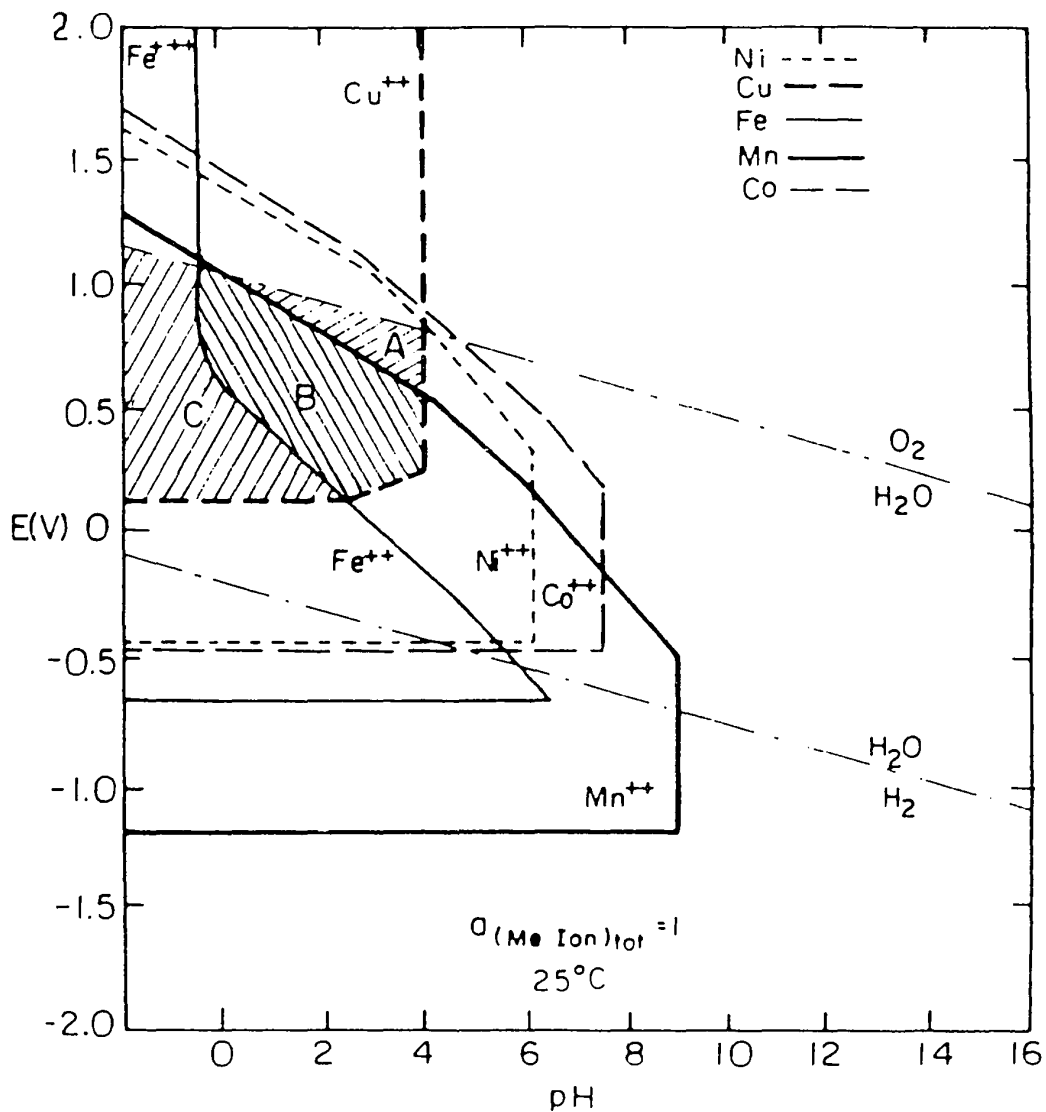


Figure 3.1 Eh - pH Diagram for the Fe - H₂O, Mn - H₂O, Cu - H₂O, Ni - H₂O, and Co - H₂O Systems at 25 °C. Only the stable dissolved ionic species for each metal at unit activity are shown (A = soluble Co, Cu, and Ni region; B = soluble Co, Cu, Mn, and Ni region; C = soluble Co, Cu, Fe, Mn, and Ni region). After Fuerstenau and Han, 1977.

3.1 Lixiviant Selection

The most promising lixiviant candidate for the *in situ* leaching of ferromanganese crust is a sulphurous/dithionate solution formed by dissolving SO_2 in sea water. The reductive dissolution mechanism of transition metal-oxides by $\text{SO}_{2(aq)}$ is much more effective than the reaction of transition metal-oxides with strong mineral acids. Figure 3.2 (Khalafalla and Pahlman, 1981) compares the solubilization of 20 gm of ferromanganese nodule material with 0.23 moles of $\text{SO}_{2(aq)}$ with pH adjusted by addition of HCl to the results of a HCl leach. The HCl leach results show the effect of hydrogen ions on the solubilization of the ferromanganese nodule metals, except for copper, where the chloride ion may also aid solubilization by forming chloro-complexes. It is clear from the data in Figure 3.2 that the leaching agent is the dissolved $\text{SO}_{2(aq)}$ and not the hydrogen ions in the $\text{SO}_{2(aq)}$ leach. The effectiveness of the reductive dissolution reaction at ambient (25°C) conditions makes it a prime candidate for potential *in situ* extraction of ferromanganese crust material.

Besides aqueous SO_2 , other generally strong reductants may be adaptable to leach ferromanganese crust at *in situ* conditions. These include hydrazine hydrate ($\text{N}_2\text{H}_4\cdot\text{H}_2\text{O}$) reported by Warren and Devuyst (1972) to extract 90% of Mn from pyrolusite particles within one hour, pyrophosphate ($\text{H}_2\text{P}_2\text{O}_7$) with hydrazine hydrate, used to reduce electrolytic MnO_2 (Malti et al., 1981), hydroxylamine hydrochloride ($(\text{NH}_2\text{OH})\text{Cl}$) with SO_2 , reported to have more rapid reaction rates than aqueous SO_2 alone (Han and Fuerstenau, 1980), potassium iodide (KI) with acetic acid, reported to be the most effective reductant for pyrolusite in domestic manganese ores (Usatenko and Ryl'kova, 1983), and nitrous acid

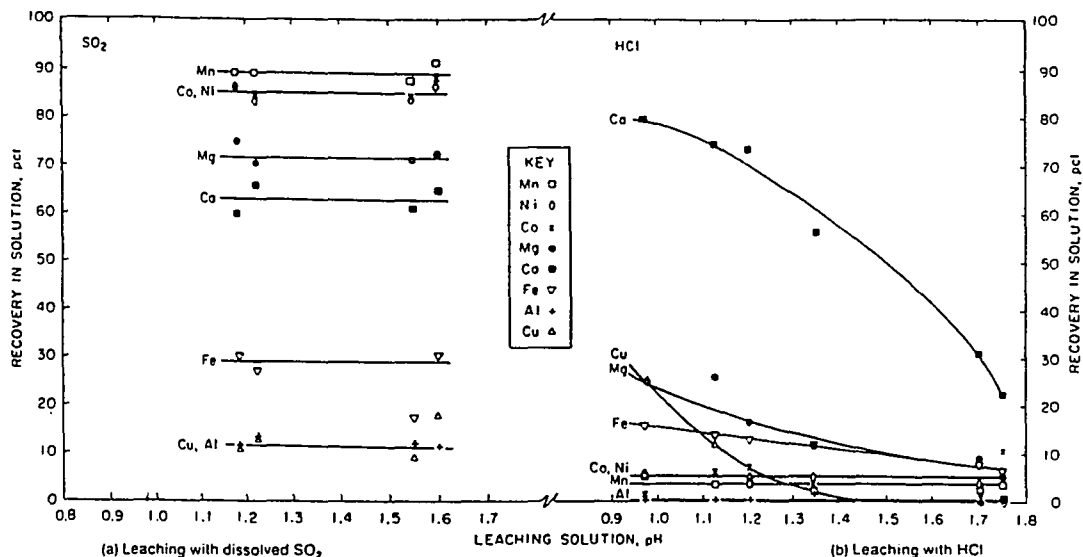


Figure 3.2 *The Effect of Solution pH on the Recovery of Metals During a 10 minute Leach of 20 gm of Ground (-100 mesh) Ferromanganese Nodule Material at 25 °C, one atm; (a) Leaching with SO₂(aq) (0.23 mole) with pH Adjusted by HCl; (b) Leaching with HCl. After Khalafalla and Pahlman (1981).*

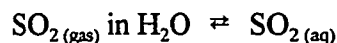
(HNO₂) solutions, reported to have slightly higher overall leach rates than aqueous SO₂ (Dresler, 1984). Most recently, hydrogen peroxide (H₂O₂) with sulfuric acid has been reported to have the least amount of noxious byproducts, and a Fe recovery of just 28% (Allen et al., 1991).

The sulfurous acid leach system, (i.e., aqueous SO₂ solution with pH adjusted by hydrochloric acid), was selected as the lixiviant candidate for this research over the other potential leach methods. This selection was based on four criteria: (1) a rapid reaction rate at low temperature; (2) nonselective reaction characteristics, for the maximum extraction of crust material; (3) relatively low potential for environmental damage; and (4) good economics, i.e., low lixiviant production cost. In comparing the seven leach systems, the

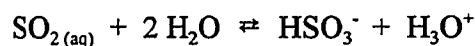
sulfurous acid leach was judged best overall, with individual criteria rankings of: third best in reaction rate, second best in nonselective characteristics, second best for environment, and best for economics.

3.2 The Sulfurous Acid System

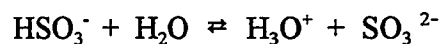
Dissolved $\text{SO}_{2(\text{gas})}$ solutions, which possess acidic properties, have long been called solutions of sulfurous acid (H_2SO_3). However, Raman studies of concentrated aqueous SO_2 solutions have shown that the H_2SO_3 molecule is not present (Cotton and Wilkinson, 1980). Instead, unchanged SO_2 (aqueous) molecules and two series of salts, the *hydrogen sulfites* (HSO_3^-) and *sulfites* (SO_3^{2-}) are present in the sulfurous acid system. The equilibria equations are represented as:



where $P_{\text{SO}_2} \approx 0.09$ at one atm and 25°C .



where $K_1 = [\text{HSO}_3^-][\text{H}^+] / ([\text{SO}_{2(\text{aq})}] - [\text{HSO}_3^-]) = 1.7 \times 10^{-2}$, and



where $K_2 = [\text{SO}_3^{2-}][\text{H}^+] / ([\text{HSO}_3^-] - [\text{SO}_3^{2-}]) = 6.4 \times 10^{-8}$.

A distribution diagram is given in Figure 3.3 for the sulfurous acid system showing the predominant species present at pH's ranging from 0 to 14. Above pH 10 the solution is predominantly SO_3^{2-} and below pH 0.0 the SO_2 in solution is 99% dissolved SO_2 .

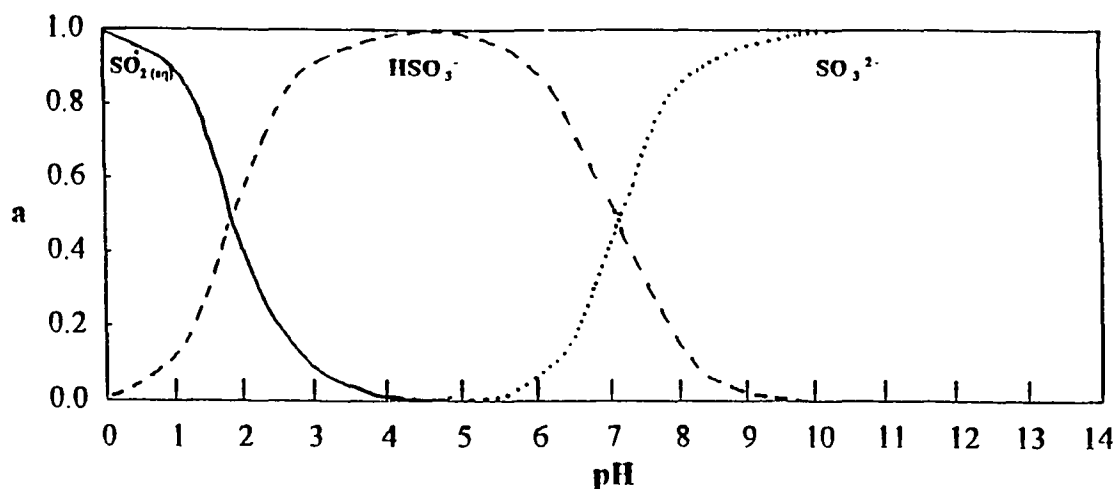


Figure 3.3 *Distribution of the Sulfurous Acid System with pH, at 1 bar and 25 °C. $\text{SO}_{2(\text{aq})} = [—]$, $\text{HSO}_3^- = [- -]$, $\text{SO}_3^{2-} = [\dots]$. Curves were Generated using $K_1 = 1.7 \times 10^{-2}$, $K_2 = 6.4 \times 10^{-8}$, $a_{\text{SO}_3} = K_1 \cdot K_2 \cdot a_{\text{SO}_2(\text{aq})} / [\text{H}^+]^2$, $a_{\text{HSO}_3} = K_1 \cdot a_{\text{SO}_2(\text{aq})} / [\text{H}^+]$, and $a_{\text{SO}_2(\text{aq})} = [\text{H}^+]^2 / ([\text{H}^+]^2 + K_1 \cdot [\text{H}^+] + K_1 \cdot K_2)$. Modified after Schein (1986).*

3.3 Review of Chemical Bonding

In mineral leaching, bond breaking of the chemical bonds between constituent atoms (ions) occurs at the solid-liquid (lixiviant) interface. One way to compare structure and reactivity between minerals and solution complexes is to review how minerals and complexes are bonded (Zoltai and Stout, 1984).

Four principle chemical bond types are found in minerals: ionic, covalent, metallic, and van der Waals'. Ionic bonding is the electrostatic attraction of oppositely charged ions at an internuclear distance where the attractive forces are balanced by the coulomb repulsive forces of the valence electron clouds. Ionic bonding occurs between cations and anions that result in filled outermost electron shells and leads to mineral lattices with highly symmetric close packing structures. The mineral lattice can be described by its *coordination number*,

i.e., the number of anions in the polyhedron in “coordination” with the given cation, and *radius ratio* (r_+/r_-), i.e., the ionic radii of the cation and anion which expresses relative size of the complex (Hurlbut and Klein, 1977). Generally, ionic bonding is important in minerals with coordination numbers of six or eight (Zoltai and Stout, 1984).

Covalent bonding occurs when one or both of the atoms of the bound pair contribute(s) one (or more) electron(s) to form a shared electron pair (*s*, *p* or *d*) in a hybridized *bonding molecular orbital* (Drago, 1977). The tendency for an atom (ion) to form a covalent bond is related to its electron configuration. Spatial symmetry and bond energy of the covalent bond is related to the atomic octahedral symmetry and geometry of the atom’s orbital energy levels. Covalent bonds are the strongest of the chemical bonds, with highly directional electrical forces localized close to the shared electrons. The strongest electron densities in covalent bonding occur in direct lines or planes between the cation and anion, and leads to mineral lattice structures lower in symmetry and coordination number than that of ionic bonding (Hurlbut and Klein, 1977).

Metallic bonding is the type of chemical bond characteristic of the metallic elements with low ionization energies (e.g., Na, K, Fe) exhibited when amassed in bulk form. The metallic bond properties of a metallic element are very different from those of its salts. X-ray diffraction analysis reveals that bulk metal samples have the regular repeating diffraction patterns of crystalline solids. In effect, the whole piece of metal *is* the molecule (Drago, 1977). The structural units of true metals in bulk samples are really the atomic nuclei bound with their outer orbital energy levels so closely spaced (gapped or overlapped) as to form for all practical purposes, an electron energy continuum *band*. The continuum *band* allows

extensive delocalization of the valence electrons (i.e., conductance) in the electron cloud surrounding the nuclei and electrons are free to drift throughout the structure without disrupting the bonding mechanism. Among minerals, only the native metals display pure metallic bonding (Hurlbut and Klein, 1977).

Van der Waals' bonding (also known as *London dispersion interaction*) is a residual electrostatic attractive force between two atoms or nonpolar molecules. It is one of the weakest of the chemical bonds and is not often encountered in minerals. The bonding force arises when a fluctuating dipole moment in one molecule induces a dipole moment in the other, and the two dipole moments then interact. When van der Waals' bonding is found in minerals, it generally defines a zone of ready cleavage and low hardness. An example is the mineral graphite, which consists of covalent bonded sheets of carbon atoms linked into a weak cohesive structure by van der Waals' bonds (Hurlbut and Klein, 1977).

The most important type of chemical bonding in many minerals is ionic bonding. However, the presence of only one bond type is rare and some degree of covalent bonding coexists in the lattice of most minerals (Hurlbut and Klein, 1977; Zoltai and Stout 1984; Jolly, 1984). The familiar *Lewis octet theory* and *valence-shell electron pair repulsion (VSEPR)* theories were early models to predict the nature of the bonding and structure of compounds with covalent bonding (Jolly, 1984; Cotton et al., 1987). Although these early theories were usually adequate for predicting the nature of non-transition-element compounds (e.g., mostly group III element combinations with expanded octets), they cannot explain observed molecular spectral properties and many aspects of transition-metal bonding and structure.

In solution, the structure and reactivity of manganese and other first-row transition metals are dominated by covalent bonding and the arrangements of valence electrons in their unfilled $3d$ shells (Petrie, 1991). When four to seven electrons are in the $3d$ shell, the electrons will be either highly-paired or unpaired. Due to low ionization potentials, these metals usually exist as $2+$ or higher oxidation state cations and tend to fill the $3d$ inner coordination shell. Metals fill their “inner shell” by bonding with ligands that can donate one electron to a covalent bond or two electrons to a *coordinate covalent bond*. Experimental evidence has shown that manganese in solution is most stable as the Mn^{2+} ion, which has five unpaired $3d$ electrons (high spin) and forms coordinate covalent bonds with six ligand sites in octahedral symmetry (Cotton and Wilkinson, 1980). In the mineral lattice, the spatial symmetry for vernadite (δ - MnO_2) has been determined by crystallography work to be randomly ordered layers of octahedral bonding ($Mn^{IV}O_6$). Vernadite samples yield diffuse X-ray diffractions of $2.40\text{-}\text{\AA}$ to $2.45\text{-}\text{\AA}$ and $1.40\text{-}\text{\AA}$ to $1.42\text{-}\text{\AA}$ and do not give good basal X-ray reflections (Burns and Burns, 1977). By carefully inclining fibrous leaflets of vernadite with respect to the electron beam, weak basal reflections with d spacing equal to $2.18\text{-}\text{\AA}$ to $2.20\text{-}\text{\AA}$ can be obtained, corresponding to a two-layer hexagonal crystal cell packing with filled octahedra sites (Haynes et al., 1985). The poor crystallinity, high specific surface area, and disordered random structure of the lattice in this mineral phase is suggested to be the result of the pervasive isostructural intergrowth of amorphous $FeOOH \cdot xH_2O$, and many vacant octahedral sites. The substitution of low-spin Co^{3+} (ionic radius $0.53\text{-}\text{\AA}$) for Mn^{4+} (ionic radius $0.54\text{-}\text{\AA}$) in the ($Mn^{IV}O_6$) octahedra of vernadite has been confirmed by photoelectron spectroscopy (Murray and Dillard, 1979). Calculation of the ionic radii ratios (r_{+}/r_{-}) for Mn^{4+}

with O^{2-} confirms the tendency for octahedral symmetry with a (r_+/r_-) ratio of 0.386 that is just below the minimum 0.414 (r_+/r_-) ratio for octahedral close packing structure (Zoltai and Stout, 1984). Although ionic bonding predominates in the lattice bonding of vernadite, at mineral-solution interfaces, exposed octahedral bonding positions about Mn centers should behave like those of solution-phase Mn coordinate covalent complexes. Therefore, models that predict chemical reactivity of solution-phase complexes can be applied to gain insight to mineral leaching reactions.

3.4 Ligand Field Theory

A covalent bonding model called the *ligand field theory* was developed specifically for the transition metals (Cotton and Wilkinson, 1980) and can be used to estimate the activation energies for substitution leaching reactions. This model focuses on what happens to the electrons only in the higher energy, essentially nonbonding and antibonding *d* orbitals. Predictions are made based on considering the repulsions that exist between the interacting ligand's electron density and the *d* electrons of the metal ion. Ligand field theory starts with the *crystal field theory model*, by considering a transition metal atom (ion) in a complex as if it were subject to purely electrostatic perturbation by its ligands. The ligands are considered simply as point charges or point dipoles. Ligand field theory modifies the crystal field theory model with the key idea (empirically dictated) that patterns of the energy levels of the *d* orbitals are split and shifted based on the spatial symmetry of the interacting ligands. The effects of both the "octahedral" ligand complex (six negative point charges at the octahedral positions) and the "tetragonal" ligand complex (four charges at the tetragonal positions) on a metal atom (ion) are shown in Figure 3.4. As depicted in Figure 3.4, the

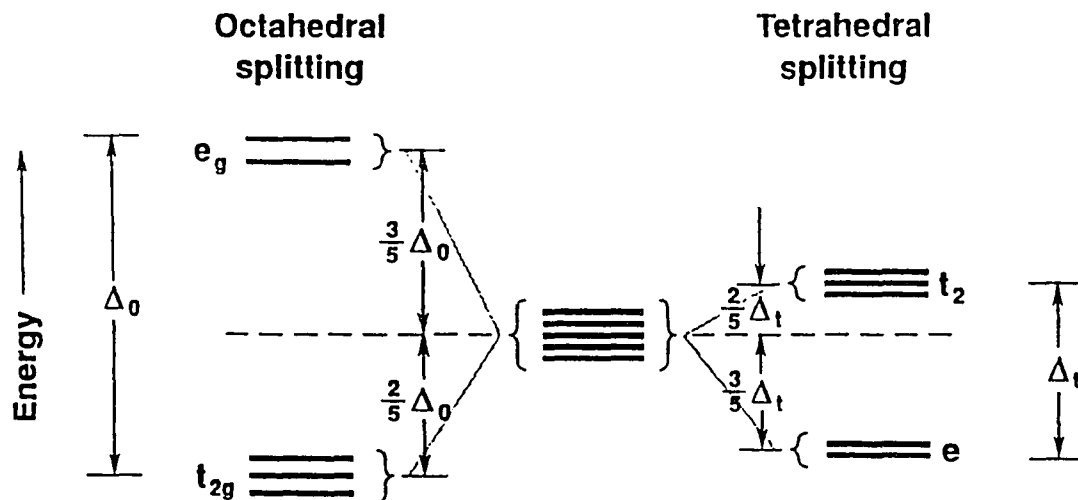


Figure 3.4 Energy Level Diagram Showing the Splitting of a Set of Metal Atom (ion) d Orbitals by Octahedral and Tetrahedral Electrostatic Ligand Fields. After Cotton and Wilkinson, 1980.

energy levels of the five d orbitals of the metal atom (ion) are initially assumed to be approximately equal, i.e., degenerate. However, as the ligand charges are brought closer to the metal atom (ion), the octahedral complex induces the $3d$ orbital energies to split producing three orbitals with lower energies (t_{2g}) and two with higher energies (e_g). The tetrahedral complex induces the $3d$ orbital energies to shift, splitting into a reverse set of three orbitals with higher energies (t_2) and two orbitals with lower energies (e). The magnitudes (Δ_o and Δ_t) of the ligand field energy splitting for actual complexes vary with metal and ligand. *Ligand field theory* has proved helpful in predicting the reactivities of the first-row transition metals (e.g., Mn, Fe, Co, Ni, and Cu) and has explained much of the experimentally observed structural, magnetic and spectroscopic properties of the transition metal-ligand complexes. However, *ligand field theory* is an incomplete model of metal-ligand bonding since it only considers the d orbitals of the metal (Petrie, 1991).

3.5 Frontier Molecular Orbital Theory

Frontier molecular orbital theory was developed to explain chemical bonding and other properties of covalent complexes while accounting for all possible molecular orbital interactions. The basic premise of *frontier molecular orbital theory* is that bonding between the atoms occurs when their atomic orbitals overlap to form molecular orbitals of concentrated electron density between their nuclei. Atomic orbital interactions are classified into three categories: (1) bonding, leading to lower energy and stabilization; (2) antibonding, leading to higher energy and destabilization; and (3) nonbonding with no significant change in energy levels (Cotton et al., 1987). Since the electrons in a molecular orbital are no longer associated with the parent atoms but with the molecule as a whole, bonding and antibonding molecular orbitals reflect spatial symmetries dependant upon types of atomic orbitals involved in the overlap. Molecular orbitals with cylindrical symmetry about the bond axis are classified as *sigma* (σ) orbitals. Molecular orbitals that have a node (i.e., wave function of zero) and do not have cylindrical symmetry along the bond axis are classified as *pi* (π) orbitals.

To construct a molecular orbital theory energy diagram for an octahedral transition metal-ligand complex, one may use the *linear combination of atomic orbitals* method as summarized by Cotton and Wilkinson (1980). "First consider the nine valence shell orbitals of the metal ion. Six of these -- d_{z^2} , $d_{x^2-y^2}$, s , p_x , p_y , and p_z -- have lobes lying along metal-ligand bond direction (i.e., are suitable for σ bonding). Three -- d_{xy} , d_{yz} , and d_{zx} -- are so oriented as to be suitable only for π bonding. Each of the metal orbitals must then be combined with its matching symmetry orbital of the ligand system to give a bonding and an antibonding molecular orbital. If the ligands also possess π orbitals, these must be combined

into symmetry orbitals constructed to overlap effectively with the metal ion π orbitals, and the bonding and antibonding molecular orbitals then formed by overlap.” Figure 3.5 depicts a representative example of a molecular orbital theory energy diagram for an octahedral transition-metal--ligand complex in which the ligands provide only σ bonding. Note, in Figure 3.5: The symbol A_{1g} represents a single orbital that has the full symmetry of for spatial orientation; the symbol T_{1u} represents a set of three orbitals that are equivalent except for spatial orientation; the subscripts g and u show whether the orbital(s) is centrosymmetric (g from the German *gerade* meaning even) or anticosymmetric (u from the German *ungerade* meaning uneven); and the asterisk “*” denotes the antibonding orbitals (Cotton and Wilkinson, 1980).

Frontier molecular orbital theory can be applied in identifying the favorable bonding conditions for mineral surface reactions (Petrie, 1991). Therefore, frontier molecular orbital theory can also be applied to identify the SO_2 reaction mechanism in the reduction of Mn^{4+} metal centers in the ferromanganese crust leach process. When two molecules meet, covalent bonding or electron transfer occurs when electron density flows from the *highest occupied molecular orbital* (HOMO) of a donor (Lewis base) molecule to the *lowest unoccupied molecular orbital* (LUMO) of an acceptor (Lewis acid) molecule. This occurs if the following conditions are met: (1) The Molecular or atomic orbitals have similar spatial symmetry for positive orbital overlap, and (2) the energy of the HOMO for the donor molecule is greater than but similar to the energy of the LUMO for the acceptor, with best results when the energy of the LUMO is within 6 eV/molecule (i.e., 579 $\text{kJ}\cdot\text{mole}^{-1}$) of the energy of the HOMO (Luther, 1987; 1990). Figure 3.6 is a qualitative molecular orbital

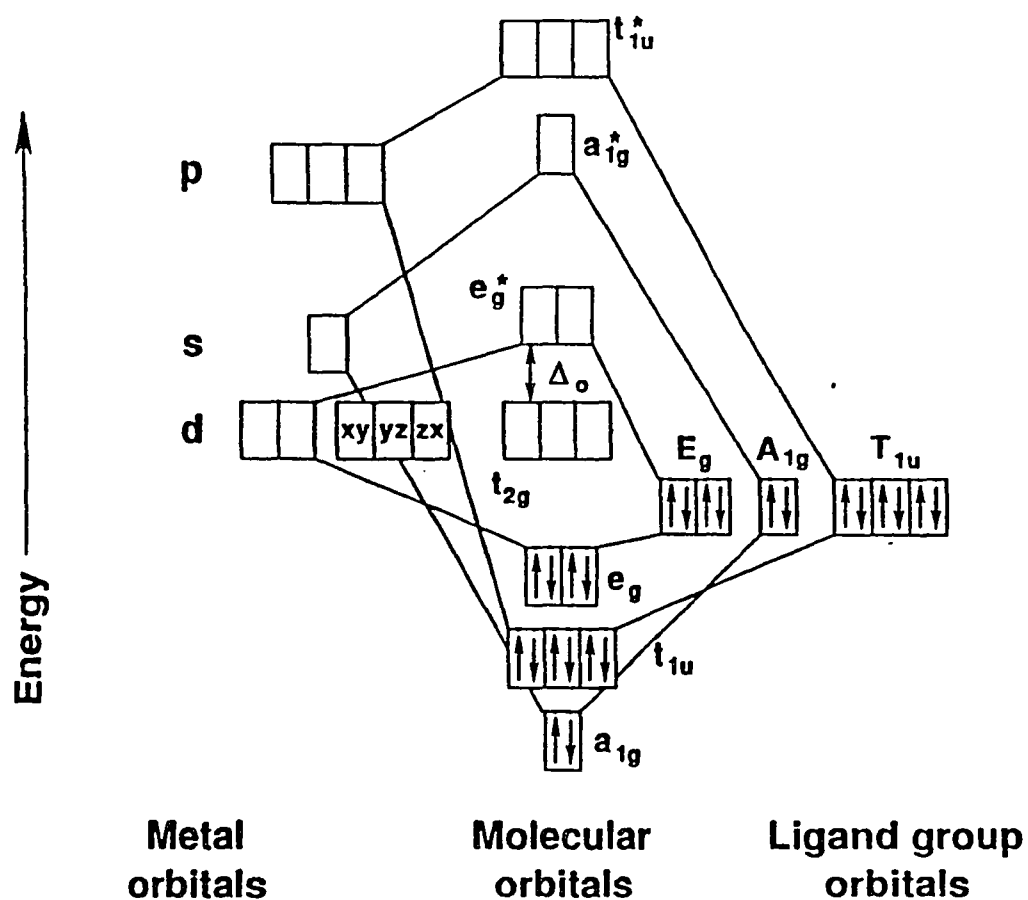


Figure 3.5 *Molecular Orbital Theory Energy Diagram for σ Bonding in an Octahedral Transition-Metal-Ligand complex (ML_6) which has No Ligand π Bonding. Adapted from Cotton and Wilkinson, 1980.*

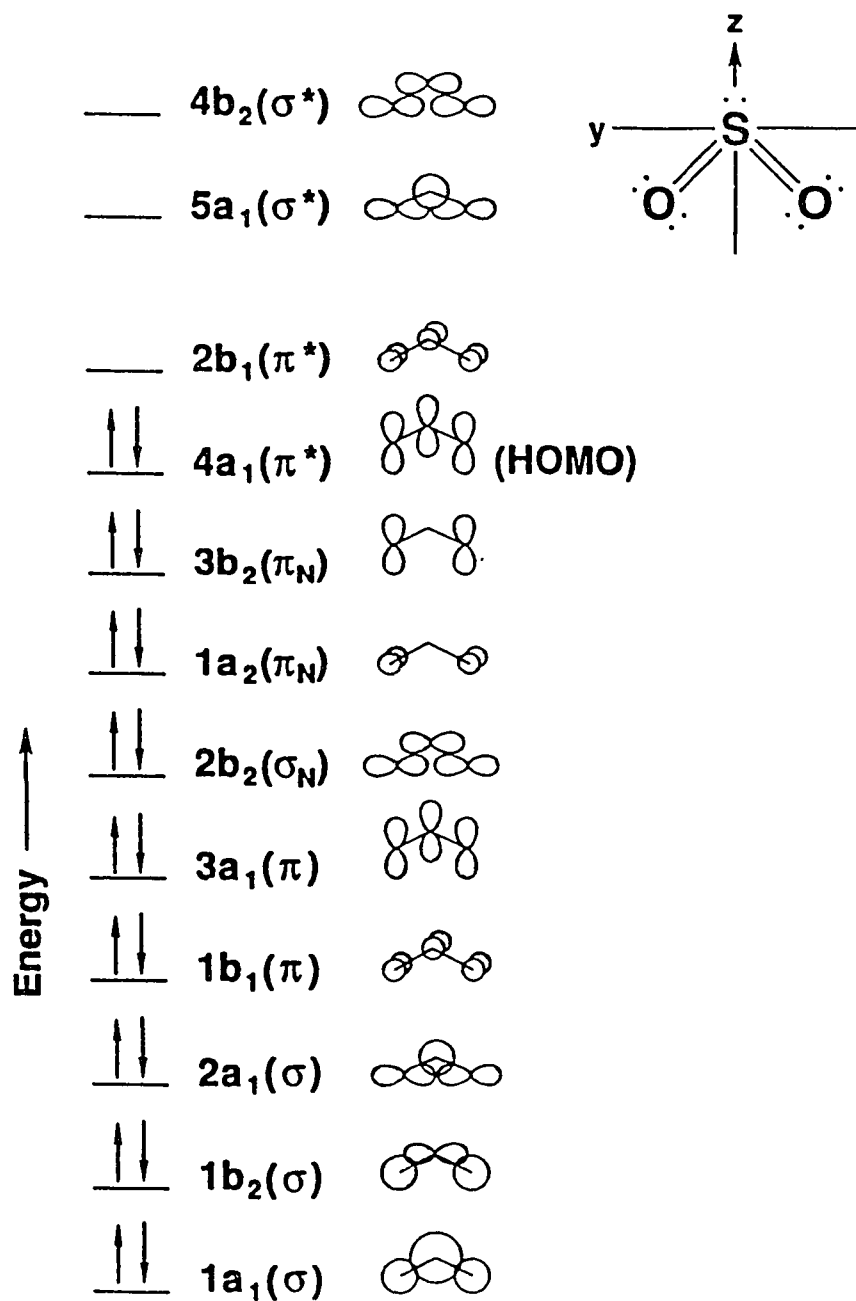


Figure 3.6 *Qualitative Molecular Orbital Theory Energy Diagram for SO₂. The x-axis is Perpendicular to the Page. "*" Denotes Antibonding and "N" Denotes Non-Bonding Orbitals. Adapted from Gimarc, 1979.*

theory energy diagram for SO_2 (Gimarc, 1979). The SO_2 molecule has bent planar symmetry with a 119.5 degree angle between the two O-S bonding axis and has stable π bonding between S and each O atom (Purser, 1989). Since sulfur and oxygen both have six electrons in their highest unfilled energy shell, 18 valence electrons are available for placement into the 12 molecular orbitals formed by one S atom and two O atoms (Petrie, 1991). This means that the HOMO for SO_2 is the antibonding π -orbital $4a_1$ as shown in Figure 3.6.

Figure 3.7 depicts the *molecular orbital diagram* showing the reduction of MnO_2 by SO_2 . The *molecular orbital diagram* shows that the first condition for electron density flow from the HOMO of SO_2 to the LUMO of MnO_2 is met. As shown in Figure 3.7, SO_2 has an ideal overlap symmetry for bonding and subsequent reduction of Mn^{4+} centers. The HOMO component of SO_2 that originates from the S atom can overlap the vacant $3d_{z^2}$ orbital of Mn^{4+} , forming a σ bond along the z-axis. The second condition, that of proper energy level for electron density flow from the HOMO of SO_2 to the LUMO of MnO_2 is also met. According to Luther (1990) the estimated energy for the HOMO of an atom or molecule is the ionization potential (IP), which for SO_2 is -12.34 eV. Also, the estimated energy of the LUMO of an atom or molecule is the electron affinity (EA), which for Mn^{4+} is -51.2 eV (values of IP and EA derived from CRC Handbook, 1980). Therefore, both orbital overlap symmetry and relative energies of the HOMO and LUMO are favorable for z-axis σ -bonding between SO_2 and Mn^{4+} . This is a π to σ type of electron transfer that requires an inner-sphere mechanism. This inner-sphere attack is necessary because the Mn in MnO_2 is a d^3 type ion with high spin ground state; that is, generally inert and not susceptible to ligand lability, even under acidic conditions (Luther, 1990). However, the correct symmetry and favorable energy

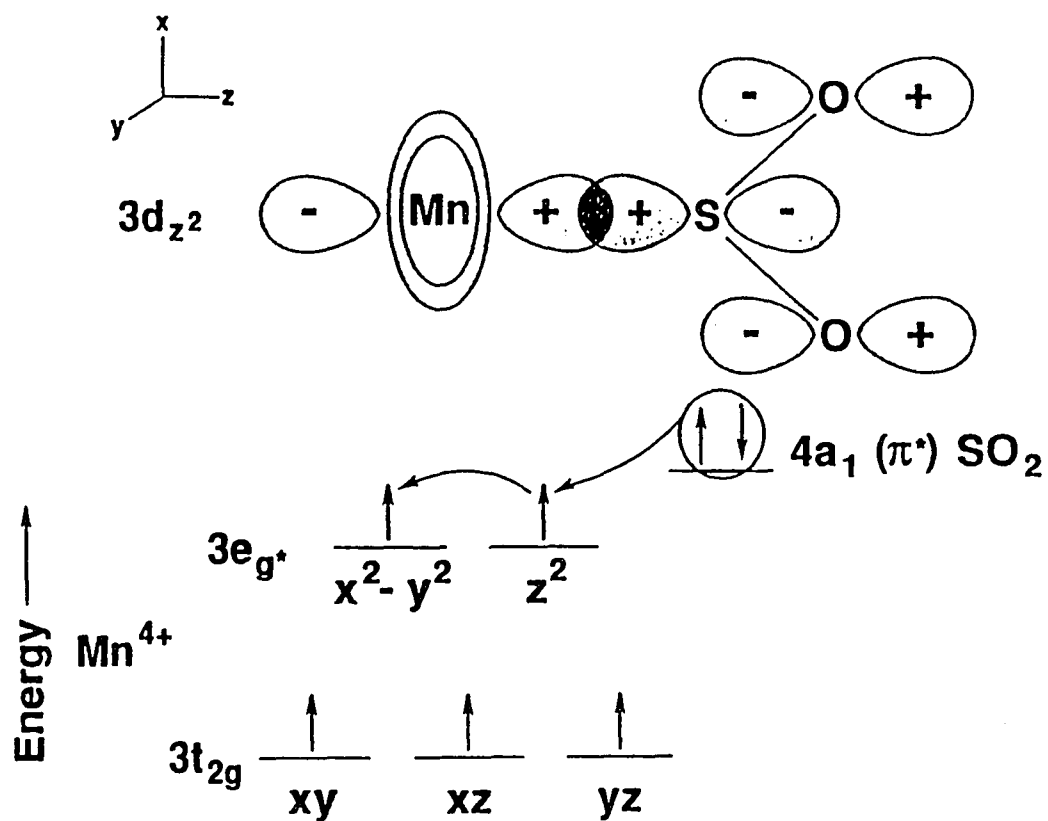


Figure 3.7 *Molecular Orbital Diagram Demonstrating the Two-Electron Reduction of Mn^{4+} by SO_2 . Electron Transfer Occurs from SO_2 $4a_1$ Orbital to Each of the Degenerate $3e_g$ Orbitals on Mn^{4+} . After Petrie (1991).*

comparison between the HOMO of SO_2 to the LUMO of Mn^{4+} permit labile formation of a σ -bond with Mn^{4+} before electron transfer (Petrie, 1991).

3.6 Proposed Mechanism of Reductive Dissolution by SO_2

The *surface coordination model* developed largely by Stumm and Morgan (1981), is based on the principle that a mineral dissolution is regulated by the formation of specific coordination complexes at the mineral surface. This model was extended to include reductive dissolutions (Stone and Morgan, 1984; 1987) and can be used to explain the mechanism of the leaching of ferromanganese crust minerals.

The detachment of a metal species from metal-oxide minerals by ligand-promoted dissolution occurs when adsorption-altered surface metal atoms have enough weakened metal-oxygen bonds to permit release into the solution. A three-step reaction mechanism for these dissolution reactions was proposed by Furrer and Stumm (1986). First, rapid adsorption of solution ligands as strong surface coordination complexes (M-ligand) occurs which weaken the M-O bonds. Second, the (M-ligand) complex breaks the M-O bonds and detaches to form a soluble complex. Third, the complex detaches and fast protonation occurs to neutralize the excess negative surface charge left behind by the departing complex. For reductive dissolutions, between the first and second steps, an intermediate inner-sphere electron transfer step reduces the transition-metal centers of the surface exposed octahedrals. This results in greater lability of the reduced metal-oxygen bond in comparison to the nonreduced metal-oxygen bond, and greater solubility, i.e., easier detachments of the reduced metal atoms (ions) from the lattice surface (Stumm and Wieland, 1990). The overall reductive dissolution mechanism for Mn^{4+} oxides by SO_2 is summarized in Figure 3.8.

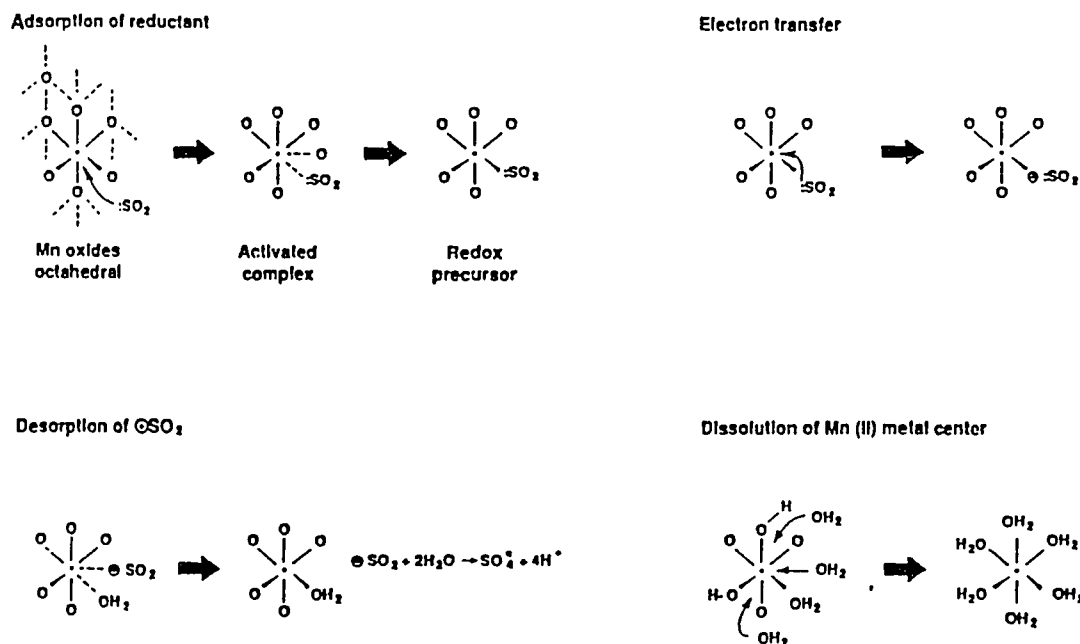


Figure 3.8 Reductive Dissolution Mechanism of Mn Oxide by SO_2 (aq) (after Petrie, 1991).

3.7 Thermodynamic Evaluation of SO_2 Reactivity

A thermodynamic evaluation can be made by comparing the *Gibbs standard free energy* (ΔG°) of the most probable chemical reactions that describe the SO_2 (aq) lixiviant dissolution of ferromanganese crust minerals. Table 3.1 shows the ΔG° results of probable overall leach reactions calculated from data in the *Handbook of Chemistry and Physics*, table of *Chemical Thermodynamic Properties* (CRC, 1980). Most of the leaching reactions shown in Table 3.1 have negative ΔG° values and are favored to occur under experimental conditions. Quartz, as expected, is not favored to leach. The thermodynamic data in Table 3.1 are listed in order of expected decrease in extraction efficiency. According to free energies for overall reaction equations, manganese minerals are strongly favored whereas iron minerals (geothite) are only slightly favored for leaching in acidic lixiviant. However, ΔG°

Table 3.1 *Thermodynamic Evaluation of Mineral Leaching in Ferromanganese Crust (at standard conditions: 25 °C and one atm).*

Mineral	Probable Overall Leaching Reaction(s)	ΔG° (kJ/mole)
vernadite	$\text{MnO}_2 + \text{SO}_2 \rightleftharpoons \text{Mn}^{2+} + \text{SO}_4^{2-}$	-209
“	$\text{MnO}_2 + 2\text{SO}_2 \rightleftharpoons \text{Mn}^{2+} + \text{S}_2\text{O}_6^{2-}$	-131
calcite	$\text{CaCO}_3 + 2\text{H}^+ \rightleftharpoons \text{Ca}^{2+} + \text{H}_2\text{O} + \text{CO}_2$	-47
goethite	$\text{FeO}(\text{OH}) + 3\text{H}^+ \rightleftharpoons \text{Fe}^{3+} + 2\text{H}_2\text{O}$	-2
quartz	$\text{SiO}_2 + 2\text{H}_2\text{O} \rightleftharpoons \text{H}_2\text{SiO}_4(\text{amorphous})$	+23

values should only be viewed as a relative tendency, i.e., whether the reactions are favored or not. The actual reaction rates depend upon the kinetics of the system.

3.8 Kinetic Evaluation of SO_2 Reactivity

Chemical kinetics is the study of the rate and sequence of reaction steps for a chemical reaction. Evidence suggests that many geochemical processes, including mineral dissolutions, may not be at equilibrium or steady-state as represented by their overall stoichiometric equations. This is because the residence times are not long enough in many reaction systems for the process mechanisms to achieve equilibrium (Petrie, 1991). However, equilibrium or steady state can often be viewed as a limiting case. This occurs when the important reactions are rapid enough in the geochemical process to result in virtually constant solution concentrations of reaction products. Kinetic evaluation of a reaction requires more intimate knowledge of the reaction and much more experimental data than that required for a

thermodynamic evaluation (Wilkinson, 1980). The overall rate of a chemical reaction is determined in large part by the rate-limiting reaction step in the sequence and summarized in an experimentally derived *rate equation*.

Herring and Ravitz (1965) reported the first actual reaction rate data for SO_2 - MnO_2 reactions. They mounted electrolytic MnO_2 in Lucite creating a flat plane of reactive mineral sites, and found that the rates of manganese dioxide reductive dissolutions were faster at lower pH values, e.g., $7.6 \mu\text{-mole}\cdot\text{min}^{-1}\cdot\text{cm}^{-2}$ at pH 1.82 versus $80.4 \mu\text{-mole}\cdot\text{min}^{-1}\cdot\text{cm}^{-2}$ at pH 1.09. These results showed that Mn dissolution is an order of magnitude faster for $\text{SO}_{2(aq)}$ leach solutions than for solutions where HSO_3^- is the dominant species. The reaction rates were also faster with increasing stirring rates, suggesting a transport-controlled reaction, with an apparent activation energy of $4.5 \pm 0.2 \text{ kcal}\cdot\text{mole}^{-1}$.

Miller and Wan (1983) also reported investigations on the reductive dissolution of MnO_2 . They used suspended electrolytic MnO_2 and pyrolusite mineral particles, sized through -25 and +48 mesh. In contrast to Herring and Ravitz, they calculated an apparent activation energy of $8.6 \text{ kcal}\cdot\text{mole}^{-1}$ and found no change in rate constants with changes in stirring rates. Miller and Wan concluded that the leach process was rate-limited by a mineral surface reduction reaction.

To resolve the controversy and clarify the mechanism; Asai, and others (1986) conducted a chemical engineering study of a SO_2 and H_2SO_4 leach in a packed bed of MnO_2 . They solved the experimental mass transfer coefficients for SO_2 in a packed bed and conclusively proved that the mineral surface reaction was not the rate-limiting step. They found that $\text{S}_2\text{O}_6^{2-}$ formation increased with increasing SO_2 concentration and increasing

lixiviant flow rates. In addition, they found that in the presence of high concentrations of SO_2 , MnSO_4 forms as the predominant reaction species.

3.9 Previous Research on the Dissolution of Selected Oxides with SO_2

Many investigations have been made using SO_2 as a reducing agent of selected oxides. Just the work concerning mining or mineral processing is presented here. Most of the research effort on processing ferromanganese (primarily nodules) focused on the selective recovery of the value metals.

Wyman and Ravotz (1947) reported the selective nature of SO_2 leaching for manganese over iron and other gangue minerals in domestic ores. Basset and Parker (1951) conducted anaerobic batch leaching experiments with SO_2 and various manganese salts. By measuring reaction products at the end of the experiment, Basset and Parker deduced that the oxidation of sulfurous acid must be occurring at the mineral surface and not in solution. Back and others (1952) conducted SO_2 processing of MnO_2 ores under aerobic conditions. They observed a decrease in $\text{S}_2\text{O}_6^{2-}$ formation with low pH and increased oxygenation. Work by Higginson and Marshall (1957) supports the conclusions of Basset and Parker (1951). They found by using different oxidants in solution, those 1-electron transfer oxidants (e.g., Fe^{3+} , Co^{3+}) produced $\text{S}_2\text{O}_6^{2-}$ formation whereas 2-electron transfer oxidants (e.g., IO_3^- , H_2O_2) produced SO_4^{2-} formation. Herring and Ravitz (1965) reported the first actual reaction rate data for anaerobic SO_2 - MnO_2 reactions, and found that the rate of manganese dioxide reductive dissolutions was faster at lower pH values. They also reported faster reaction rates with increasing stirring rates, suggesting a transport-controlled reaction. Miller and Wan (1983) also conducted work devoted to the kinetics of reductive dissolutions of MnO_2 , but

in contrast to Herring and Ravitz, reported a mineral surface reduction reaction rate-limiting step. Asai, and others (1986) conducted a study of diffusion-controlled transport of SO_2 and H_2SO_4 lixiviant in a packed bed of MnO_2 . Their results confirmed the results of Herring and Ravitz. Dixit and Raison (1987, 1988) showed that high concentrations of dissolved O_2 ($P_{\text{O}_2} \geq 11.15$ bar) in an autoclave at 35°C , will suppress the reductive dissolution of MnO_2 by SO_2 . They also reported that dissolution rates of MnO_2 fit an equation for diffusion-controlled release of Mn^{2+} through an unreacted product layer.

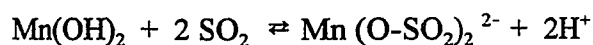
Low temperature sulfurous acid reduction methods of ferromanganese nodules were first suggested by Mero (1962) as a way to separate cobalt and other value metals from the iron phase. Han (1972) extracted less than 10% of the Fe while recovering more than 90% of the Mn, Ni, Co, and Cu after five hours of leaching with dilute 0.2% $\text{SO}_{2(\text{aq})}$ solution at pH 3 and 25°C . Similar results were obtained by Lee (1979). Kane and Cardwell (1974a, 1974b, 1975) have several patents related to low temperature sulfation, in which nodule material is treated with SO_2 without O_2 , washed with H_2O to separate the soluble Mn^{2+} , followed by an oxygenated SO_2 leach to recover the soluble sulfates of Cu, Ni, and Co from the remaining iron phase. These claims were met with considerable skepticism (Schein, 1986) as considerable research (Lee, et al., 1978; Lee, 1979; Schein, 1986) showed that soluble dithionates would exist in the leach solutions, seriously compromising selective leach extractions by the methods of Kane and Cardwell. Several researchers (Van Hecke and Bartlett, 1973; Faugeras et al., 1977) obtained selective recovery of metals by low temperature sulfation by adding SO_2 to a nodule slurry maintained at pH 2 - 4 with H_2SO_4 . As iron sulfate is only slightly soluble, this method significantly reduced Fe recovery.

Khalafalla and Pahlman (1981) conducted a series of SO₂ batch leaching experiments of ferromanganese nodules that showed the selective extraction of metals in a preferential leach order of: Mn > Ni > Co >> Fe, Al, Cu by increasing the molar ratio of SO₂ (i.e., concentration) in the lixiviant to the weight of the nodules being leached. As shown in Figure 3.9, Fe, Al, and Cu were leached only after most of the Mn, Ni, and Co had been leached. However, using an excess of SO₂ (> 7%) will result in nonselective sulfation. Khalafalla and Pahlman predicted that MnO₂ could not directly complex with SO₂ (contrary to what is now known) and proposed a dissolution reaction using a complexometric titration theory by the following reaction steps:

First the Mn⁴⁺ metal center in the MnO₂ lattice is reduced by SO₂ to Mn²⁺:



The formed manganese (II) hydroxide would then react with other SO₂ molecules that exchange with exposed protonated oxygens to yield a soluble disulfitomanganese(II) complex:



Schein (1986) confirmed the findings of Khalafalla and Pahlman (1981) and developed a method of forming sulfurous acid solutions by pH adjustment of sulfite salts. Schein also did the first low temperature SO_{2(aq)} leach experiments on ferromanganese crust and showed that crust has similar leaching behavior to nodules. Petrie (1991) proposed an intermediate inner-sphere electron transfer step mechanism for the dissolution reaction using frontier molecular orbital theory (depicted in Figure 3.7). Petrie also identified two separate leaching reactions for the reductive dissolution of manganese oxides that occur simultaneously:

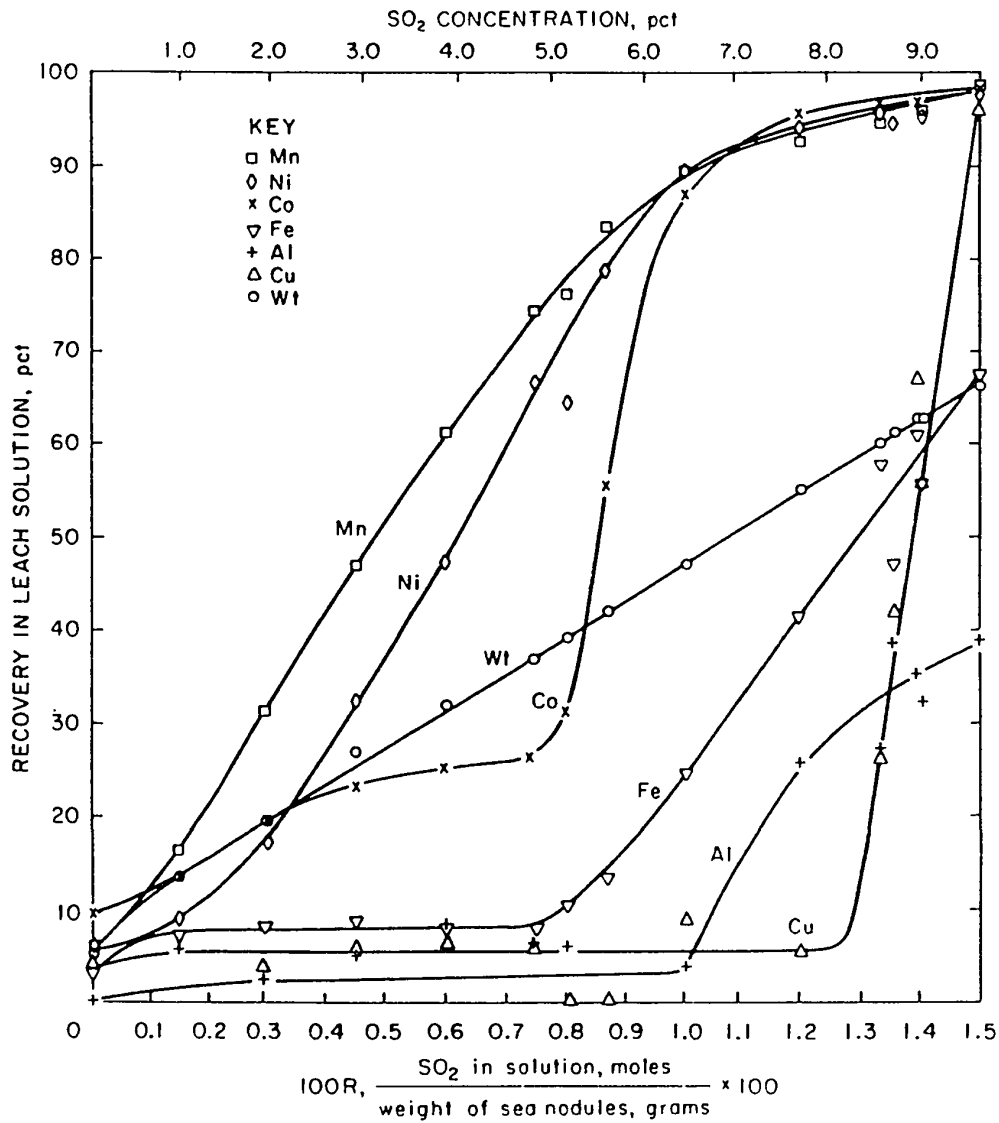
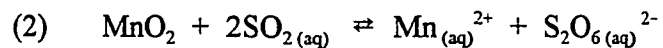
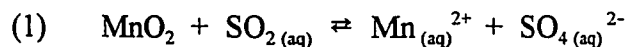


Figure 3.9 Leaching Curves (10 minutes) for Several Metal Values from 20 Grams of -200 Mesh Ferromanganese Nodule Particles in Water Containing Various Quantities of SO₂ (Wt = nodule weight % recovered). After Khalafalla and Pahlman (1981).



Reaction (1) which proceeds by the inner-sphere electron transfer mechanism, forms sulfate (SO_4^{2-}) and consumes one mole of SO_2 for every mole of Mn dissolved. Reaction (2) which parallels the complexometric titration mechanism of Khalafalla and Pahlman, forms dithionate ($\text{S}_2\text{O}_6^{2-}$) and consumes two moles of SO_2 for every mole of Mn dissolved. The thermodynamic evaluation of the two reactions (Table 3.1) suggests that reaction (1) may be favored. However, actual percentages of sulfate and dithionate produced during leach experiments depends on the manganese oxide mineral structure, pH and oxygen content of the solution (Petrie, 1991; Saini-Eidukat et al., 1992).

CHAPTER 4 RESEARCH GOALS AND METHODS

The leach method selected as the lixiviant candidate for this research (Section 3.1) is the sulfurous acid leach system. This research expands on the previous investigations of Khalafalla and Pahlman (1981; 1988) and Schein (1986). However, it differs significantly from previous work, in that for the first time, the nature of the sulfurous acid leach system as a hydrometallurgical processing method is investigated as an *in situ* solution extraction process for cobalt-rich ferromanganese crust. Using sea water as the working fluid for the lixiviant is another innovation. This is also the first investigation of sulfurous acid reactivity with ferromanganese at temperatures below 25°C, and hydrostatic pressure of up to 200 atm. Theoretical estimates of the effects of temperature and pressure at *in situ* conditions are presented in the following sections 4.1.1 and 4.1.2.

4.1 Experimental Research Goals

Specific goals are:

1. To do a baseline elemental analysis for the major transition metals in crust study medium produced for batch leach experiments.
2. To do batch experiments, leaching portions of crust study medium with sulfurous acid solutions, over the stated ranges of the following variables:

Pressure: 1 atm → 200 atm

Temperature: 0°C → 25°C

pH: 0.5 → 5.0

3. To analyze the leach filtrate (pregnant leach liquor) from the batch experiments to determine metal recovery as a function of temperature, pressure and concentration of leachate reactants.
4. To leach whole crust (~1 cm³ cubes) in semi-batch experiments to learn physicochemical nature of whole crust dissolutions.
5. To compare results of the batch leach experiments and whole crust semi-batch experiments, and determine whether leach reaction is limited by the reaction rate or by surface layer diffusion at the reactant surface

4.1.1 *Effect of Temperature*

The effect of temperature (T) on reaction rates is described by the empirical Arrhenius Equation, first postulated in 1889:

$$k = Ae^{-E_a/RT}$$

Where k is the rate constant, A is the temperature independent frequency factor or pre-exponential factor, E_a is the activation energy for reaction, and R is the gas constant. This logarithmic relation predicts a significant negative effect on reaction rates at the expected *in situ* temperature at ferromanganese crust locations. If the apparent activation energy, $E_a = 4.5 \pm 0.2 \text{ kcal} \cdot \text{mole}^{-1}$, reported from the SO_2 - MnO_2 reductive dissolution experiment of Herring and Ravitz (1965) is assumed, the change in the rate constant from $T = 25^\circ\text{C}$ to 4°C can be expressed as:

$$\log (k_{4^\circ\text{C}} / k_{25^\circ\text{C}}) = \log (e^{-E_a/ R(277^\circ\text{K}) + E_a/ R(298^\circ\text{K})}) = -0.25$$

This yields an estimated decrease in the reaction rate of 25%. If the higher activation energy,

$E_a = 8.6 \text{ kcal}\cdot\text{mole}^{-1}$, calculated by Miller and Wan (1983) is used, the estimated decrease in reaction rate is 48%. Although the $\text{SO}_2 - \text{MnO}_2$ reductive dissolution reaction is considered very “fast,” a decrease in the reaction rate of this amount could have significant impact on the commercial feasibility of crust mining by the *in situ* solution batch reactor system. However, the effect of temperature may be partially compensated by the effect of pressure.

4.1.2 *Effect of Pressure*

The effects of pressure (P) on reaction rates in solutions are related to the *volume of activation*, which is the difference between the molar volumes of the transition and reactant states. In addition, pressure effects on equilibria may change the forms and concentrations of the reactants (Brezonik, 1994). The effects of pressure on chemical equilibria were first described by Planck in 1887. He related the change in equilibrium constants with P to volume changes between products and reactants (*ibid.*):

$$\left(\frac{\partial \ln K}{\partial P}\right)_T = - \Delta V^\circ / RT$$

Where K is the equilibrium constant, ΔV° is the difference in partial molal volumes between products and reactants, and R is the gas constant.

From *Activated Complex Theory*, the argument can be reformed in terms of activated complex (Laidler, 1987) where k is the rate constant expressed by:

$$k = kT / h \cdot K_c^*$$

Where K_c^* is the equilibrium constant for formation of an activated complex, k is Boltzmann's constant, and h is Planck's constant (number of degrees of freedom). Also, the influence of pressure on the rate constant can be expressed by the van't Hoff equation, described in 1901:

$$\left(\frac{\partial \ln k}{\partial P}\right)_T = - \Delta^*V^\circ / RT$$

Where Δ^*V° in the equation is the overall change in the standard volume of activation. If the reactant state is larger than the transition state, i.e., when the volume of the activated complex AB^* is less than the volume of the reactants A and B ($\Delta^*V^\circ < 0$), the rate increases with increasing P . Experimentally derived plots of $\ln k$ versus P depart from linearity at high pressures (1000s of atm), which implies that the reactant and transition states usually have different molar compressibilities. Thus, Δ^*V° varies with P . However, at lower pressures, the slope of $\ln k$ versus P is essentially constant, and for the low (< 1000 atm) P case, the van't Hoff equation can be integrated to:

$$\ln(k_P / k_{1 \text{ atm}}) = - \Delta^*V^\circ (P - 1) / RT$$

This equation can be used to predict the importance of pressure effects on reactions at *in situ* conditions. Figure 4.1 shows the relationship between $k_P / k_{1 \text{ atm}}$ and the change in volume of activation, Δ^*V° , for average *in situ* crust conditions ($P = 200$ atm, $T = 4^\circ\text{C}$). Values of Δ^*V° are known for only a few geochemical reactions, but reported values generally are between -20 and $+20$ cm^3/mole (Brezonik, 1994). Conversion of reactants into a transition state causes a volume decrease for bimolecular processes. However, large volume decrease is usually indicative of “slow” reactions compared to transport-limited or “fast” reactions (Stumm and Morgan, 1981). Nevertheless, it is reasonable to consider the effect on reaction rates at $\Delta^*V^\circ = -20$ cm^3/mole , as a maximum estimate. From Figure 4.1, this maximum estimate is an increase in the rate constant by a factor of 0.07 (7%).

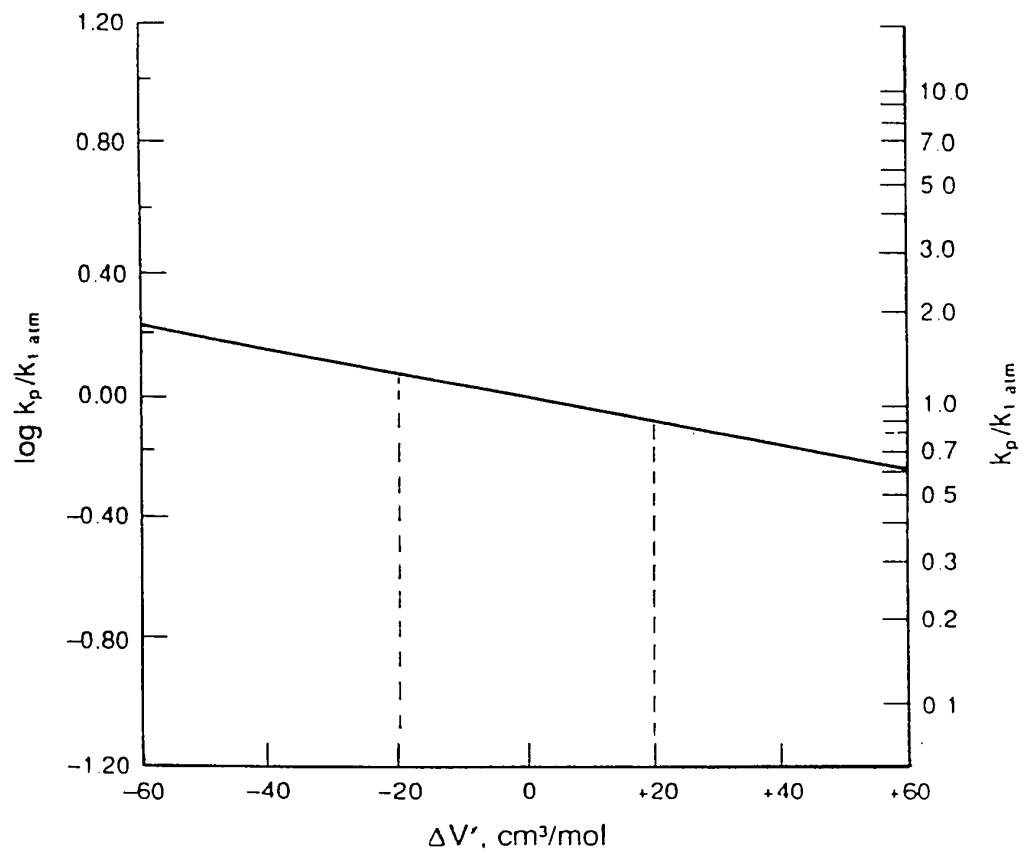


Figure 4.1 Relationship Between $k_p / k_{1 \text{ atm}}$ and Volume of Activation, $\Delta V'$, for Average In Situ Ferromanganese Crust Conditions ($P = 200 \text{ atm}$, $T = 4^\circ\text{C}$). The Dashed Lines Delineates General Range of $\Delta V'$ for Geochemical Reactions. Modified After Brezonik (1994).

4.2 Experimental Methods

Unless otherwise stated, all solutions were prepared from reagent grade chemicals and analytical grade, type I, deionized-water (DIW). Research grade N₂ and SO₂ gas used to sparge leach solutions was supplied from gas cylinders using special-service two-stage regulators to control flow rates. All labware was soaked in 10% HNO₃ overnight, thoroughly rinsed (three times) with DIW, and air dried before use. An Orion Research laboratory model 720A pH/ISE meter was used to measure direct redox potential (ORP) using an Orion model 96-78 platinum redox electrode and pH with a ROSS Combination pH electrode and automatic temperature compensator probe. Chemical analyses of metals in solution were completed in duplicate by inductively coupled plasma atomic emission spectrometry (ICP/AES), using a Leeman Labs Plasma Spec I high-resolution rapid-sequential echelle grating spectrometer. Analytical precision and accuracies are presented in Appendix A.

4.2.1 Batch Leach Experiments

A study medium was produced by carefully hand picking about two kilograms of ferromanganese crust from a large flat boulder recovered from *Hancock Seamount* (29° 40.1' N 179° 16.8' E) during the University of Hawaii, *Kana Keoki* cruise 84-04-28-05 (DeCarlo et al., 1987). The crust material was ground, sieved to < 105 microns (-100 nylon mesh), thoroughly mixed, oven dried for several days at 110°C, then stored in glass vials kept in desiccators. Chemical analysis of the study medium was done on sub-sample portions from widely separated locations within the bulk sample. Five sub-sample portions of 252 - 255 mg were weighed on a micro-balance and transferred to Teflon™ microwave digestion crucibles.

Five ml of *aqua regia* (2 ml concentrated HNO₃ + 2 ml concentrated HCl + 1 ml HF) was added to each crucible, the crucibles were sealed, then digested in a microwave oven for 60 seconds at high power. After cooling for one hour, the contents of each crucible were transferred to a volumetric flask and adjusted to 100 ml with 0.5 M H₃BO₃. Quantitative analysis of the five major transition metals, Mn, Fe, Co, Ni, and Cu in each sub-sample were completed by ICP/AES. The accuracies of the determinations were determined by simultaneous analysis of *USGS standard nodules A-1*, with precision better than $\pm 6\%$ of the reported value for each element.

The batch leach kinetics experiments used a refrigerated pressure bomb apparatus to produce simulated *in situ* conditions. The apparatus was assembled by coiling 20 meters of nominal “half-inch” copper tubing around a HIP R4-16-20 stainless steel pressure bomb (20,000 psi rated). The pressure bomb and copper tubing were placed into an insulated canister filled with water to enhance heat conduction between bomb and refrigerating tubing. A 50% ethylene-glycol solution (coolant) was circulated through the copper tubing coil to/from the 30-liter reservoir of a NESLAB HL-75 Recirculating Chiller which maintained a stability of $\pm 0.1^\circ\text{C}$ over a temperature range of 3°C to 35°C . Hydraulic pressures were applied to the pressure bomb with an Enerpac 11-100 (10,000 psi rated) High Pressure Hand Pump, using DIW as the working fluid. A series of batch experiments were also done at $\sim 0^\circ\text{C}$ (below the temperature range of the refrigerated pressure bomb apparatus) in an ice bath at 1 atm pressure.

An electromagnetic stirrer unit for use in the refrigerated pressure bomb was assembled by cementing two small disc-shaped ceramic magnets onto a spin-bar attached to

a small direct current (DC) electric motor. The motor with attached magnet spin-bar was mounted in a two oz. polypropylene container with a snug fitting snap-shut lid and was filled with fresh ethanol (taking care to ensure the container contained no air space) before every experiment. Immediately after each high pressure experiment, the ethanol solution (including any water that seeped into the housing) was drained from the stirrer container, the stirrer motor bearings and windings were flushed with a silicon-based electrical contact cleaner and lubricated with light machine oil. Electrical leads for the stirrer motor were attached to insulated electrical pass-throughs in the high pressure vessel cover. A 115 VAC transformer provided a 4 VDC power supply and a rheostat regulated the current to control stirrer speed.

To conduct a batch leach experiment, an analytical portion of about one gram of ferromanganese crust study medium is weighed on a micro-balance. The weighed portion of crust is placed into a 250 ml Teflon™ wide mouthed reaction bottle, along with a Teflon™ coated magnetic stir-bar. Next, the crust portion is carefully washed down to the bottom of the reaction bottle with 55 ml of saturated NaCl brine. The reaction bottle is then capped, labeled, and cooled down to the desired experiment temperature in a chill water bath or refrigerator. The saturated NaCl brine, which covers the crust study medium and stir bar in the reactor bottle, serves two purposes: (1) to provide a density layer to keep the study medium separated from the leaching solution until the desired experiment pressure and temperature is achieved; and (2) to produce a leachate with the approximate salinity of natural seawater, when the leaching experiment is started. Most batch leach experiments used saturated brine made from reagent grade NaCl, as it was much easier to produce and had comparable leach results to experiments using brine produced from evaporated sea water.

The majority of the sulfurous acid pre-leach solutions were produced by the pH adjustment of sodium sulfite (Na_2SO_3) solutions, after the method developed by Schein (1986). This method of sulfurous acid production ensures more consistent experimental SO_2 (aq) leach concentrations than sulfurous acid solutions produced by sparging SO_2 gas through DIW (Schein found that sulfurous acid solutions produced by sparged SO_2 gas would lose up to 6% in normality within an hour, even when stored in sealed containers). However, a few experiments were done, using sulfurous acid solutions produced by sparged SO_2 gas for comparison. Prepared sulfurous acid pre-leach solutions were kept in sealed flasks and placed in a chill water bath or refrigerator to cool down to the experiment temperature.

When the refrigerated pressure bomb apparatus has stabilized at the desired experiment temperature, one can begin. First, the pre-leach solution is added into the reactor bottle, taking great care not to disturb the saturated brine density layer. A thin disc of DIW ice may be placed on top of the saturated brine layer with forceps as an aid. However after some practice, the chilled pre-leach solution can be transferred into the reaction bottle by merely pouring very slowly while guiding the flow stream to the inner side of the bottle with a glass or Teflon™ stir rod. Any remaining head-space in the reaction bottle is filled with chilled DIW and the bottle is capped. Next, the prepared reactor bottle is placed on top of the electromagnetic stirrer unit, again taking care to avoid prematurely mixing the stratified density layers, and secured in place using duct tape. Finally, the prepared reactor bottle and attached stirrer unit are slowly lowered into the refrigerated pressure bomb, the bomb vessel cover is secured and hydraulic pressure is applied. After the desired experiment pressure is achieved, the leach experiment is started by turning on the electromagnetic stirrer that mixes

the crust portion, brine and pre-leach solutions into a leach slurry. At completion of the experiment's allotted leach time, the stirrer is turned off, bomb pressure is released, and the reactor is removed from the bomb apparatus. The pregnant leachate is vacuum filtered under an exhaust fume hood, through 0.45 μm micropore nylon filter membranes. The filtrate is adjusted to 500 ml with pH \sim 2.0 solution, and concentrations of Fe, Mn, Co, Ni, and Cu are determined by ICP/AES. To determine bulk crust dissolutions (change in crust portion mass), the filter membrane and residual solids from the leach are transferred to an aluminum weighing dish, dried overnight in an oven at 110°C. After the contents of the dish are cooled to ambient temperature in a desiccator, the residual solids are weighed on a micro-balance.

4.2.2 *Semi-Batch Intact Crust Experiments*

In the semi-batch *intact crust* experiments, \sim 1 cm^3 cubes of intact ferromanganese crust were suspended in a 500 ml Erlenmeyer reactor flask containing 300 ml of \sim 9% anoxic sulfurous acid solution.

The sulfurous acid solution was produced by sparging SO_2 gas from a compressed gas cylinder through a porous glass frit submerged in a vented 1.5 liter Erlenmeyer flask containing one liter of 0.58 M NaCl solution (synthetic sea water) with pH of \sim 1.0 under a fume hood. The solution was first deoxidized by sparging N_2 gas through it for 15 minutes, followed by sparging SO_2 gas for one hour to ensure saturation. The production flask was then placed into a 4°C chill water tank (also under the fume hood) and a \sim 5 psi N_2 overpressure was applied to prevent loss of volatile SO_2 or solution oxidation. Quantities of

prepared $\text{SO}_{2(aq)}$ leach solution was then readily available on demand by stopping the vent causing the N_2 overpressure to force leach solution out through a siphon tube.

The semi-batch *whole crust* reactor flask apparatus is shown in Figure 4.2. It consists of a 500 ml heavy Erlenmeyer flask with a tubing nipple on the neck placed into the 4°C chill water tank under the exhaust fume hood. The flask is secured by a clamp on a bracket in the tank, is partially submerged to just below the tubing nipple and positioned on top of a submerged electromagnetic stirrer. A two-hole stopper in the flask mouth provides venting of N_2 (N_2 overpressure is applied at the tubing nipple) and support for a siphon tube and the crust “suspension harness.” Suspension harnesses for crust fragments are fashioned from fine bell wire with thick continuous polyethylene insulation coating (for acid resistance), which are looped two or more times around intact $\sim 1 \text{ cm}^3$ pieces of crust and twisted to tighten the loops. This harness provides a secure method to hold and retrieve crust samples. A 20 ml syringe is attached to the outer end of the siphon tube for periodic extraction and replacement of leach solution and a large Teflon™ stir-bar is placed inside the flask.

To conduct a semi-batch *whole crust* leach experiment, a cube shaped crust fragment is secured in a suspension harness and prepared by soaking overnight in a beaker of synthetic seawater in a refrigerator to ensure saturation of crust pore spaces at near *in situ* temperature. A 100 ml (4 oz) polyethylene weighing cup is prepared by adding 60 ml of 4°C deaerated (sparged with N_2) synthetic seawater siphoned from a sparging flask. The crust sample and its harness are removed from the soaking beaker and placed into the weighing cup and the total weight is measured on a micro-balance. Next, the crust sample and its harness are quickly transferred to the reactor flask containing 300 ml of prepared $\text{SO}_{2(aq)}$ leach solution,

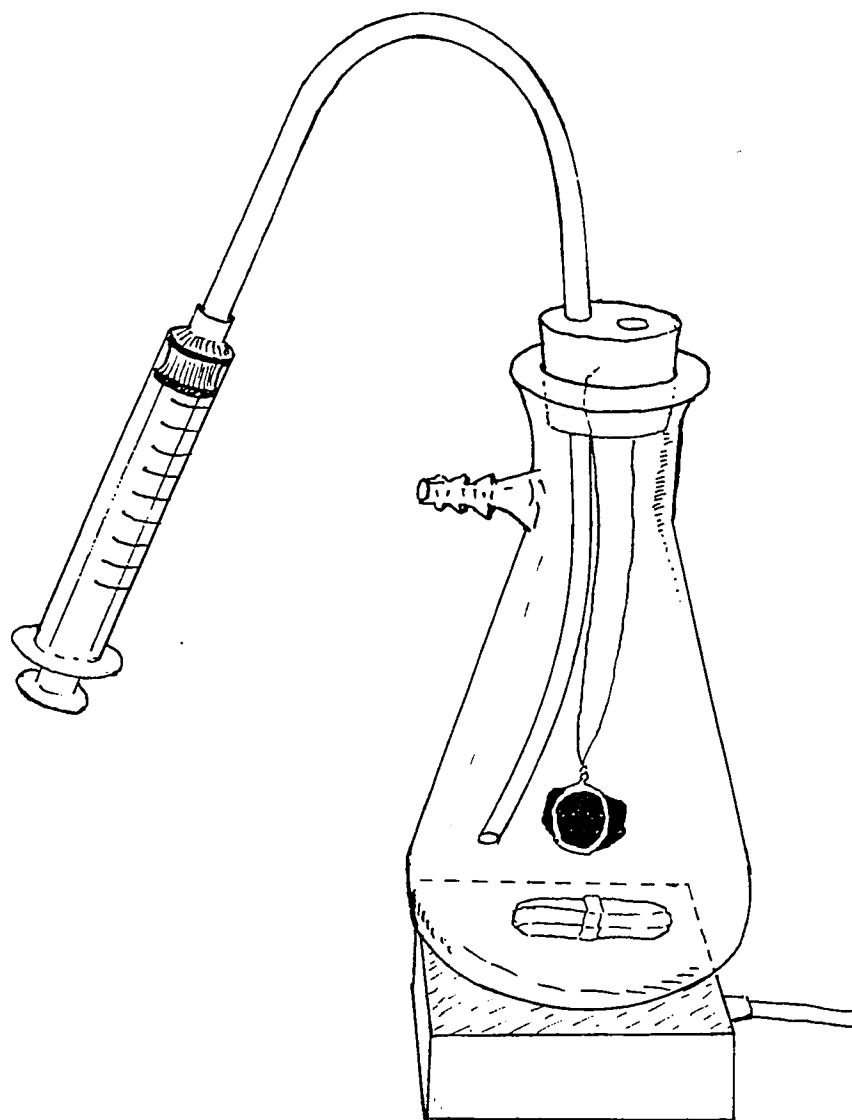


Figure 4.2 *Semi-Batch Whole Crust Reactor Flask Apparatus for SO_2 (aq) Leaching of Intact Ferromanganese Crust Fragments.*

and the weighing cup with synthetic seawater are measured to determine the weight difference. The leach experiment in the reactor continues for up to six hours. Periodically, every ten minutes, 20 ml of leach solution is extracted using the syringe on the siphon tube (aided by increasing N₂ overpressure in the flask) and replaced with fresh leach solution. Every 30 minutes, the crust sample and its harness is quickly transferred to a freshly prepared weighing cup, measured on the micro-balance, and the difference in weight determined when the crust sample and harness are replaced in the leach. As necessary, the suspension harness is adjusted to keep the crust fragment secure, taking care to avoid altering the leached crust surface as much as possible. At the completion of the experiment, the suspension harness is removed from any residual crust sample, measured on the micro-balance, and crust recovery (dissolution) versus leach time is calculated. The pH and temperature of the leach solution are monitored and the stirring rates kept constant for all experiments.

The procedure for two semi-batch *whole crust* leach experiments was modified to determine the effect on crust leaching due to the presence of oxygen. In these trials the stopper in the flask mouth was left off and N₂ overpressure was not supplied. The crust sample and harness were simply hung from a small wood stick laid across the flask mouth and lixiviant transfer was made by pipette.

CHAPTER 5

RESULTS AND DISCUSSION

More than 260 batch leach experiments were completed at a hydrometallurgical laboratory set up at the University of Hawaii Marine Center (Snug Harbor) in Honolulu. Filtrate from these experiments were analyzed by inductively coupled plasma atomic emission spectroscopy (ICP/AES) and percent recovery of Co, Cu, Fe, Mn and Ni determined. These data are presented in Appendix A. In each of the experimental trials, one gram of ferromanganese crust study medium (approximately 0.011 moles of metal oxides) was mixed with a 1% sulfurous acid leach (0.030 moles of aqueous SO₂ species) produced by the pH adjustment and dissolution of sodium sulfite salt in synthetic seawater.

Six semi-batch intact crust experiments were also completed. The results of the semi-batch experiments are displayed in Section 5.5.

5.1 Effect of Temperature on Batch Leach Experiments

The effects of temperature on leach reaction recoveries (Co, Cu, Fe, Mn and Ni) are shown in Figures 5.1.1 to 5.1.18. Three-dimensional *ribbon charts* were selected to show the interrelation among the five transition metals. However, for clarity, error bars are not shown. The variance is high for some data points, especially for copper at low recoveries close to ICP/AES detection limits. Each ribbon graph should be considered only as a trend, particularly when viewing specific details such as inflection points. Standard deviation and replicate number for each data point are given in Appendix A.

The Arrhenius Equation predicted decrease in reaction rate with decreasing temperature (previous Chapter, Section 4.1.1). This relation is seen in the series of batch

experiments where $\text{pH} = 1.0$. However, the results do not appear to approach the projected 25% to 48% decrease in reaction rate predicted at *in situ* crust temperature. Also, the experimental results are mixed when $\text{pH} \geq 2.0$, with most series showing evidence of increased recovery with lower temperature. The unexpected results when $\text{pH} \geq 2.0$, may be due to a temperature induced change in aqueous SO_2 species distribution, in the $\text{SO}_{2(\text{aq})} \leftrightarrow \text{HSO}_3^-$ system. This is important because in the leach, $\text{SO}_{2(\text{aq})}$ is a reductant and HSO_3^- is an oxidant. An increase in the HSO_3^- fraction is expected to decrease the dissolution reaction recovery rate by reducing the concentration of the $\text{SO}_{2(\text{aq})}$ reactant. Figure 3.3 (in Chapter 3) shows that at 25°C , the distribution of $\text{SO}_{2(\text{aq})}$ and HSO_3^- are approximately at parity. The experimental results of this research suggest decreasing temperature slightly shifts the $\text{SO}_{2(\text{aq})} \leftrightarrow \text{HSO}_3^-$ system equilibria in favor of the $\text{SO}_{2(\text{aq})}$ fraction. Thus, instead of a negative impact, lower temperatures may tend to aid *in situ* crust extraction at higher pH levels.

The data also shows that temperature induced change in recovery affects Mn the least of the five major crust metals. Typically, change in recovery level is negligible for Mn and when $\text{pH} \geq 3.0$, Mn may be preferably leached at the expense of the other metal species. This leach selectivity for Mn^{2+} is probably due to the lower equilibrium constants for formation of Mn complexes in aqueous solution compared with those of the succeeding elements (Fe, Co, Ni, Cu).

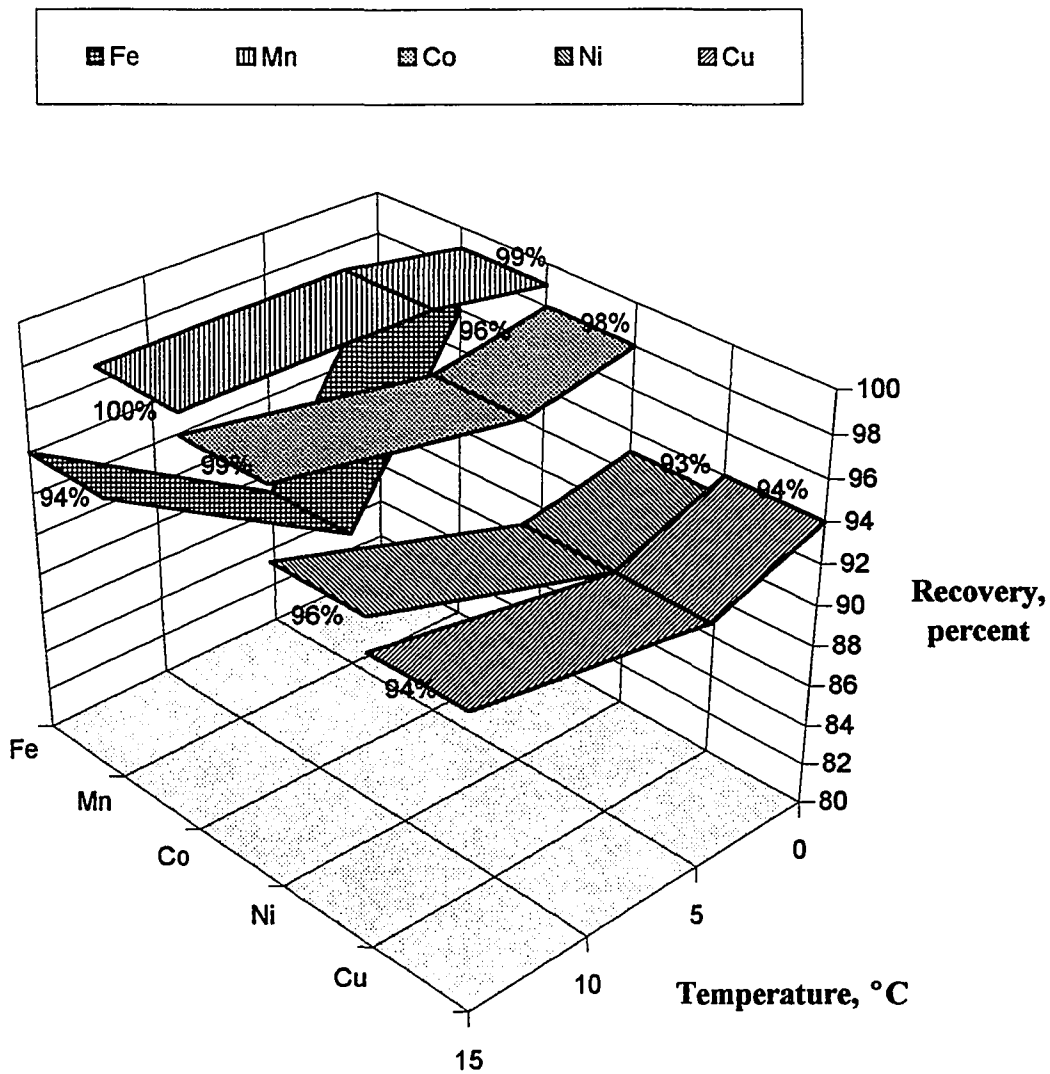


Figure 5.1.1 *Effect of Temperature on Metal Recovery of Ferromanganese Crust in 1% Sulfurous Acid Batch Leach, 5 Minute Leach Time, pH = 1.0, Pressure = 1 atm, 400 rpm Stir Rate.*

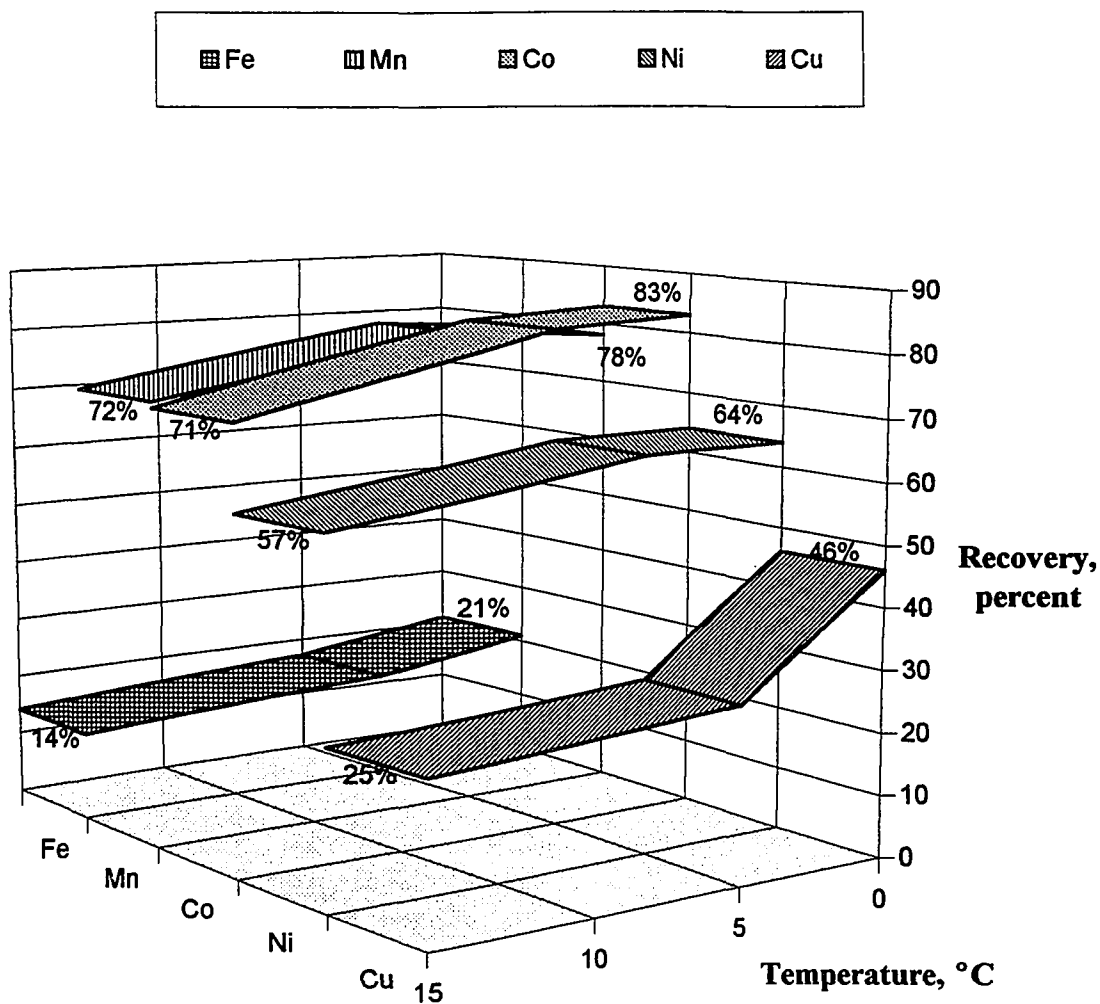


Figure 5.1.2 *Effect of Temperature on Metal Recovery of Ferromanganese Crust in 1% Sulfurous Acid Batch Leach, 5 Minute Leach Time, $pH = 2.0$, Pressure = 1 atm, 400 rpm Stir Rate.*

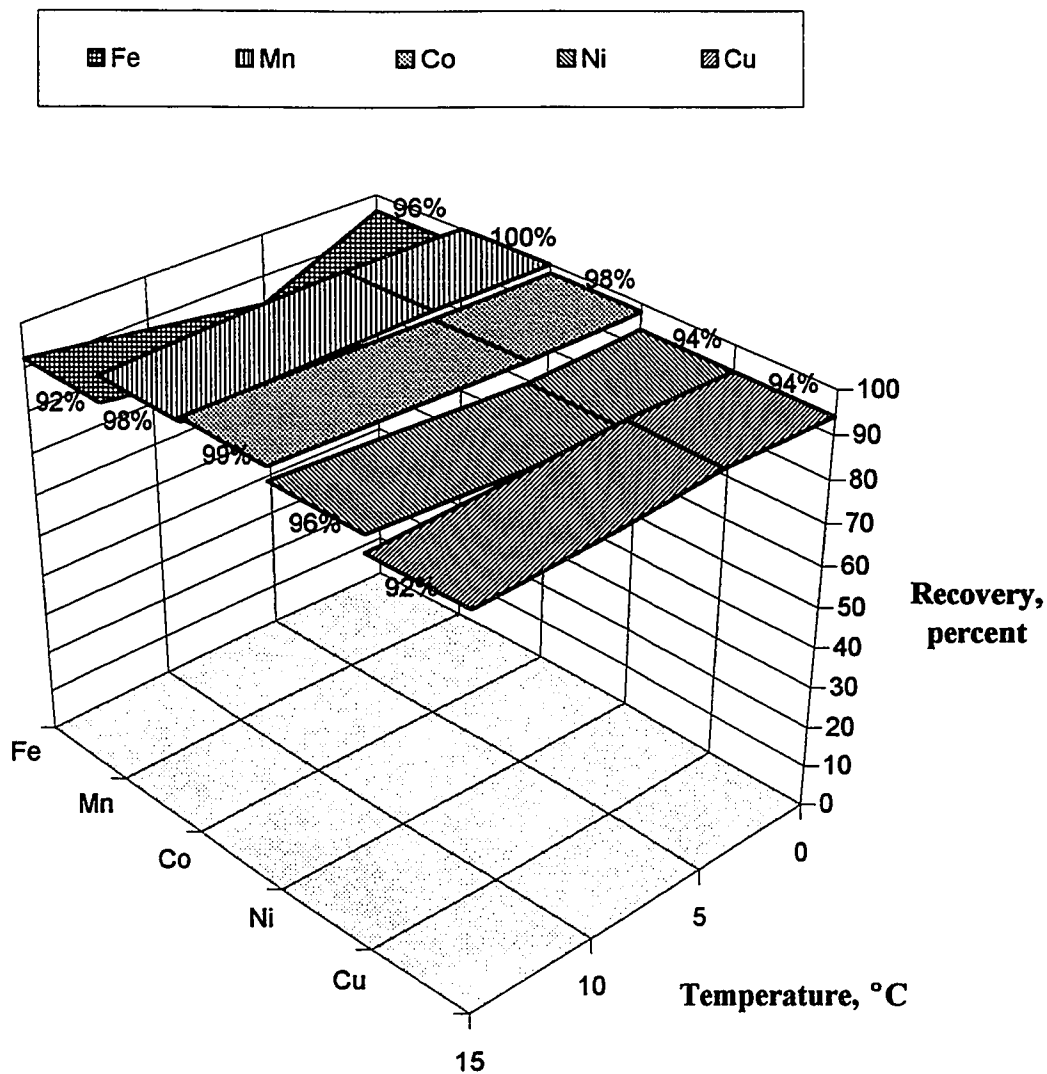


Figure 5.1.3 *Effect of Temperature on Metal Recovery of Ferromanganese Crust in 1% Sulfurous Acid Batch Leach, 15 Minute Leach Time, pH = 1.0, Pressure = 1 atm, 400 rpm Stir Rate.*

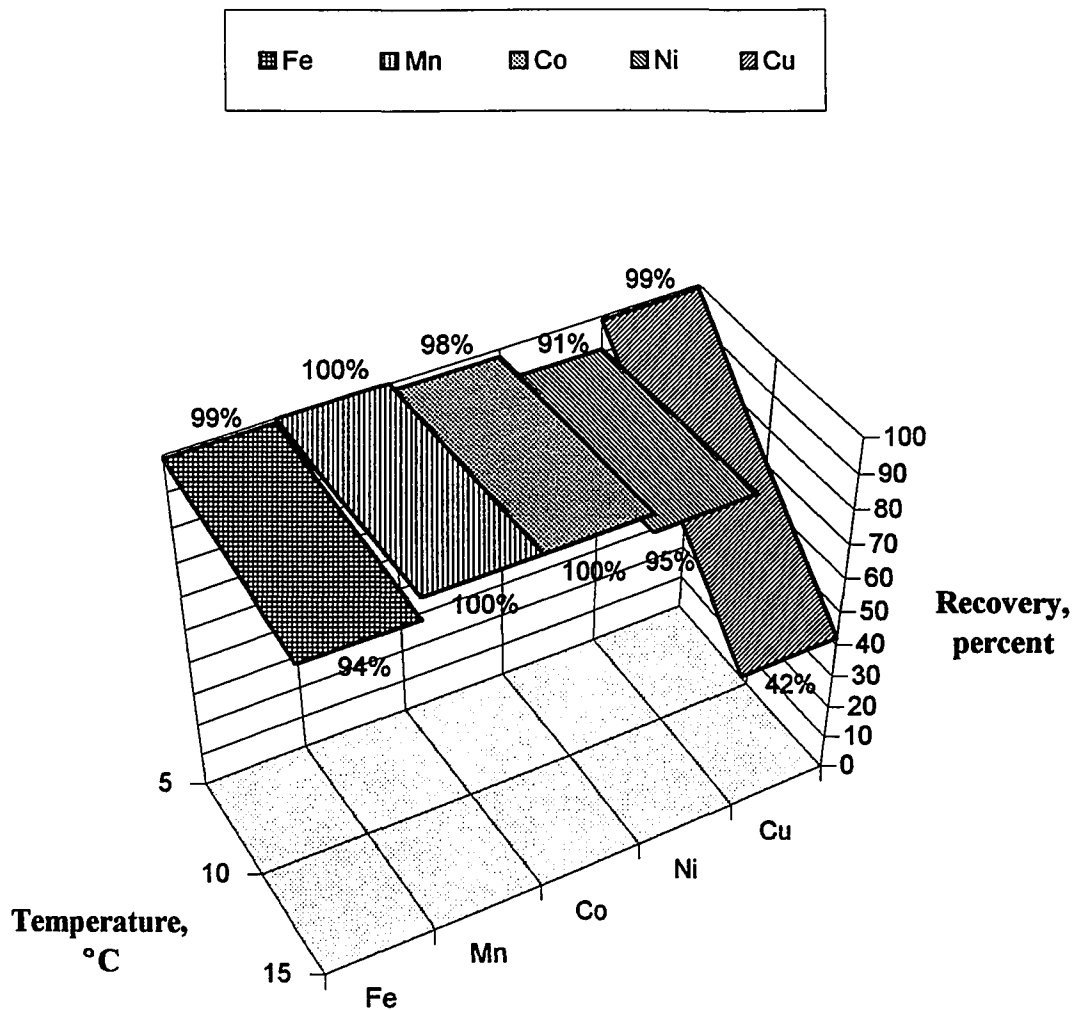


Figure 5.1.4 *Effect of Temperature on Metal Recovery of Ferromanganese Crust in 1% Sulfurous Acid Batch Leach, 15 Minute Leach Time, pH = 1.0, Pressure = 100 atm, 400 rpm Stir Rate.*

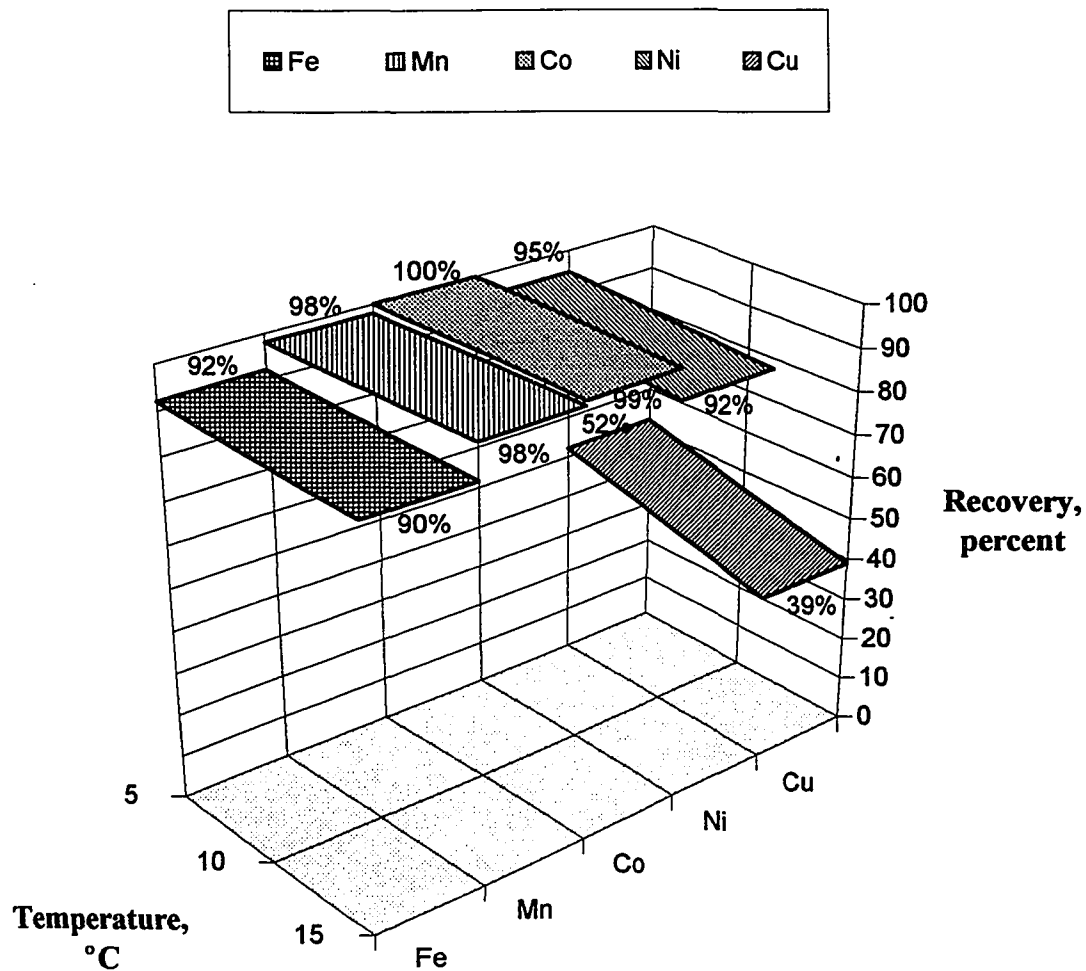


Figure 5.1.5 *Effect of Temperature on Metal Recovery of Ferromanganese Crust in 1% Sulfurous Acid Batch Leach, 15 Minute Leach Time, pH = 1.0, Pressure = 200 atm, 400 rpm Stir Rate.*

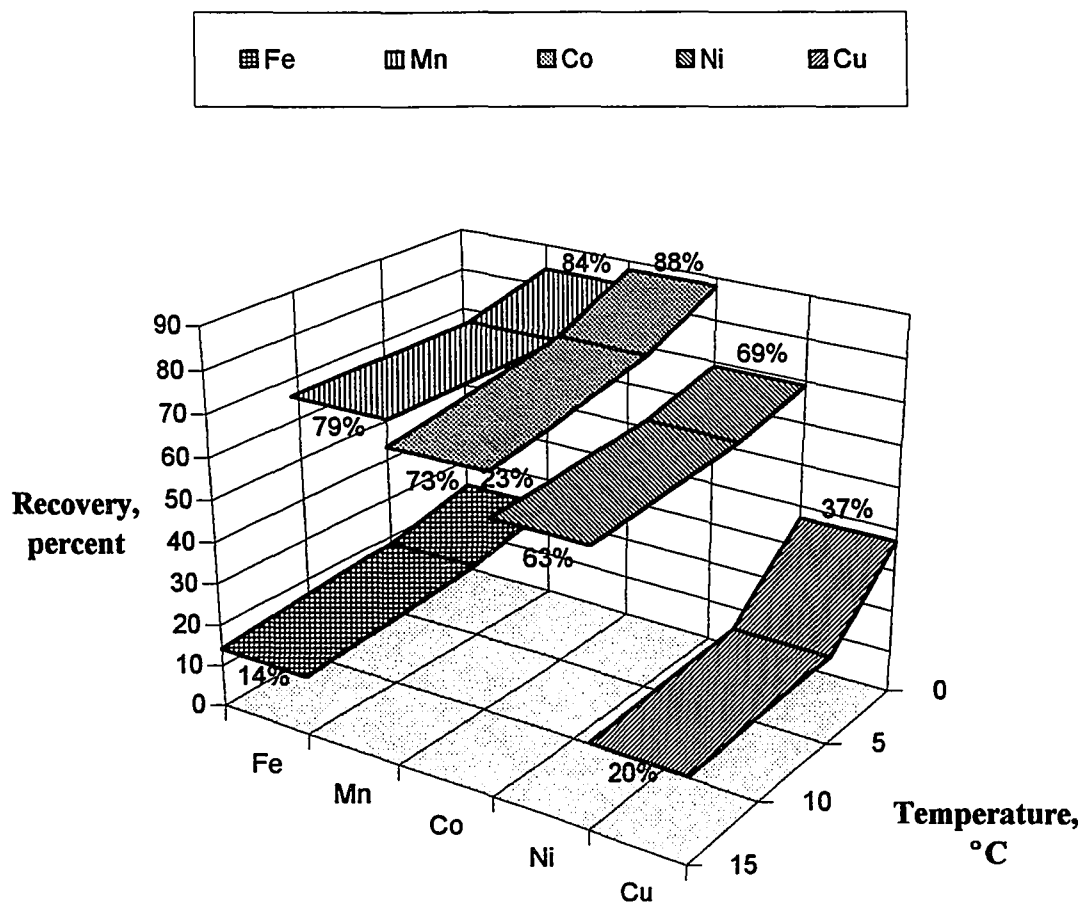


Figure 5.1.6 *Effect of Temperature on Metal Recovery of Ferromanganese Crust in 1% Sulfurous Acid Batch Leach, 15 Minute Leach Time, $pH = 2.0$, Pressure = 1 atm, 400 rpm Stir Rate.*

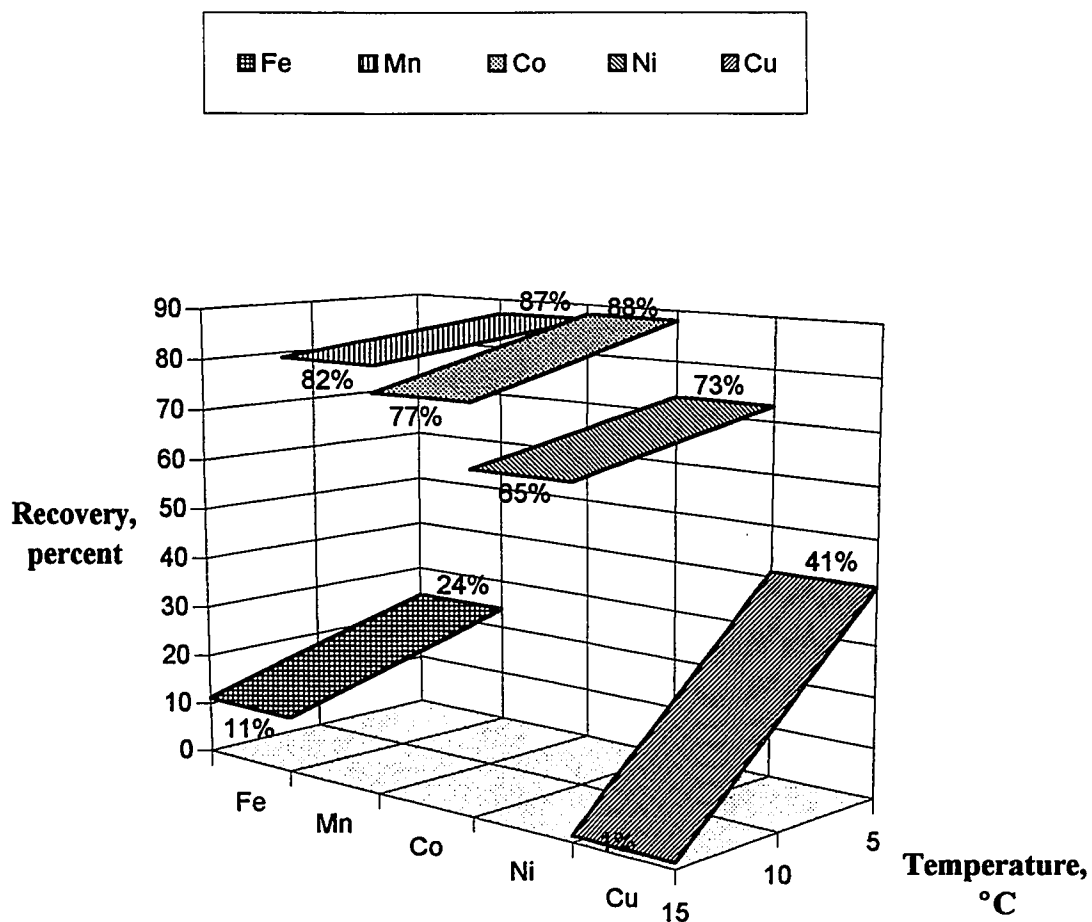


Figure 5.1.7 *Effect of Temperature on Metal Recovery of Ferromanganese Crust in 1% Sulfurous Acid Batch Leach, 15 Minute Leach Time, pH = 2.0, Pressure = 100 atm, 400 rpm Stir Rate.*

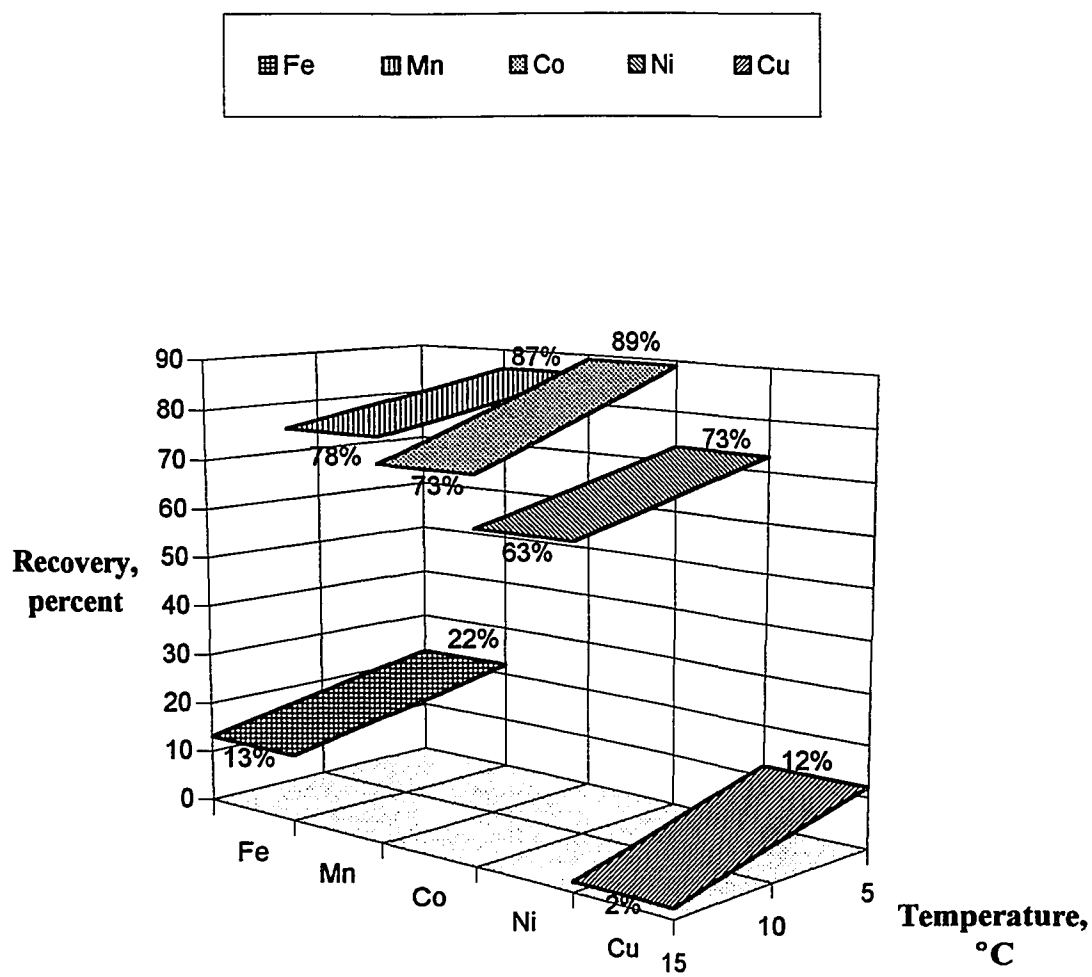


Figure 5.1.8 *Effect of Temperature on Metal Recovery of Ferromanganese Crust in 1% Sulfurous Acid Batch Leach, 15 Minute Leach Time, pH = 2.0, Pressure = 200 atm, 400 rpm Stir Rate.*

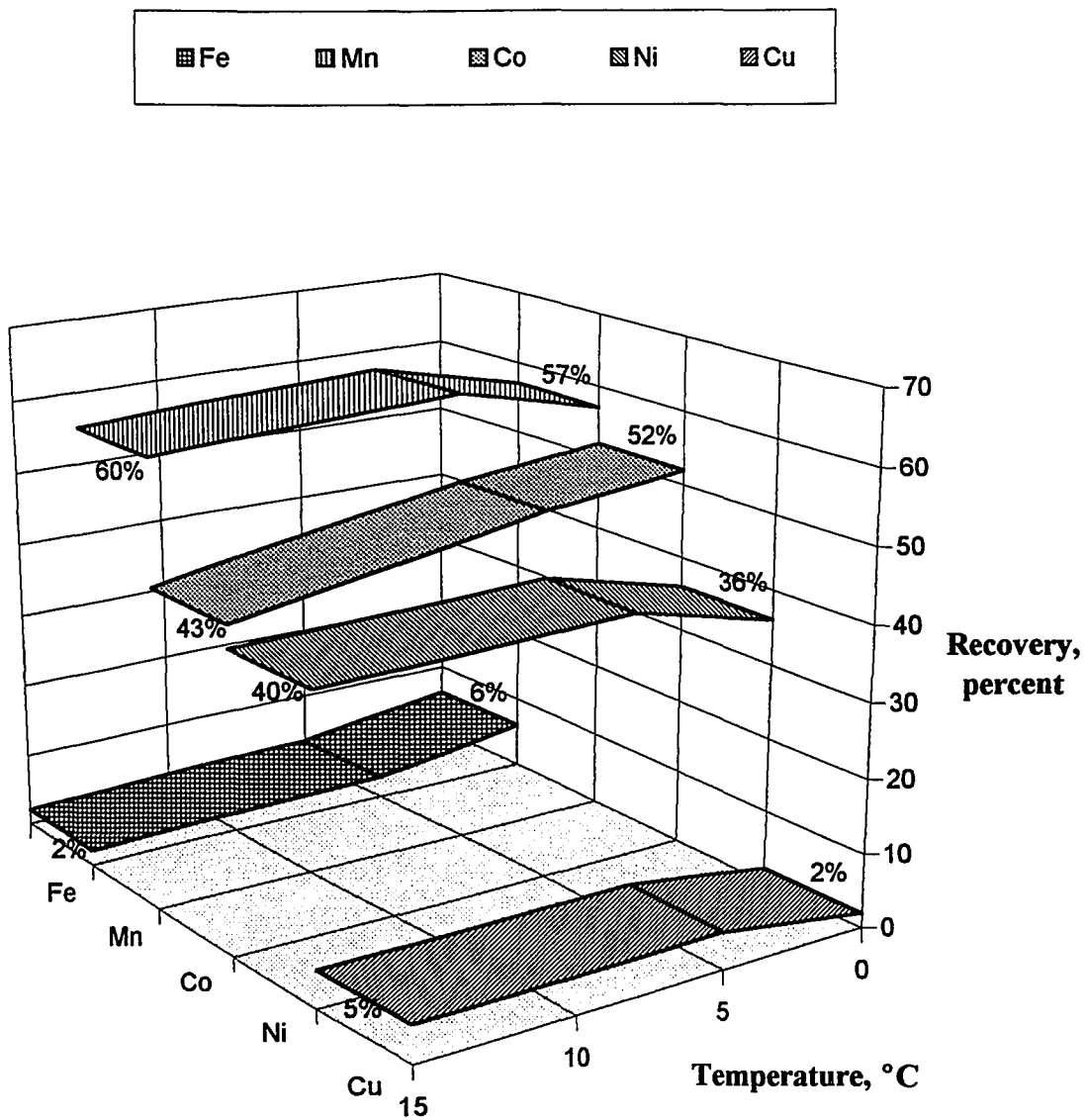


Figure 5.1.9 *Effect of Temperature on Metal Recovery of Ferromanganese Crust in 1% Sulfurous Acid Batch Leach, 15 Minute Leach Time, $pH = 3.0$, Pressure = 1 atm, 400 rpm Stir Rate.*

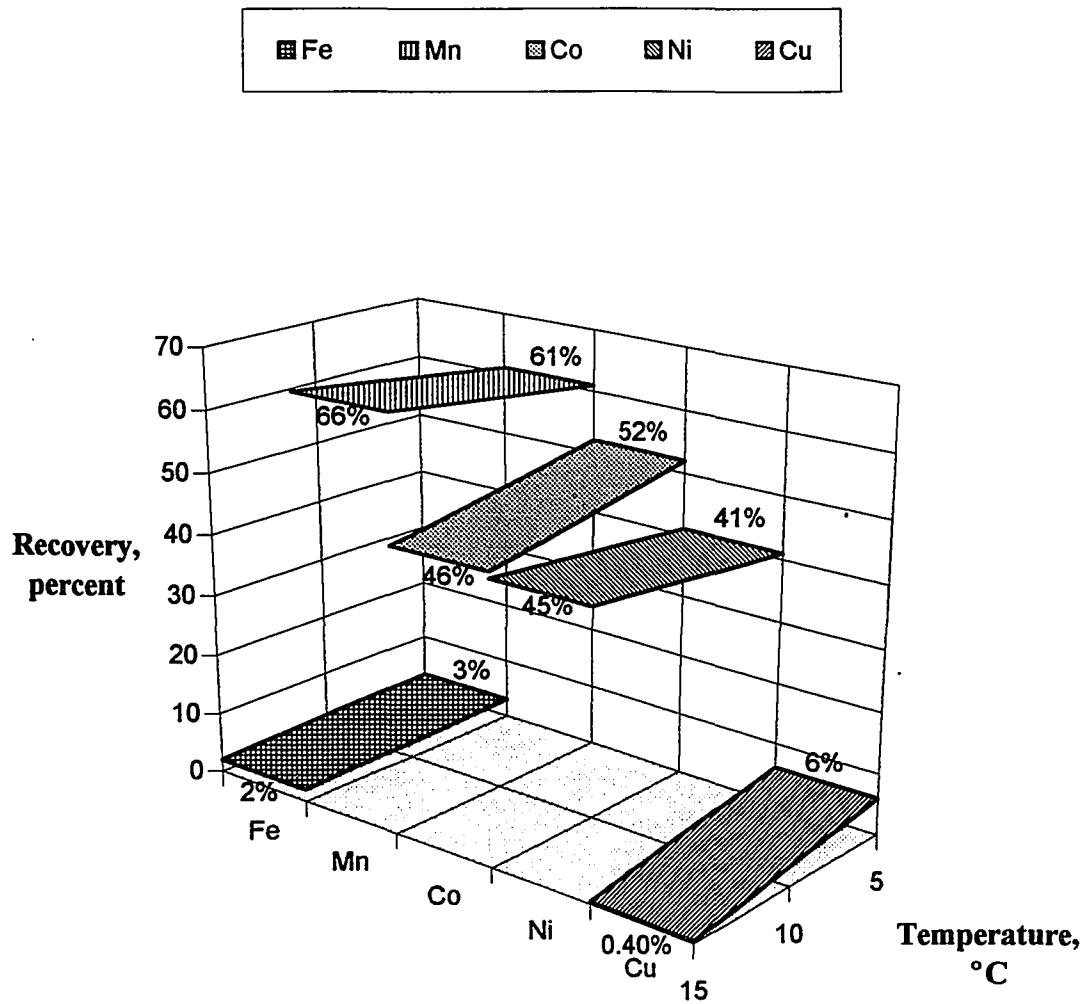


Figure 5.1.10 *Effect of Temperature on Metal Recovery of Ferromanganese Crust in 1% Sulfurous Acid Batch Leach, 15 Minute Leach Time, pH = 3.0, Pressure = 100 atm, 400 rpm Stir Rate.*

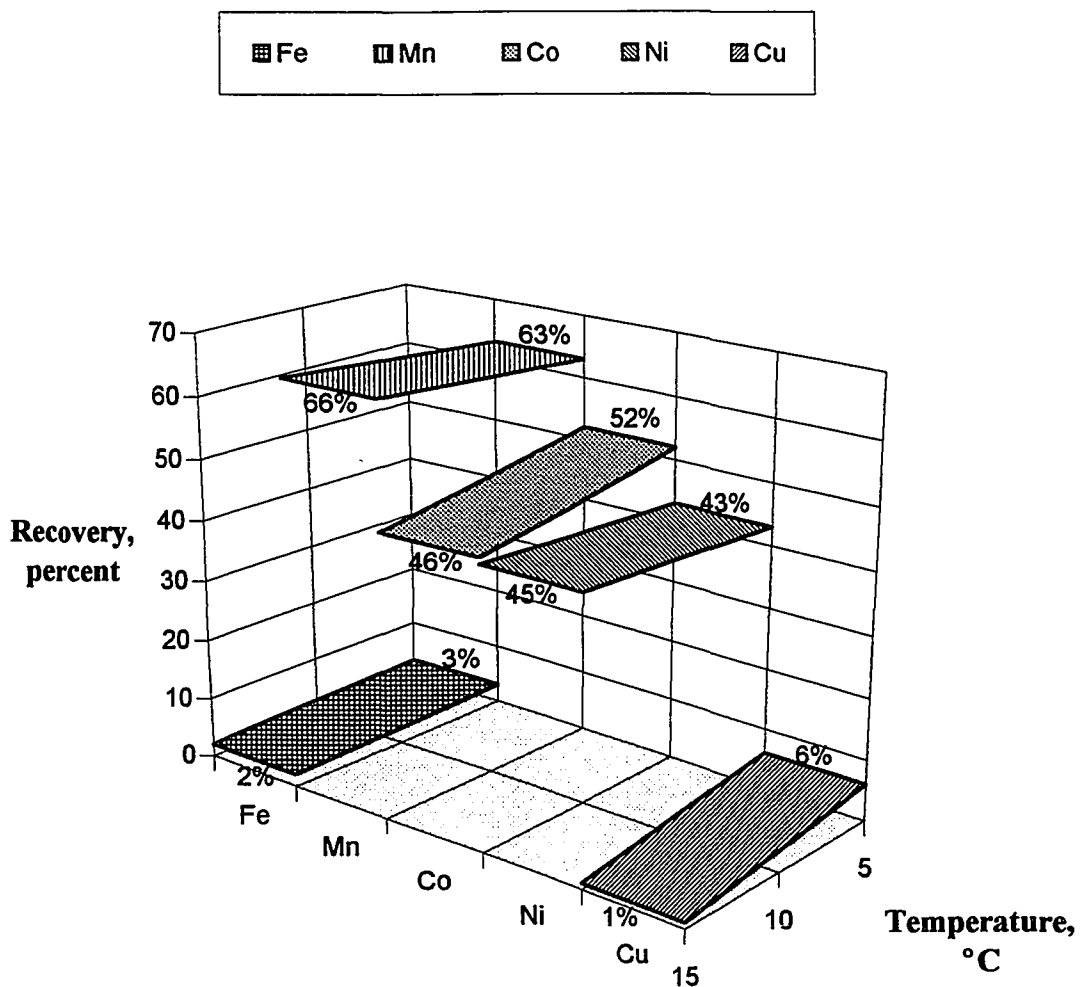


Figure 5.1.11 *Effect of Temperature on Metal Recovery of Ferromanganese Crust in 1% Sulfurous Acid Batch Leach, 15 Minute Leach Time, pH = 3.0, Pressure = 200 atm, 400 rpm Stir Rate.*

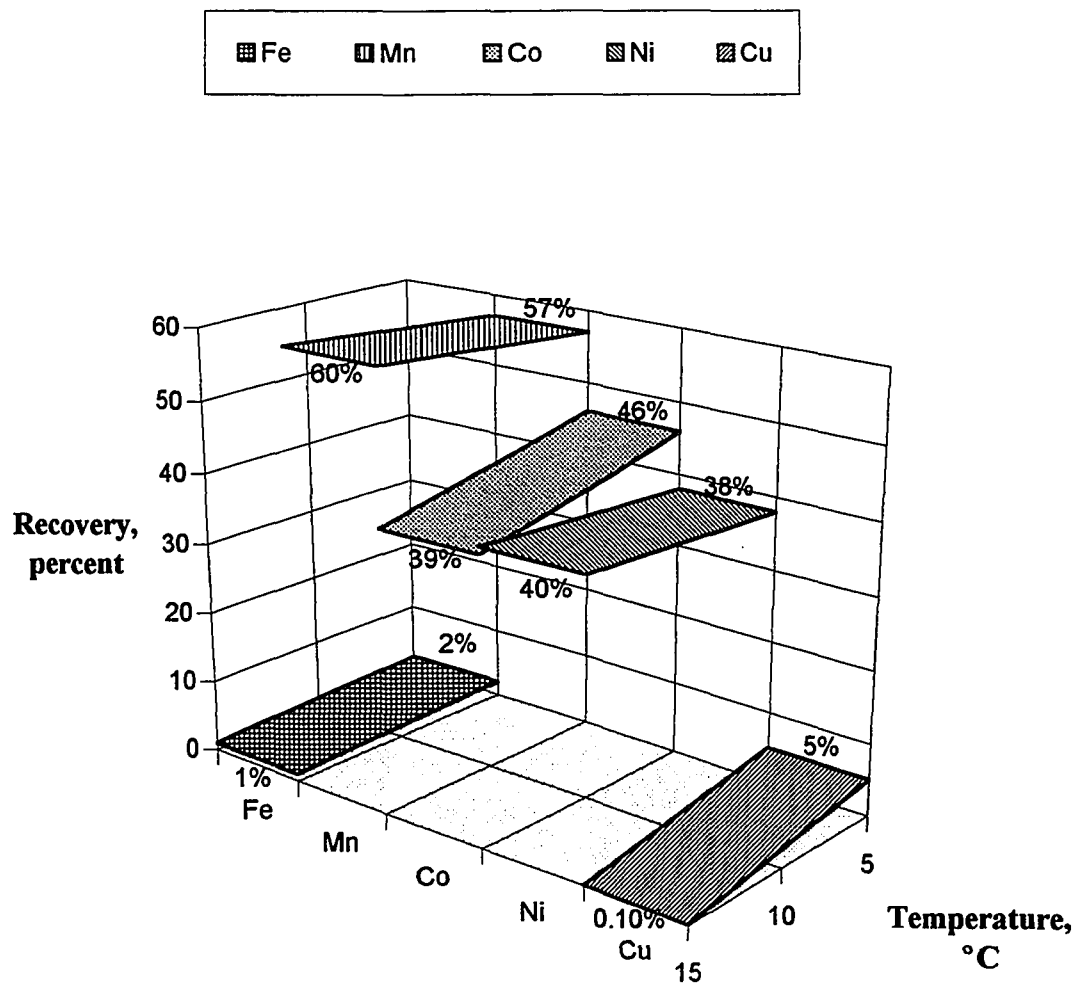


Figure 5.1.12 *Effect of Temperature on Metal Recovery of Ferromanganese Crust in 1% Sulfurous Acid Batch Leach, 15 Minute Leach Time, $pH = 5.0$, Pressure = 100 atm, 400 rpm Stir Rate.*

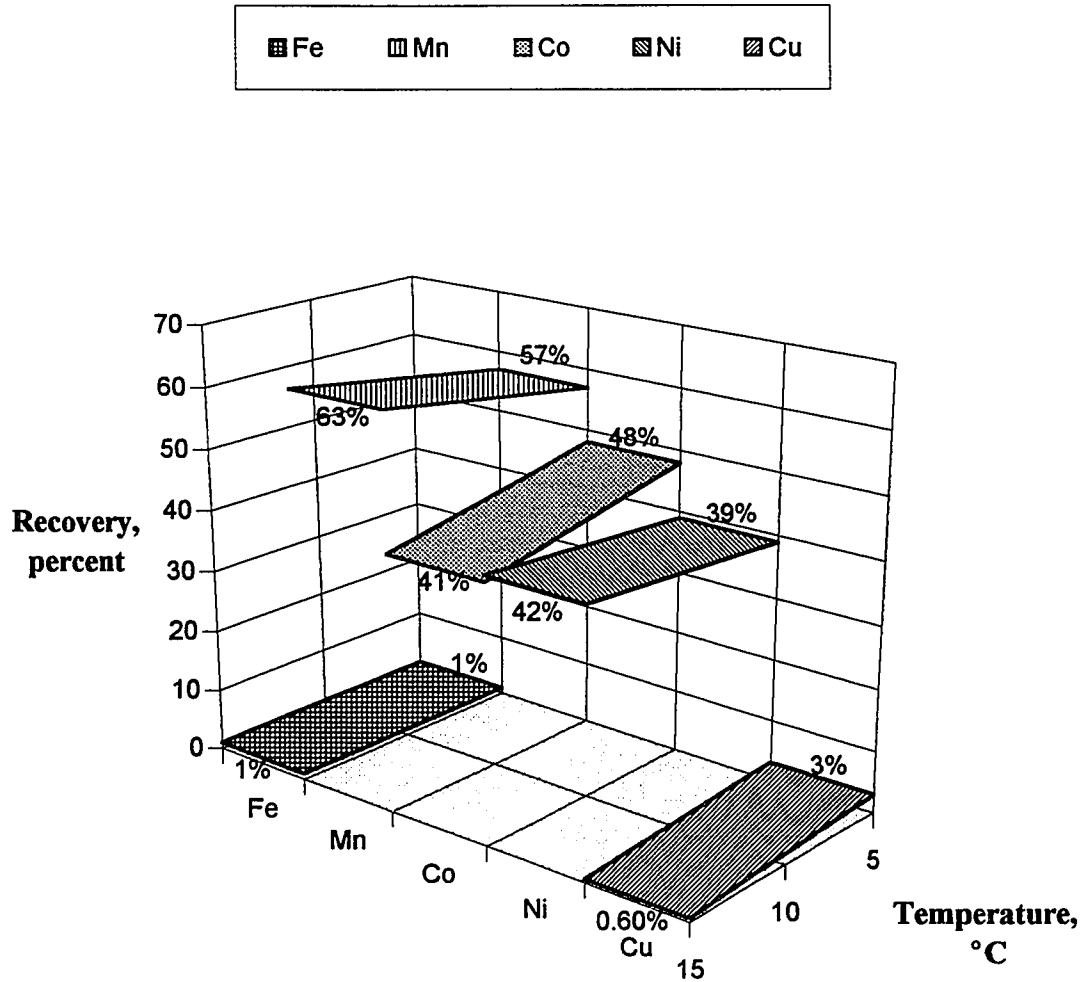


Figure 5.1.13 *Effect of Temperature on Metal Recovery of Ferromanganese Crust in 1% Sulfurous Acid Batch Leach, 15 Minute Leach Time, pH = 5.0, Pressure = 200 atm, 400 rpm Stir Rate.*

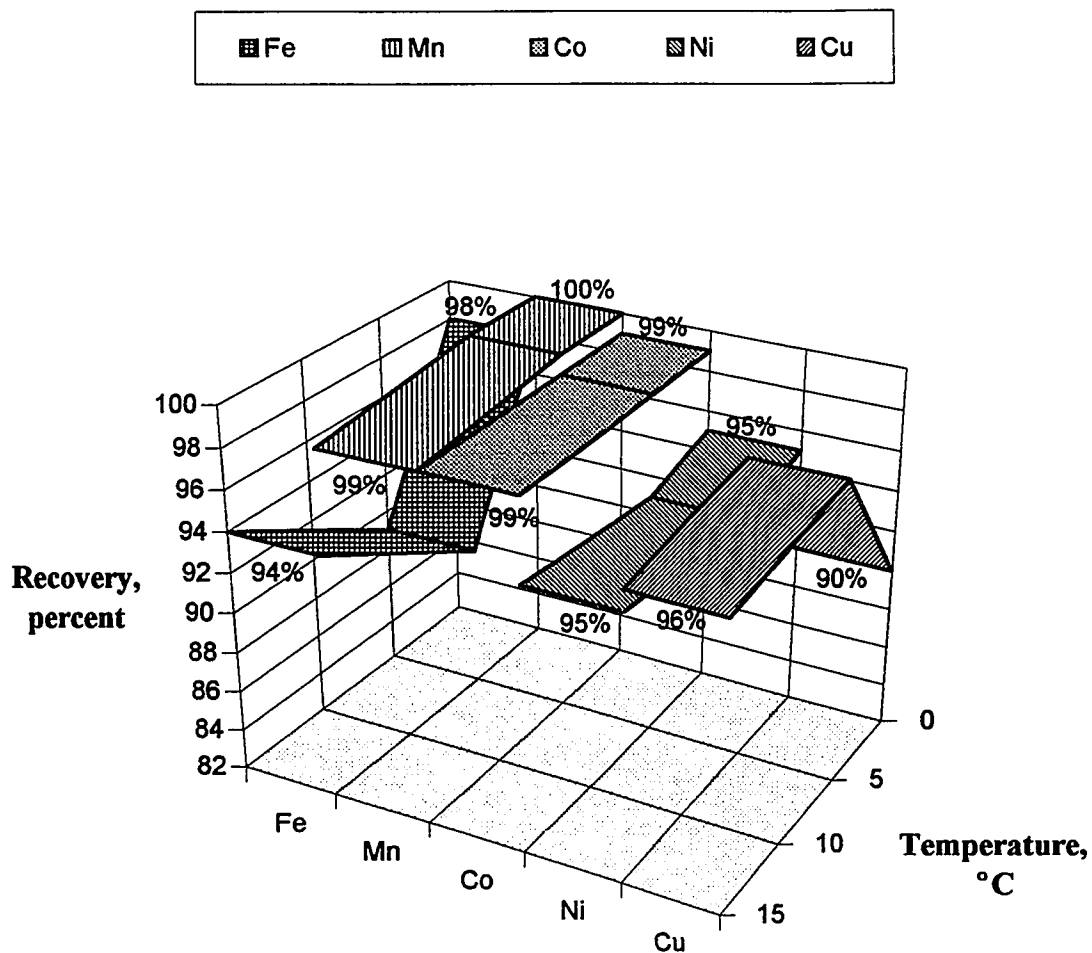


Figure 5.1.14 *Effect of Temperature on Metal Recovery of Ferromanganese Crust in 1% Sulfurous Acid Batch Leach, 30 Minute Leach Time, pH = 1.0, Pressure = 1 atm, 400 rpm Stir Rate.*

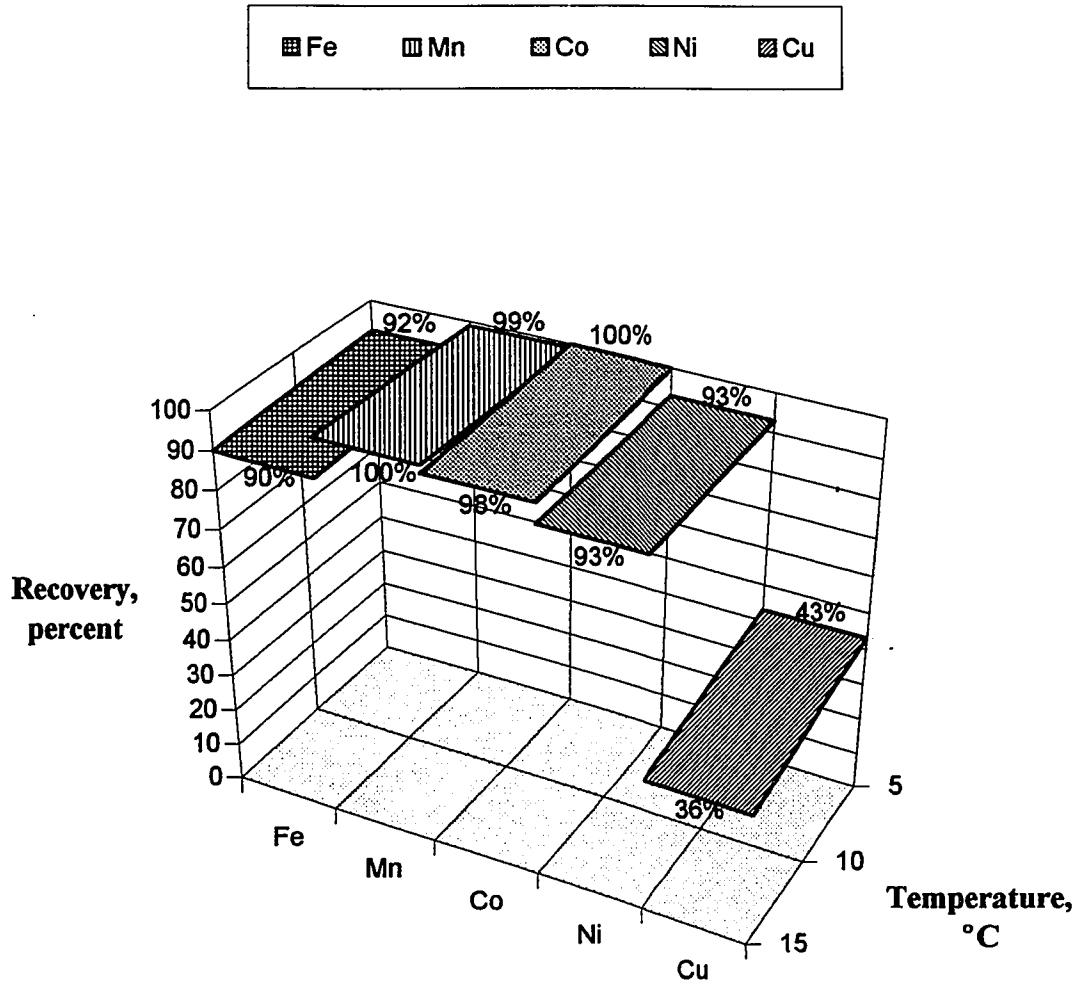


Figure 5.1.15 *Effect of Temperature on Metal Recovery of Ferromanganese Crust in 1% Sulfurous Acid Batch Leach, 30 Minute Leach Time, pH = 1.0, Pressure = 100 atm, 400 rpm Stir Rate.*

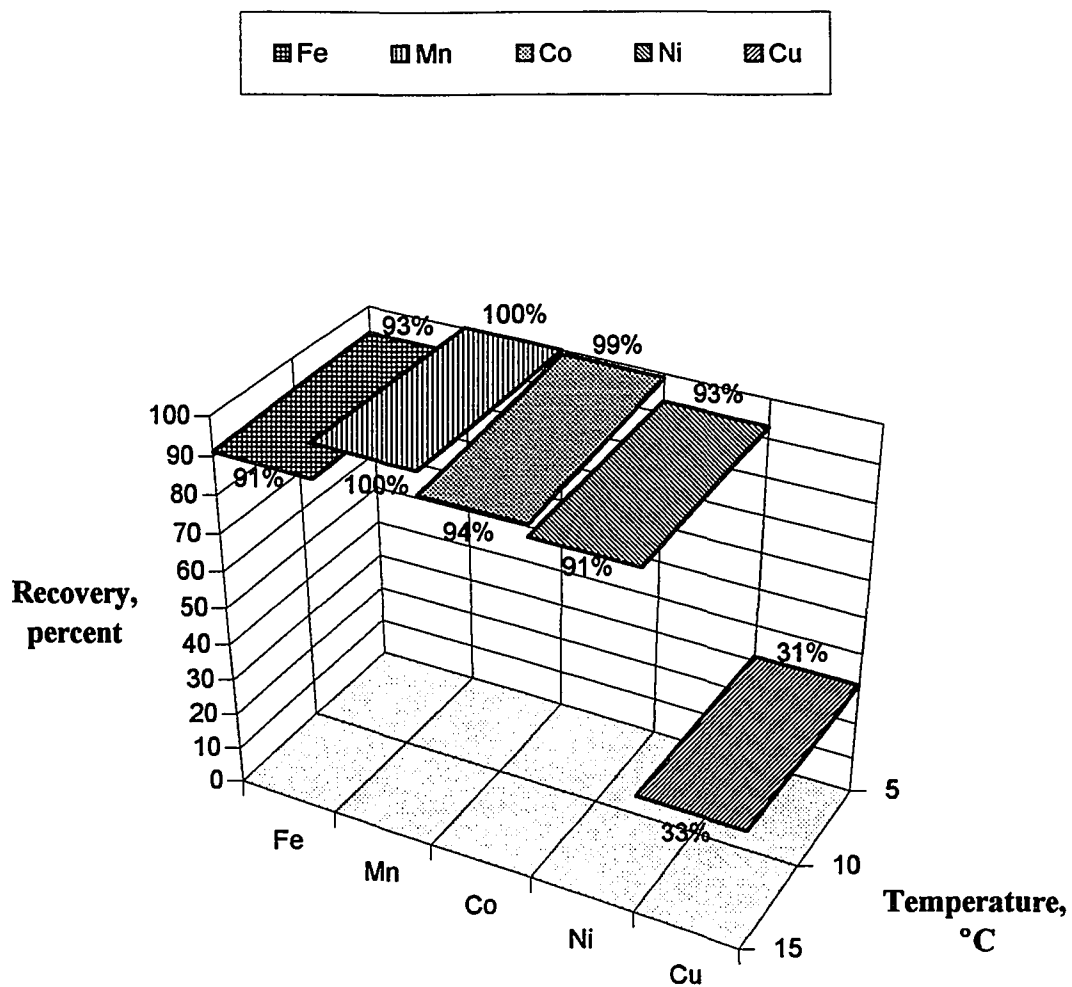


Figure 5.1.16 *Effect of Temperature on Metal Recovery of Ferromanganese Crust in 1% Sulfurous Acid Batch Leach, 30 Minute Leach Time, pH = 1.0, Pressure = 200 atm, 400 rpm Stir Rate.*

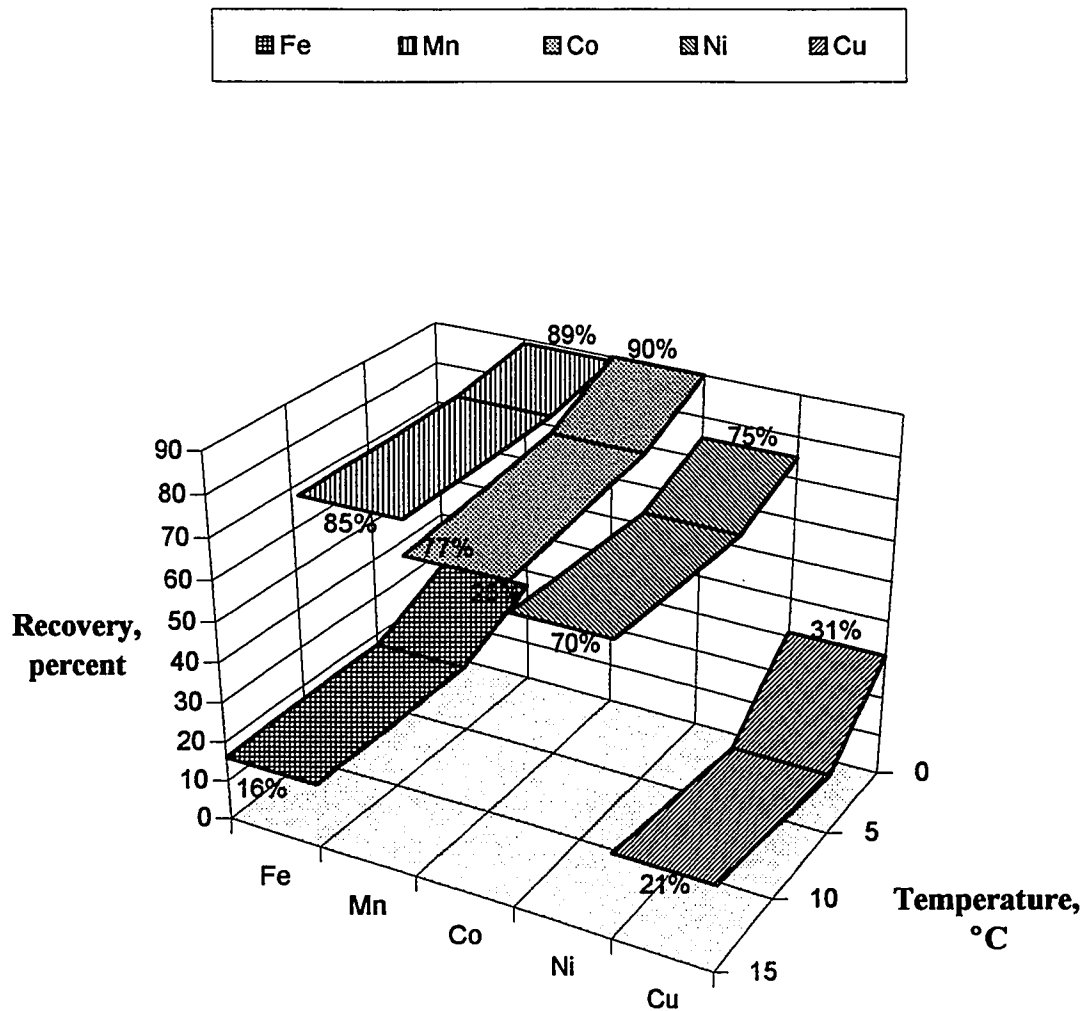


Figure 5.1.17 *Effect of Temperature on Metal Recovery of Ferromanganese Crust in 1% Sulfurous Acid Batch Leach, 30 Minute Leach Time, $pH = 2.0$, Pressure = 1 atm, 400 rpm Stir Rate.*

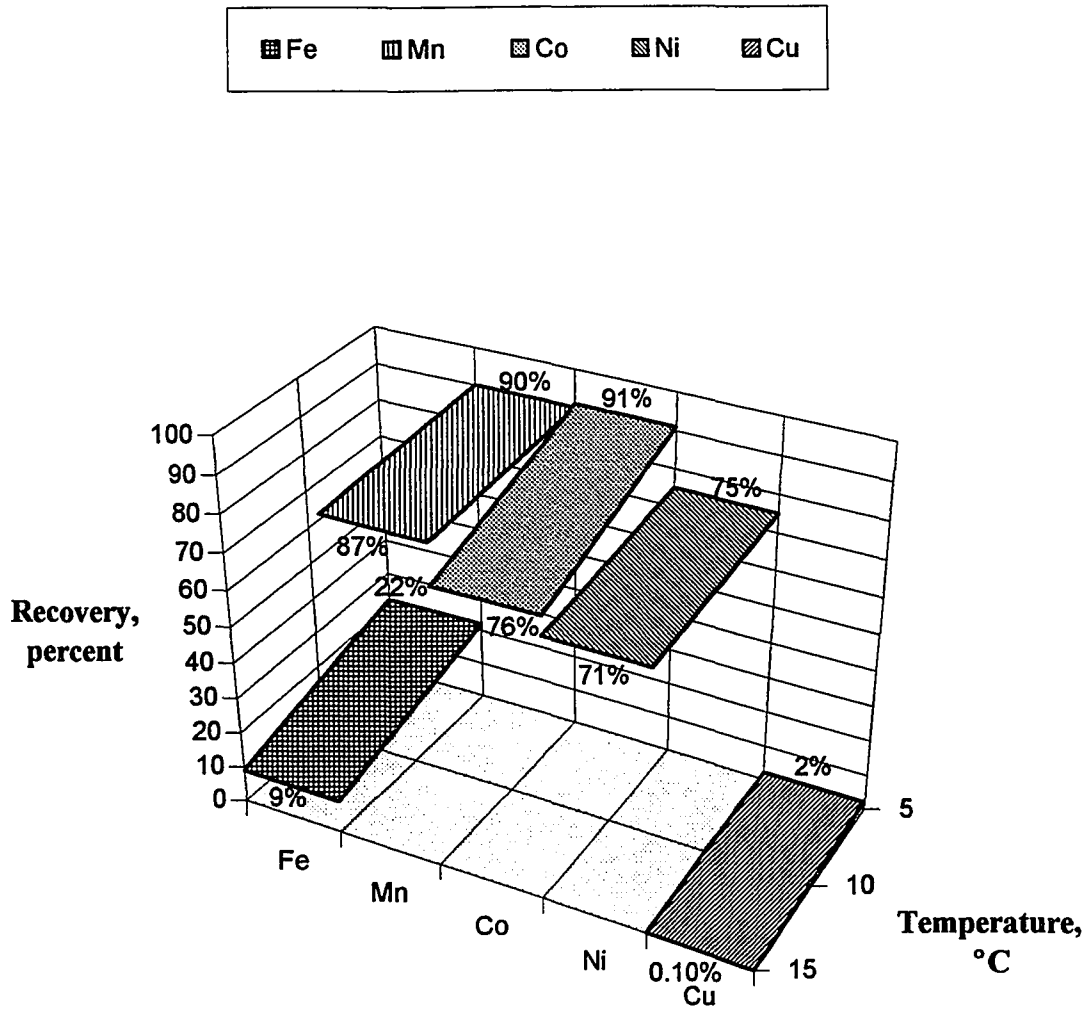


Figure 5.1.18 *Effect of Temperature on Metal Recovery of Ferromanganese Crust in 1% Sulfurous Acid Batch Leach, 30 Minute Leach Time, pH = 2.0, Pressure = 100 atm, 400 rpm Stir Rate.*

5.2 Effect of Pressure on Batch Leach Experiments

The effects of pressure on leach reaction recoveries (Co, Cu, Fe, Mn and Ni) are shown in Figures 5.2.1 to 5.2.12. As before, three-dimensional *ribbon charts* were selected to show the interrelation among the five transition metals. Standard deviation and replicate number for each data point are given in Appendix A.

The pressure effect on chemical equilibria is expected to increase the dissolution reaction (i.e., metal recovery) rate by a maximum factor estimated at 7% (previous Chapter, Section 4.1.2). The experimental data shows for the Fe, Mn, Co, and Ni species, very slight to no discernable increase of recovery with increasing pressure when $\text{pH} = 1.0$ and strong correlation of an increase of recovery with increasing pressure when $\text{pH} \geq 2.0$.

A very different trend is seen for the Cu species. In nearly every series, Cu shows a marked decrease in recovery with increasing pressure. This effect may be due to pressure induced hydration causing precipitation of $\text{Cu}(\text{OH})_2$ or possibly a shift in the Eh dependant boundary between the soluble Cu^{2+} and solid Cu species with pressure. Measured direct redox potential of prepared pre-leach solutions for all leach experiments was 0.18 ± 0.04 V. Figure 5.2.13 depicts the simple Cu-O-H system and shows that the batch experiment pre-leach redox level is right at the Eh dependant boundary between the soluble and solid Cu species. The experimental result of this research suggests a shift in the Eh dependant boundary between the soluble and solid Cu species to a more oxidizing level with increasing pressure. However, there is little in the literature to support this boundary shift mechanism. Most Eh-pH data are limited to equilibrium conditions at 1 atm and 25°C (Brookins, 1988).

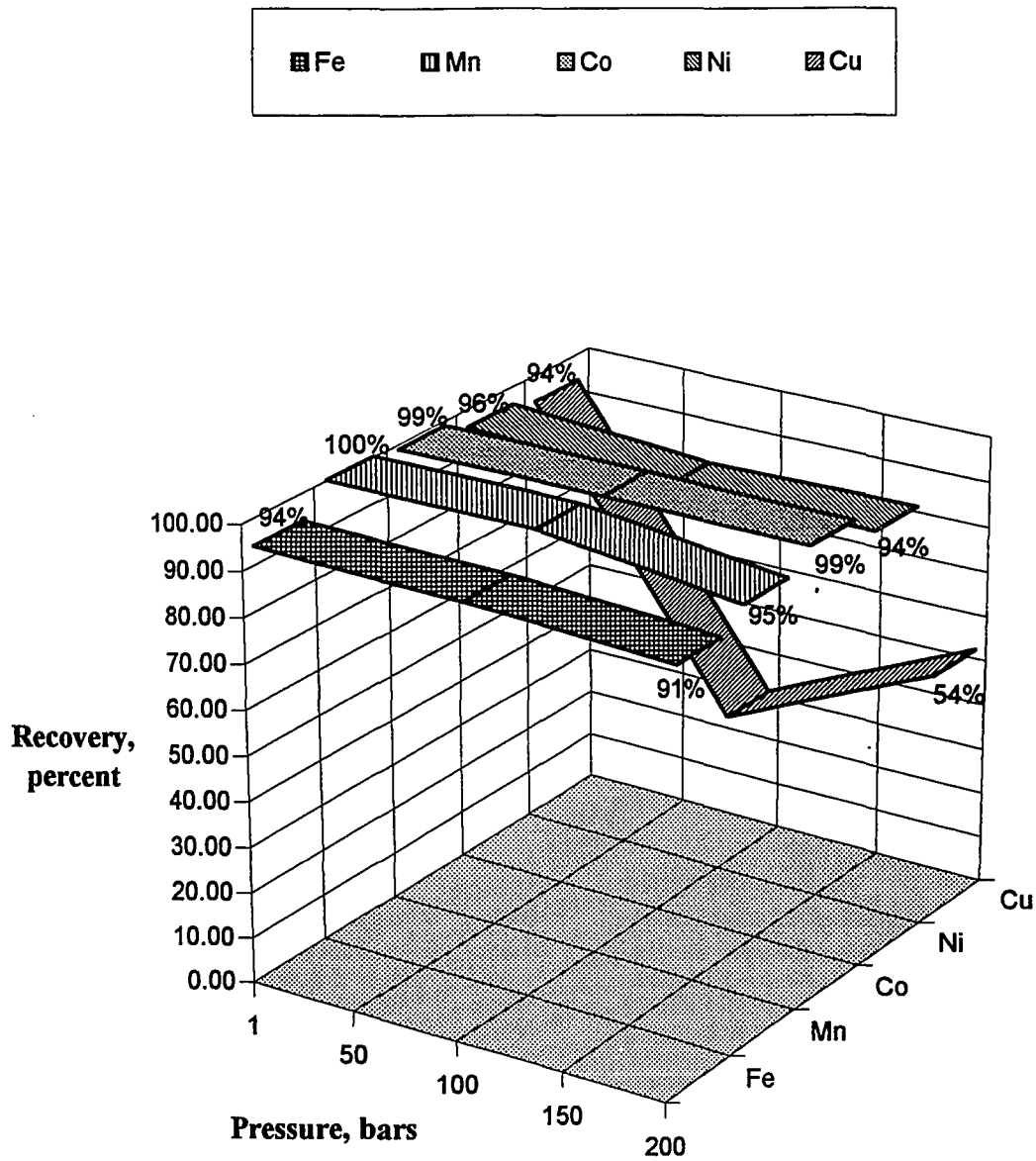


Figure 5.2.1 *Effect of Pressure on Metal Recovery of Ferromanganese Crust in 1% Sulfurous Acid Batch Leach, 5 Minute Leach Time, pH = 1.0, Temperature = 15 °C, 400 rpm Stir Rate.*

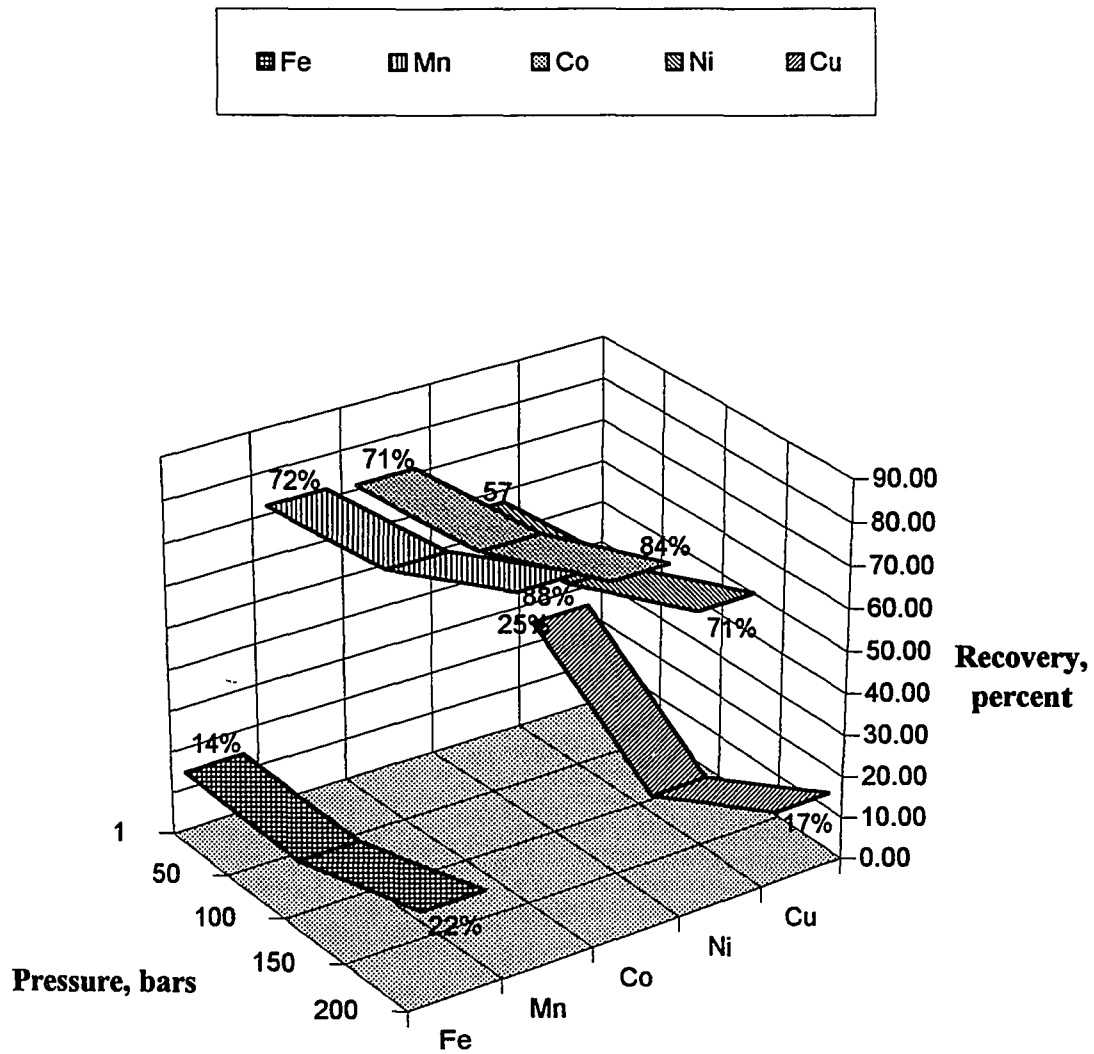


Figure 5.2.2 *Effect of Pressure on Metal Recovery of Ferromanganese Crust in 1% Sulfurous Acid Batch Leach, 5 Minute Leach Time, $pH = 2.0$, Temperature = 15 °C, 400 rpm Stir Rate.*

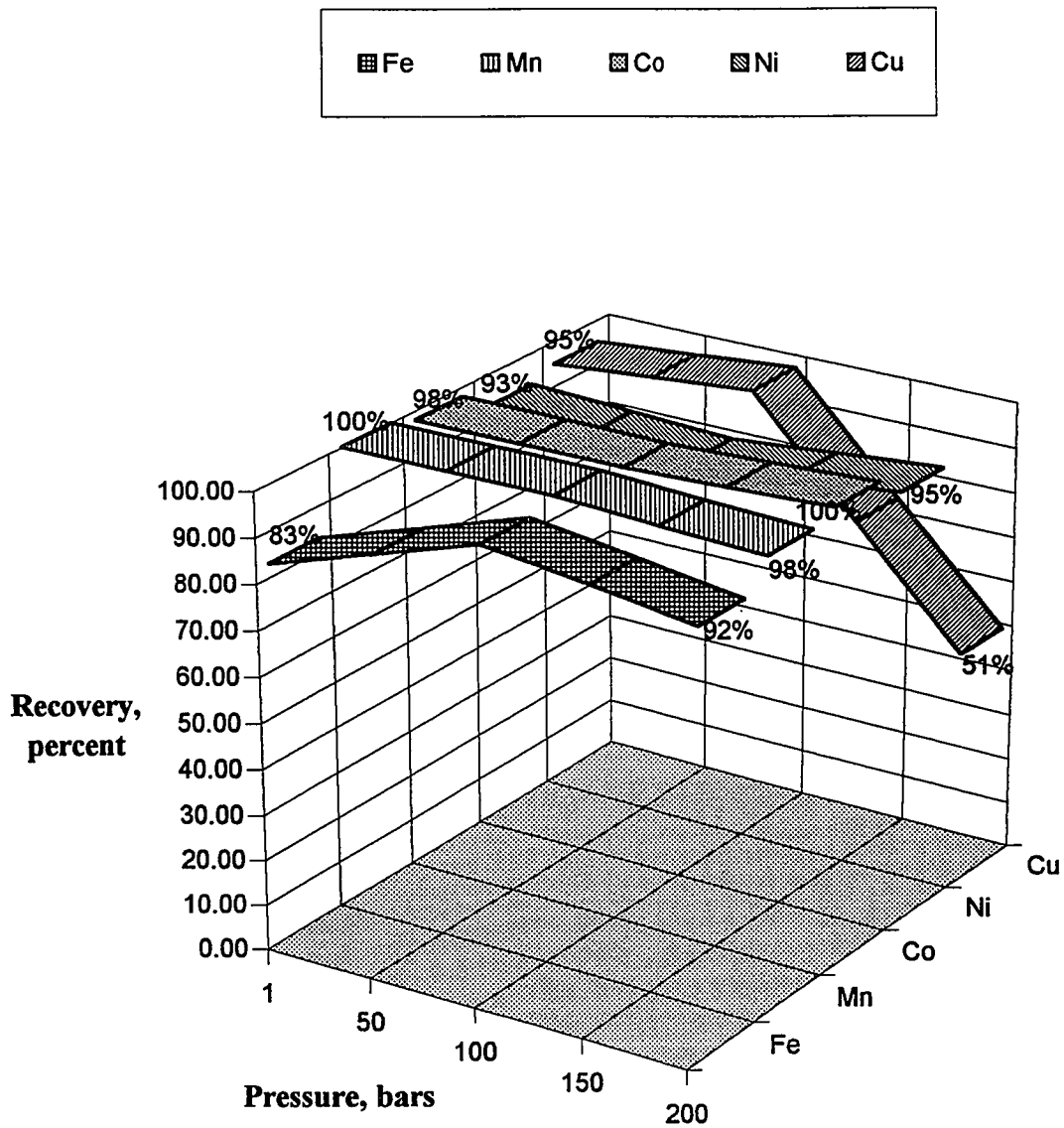


Figure 5.2.3 *Effect of Pressure on Metal Recovery of Ferromanganese Crust in 1% Sulfurous Acid Batch Leach, 15 Minute Leach Time, pH = 1.0, Temperature = 5 °C, 400 rpm Stir Rate.*

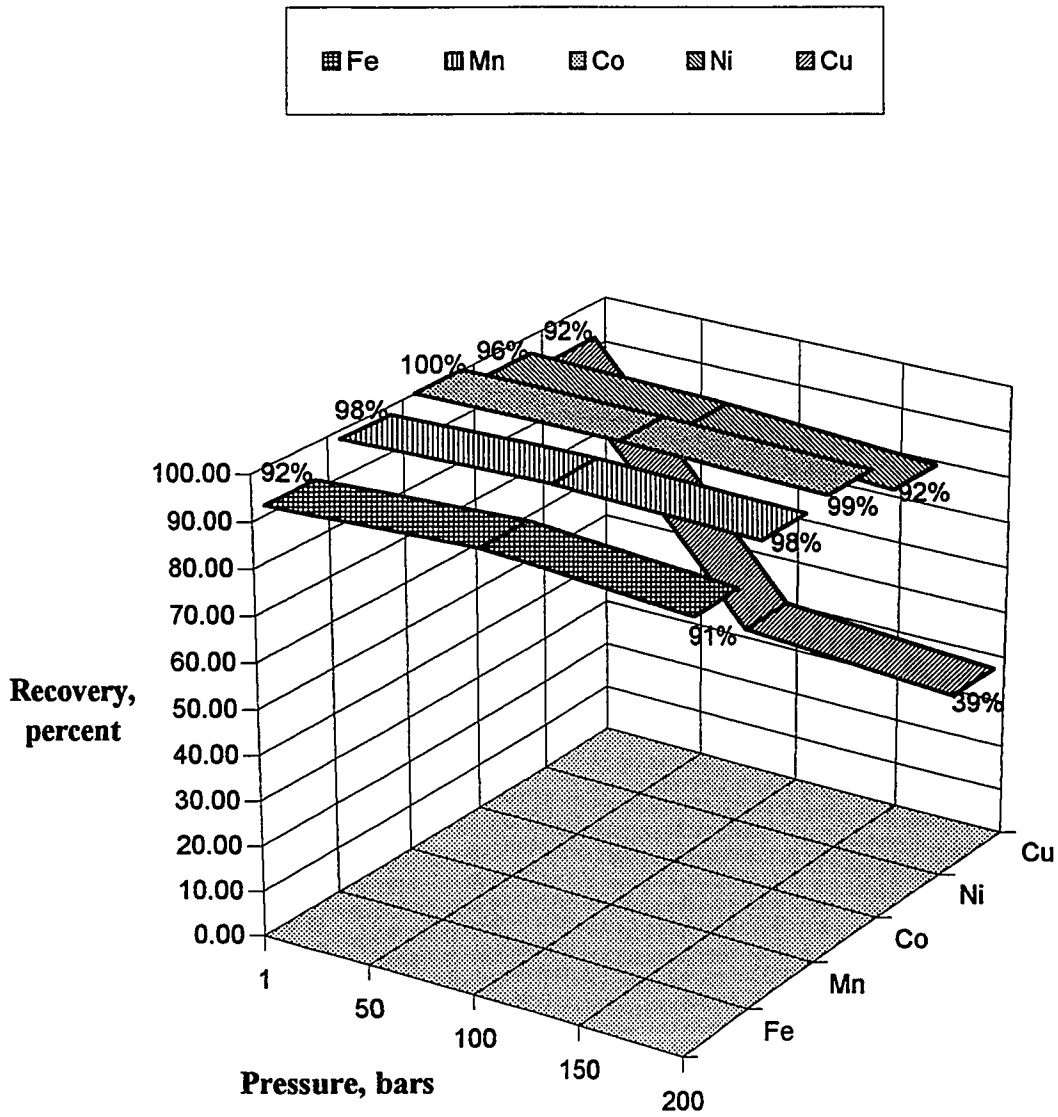


Figure 5.2.4 *Effect of Pressure on Metal Recovery of Ferromanganese Crust in 1% Sulfurous Acid Batch Leach, 15 Minute Leach Time, pH = 1.0, Temperature = 15 °C, 400 rpm Stir Rate.*

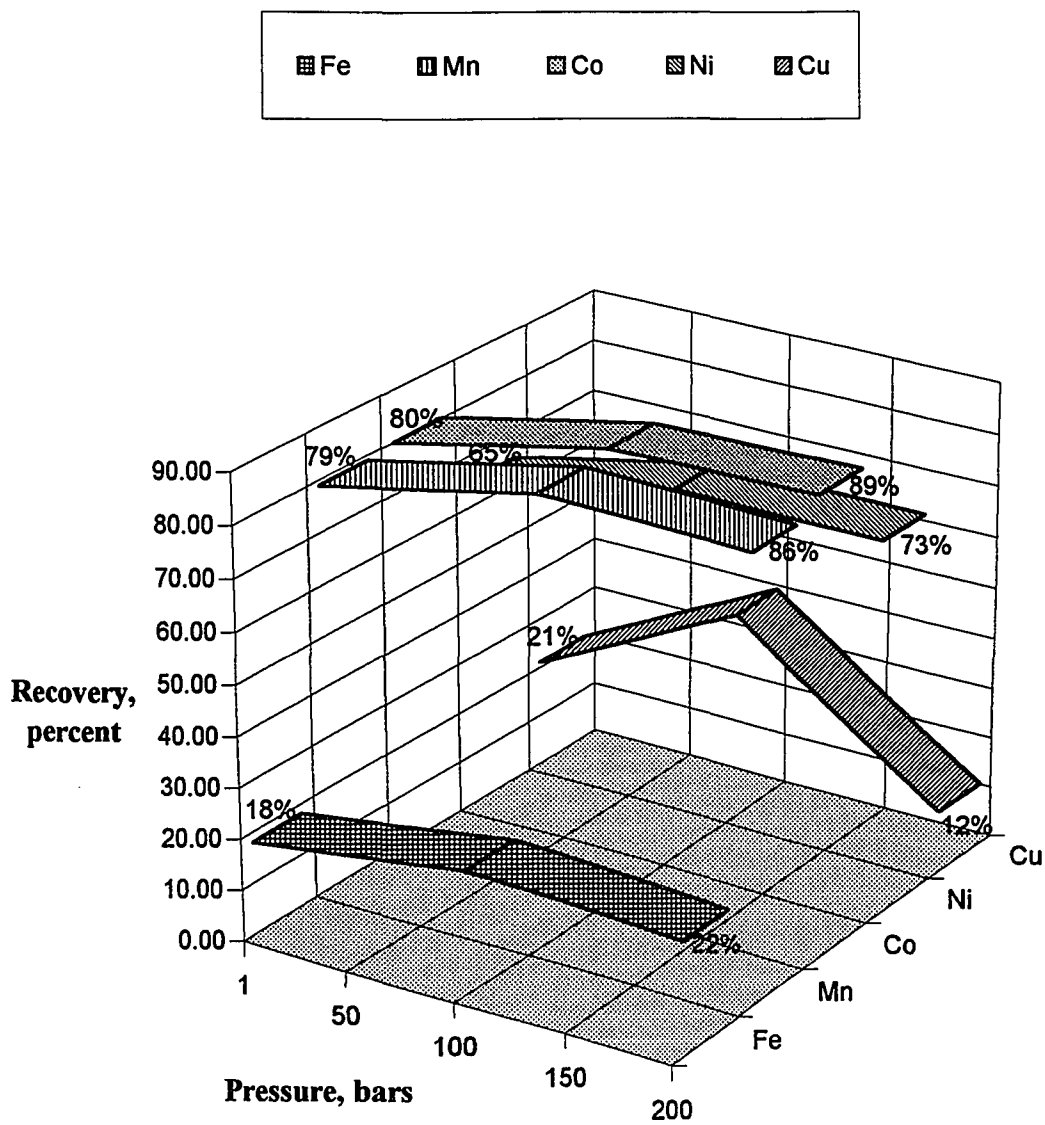


Figure 5.2.5 *Effect of Pressure on Metal Recovery of Ferromanganese Crust in 1% Sulfurous Acid Batch Leach, 15 Minute Leach Time, $pH = 2.0$, Temperature = $5^{\circ}C$, 400 rpm Stir Rate.*

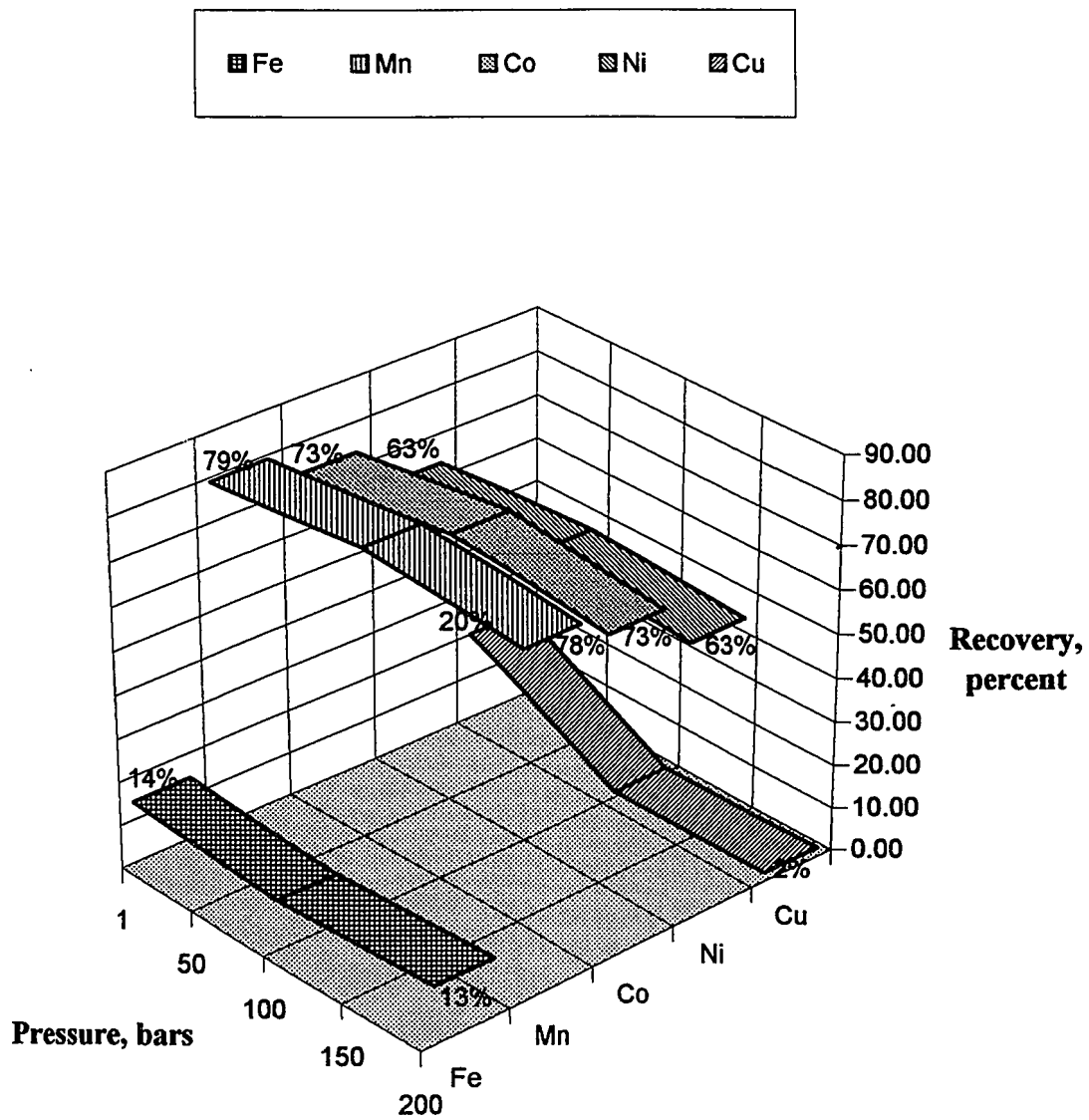


Figure 5.2.6 *Effect of Pressure on Metal Recovery of Ferromanganese Crust in 1% Sulfurous Acid Batch Leach, 15 Minute Leach Time, pH = 2.0, Temperature = 15 °C, 400 rpm Stir Rate.*

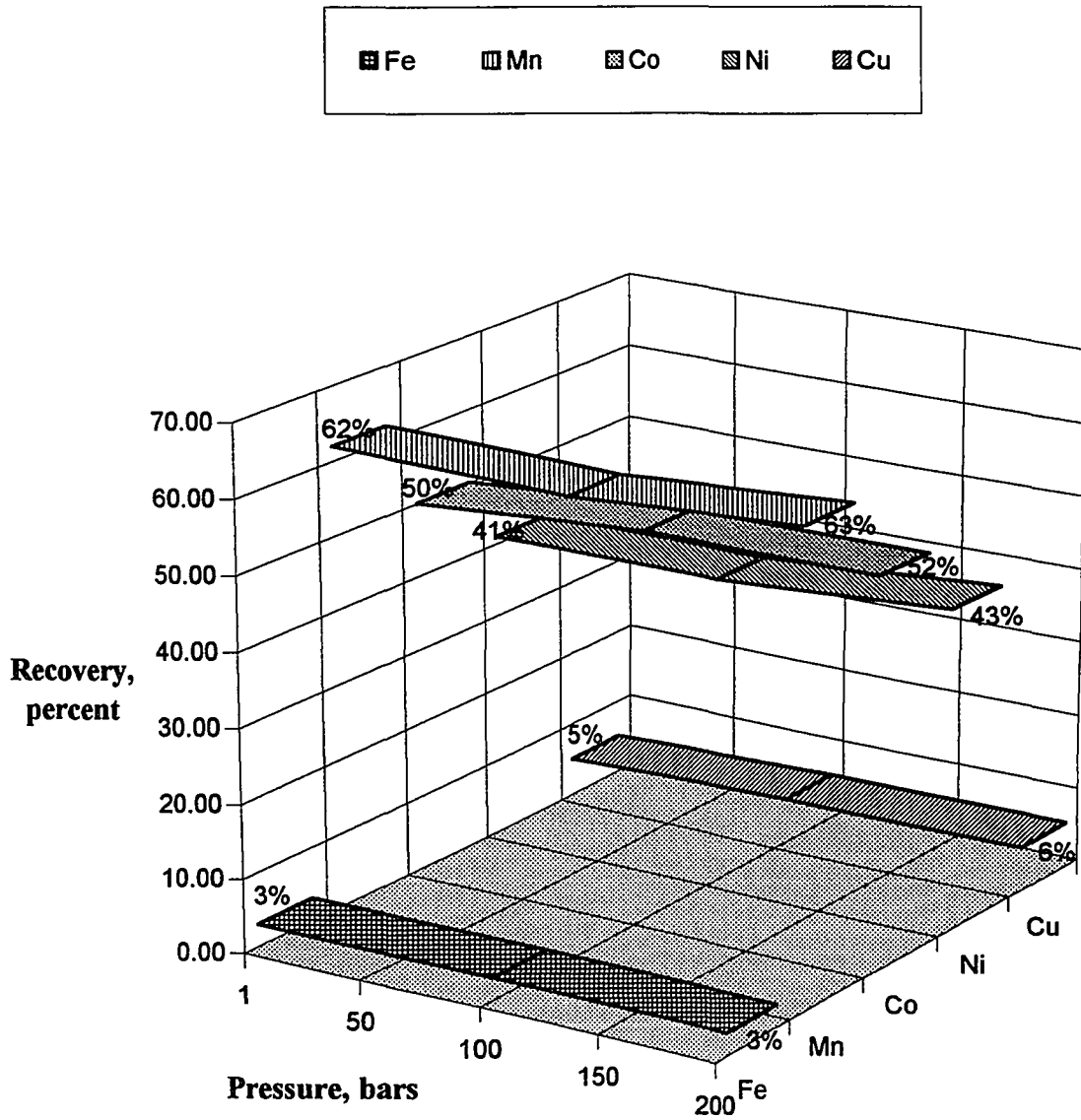


Figure 5.2.7 *Effect of Pressure on Metal Recovery of Ferromanganese Crust in 1% Sulfurous Acid Batch Leach, 15 Minute Leach Time, $\text{pH} = 3.0$, $\text{Temperature} = 5^\circ\text{C}$, 400 rpm Stir Rate.*

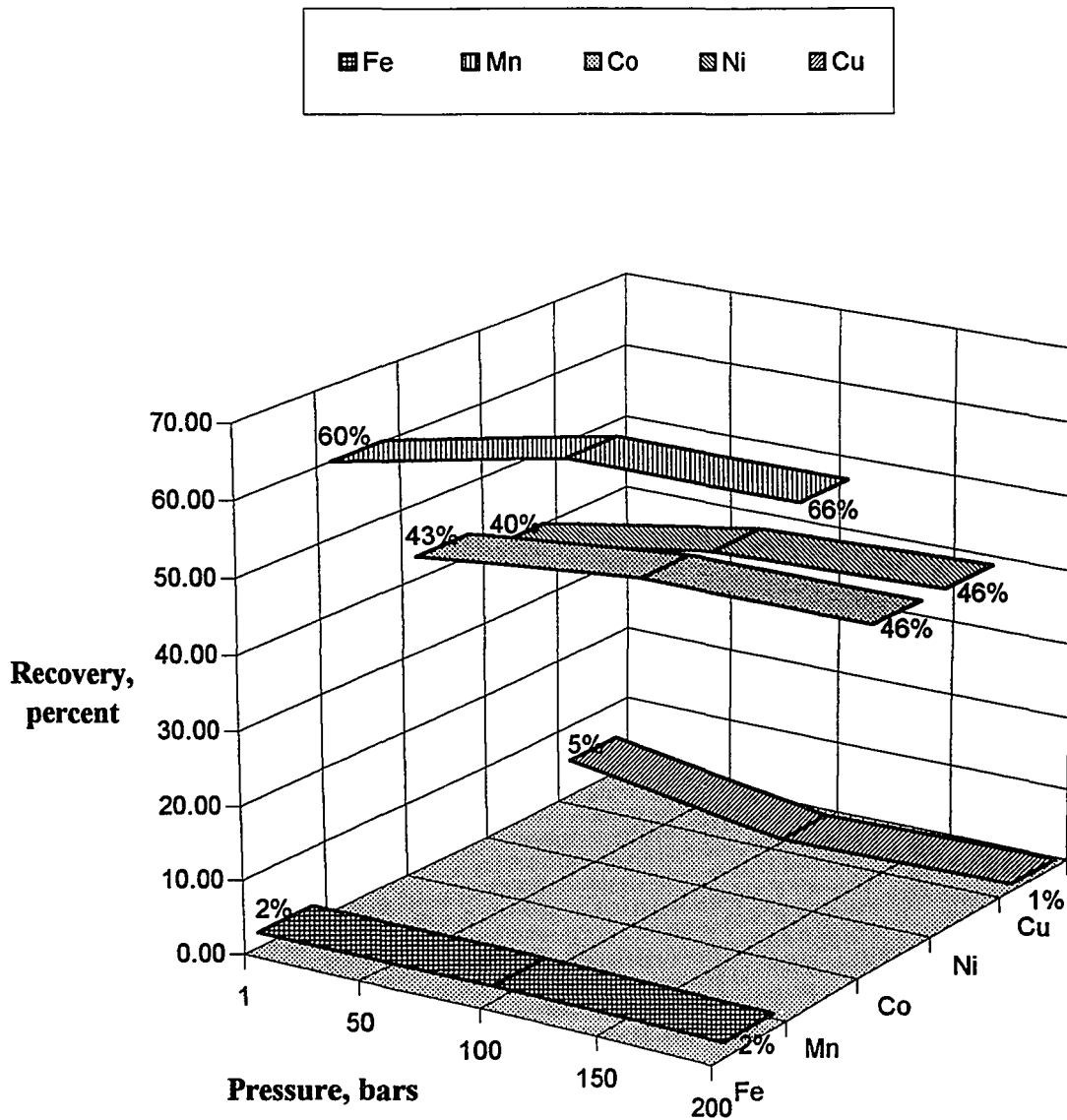


Figure 5.2.8 *Effect of Pressure on Metal Recovery of Ferromanganese Crust in 1% Sulfurous Acid Batch Leach, 15 Minute Leach Time, pH = 3.0, Temperature = 15 °C, 400 rpm Stir Rate.*

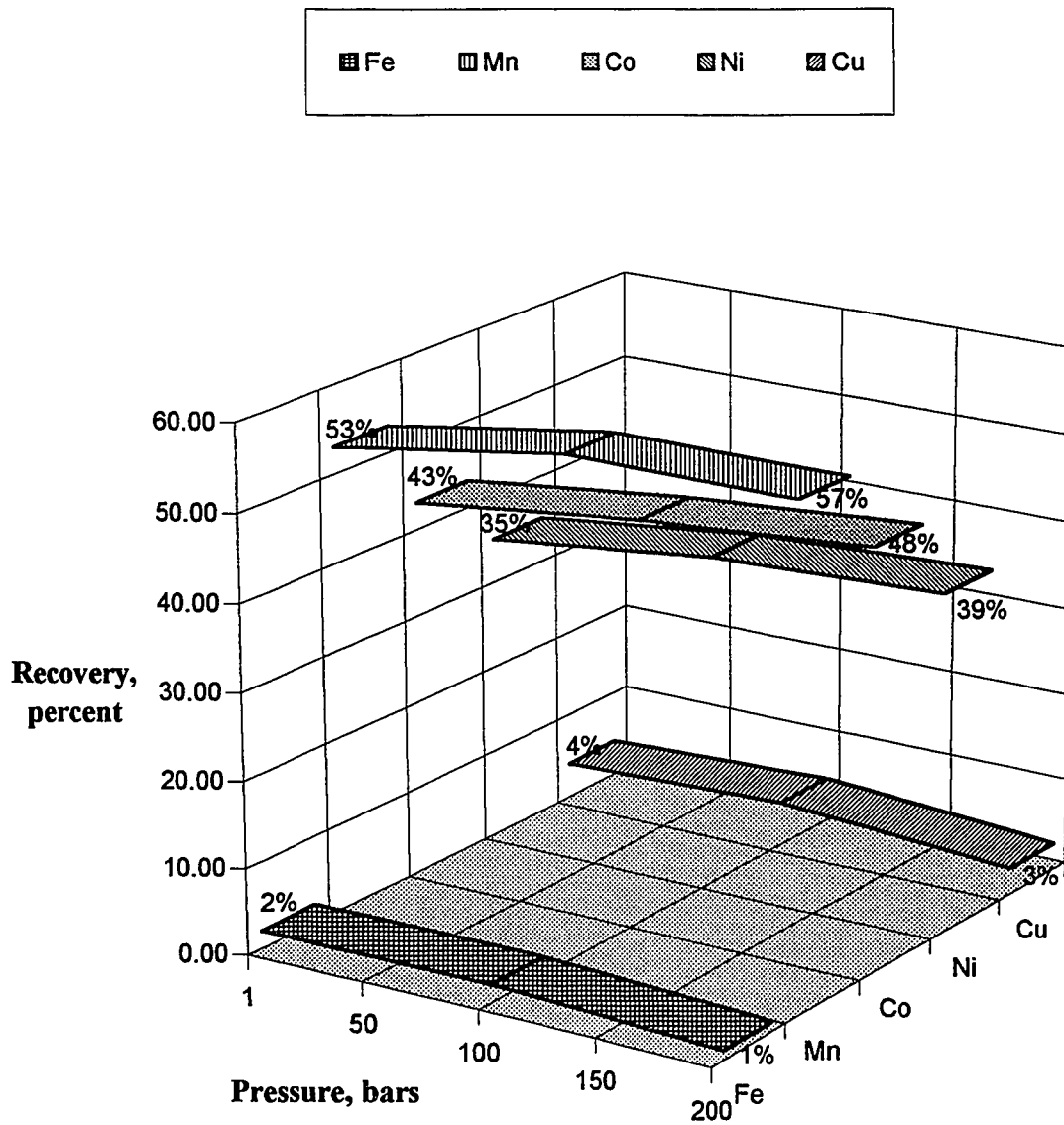


Figure 5.2.9 *Effect of Pressure on Metal Recovery of Ferromanganese Crust in 1% Sulfurous Acid Batch Leach, 15 Minute Leach Time, pH = 5.0, Temperature = 5 °C, 400 rpm Stir Rate.*

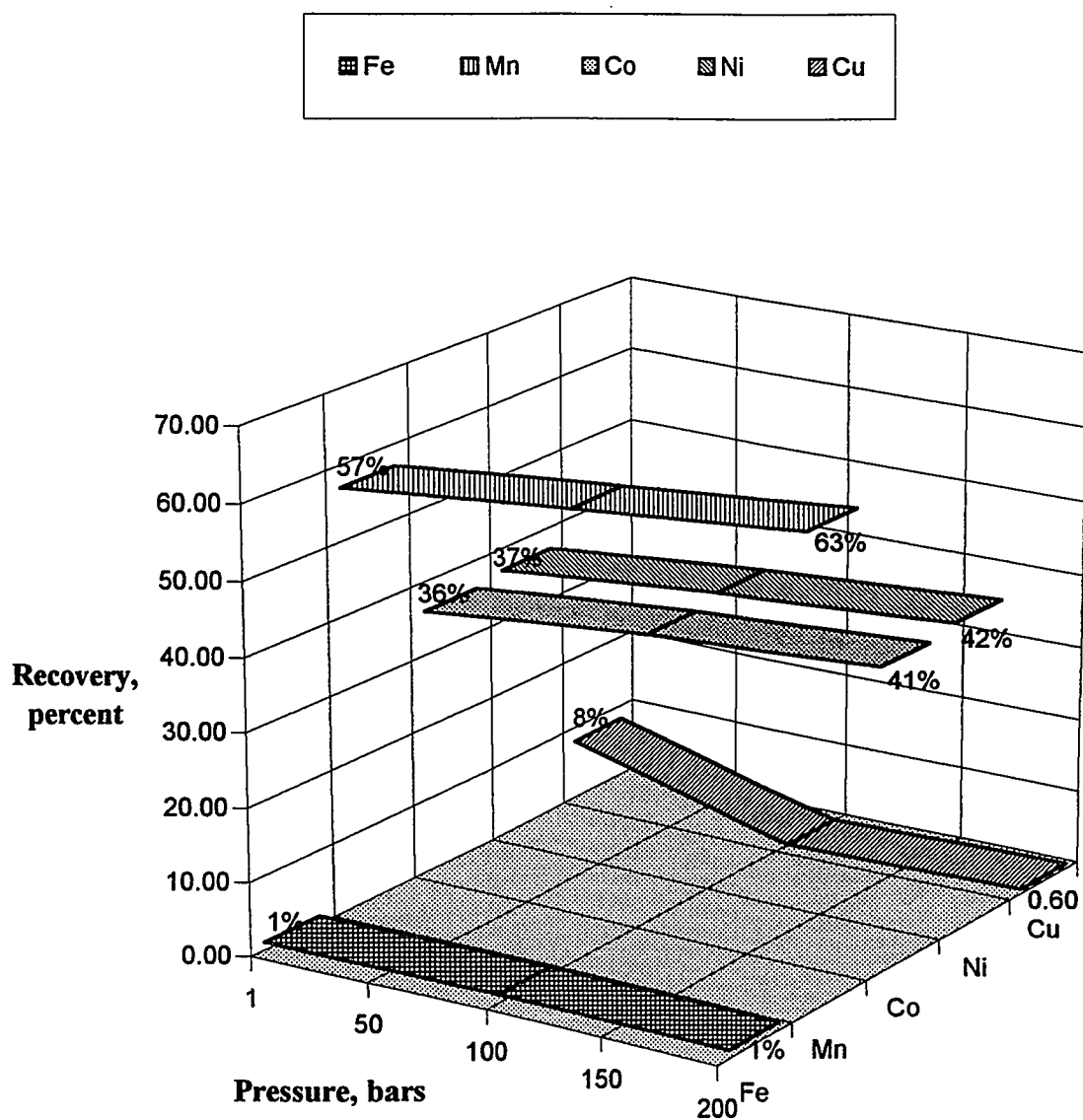


Figure 5.2.10 *Effect of Pressure on Metal Recovery of Ferromanganese Crust in 1% Sulfurous Acid Batch Leach, 15 Minute Leach Time, pH = 5.0, Temperature = 15 °C, 400 rpm Stir Rate.*

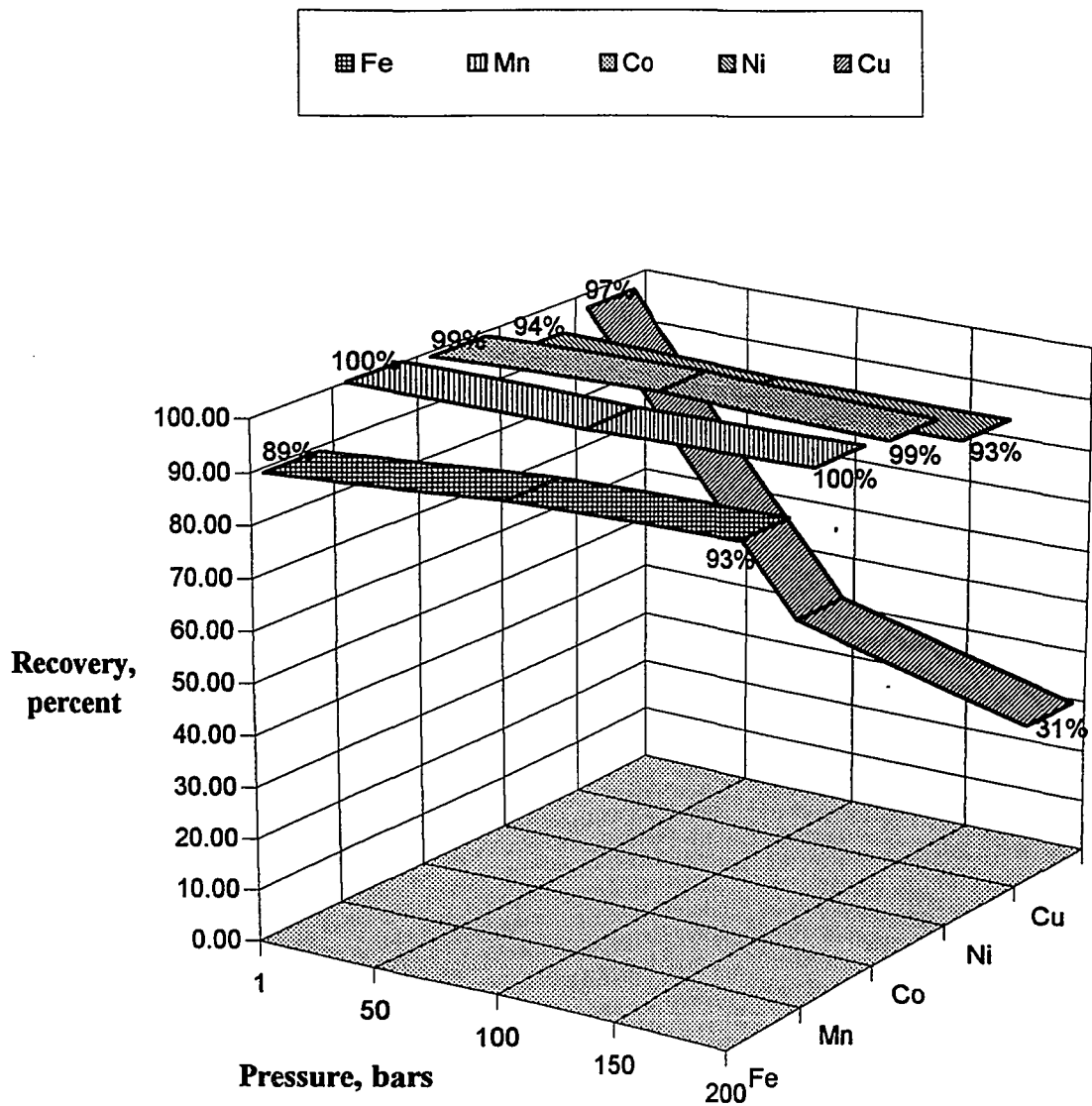


Figure 5.2.11 *Effect of Pressure on Metal Recovery of Ferromanganese Crust in 1% Sulfurous Acid Batch Leach, 30 Minute Leach Time, pH = 1.0, Temperature = 5 °C, 400 rpm Stir Rate.*

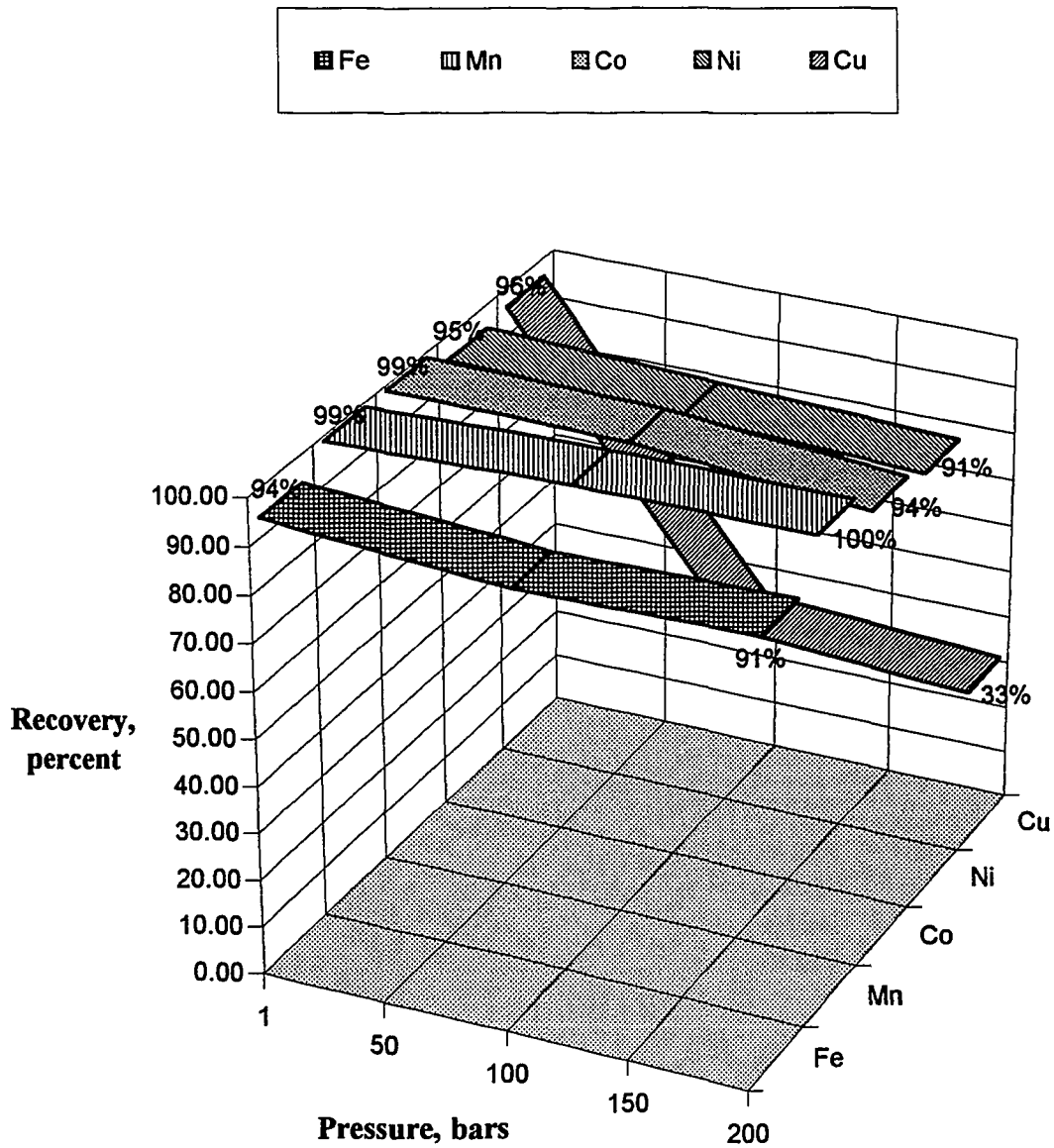


Figure 5.2.12 *Effect of Pressure on Metal Recovery of Ferromanganese Crust in 1% Sulfurous Acid Batch Leach, 30 Minute Leach Time, pH = 1.0, Temperature = 15 °C, 400 rpm Stir Rate.*

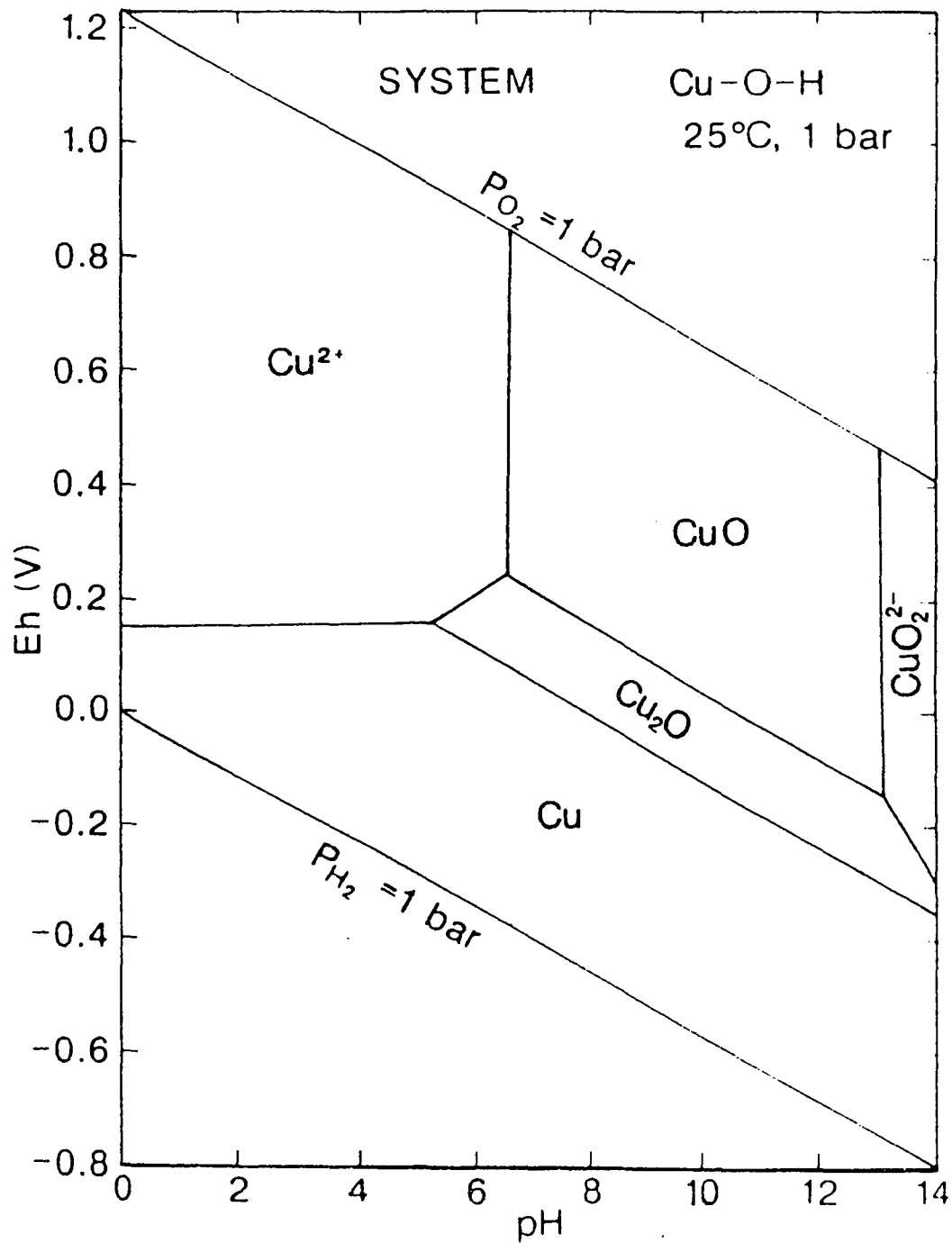


Figure 5.2.13 Eh-pH Diagram for the Simple Cu-O-H Geochemical System. The Assumed Activity for Dissolved Cu = 10^{-6} . After Brookins (1988).

5.3 Effect of pH on Batch Leach Experiments

Previous work (Khalafalla and Pahlman, 1981; Schein, 1986) on the sulfurous acid dissolution of ground ferromanganese nodules at 25°C, showed that the reaction rate is very dependant on pH, and less sensitive to minor change in $\text{SO}_{2(\text{aq})}$ concentration. Since the rate of reaction is very fast, batch experiment reactions go to near completion in less than ten minutes over a range in $\text{SO}_{2(\text{aq})}$ concentrations from 1% to ~9% (saturation). This holds true if the stoichiometry of the reactants is above a minimum threshold level, i.e., $\text{SO}_{2(\text{aq})} \geq 0.015$ moles per gram of ferro-manganese oxide (~ 0.011 moles). A few early trials confirmed this relative insensitivity to concentration, so nearly all of the batch leach experiments were performed using 0.030 moles of Na_2SO_3 dissolved in a pre-leach solution. This pre-leach solution when mixed with the brine density fluid in the reactor bottle, produced a synthetic seawater leach with $\text{SO}_{2(\text{aq})}$ concentration of ~ 1%. The primary reason for selecting the 1% $\text{SO}_{2(\text{aq})}$ concentration as the standard for the batch leach experiments was human comfort. Using $\text{SO}_{2(\text{aq})}$ concentrations of 1% greatly reduced the amount of volatile SO_2 gas released from solution during laboratory procedures compared with 5% or greater concentrations.

The effect of pH on leach chemistry is a major controlling factor as pH controls the speciation of SO_2 in the sulfurous acid system. As shown previously in Figure 3.3 (in Chapter 3), the reactive species, $\text{SO}_{2(\text{aq})}$ is predominant only when $\text{pH} < 2.0$. Consequently, an increase in pH above 2.0 drastically reduces the batch experiment dissolution rate (metal recovery). This dramatic decrease in recovery is clearly apparent in every series investigated, shown in Figures 5.3.1 to 5.3.10.

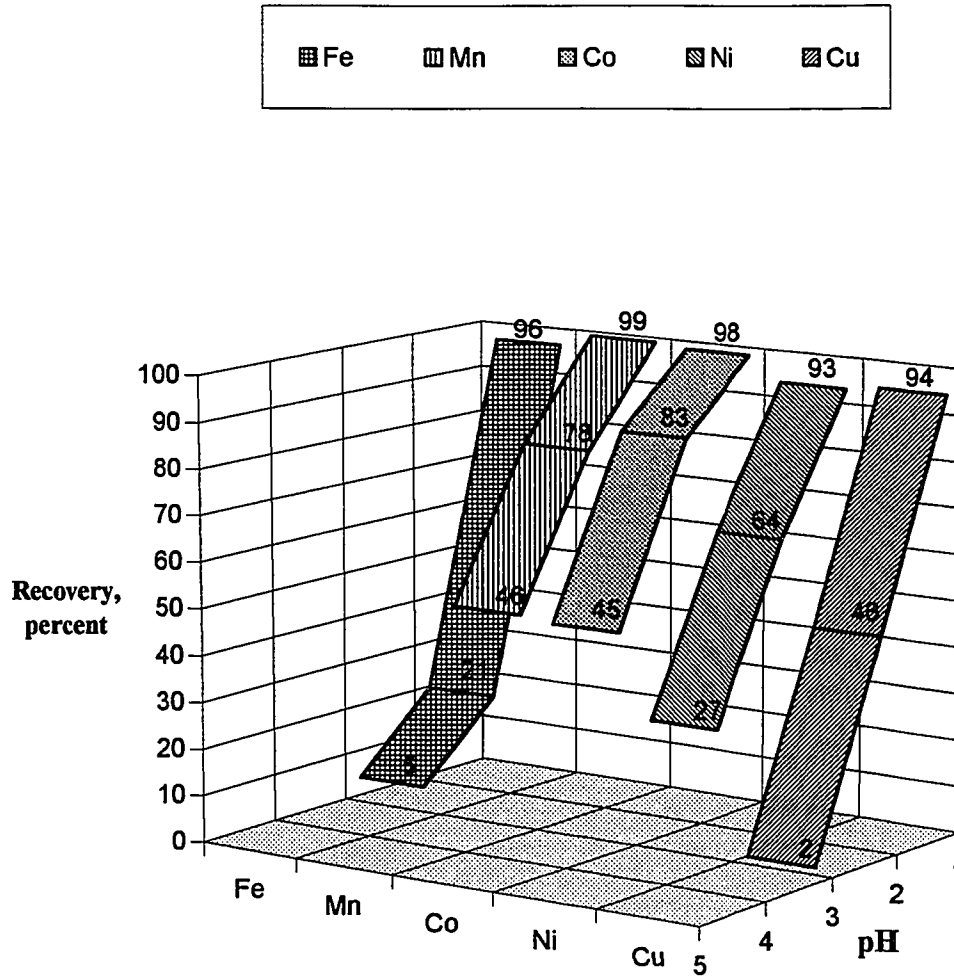


Figure 5.3.1 *Effect of pH on Metal Recovery of Ferromanganese Crust in 1% Sulfurous Acid Batch Leach, Leach Time = 5 Minutes, Temperature = 0.1 °C, Pressure = 1 atm, 400 rpm Stir Rate.*

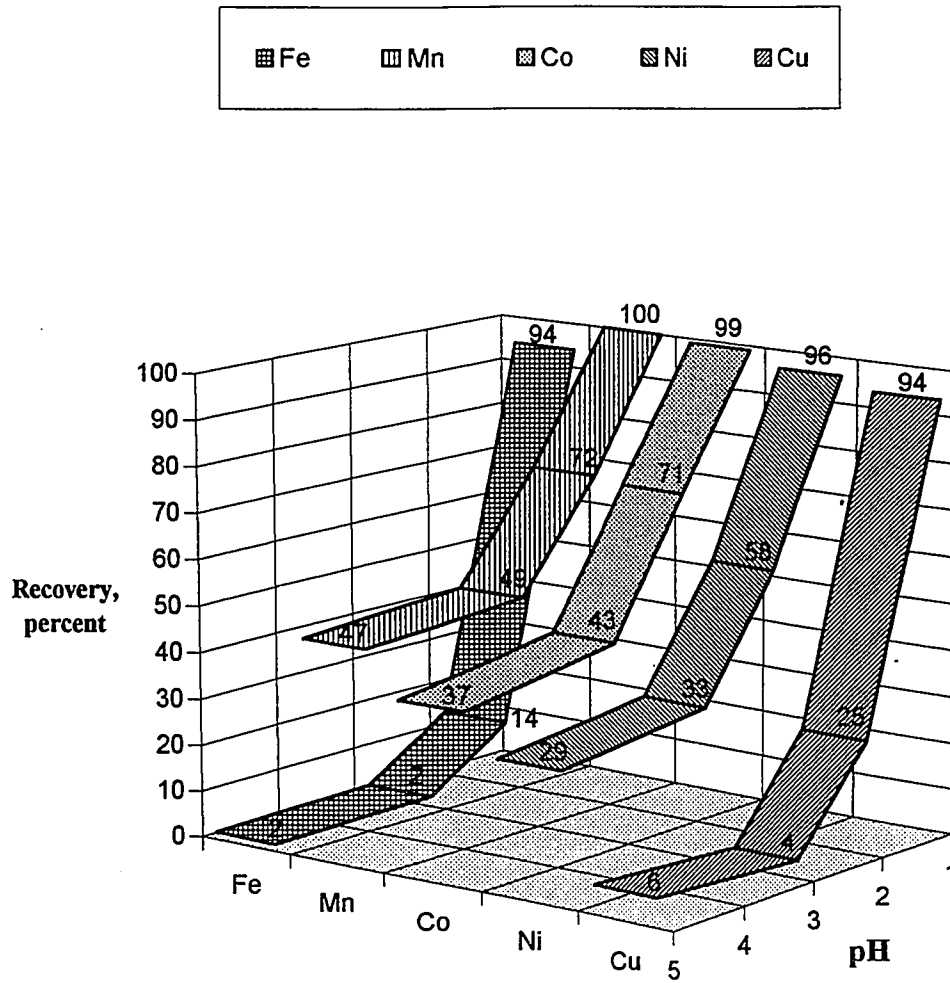


Figure 5.3.2 *Effect of pH on Metal Recovery of Ferromanganese Crust in 1% Sulfurous Acid Batch Leach, Leach Time = 5 Minutes, Temperature = 15 °C, Pressure = 1 atm, 400 rpm Stir Rate.*

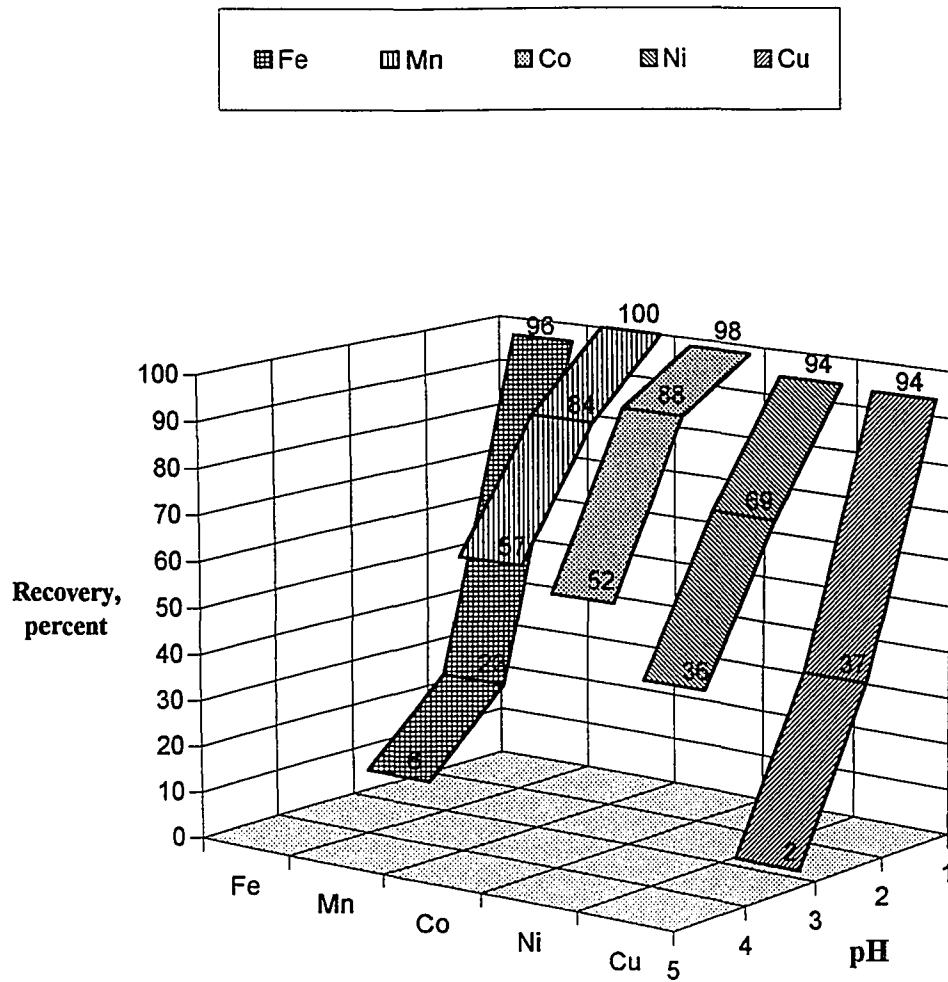


Figure 5.3.3 *Effect of pH on Metal Recovery of Ferromanganese Crust in 1% Sulfurous Acid Batch Leach, Leach Time = 15 Minutes, Temperature = 0.1 °C, Pressure = 1 atm, 400 rpm Stir Rate.*

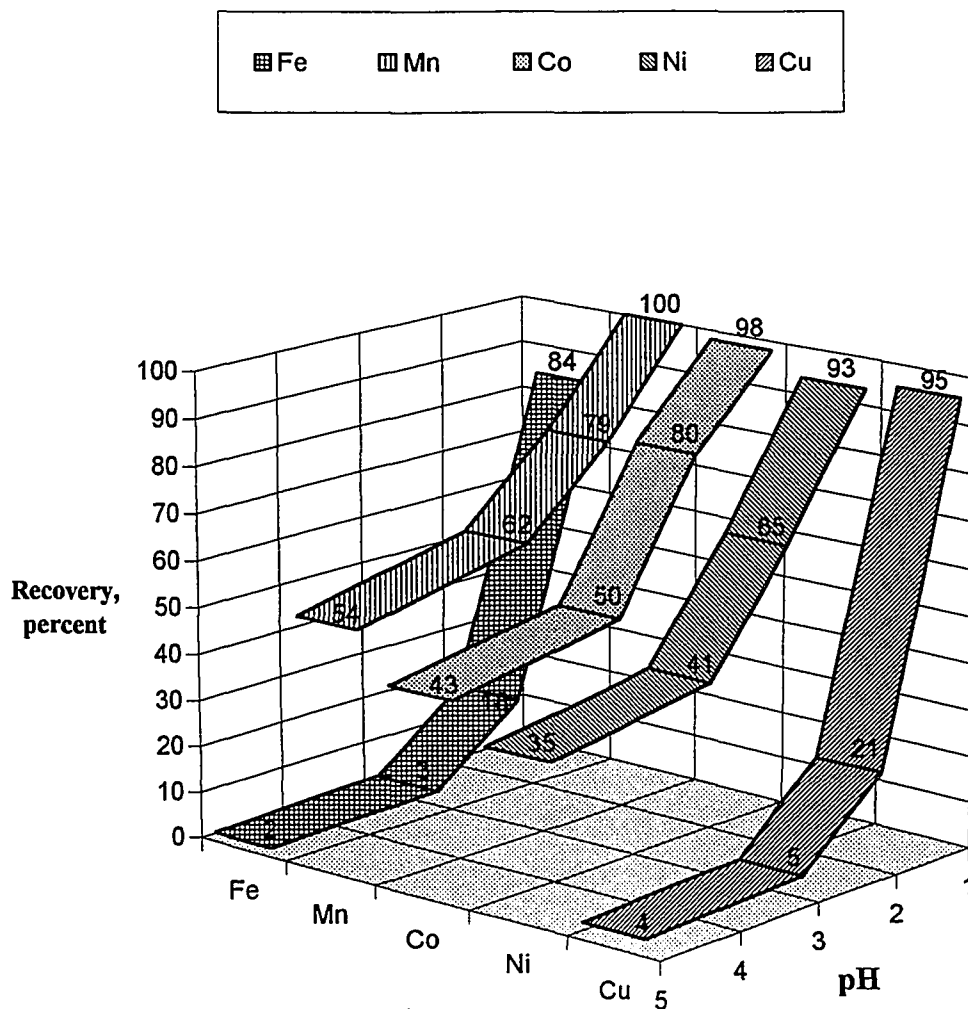


Figure 5.3.4 *Effect of pH on Metal Recovery of Ferromanganese Crust in 1% Sulfurous Acid Batch Leach, Leach Time = 15 Minutes, Temperature = 5 °C, Pressure = 1 atm, 400 rpm Stir Rate.*

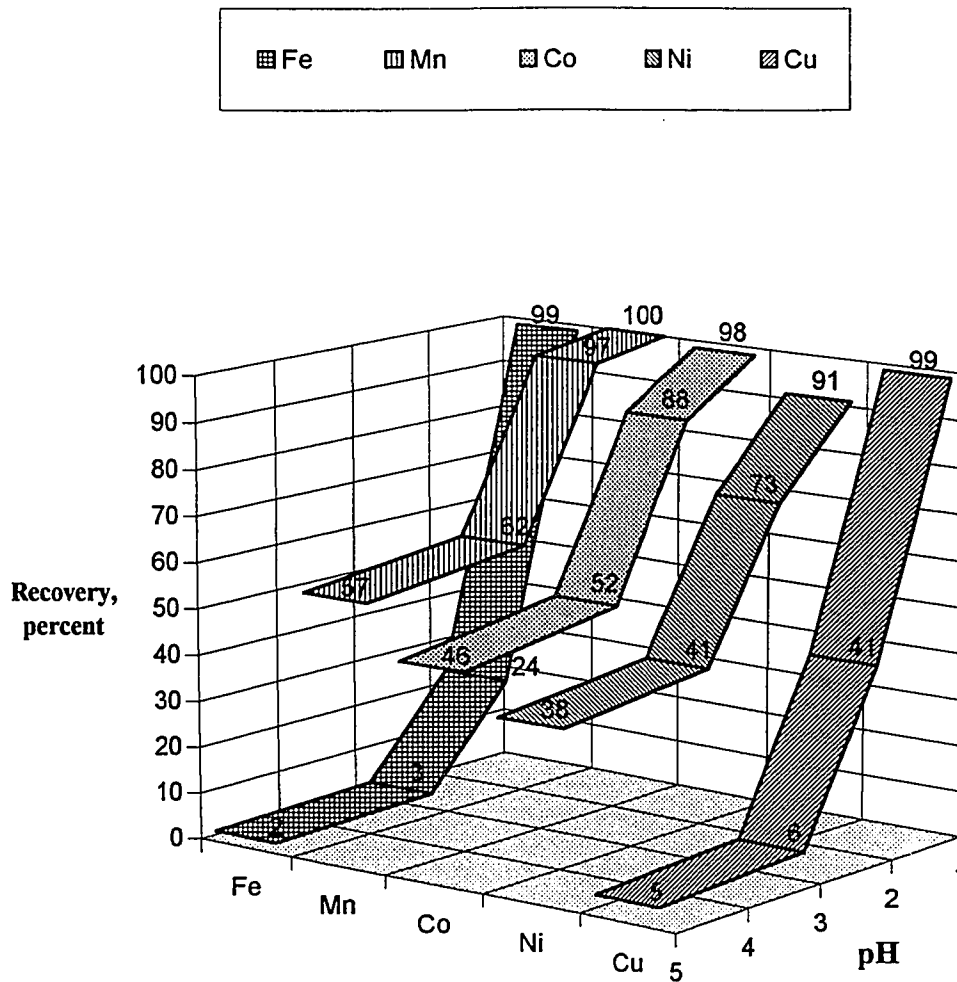


Figure 5.3.5 *Effect of pH on Metal Recovery of Ferromanganese Crust in 1% Sulfurous Acid Batch Leach, Leach Time = 15 Minutes, Temperature = 5 °C, Pressure = 100 atm, 400 rpm Stir Rate.*

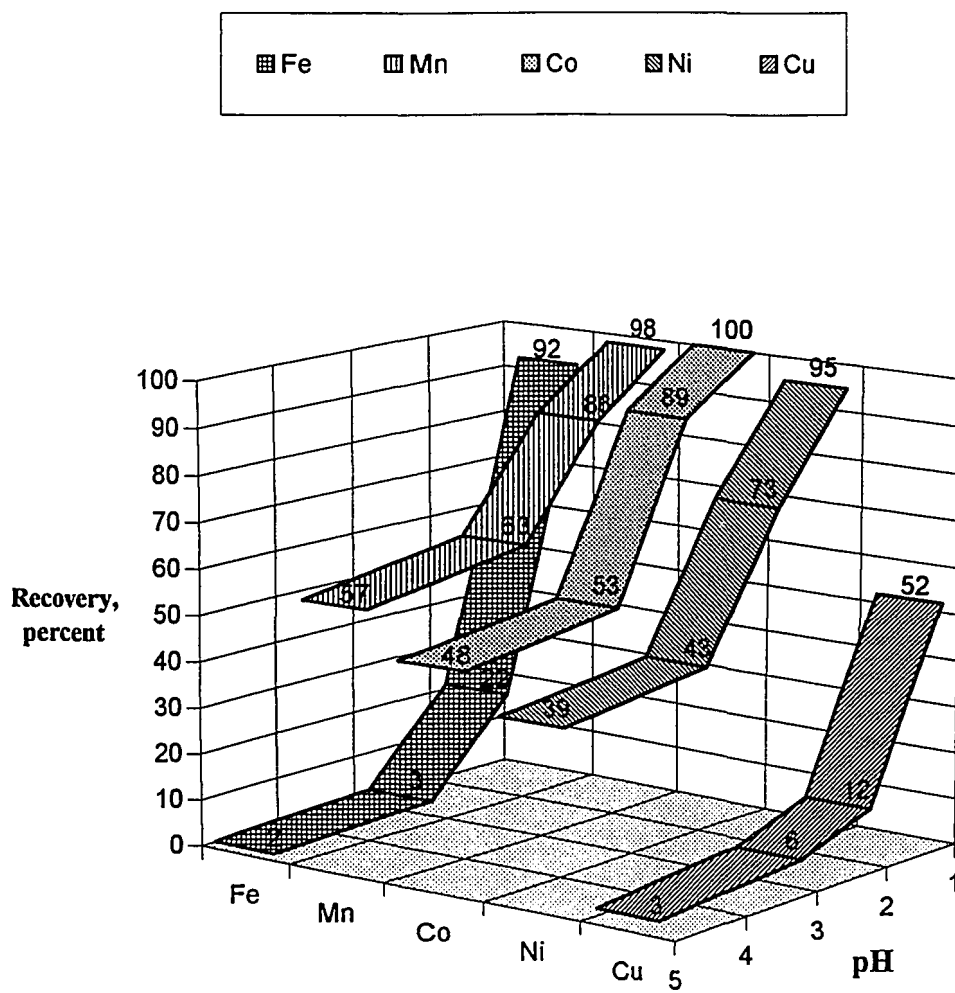


Figure 5.3.6 *Effect of pH on Metal Recovery of Ferromanganese Crust in 1% Sulfurous Acid Batch Leach, Leach Time = 15 Minutes, Temperature = 5 °C, Pressure = 200 atm, 400 rpm Stir Rate.*

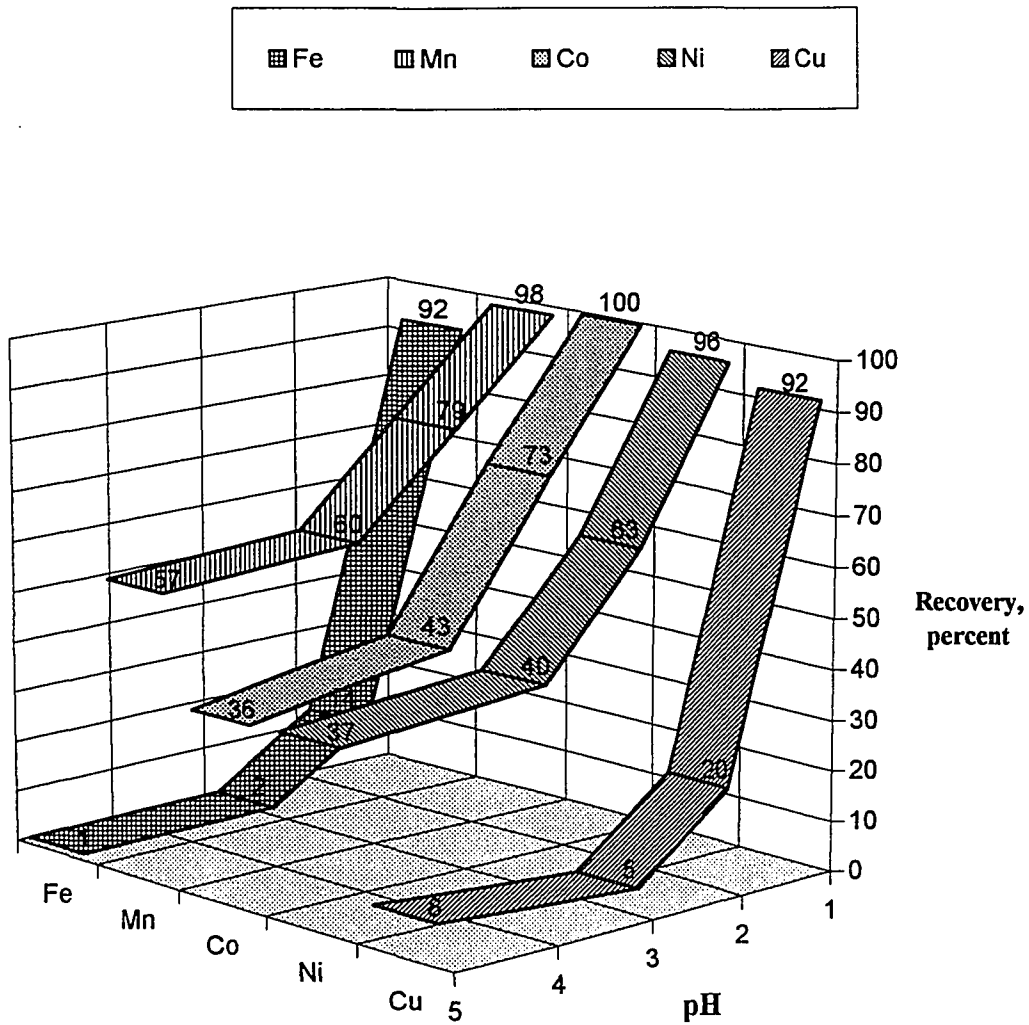


Figure 5.3.7 *Effect of pH on Metal Recovery of Ferromanganese Crust in 1% Sulfurous Acid Batch Leach, Leach Time = 15 Minutes, Temperature = 15 °C, Pressure = 1 atm, 400 rpm Stir Rate.*

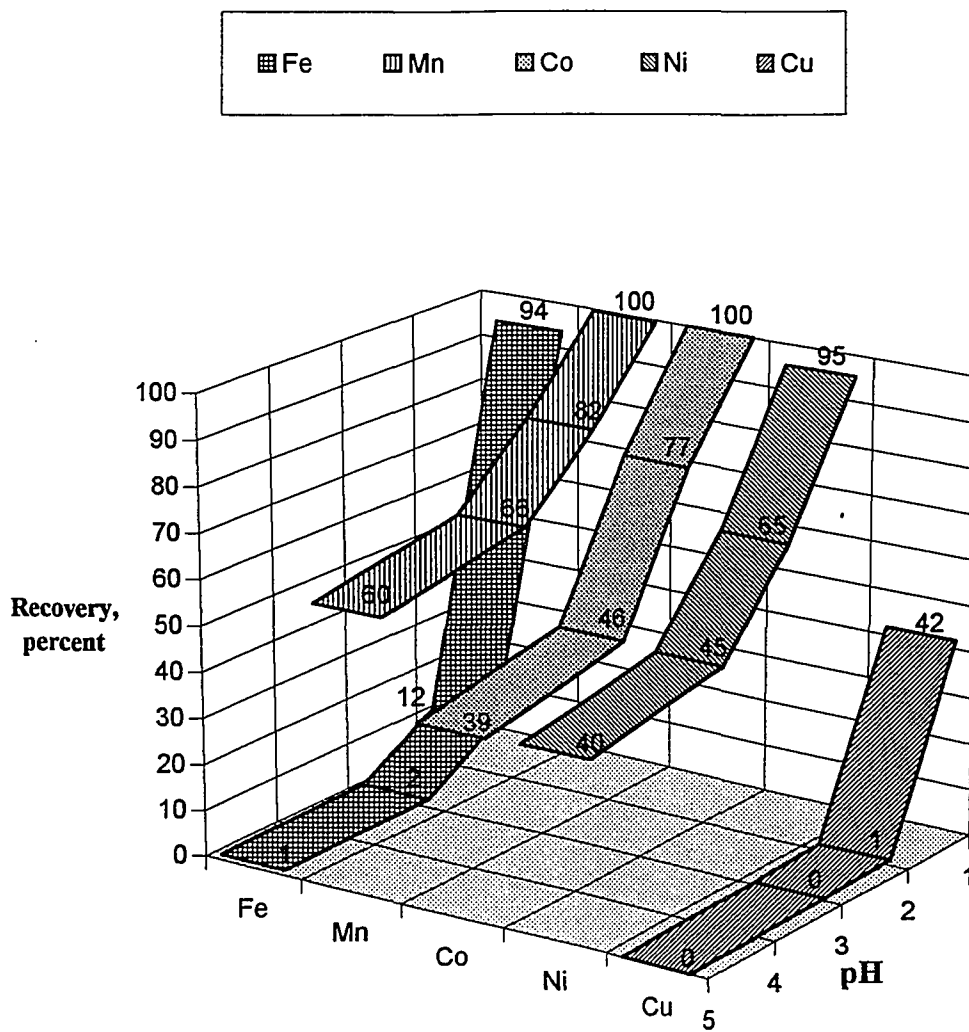


Figure 5.3.8 *Effect of pH on Metal Recovery of Ferromanganese Crust in 1% Sulfurous Acid Batch Leach, Leach Time = 15 Minutes, Temperature = 15 °C, Pressure = 100 atm, 400 rpm Stir Rate.*

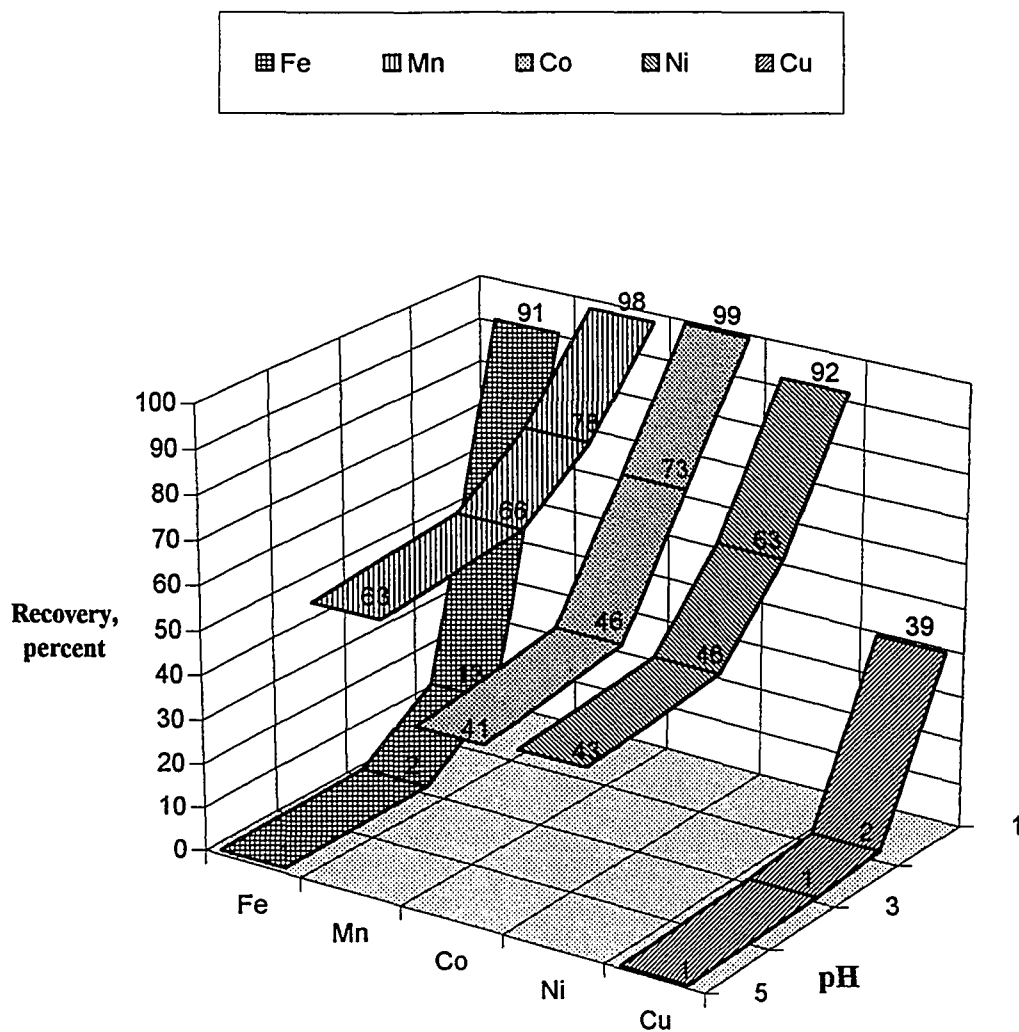


Figure 5.3.9 *Effect of pH on Metal Recovery of Ferromanganese Crust in 1% Sulfurous Acid Batch Leach, Leach Time = 15 Minutes, Temperature = 15 °C, Pressure = 200 atm, 400 rpm Stir Rate.*

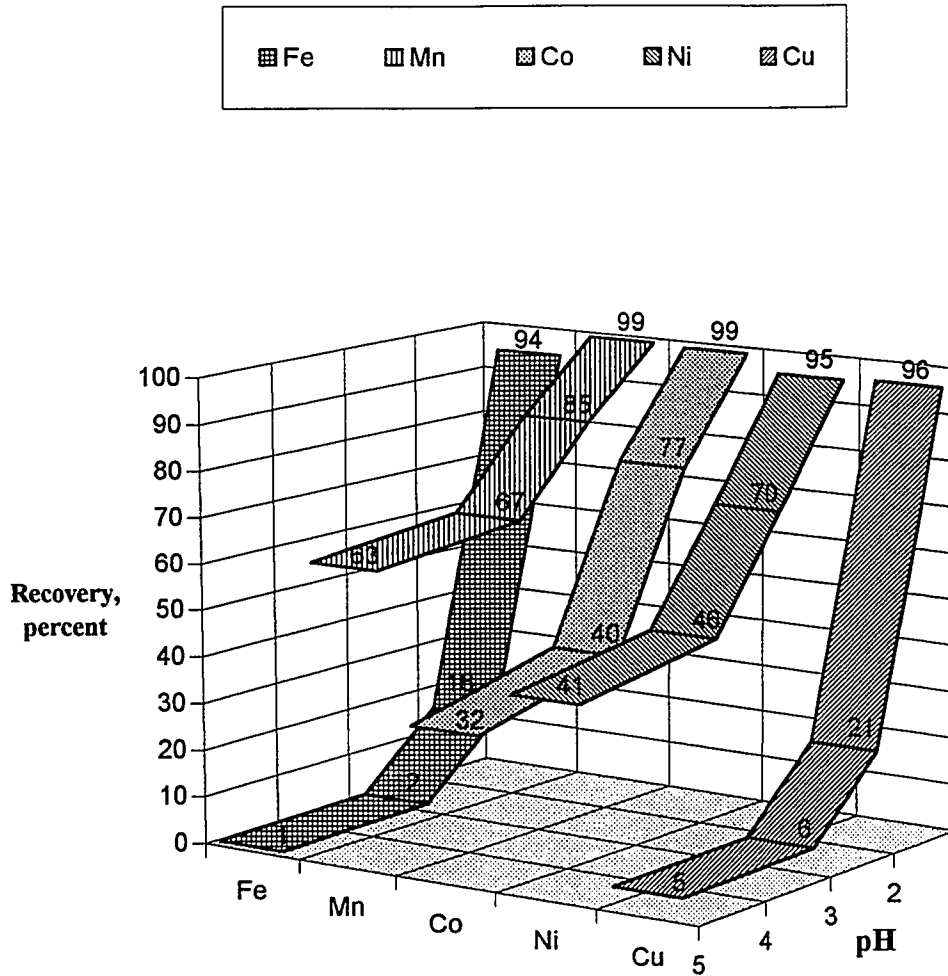


Figure 5.3.10 *Effect of pH on Metal Recovery of Ferromanganese Crust in 1% Sulfurous Acid Batch Leach, Leach Time = 30 Minutes, Temperature = 15 °C, Pressure = 1 atm, 400 rpm Stir Rate.*

5.4 Effect of Leach Duration on Batch Leach Experiments

The effect of leach time on metal recovery on the $\text{pH} = 1.0$ series of batch leach experiments (Figures 5.4.1 to 5.4.5) is very consistent. As the rate of reaction is very fast, leach experiments are essentially completed by five minutes, i.e., the metal recoveries attain maximum value and remain there. Of note is the striking loss in the maximum value of recovered copper due to the effect of pressure (Figures 5.4.4 and 5.4.5). However, even in the high pressure series, the reaction is essentially complete at five minute, as no further increase in Cu recovery is apparent. The series of batch leach experiments where $\text{pH} = 2.0$ (Figures 5.4.6 to 5.4.11) are also near completion at five minutes. However, gradual increase in the recoveries of Fe (except at high pressure), Mn, Co, and Ni continue until the end of the experiment study duration (30 minutes). A slight negative trend in copper is evident and may reflect a possible precipitation reaction or sorption mechanism on refractory material. For the series of batch leach experiments where $\text{pH} \geq 3.0$ (Figures 5.4.12 and 5.4.13), only Mn and Ni continue the trend of a gradual increase with time. A gelatinous (amorphous) white precipitate (presumably $\text{Fe}(\text{OH})_3$) also settled out in the filtrate of batch leach experiments with $\text{pH} \geq 3.0$ after sitting overnight. This process suggests a hydrolysis reaction of ferric sulfate in solution forming ferric hydroxide precipitates (discussed further in Section 5.5) which may also serve as a source of sorption sites for the removal of Co and Cu.

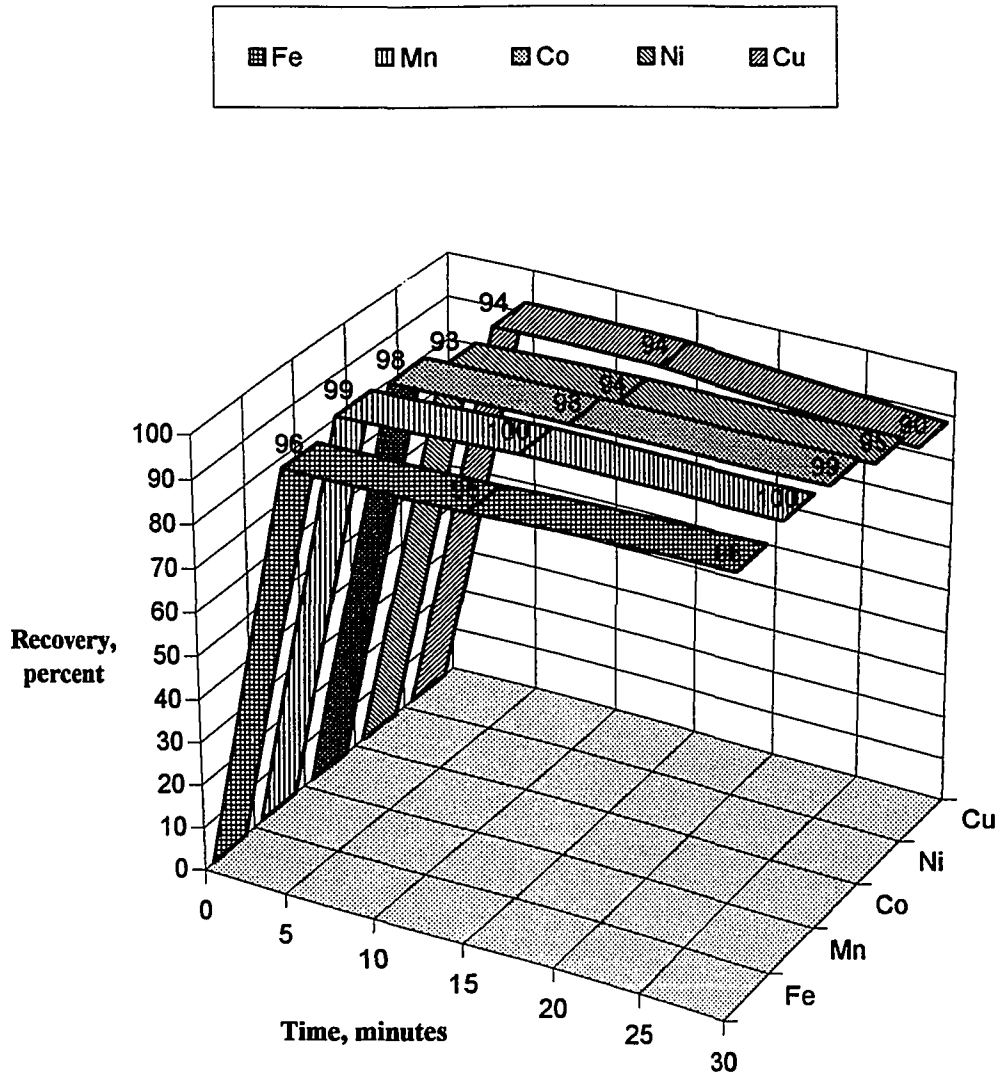


Figure 5.4.1 *Effect of Leach Time on Metal Recovery of Ferromanganese Crust in 1% Sulfurous Acid Batch Leach, pH = 1.0, Temperature = 0.1 °C, Pressure = 1 atm, 400 rpm Stir Rate.*

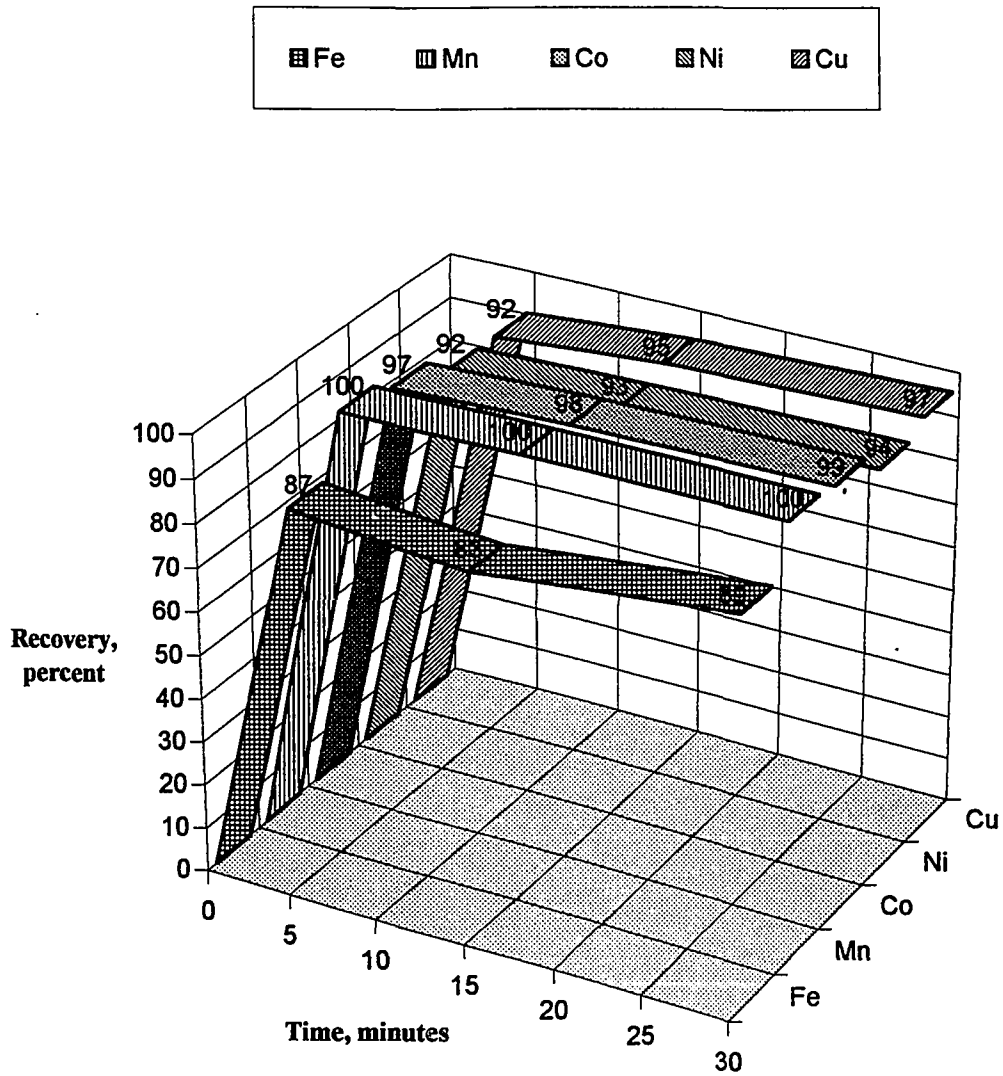


Figure 5.4.2 *Effect of Leach Time on Metal Recovery of Ferromanganese Crust in 1% Sulfurous Acid Batch Leach, pH = 1.0, Temperature = 5 °C, Pressure = 1 atm, 400 rpm Stir Rate.*

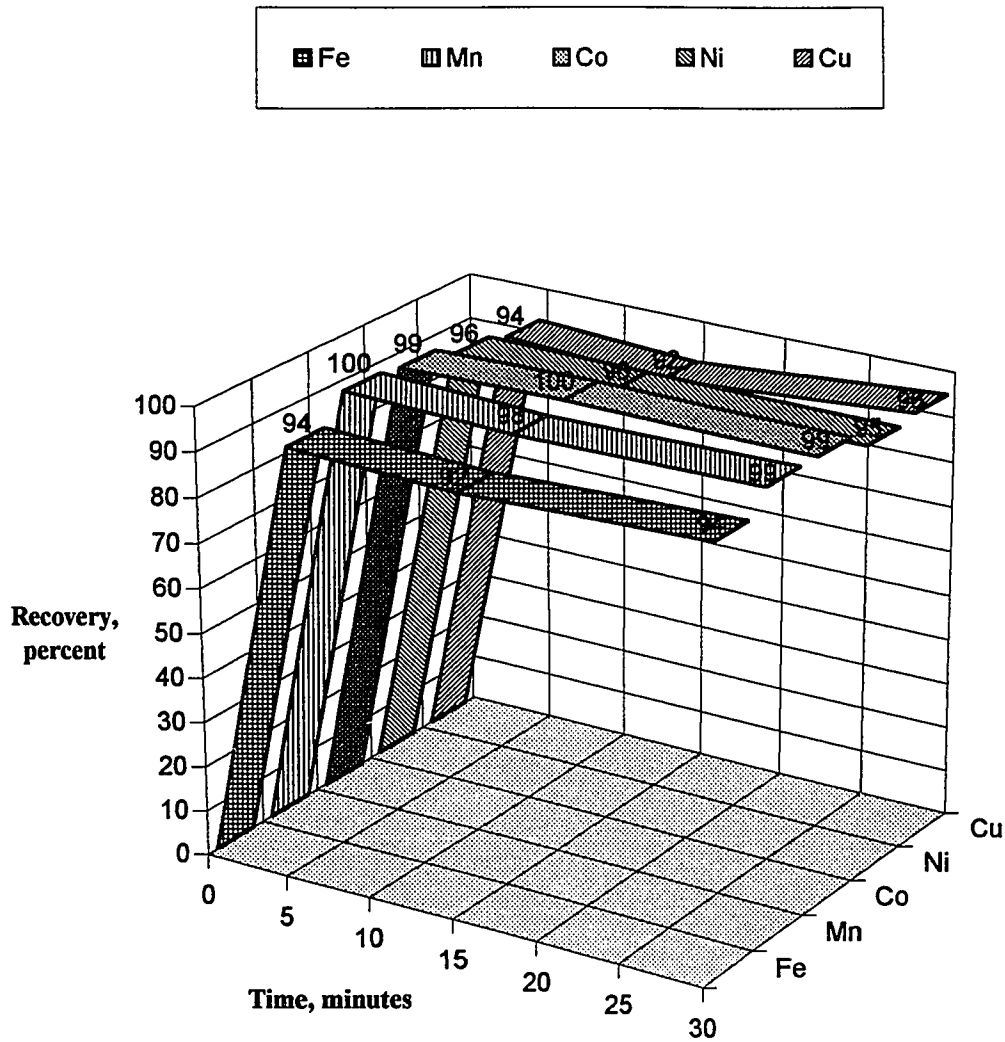


Figure 5.4.3 *Effect of Leach Time on Metal Recovery of Ferromanganese Crust in 1% Sulfurous Acid Batch Leach, pH = 1.0, Temperature = 15 °C, Pressure = 1 atm, 400 rpm Stir Rate.*

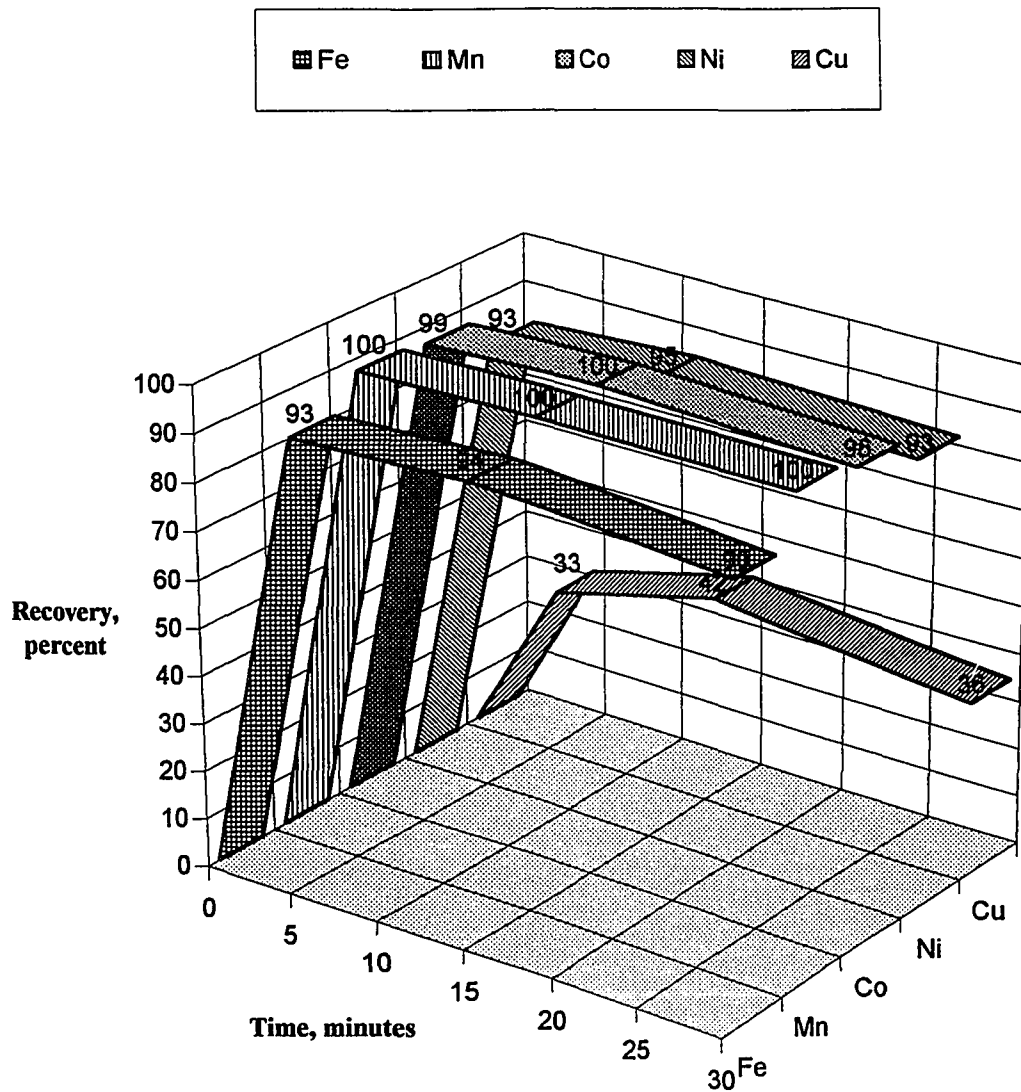


Figure 5.4.4 *Effect of Leach Time on Metal Recovery of Ferromanganese Crust in 1% Sulfurous Acid Batch Leach, pH = 1.0, Temperature = 15 °C, Pressure = 100 atm, 400 rpm Stir Rate.*

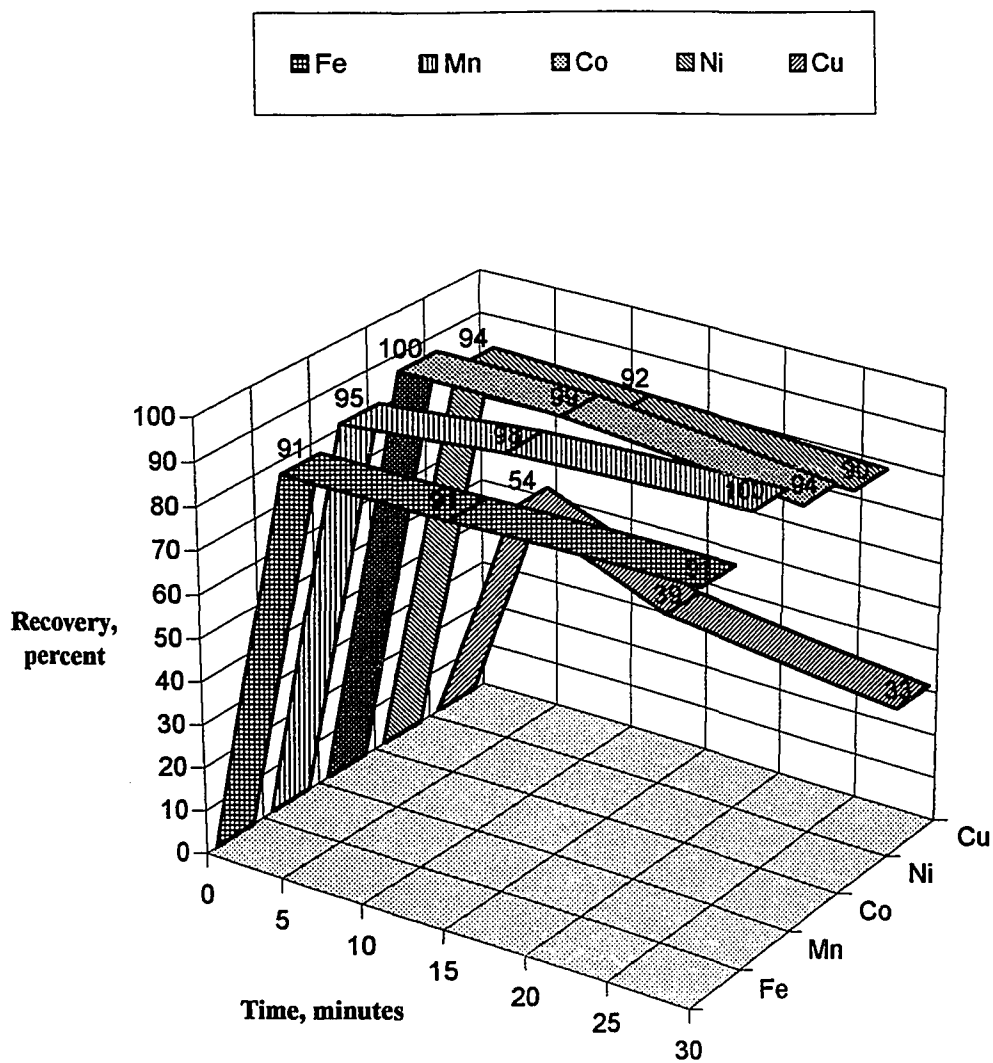


Figure 5.4.5 *Effect of Leach Time on Metal Recovery of Ferromanganese Crust in 1% Sulfurous Acid Batch Leach, pH = 1.0, Temperature = 15 °C, Pressure = 200 atm, 400 rpm Stir Rate.*

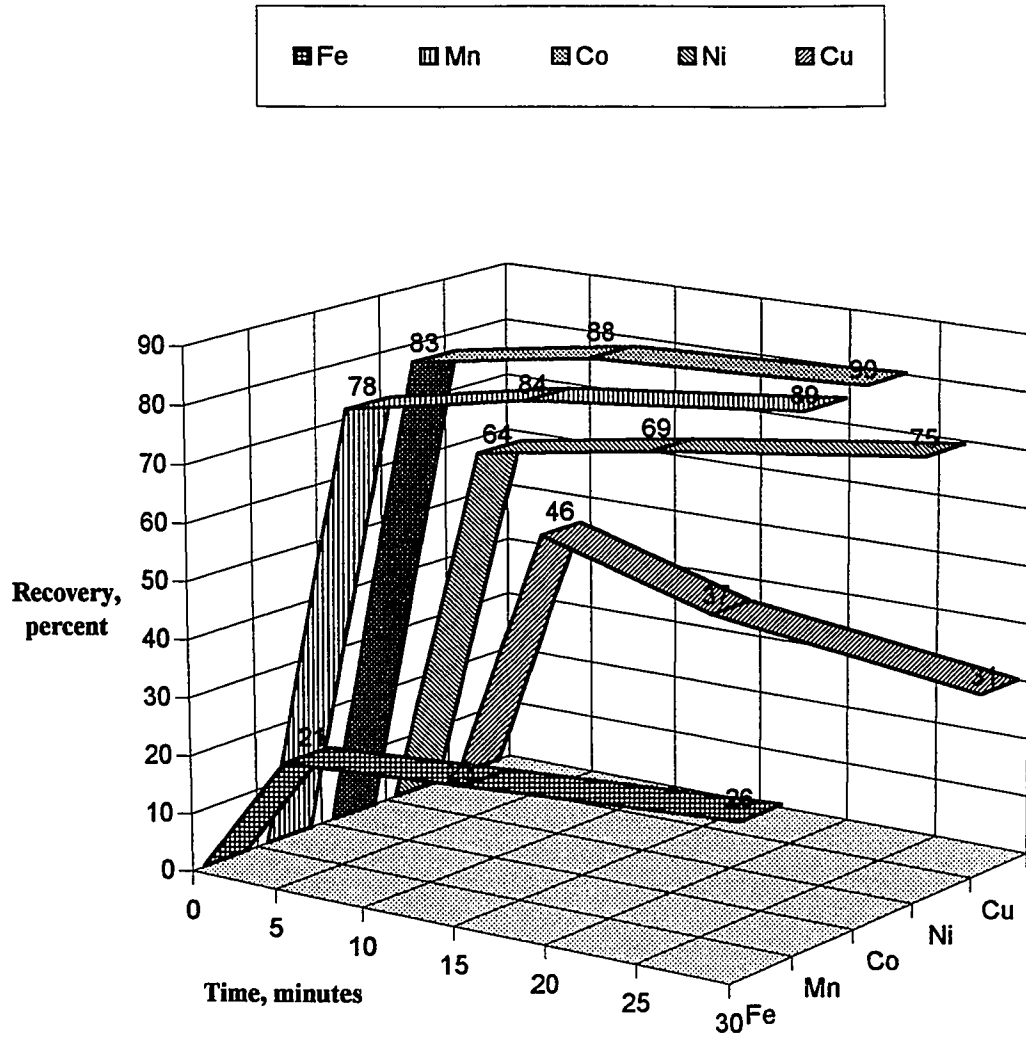


Figure 5.4.6 *Effect of Leach Time on Metal Recovery of Ferromanganese Crust in 1% Sulfurous Acid Batch Leach, $pH = 2.0$, $Temperature = 0.1^{\circ}C$, $Pressure = 1 atm$, 400 rpm Stir Rate.*

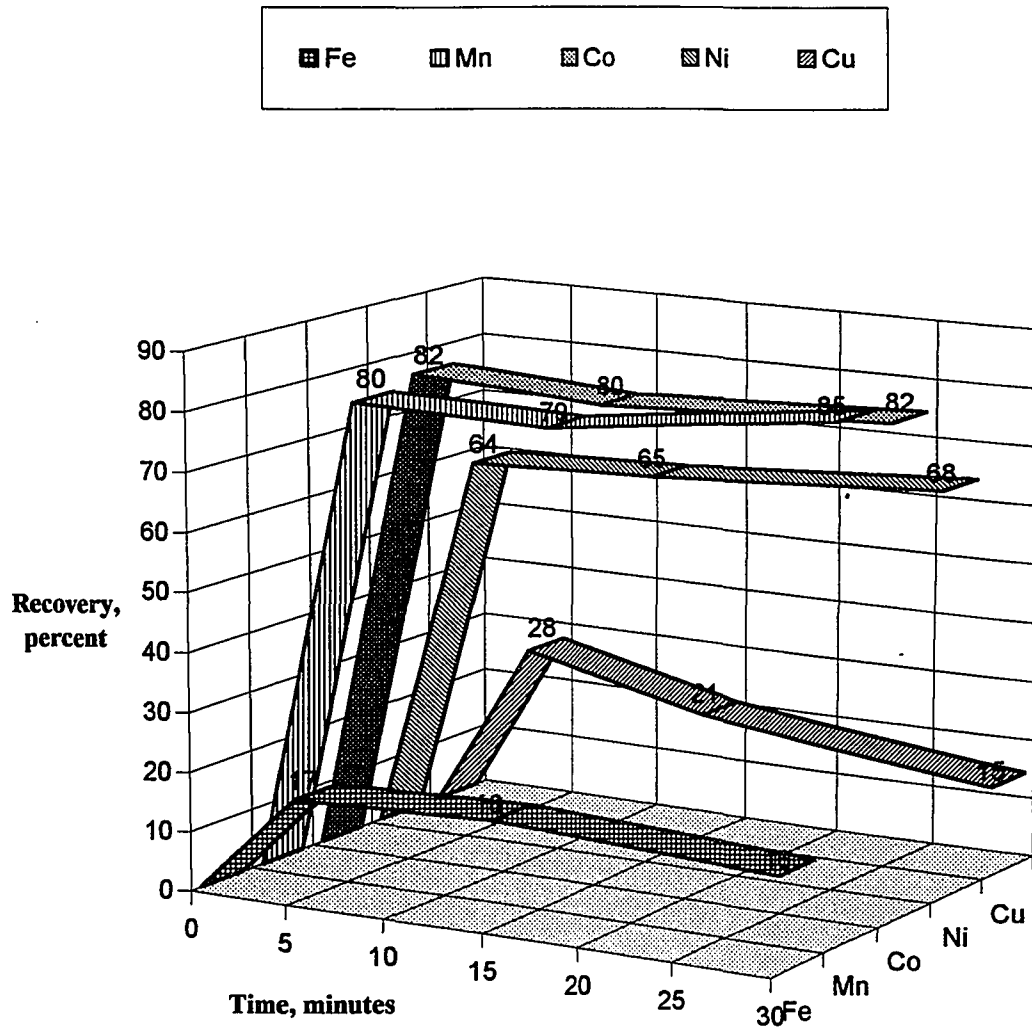


Figure 5.4.7 *Effect of Leach Time on Metal Recovery of Ferromanganese Crust in 1% Sulfurous Acid Batch Leach, pH = 2.0, Temperature = 5 °C, Pressure = 1 atm, 400 rpm Stir Rate.*

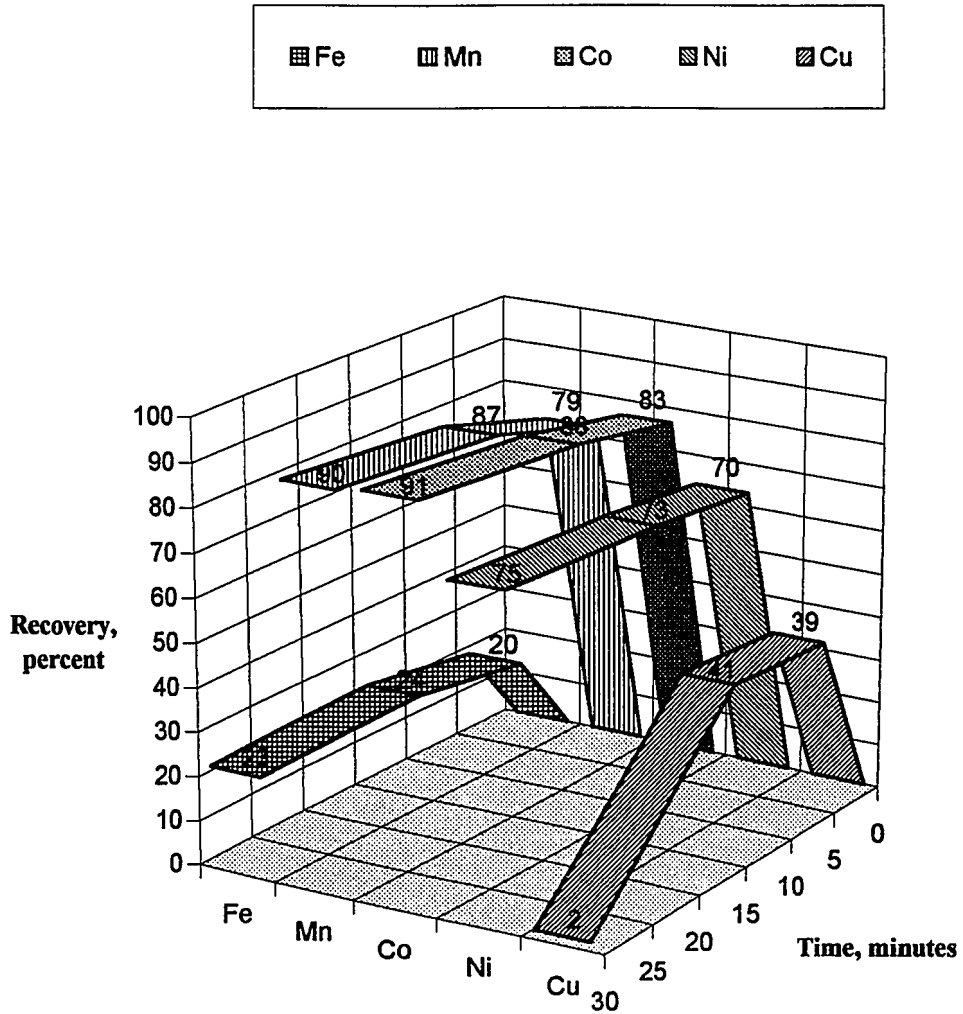


Figure 5.4.8 *Effect of Leach Time on Metal Recovery of Ferromanganese Crust in 1% Sulfurous Acid Batch Leach, pH = 2.0, Temperature = 5 °C, Pressure = 100 atm, 400 rpm Stir Rate.*

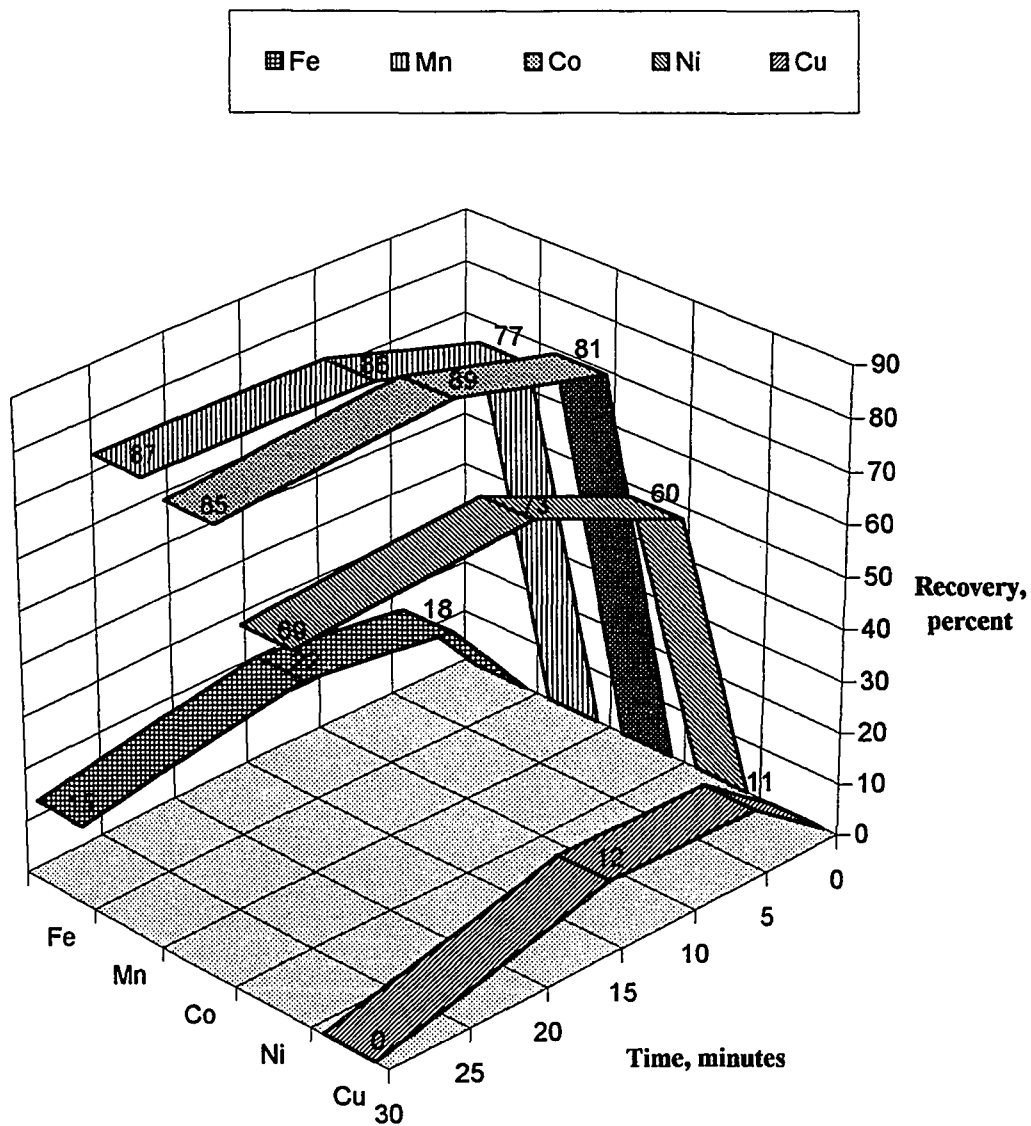


Figure 5.4.9 *Effect of Leach Time on Metal Recovery of Ferromanganese Crust in 1% Sulfurous Acid Batch Leach, pH = 2.0, Temperature = 5 °C, Pressure = 200 atm, 400 rpm Stir Rate.*

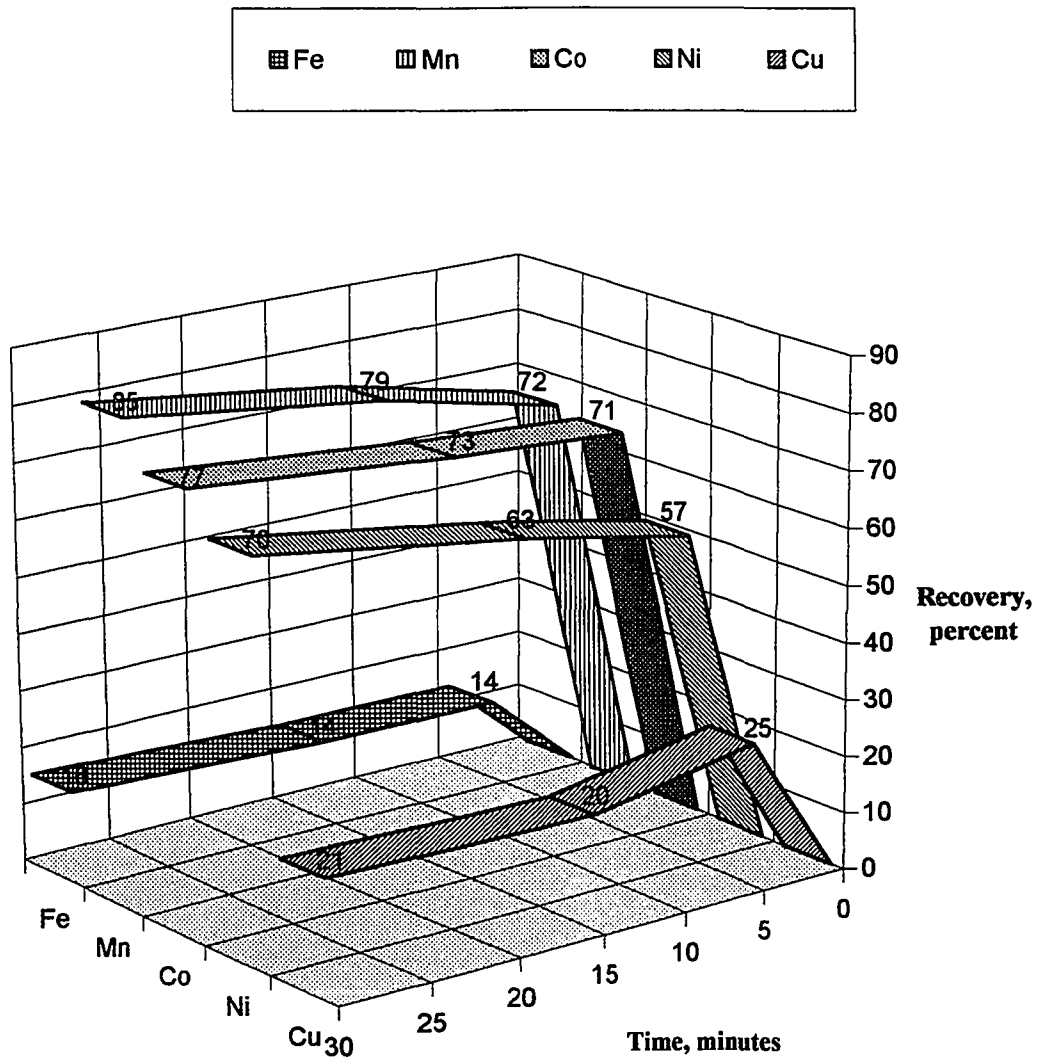


Figure 5.4.10 *Effect of Leach Time on Metal Recovery of Ferromanganese Crust in 1% Sulfurous Acid Batch Leach, pH = 2.0, Temperature = 15 °C, Pressure = 1 atm, 400 rpm Stir Rate.*

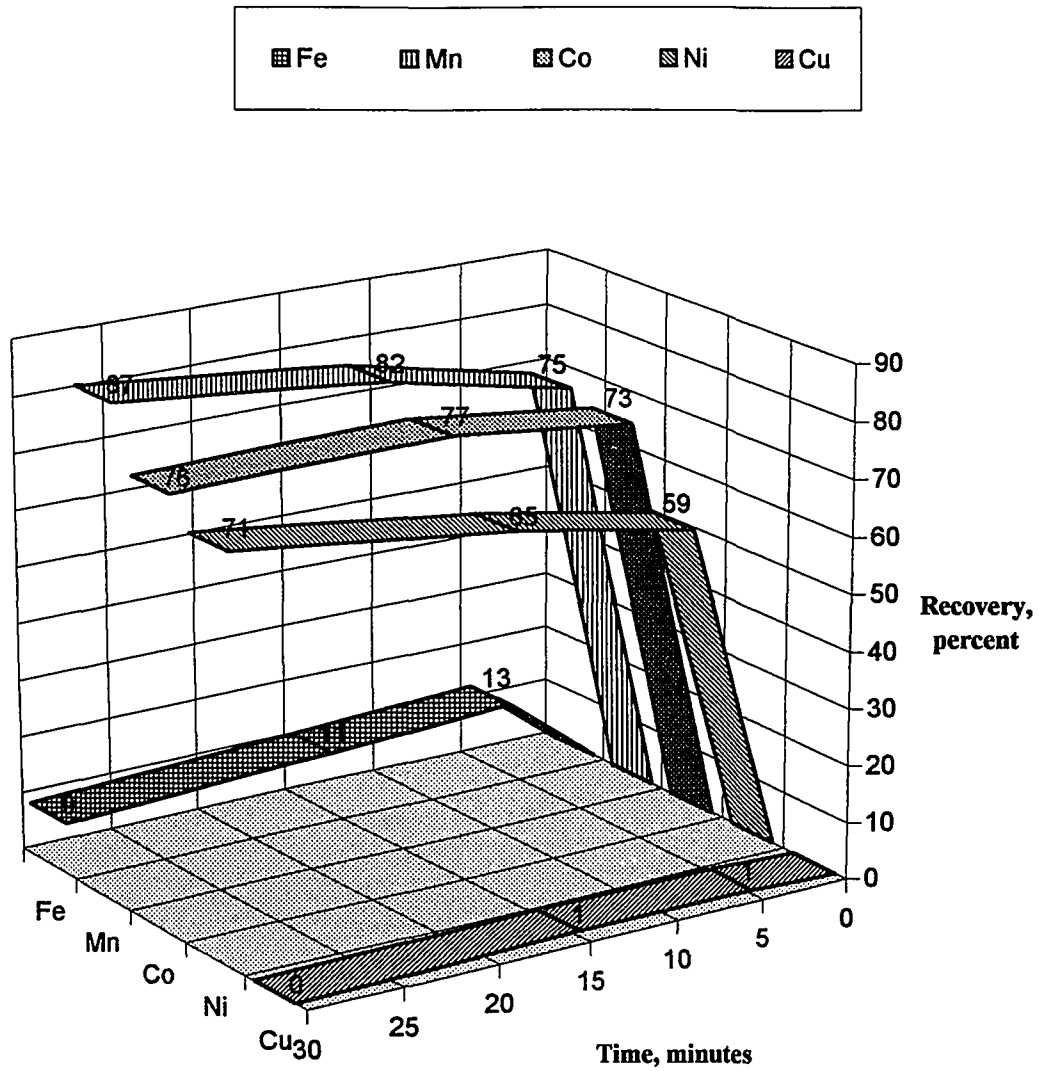


Figure 5.4.11 *Effect of Leach Time on Metal Recovery of Ferromanganese Crust in 1% Sulfurous Acid Batch Leach, pH = 2.0, Temperature = 15 °C, Pressure = 100 atm, 400 rpm Stir Rate.*

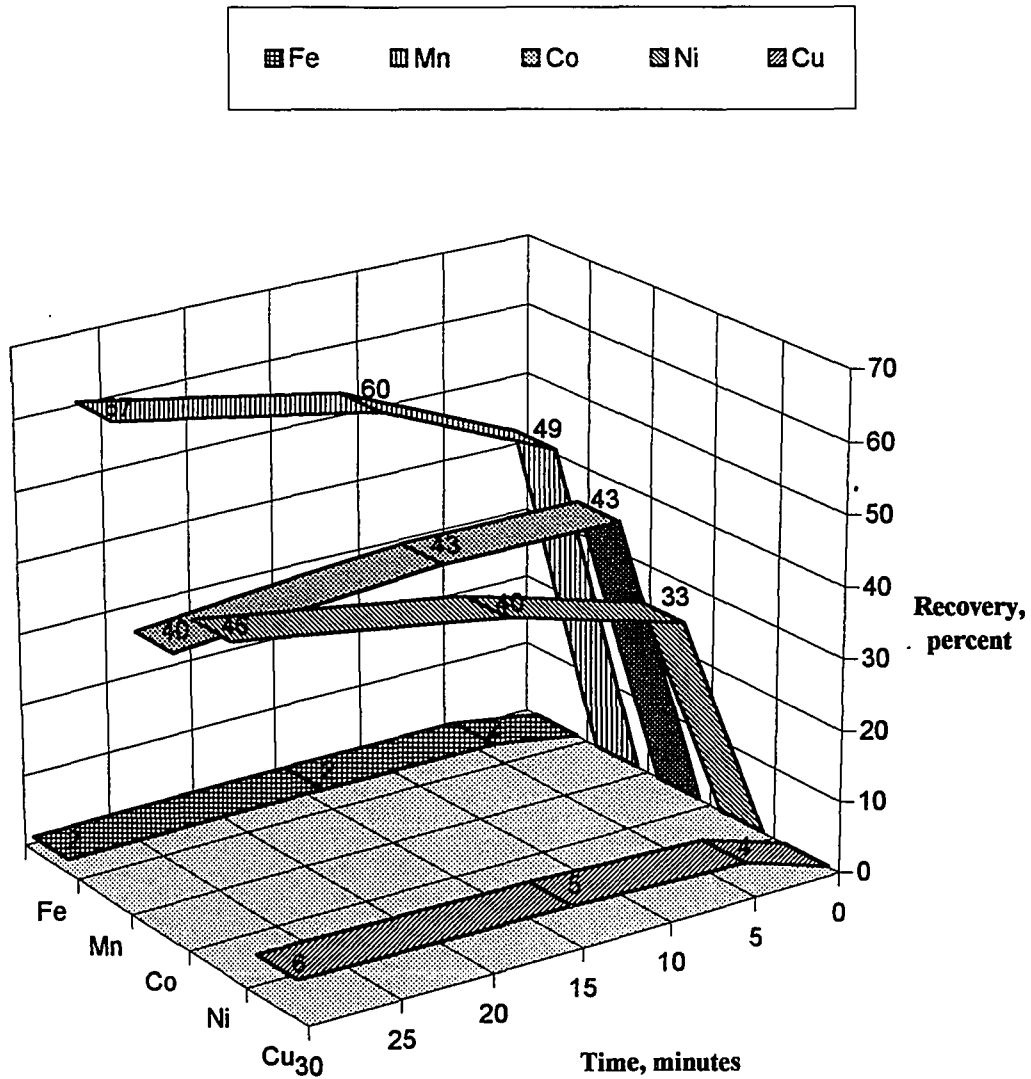


Figure 5.4.12 *Effect of Leach Time on Metal Recovery of Ferromanganese Crust in 1% Sulfurous Acid Batch Leach, $pH = 3.0$, Temperature = $15^{\circ}C$, Pressure = 1 atm, 400 rpm Stir Rate.*

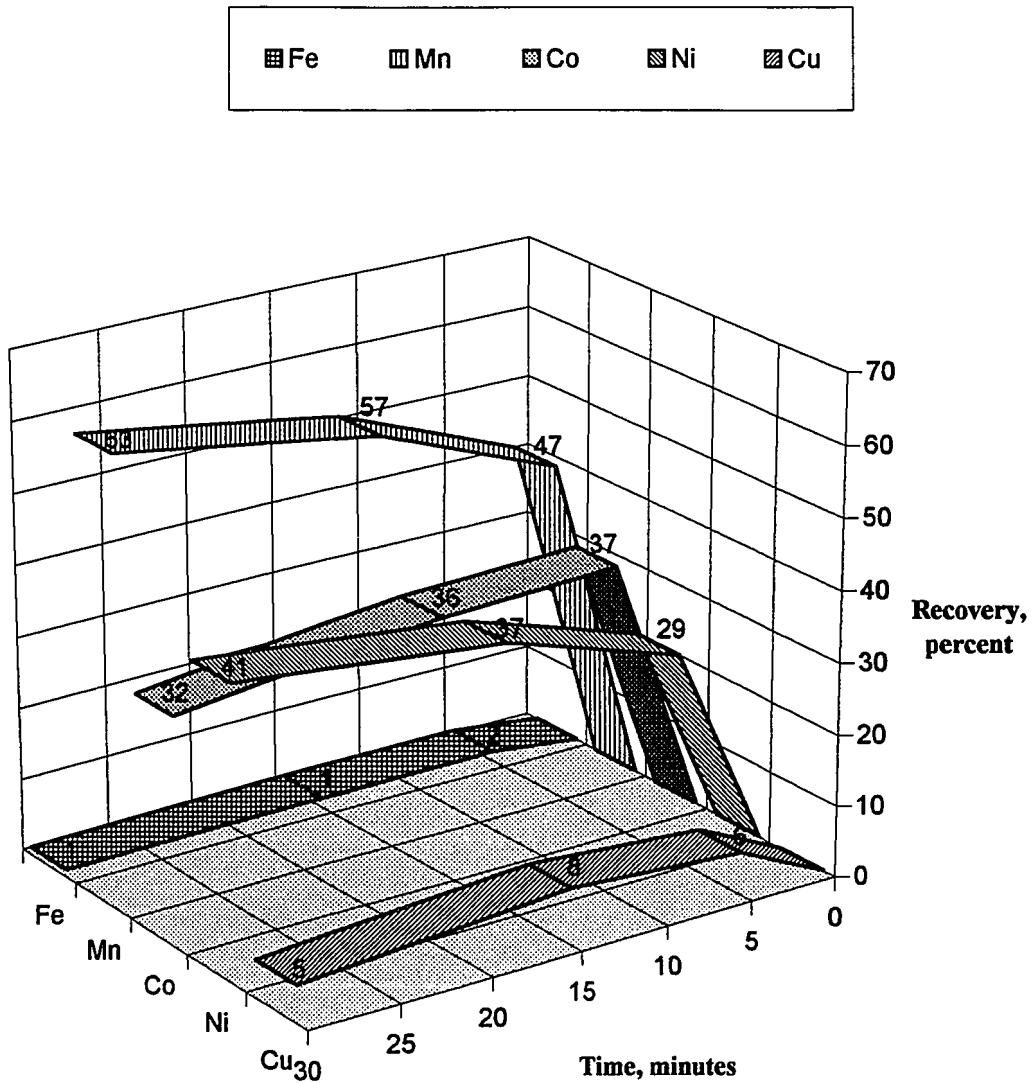


Figure 5.4.13 *Effect of Leach Time on Metal Recovery of Ferromanganese Crust in 1% Sulfurous Acid Batch Leach, $pH = 5.0$, Temperature = $15^{\circ}C$, Pressure = 1 atm, 400 rpm Stir Rate.*

5.5 Semi-Batch Intact Crust Leach Experiment Results

Two significant factors governing the dissolution of intact ferromanganese crust were identified in the semi-batch intact crust leach experiments: (1) Specific crust textural structure on dissolution behavior, and (2) The presence of oxygen.

Figure 5.5.1 shows the dissolution of *Hancock Seamount* crust fragments from the same dredge haul (*Kana Keoki* cruise 84-04-28-05) used to produce the study medium for the Batch Leach experiments. This crust material was collected off a large flat boulder, which was air dried and kept in a large synthetic fiber sack. The textures of the *Hancock Seamount* crust fragments were of the compact (massive) type, without much internal structure. These crust fragments did not achieve a total dissolution within the six-hour period of the semi-batch leach experiments.

Figure 5.5.2 shows the dissolution of *Karin Seamount Range* ($16^{\circ}40' \text{ N } 168^{\circ}15' \text{ W}$) crust collected on *Kaimikai-O-Kanaloa* cruise 93-11, RD1-1. Crust fragments were collected from an encrusted medium sized cobble kept stored in a bucket of seawater. The textural structure of the *Karin Seamount Range* crust was botryoidal, very friable and porous. This crust texture, as expected, proved much more amenable for leach dissolutions than the compact texture of the *Hancock Seamount* samples. The *Karin Seamount Range* crust samples disintegrate by flaking during the leach process leaving leach product residue suspended in the reactor flask, and achieved total dissolution in anoxic leach within the six-hour period of the experiments. Results of the semi-batch intact crust leach experiments show that crust texture is an overriding factor in crust recovery.

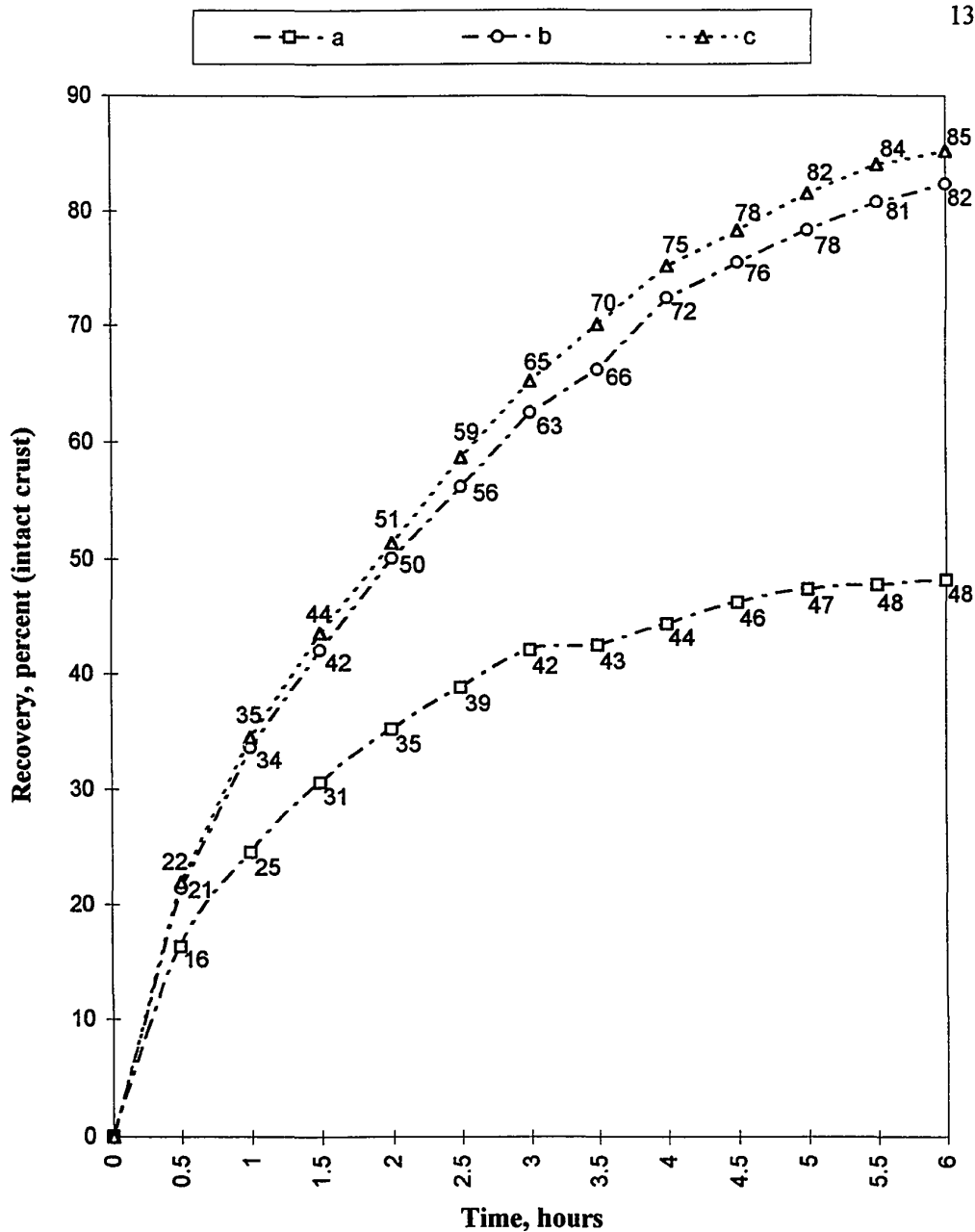


Figure 5.5.1 *Semi-Batch Intact Crust Leach Experiment: Hancock Seamount Crust in 9% Sulfurous Acid Batch Leach, Temperature = 4 ° C pH = 1.0, Pressure = 1 atm, 400 rpm Stir Rate. (a) 2.86 g (wet) in oxygenated leach, (b) 2.93 g (wet) in anoxic leach, (c) 2.91 g (wet) in anoxic leach.*

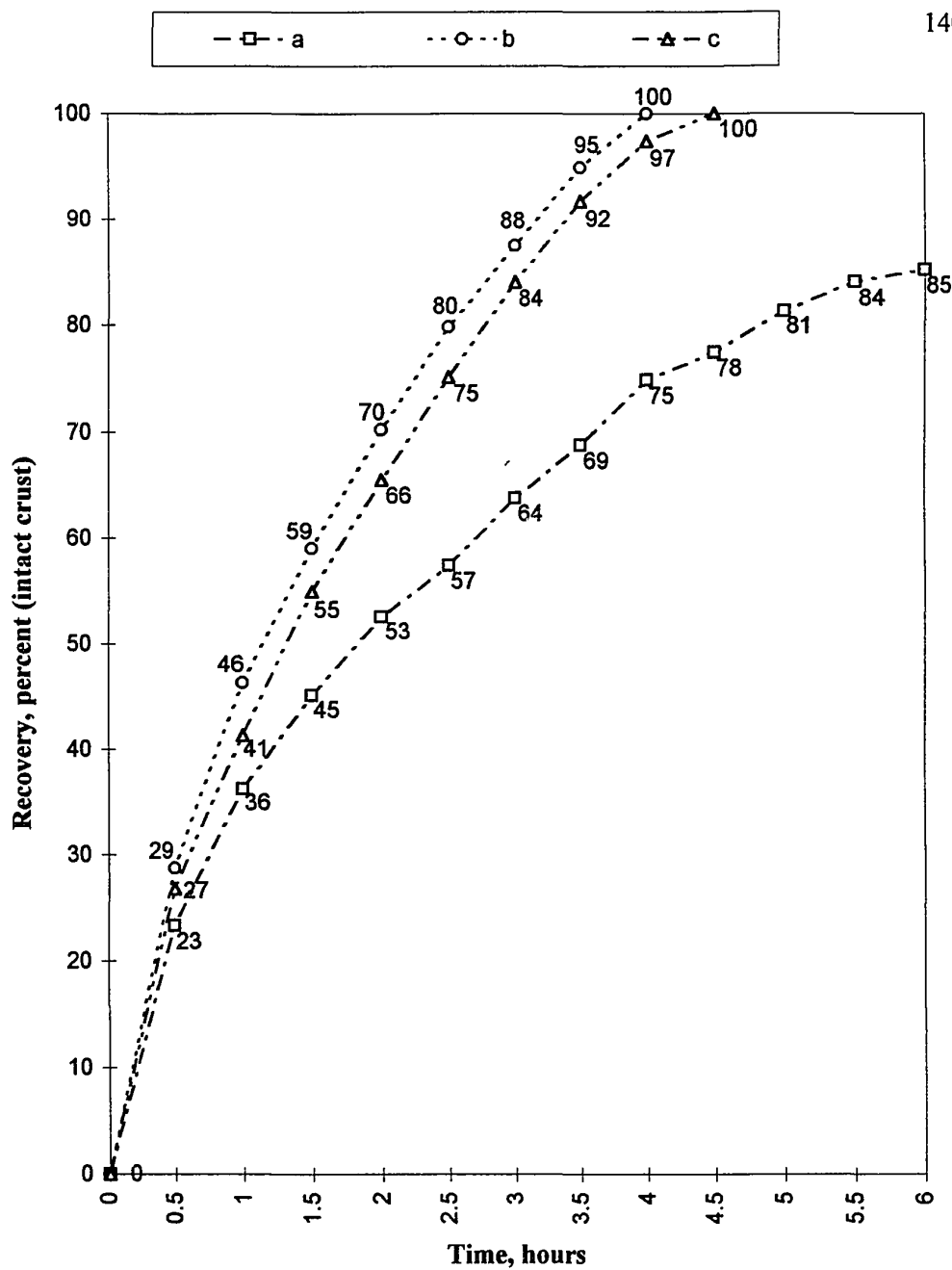


Figure 5.5.2 Semi-Batch Intact Crust Leach Experiment: Karin Seamount Range Crust in 9% Sulfurous Acid Batch Leach, $pH = 1.0$, Temperature = $4^\circ C$, Pressure = 1 atm, 400 rpm Stir Rate. (a) 2.95 g (wet) in oxygenated leach, (b) 2.98 g (wet) in anoxic leach, (c) 2.89 g (wet) in anoxic leach.

The semi-batch leach experiments also show that a leached product layer forms as a blanket on the surface of crust during the leach process. This leached surface product layer builds to a thickness of several millimeters or more and creates resistance to the diffusive flux of lixiviant to unreacted crust minerals and dissolved products away from the crust. As shown in the crust recovery curves in Figures 5.5.1 and 5.5.2, the build up of surface product layers reduces the crust dissolution rate with time. The crust recovery curves of the semi-leach batch experiments generally resemble curves that fit the empirical metallurgical equation for release of a dissolved product when product layer diffusion is the controlling resistance (Levenspiel, 1972):

$$Dissolution\ Rate = kt = 1 - 3(1 - \alpha)^{2/3} + 2(1 - \alpha)$$

Where: k = empirical dissolution rate constant, t = time, and α = fraction of solid released as dissolved product.

The mineralogy of the leached crust surface product layer was studied using a *Scintag PAD-V* automated biphasic X-ray powder diffractometer. Figure 5.5.3 shows the diffractometer record of 2θ angle diffraction maxima from Hancock Seamount crust leached product layer collected after a semi-batch leach experiment (Figure 5.5.1 (a)) that was ground to a fine powder and mounted on a *null background* glass slide. The diffraction maxima pattern shows dominant mineral phases of quartz (SiO_2), jarosite ($(\text{KH}_3\text{O})\text{Fe}_3(\text{SO}_4)_2(\text{OH})_6$), plagioclase series feldspars (anorthite shown; $\text{CaAl}_2\text{Si}_2\text{O}_8$), and a minor phase of gypsum ($\text{CaSO}_4 \cdot 2\text{H}_2\text{O}$) in the leached surface product layer specimen. The broad diffraction “hump” between 2θ angles of 18° and 34° (Figure 5.5.3) shows a substantial fraction of amorphous (lacking crystal structure) material in crust leached surface products.

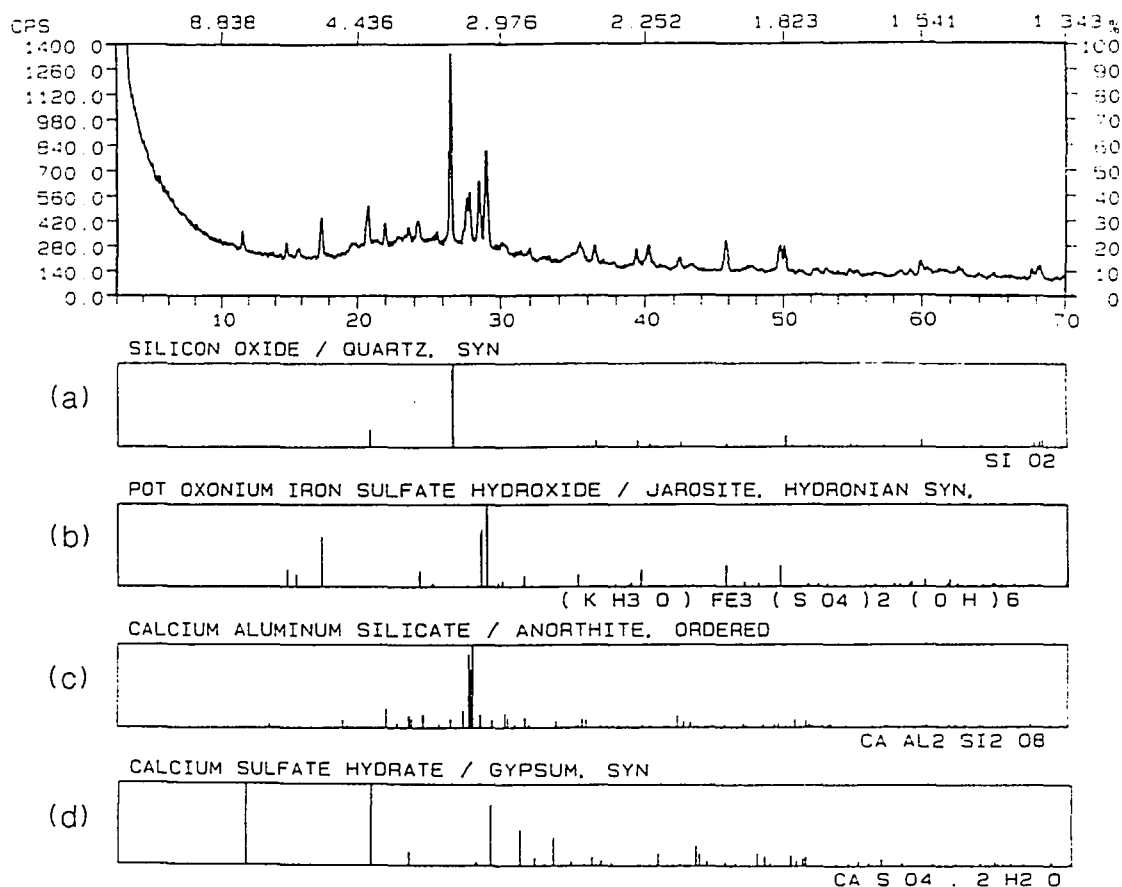


Figure 5.5.3 X-ray Powder Diffractometer Record of Hancock Seamount Crust Leached Surface Product. Instrument Settings: Preset Time = 1.8 seconds, Step Size = 0.030° , Wave Length = 1.54060 \AA . Top Diagram: Left Ordinate = Counts Per Second, Right Ordinate = Relative Peak Height in Percent, Bottom Abscissa = 2θ Angle (degrees), Top Abscissa = d Spacing (angstroms). (a) X-ray Diffraction Lines of Quartz (SiO_2). (b) X-ray Diffraction Lines of Jarosite ($(\text{KH}_3\text{O})\text{Fe}_3(\text{SO}_4)_2(\text{OH})_6$). (c) X-ray Diffraction Lines of Anorthite ($\text{CaAl}_2\text{Si}_2\text{O}_8$). (d) X-ray Diffraction Lines of Gypsum ($\text{CaSO}_4 \cdot 2\text{H}_2\text{O}$).

Microanalysis of the leached crust surface product layer was performed using a *Zeiss DSM 962* scanning electron microscope interfaced to an *Oxford Instruments* energy dispersive X-ray fluorescence spectrometer (SEM/EDS). Samples of Hancock Seamount crust leached surface product layer were embedded in resin and coated with an ultra-thin coat of high purity carbon for stability under the electron beam. An accelerating voltage of 20 kV was used for optimal count rate and backscatter imaging resolution. Figure 5.5.4 is a typical scanning electron micrograph showing the highly etched and porous texture and the friable nature of leached crust surface products. Elemental analysis was determined by the “ZAF” (secondary atomic fluorescence) method. Figure 5.5.5 shows the “ZAF” elemental peaks of a Hancock Seamount crust leached surface product layer specimen recorded by the EDS. The peaks (apparent elemental concentrations) of the “ZAF” method were normalized to data base standards with resulting leached surface product element fractions (expressed in atomic percent) of: O = 66.15%, Si = 15.67%, Fe = 7.62%, S = 5.24%, Na = 1.32%, Al = 1.03%, and all other elements < 1%. This analysis confirms that crust leached surface product layers are composed of residual silica, amorphous ferric hydroxide and ferric sulfate, and minor amounts of other refractory minerals.

Experimental results suggest that the presence of oxygen in the leach solution is a significant factor in forming (detrimental) leached product layers. Crust recovery from sulfurous leaches with oxygen present (*curves (a)* for *Hancock Seamount* and *Karin Seamount Range* crust fragments in Figures 5.5.1 and 5.5.2), show dramatic decrease compared with the crust recovery of the anoxic leaches. This may be due to a change in the amount of soluble iron products in the leach reaction when oxygen is present.




20 microns 

Figure 5.5.4 Scanning Electron Micrograph Showing Texture of Hancock Seamount Leached Crust Surface Product. Backscattered Electron Imaging. Scale Bar is 20 μ m.

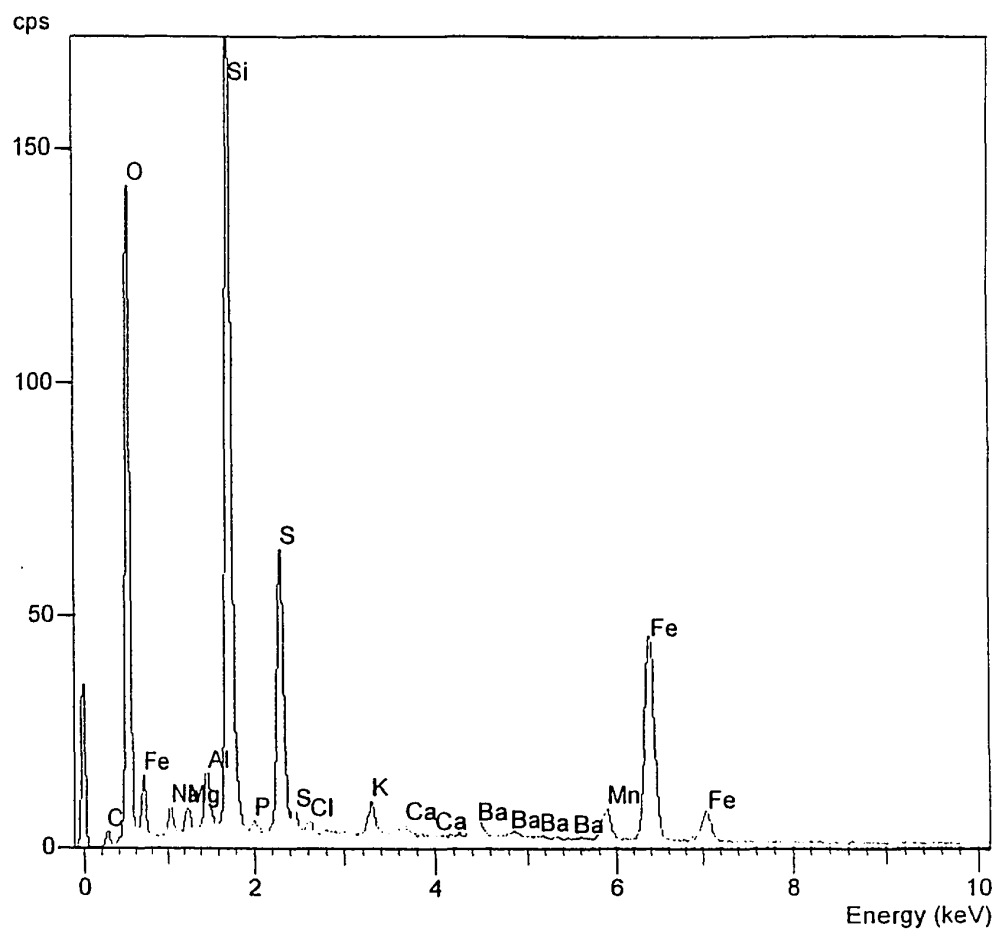
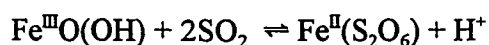


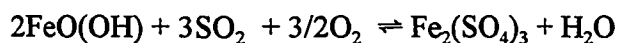
Figure 5.5.5 *Energy Dispersive X-ray Fluorescence Spectrometer Record Showing Apparent Elemental Concentration Peaks of Hancock Seamount Crust Leached Surface Product Layer Material.*

Lee and others (1978) used a vacuum line reaction tube apparatus to study the reaction of ground ferromanganese nodules with gaseous SO₂ and O₂ over a range of 25° to 95°C. Two competing reactions for Fe^{III} were identified:

(1) A reduction reaction of goethite by SO₂ to soluble ferrous dithionate:

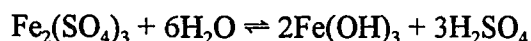


(2) A reaction in the presence of oxygen that produces slightly soluble ferric sulfate:



The presence of oxygen enhances sulfate formation at the expense of dithionate production. Using an IR spectrometer to estimate relative sulfate–dithionate end-product concentrations, Lee and others determined that in the absence of oxygen, goethite reaction with SO₂ yields > 95% dithionate. The amount of dithionate versus sulfate formed was also found to decrease with increasing oxygen concentration and temperature. A reaction with ground ferromanganese nodules and 1:1 mole ratio of gaseous SO₂ and O₂ at 25°C, produced an estimated yield of 21% dithionate in the sulfate–dithionate end-product. With temperature elevated to 95°C, only trace levels of dithionate in the sulfate–dithionate end-product were detected.

Reducing the production of ferric sulfate in the leach reaction is very important for effective *in situ* crust solution extraction. As ferric sulfate is only slightly soluble, its formation will significantly contribute to the build up of leached crust surface product layers. In addition, ferric sulfate readily undergoes hydrolysis under leach conditions, to form a white gelatinous precipitate of insoluble amorphous ferric hydroxide:



This worrisome reaction is favored by increasing pressure in aqueous solutions, as hydration equilibria are significantly affected by the closer packing of water molecules above ~50 atm (Bradley and Munro, 1965).

5.6 Discussion

The result of the collective leach experiments provides insight on leach characteristics of the sulfurous acid system at *in situ* conditions of seamount crust mine sites. Batch ground crust leach experiments show that despite low temperature, leach kinetics is still favorable for rapid reductive dissolutions of crust material. Lower temperature may also slightly aid leach chemistry by increasing the fraction of the reducing $\text{SO}_{2(aq)}$ species in the $\text{SO}_{2(aq)} \leftrightarrow \text{HSO}_3^-$ system. Increasing pressure tends to increase recoveries of Fe, Mn, Co, and Ni. A decrease in copper recovery with increasing pressure may be due to a pressure effect on redox solubility. However, as copper is just a minor constituent, recovery loss should not be too significant. Result of semi-batch whole crust experiments illuminate the overriding importance of specific crust textures on reaction rates. Semi-batch experiments also showed the detrimental effect of leached surface product layer formation on reaction rates. However, it was determined that detrimental surface product layer formation can be mitigated by eliminating free oxygen in the lixiviant. A surface product layer still forms in an anoxic leach. However, it appears to have much higher transmissivity and flakes off more readily than surface products in an oxygenated leach.

The lixiviant best suited for the *in situ* extraction of ferromanganese crust was determined to be a SO_2 saturated, anoxic seawater solution with $\text{pH} \approx 1.0$. If the leach circuit

is isolated from a significant influx of ambient seawater, the leach process is expected to extract crust at a seamount mine site successfully. Extraction continues until diffusion through a leach surface product layer becomes ineffective (i.e., uneconomic). At this point, depending on the local crust texture, an equivalence of 0.70 - 1.80 cm of crust thickness will have been extracted. In fact, crust extraction could continue, although at a slow rate, until the crust material is exhausted. However, for preliminary feasibility evaluation, a subjective choice must be made about when diminishing return warrants' cessation of mining. If the anoxic leach curves of the more conservative compact (massive) textured crust in Figure 5.5.1 are projected with the same exponential rate of decline, crust recoveries at the 12-hour point are down to 1-2% an hour. Therefore, twelve hours is selected as the design period for preliminary system evaluation.

SO₂ saturated, anoxic seawater lixiviant can be produced cheaply on the mining ship. Seawater is degassed using a *deaerating feed tank* system. Superheated dry steam (10 atm, 200°C) is shot through clean (filtered) seawater while it is sprayed through a venturi nozzle into a feed (holding) tank. The feed tank is kept under a vacuum to vent expelled gases to the atmosphere. Degassed seawater is next pumped through a series of shell-in-tube heat exchangers to cool down for improved SO₂ solubility. If necessary, a small amount of an inexpensive antioxidant, such as ethanol can be added. SO₂ gas is produced by combustion of sulfur and compressed using corrosion resistant lobe pumps. Lixiviant is produced by sparging the degassed seawater with compressed SO₂ and adjusting pH with an in line proportioner.

Since *in situ* conditions cannot be truly duplicated in the laboratory, some uncertainty exists in making real world predictions from collective leach experiments. The semi-batch whole crust leach experiments could not simulate *in situ* pressure, so pressure effects must be inferred from batch leach results. However, the effect of pressure induced change in hydration equilibria is a significant unknown concerning crust metal species, and may contribute to surface product layer formation. Batch experiments suggest that this may be a mechanism contributing to the loss of Cu recovery at simulated *in situ* pressure. Hydration effects also account for the loss of Fe in the presence of free O₂, and this process may be accelerated with increasing pressure. The insolubility of Cu is probably insignificant in affecting the rate of crust extraction. However, Fe would be problematic. Uncertainty also exists in the treatment of whole crust fragments in the semi-batch leach experiments. Irreversible physical changes occur to crust material in the sample collection process, when raised to the surface from the ocean floor. As ambient pressure is reduced, the release of pore water pressure within the crust alters the physical properties of the sample by inducing fracture porosity and rendering it more friable. Subtle physical change in crust fabric may affect laboratory semi-leach process results. In addition, the procedure of suspending crust fragments in a stirred reactor flask may be an inadequate model of *in situ* crust leaching. The net effect of laboratory artificiality may be favorable or unfavorable. In any event, an important future goal is to validate laboratory-based assumptions by actual *in situ* experiments.

CHAPTER 6 ECONOMIC ASSESSMENT

The culmination of the laboratory work of the two previous chapters attained the first four research goals outlined in the Research Objectives (Section 1.8) and validated the viability hypothesis: *The leach kinetics and physicochemical hydrodynamics at in situ conditions will be favorable for the economically viable recovery of metal cations in crusts.* Therefore, an economic analysis to evaluate the potential feasibility of *in situ* crust mining is warranted.

A preliminary economic assessment of the novel *in situ* batch reactor solution mining system was completed in collaboration with Thomas A. Loudat, Ph.D., an economist with considerable expertise in mineral production analysis, and John C. Wiltshire, Ph.D., a leading researcher in the marine mining field. This work culminated in a report submitted to the *State of Hawaii Department of Business, Economic Development, and Tourism* (Loudat, Zaiger, and Wiltshire, 1994). With permission from coauthors, many pertinent sections of the report are reproduced in this chapter. Reference is made here to preclude repetitive citation.

6.1 Basic Assumptions

The novel *in situ* batch reactor solution mining system differs considerably from proposed mechanical crust mining systems (discussed in Chapter 2). One important difference is mining site selection for economic operation. Unlike mechanical systems, thickness of crust is less important than areal coverage for solution mining. Maximizing areal coverage is most important for *in situ* solution mining as the extraction method is a surface dissolution procedure that loses recovery efficiency with the buildup of a leach surface

product layer. Thus, it is best to select crust mine sites with 75% or greater coverage to maximize production rates.

The projected output of the solution mining system is based on the following assumptions.

1. Crusts have a mean thickness of 2.5 cm and mean areal coverage of 50%.
2. Mine sites are selected with a target coverage of 75% or better to maximize solution mining production rates (assume 75% coverage for the economic study).
3. The containment and regulation cover (CRC) - batch leach system has an extraction efficiency of 50% (dissolution of intact crust) for an on site leaching time of 12 hours.
4. Three systems of alternating (200m × 200m) CRCs each require 1.5 days for a recovery/deployment, test and leach cycles.
5. One day is required for processing ship setup and leach time per CRC site.
6. Annual operation is 300 days per year with the remaining 65 days used for repair/maintenance, travel to and from home port and downtime related to weather.

Based on these assumptions, the projected daily output per CRC-day is 335 mt and the expected annual processing throughput is 302,000 dry tons of crust per year.

6.2 System Costs

The solution mining system is divided into six subsystems for economic evaluation. (1) The CRC subsystem, (2) the processing subsystem, (3) the auxiliary support subsystem, (4) the marine transport subsystem, (5) the mining support system, and (6) the research and development subsystem.

The first subsystem costed is the CRC subsystem, the heart of the solution mining operation. The CRC subsystem consists of the CRC membrane and distribution network system (described in chapter 2, section 2.3.1), submersible electric pumps, a primary mooring buoy with a coaxial electric, telemetry lines and lixiviant lines attached, two other mooring buoys, each with two lift lines (wire rope/hawser) used for CRC recovery and deployment, two submersible slurry tanks (6m × 6m × 3m) pump systems that hold/distribute weighting fluid used to seal the CRC edge, and two remotely operated vehicles (ROVs) for CRC inspection and repair.

Table 6.1 shows the capital costs of the CRC subsystem. All pumps are submersible, multistage centrifugal pumps. The lixiviant hoses are 30 inch (diameter) kevlar-reinforced hoses. The ROV's can do in place repairs and maintenance of CRC components.

The labor and fuel cost of operating the CRC subsystem are included in the processing and auxiliary subsystem operating cost amounts. Insurance costs are estimated at 1.0 percent of fixed capital costs. CRC subsystem operating costs include maintenance and repair/replacement of major components amortized over the life of the mining venture. Total annual CRC operating costs based on these assumptions is \$2.28 million.

The second subsystem is the processing subsystem. The major components of this subsystem are the hydrometallurgical processing ship, deck handling and stowage equipment, a spare CRC system, "sulfur roaster" (SO₂ gas generation plant), solvent extraction/electrowinning plant, and a manganese calcination plant. The processing ship is a 40,000 dwt converted-tanker with a maximum 13,000 shaft horsepower (HP) capacity (9,850 average continuous shaft HP output assumed) that: (1) transfers and stores bulk commodities received

Table 6.1 CRC Subsystem Capital Costs (1993 dollars). After Loudat, Zaiger, and Wiltshire (1994).

<u>Item</u>	<u>Unit Cost</u>	<u>No. of Units</u>	<u>Total Cost</u>
Membrane	\$474,000	3	\$1,422,000
Pump Systems	\$140,000	3	\$420,000
Lines and Hoses	\$720,000	3	\$2,160,000
Weighting Slurry	\$37,700	3	\$113,100
Mooring Buoy	\$75,000	6	\$450,000
Sludge Tanks	\$50,000	6	\$300,000
ROV	\$1,500,000	2	\$3,000,000
Total Fixed Capital			\$7,865,100
Working Capital	13.86%		\$1,090,212
Total Capital Costs			\$8,955,312

from the marine transfer system required for processing, (2) prepares lixiviant and supplies it to the CRC, (3) processes the leachate to extract the target metals, (4) returns the process slime/bleed stream to a leach site, and (5) transfers the processed metals to the bulk commodity transport subsystem. The lixiviant is gravity fed from the processing ship to the CRC where it remains circulating on the mine site for the appropriate leach time (12 hours), and is then pumped back to the processing ship by CRC pumps. The metals are then removed from the pregnant leach solution using the solvent extraction/electrowinning process system (described in Chapter 2, Section 2.3.6, Figure 2.6). Cathode cobalt, nickel and manganese carbonate are the end-result products. The manganese carbonate is calcined at sea using CO₂ from the processing ship's stack emissions. Calcining the manganese at sea allows direct marketing of the product from the processing ship and avoids onshore processing plant and transportation system capital and operating costs.

Table 6.2 shows the processing subsystem capital costs. These values are cost approximations for the processing ship and other subsystem components required for the solution mining system. Detailed engineering cost studies are needed to provide more accurate cost estimates for this subsystem.

The solvent extraction/electrowinning capital costs for the solution mining system are derived from Bennet and Jeffers (1988). To their fixed capital costs (\$18.6 million) for a solvent extraction/electrowinning system is added the estimated costs for an additional solvent extraction and electrowinning circuit for nickel. These are estimated to be 50 percent of the capital costs for these equipment items in the cobalt circuit (\$1.09 million \times 50%). This sum is multiplied by the ratio of the projected plant capacity of the processing ship (4,400 gpm) to the plant capacity in Bennet and Jeffers (1988) (10,000 gpm) and converted to 1993 dollars using the Mining Equipment Cost Index (U.S. Department of Commerce, 1993).

**Table 6.2 Processing Subsystem Capital Cost (millions of 1993 dollars).
After Loudat, Zaiger, and Wiltshire (1994).**

<u>Equipment Item</u>	<u>(mil. \$) Unit Cost</u>	<u>No. of Units</u>	<u>(mil. \$) Total Cost</u>
Process Shipping Ship	\$50.0	1	\$50.0
Handling and Stowage Equip.	\$3.0	1	\$3.0
Spare CRC System	\$1.5	1	\$1.5
Sulfur Roaster System	\$9.4	1	\$9.4
Solvent Ext/Electrowinning Sys.	\$9.9	1	\$9.9
Mn Calcination System	\$6.3	1	\$6.3
Total Fixed Capital			\$80.1
Working Capital	13.86%		\$11.1
Total Capital Costs			\$91.2

Capital costs for the other processing subsystem components are derived from Bureau of Mines (1987). Reported cost values are converted to 1993 dollars using the Mining Equipment Cost Index. Clearly the most significant processing subsystem capital cost is the processing ship comprising more than 60 percent to total subsystem capital costs.

Table 6.3 shows the operating costs for the processing subsystem. Operating costs for the processing subsystem are derived as follows:

1. The materials required for leaching are sulfur, lime, ammonia and hydrochloric acid. Materials required for solvent extraction are dextrose, ion exchange resin (cyanex 272) and DEHPA solvent. Collectively these would cost \$27.09 million annually.
2. It is assumed that the processing ship's generating capacity operates continuously and provides sufficient power (average 9,850 diesel-electric shaft HP) to: (1) deploy the processing ship in a mine site area and travel to and from home port, and (2) meet the electrical requirements for mining and processing activities that take place on the processing ship. Fuel cost is estimated at \$2.61 million annually.
3. Labor costs are for manning the processing ship (20 member ship crews) and for operating the mining/processing activities occurring on the processing ship (12 man processing crews). It is assumed that a crew spends two weeks at the mine site and returns to their home port, being replaced by an alternate crew. Labor costs include hourly wages for normal and estimated overtime, benefit costs and costs for crew food and supplies.

Table 6.3 Processing Subsystem Operating Costs (millions of 1993 dollars). After Loudat, Zaiger, and Wiltshire (1994).

<u>Item</u>	<u>(mil. \$)</u> <u>Annual Cost</u>	<u>%</u> <u>Distrib.</u>
Direct Costs		
Materials and Supplies	\$27.09	63.25%
Fuel	\$2.61	6.10%
Labor	\$7.08	16.53%
Maintenance and Repairs	\$2.51	5.85%
Operating Supplies	\$0.50	1.17%
Indirect Costs	\$1.44	3.36%
Fixed Costs		
Taxes	\$0.80	1.87%
Insurance	\$0.80	1.87%
Total Costs	\$42.80	100%

4. Maintenance and repair are estimated at 2 percent of the processing ship fixed capital cost plus 5 percent of the remaining fixed capital cost of the processing system.
5. Ship and equipment operating supplies are estimated at 20 percent of maintenance and repair costs.
6. Indirect costs are estimated at 15 percent of labor plus repair and maintenance costs.
7. Fixed costs are estimated at 1 percent of the processing system fixed capital cost for each fixed costs item.

The third subsystem is the auxiliary support subsystem that includes two ocean going vessels with specialized handling equipment. This subsystem deploys and recovers the CRC system from one mine site to another by towing the CRC hose mooring buoy and submersed pump station components while simultaneously lifting and moving the CRC and mud-slurry tanks.

The capital costs for the auxiliary support subsystem are \$29.60 million. This includes two \$12 million tugs which are 50m long, 8,000 shaft HP ocean going vessels. Each vessel is equipped with twin-screws, bow thrusters and heavy duty winches that can lift and maneuver the CRCs (360 mt static loads). Handling equipment and working capital comprise the balance of capital costs for this subsystem.

The operating cost assumptions for the auxiliary support subsystem are the same as the corresponding items outlined for the processing subsystem operating costs with the following changes. The average continuous power output of each tug is assumed to be 4,000 shaft HP. Each tug is assumed to have an 8-man crew and indirect costs are estimated at 10 percent of labor plus repair and maintenance costs. Annual auxiliary support subsystem operating costs are estimated at \$5.90 million.

The fourth subsystem is the marine transport subsystem that transfers bulk commodities to and from the processing ship. Bulk commodities transported to the ship are those materials required for processing. Bulk commodities transported from the processing ship are the target metals recovered from the crusts. A single tug and barge unit is expected to provide the required bulk transport capacity to and from an assumed home port of Los Angeles and the mining area. The tug is assumed to be similar to the vessels used for the auxiliary support subsystem and a barge is estimated to cost \$2 million. Thus, the capital cost for the marine transport subsystem is \$14 million.

Given expected bulk tonnage's, the marine transport system will only be required to provide transportation services once per month. A round-trip voyage between the mine site (assumed Johnston Island EEZ) and the assumed Los Angeles home port will require

approximately 17 days and loading and discharging an additional 3-4 days. Thus, the expected annual operating cost of the marine transportation subsystem is \$1.96 million.

The fifth subsystem is the mining support subsystem that covers support costs not accounted for in the previous subsections, primarily consisting of a mining ship servicing vessel that transports crews and supplies to the mining area. Capital costs are estimated at \$1.90 million and annual mining support subsystem operating costs are estimated at \$1.20 million.

The final subsystem is the research and development subsystem that includes all non-mining system research and development costs. It is estimated as 1.0 percent of the processing system annual operating costs.

6.3 Cost Summaries

Table 6.4 shows the capital cost summary of an ocean mining venture based on the solution mining system. The total capital cost is \$145.7 million. For comparison to other mining technologies, capital costs can be expressed as *cost per ton of crust processing capacity*. The *per ton crust capacity* capital cost of the Solution Mining system is \$482. This is much less than the *per ton crust capacity* capital cost derived by similar analysis (Loudat et al., 1994; Loudat, Zaiger and Wiltshire, 1994) for crust mining by robotic mechanical miner using high temperature, high pressure sulfuric acid processing (\$747) and crust mining by robotic mechanical miner using acid/hydrogen peroxide processing (\$665). Detailed costing of the continuous line bucket crust mining system is not yet available, but will be analyzed in the future.

Table 6.4 Total Solution Mining System Capital Cost Summary (millions of 1993 dollars). After Loudat, Zaiger, and Wiltshire (1994).

<u>Subsystem</u>	<u>(mil. \$) Capital Cost</u>	<u>% Distrib.</u>
CRC Subsystem	\$9.0	6.15%
Processing Subsystem	\$91.2	62.62%
Auxiliary Support Subsystem	\$29.6	20.32%
Marine Transport Subsystem	\$14.0	9.61%
Mining Support Subsystem	\$1.9	1.30%
Total Costs	\$145.7	100%

Table 6.5 shows the operating cost summary across all the ocean mining venture subsystems using the solution mining system for the mining and processing subsections. The total annual operating cost is \$67.8 million. This is a cost of \$224.50 per ton of crust processed. The estimated cost per ton of crust processed by the robotic mechanical miner system (*ibid.*) using high temperature, high pressure sulfuric acid processing is \$262.20 (greater by approximately 17%). If the robotic mechanical miner uses acid/hydrogen peroxide processing, the estimated cost per ton of crust processed is \$235.00 approximately 5 percent greater than the estimated operating costs per ton processed by the solution mining system.

6.4 Economic Analysis

The economic analysis of the solution mining system was conducted using the spreadsheet financial model presented in Loudat and others (1994). In this model, integration of capital and operating cost estimates for the collective subsystems yield revenue projections based on mineral prices, recovery efficiencies, mine site crust grade and tonnage. Economic viability estimates of the mining venture are made from the cost data and revenue projections.

Table 6.5 Total Solution Mining System Operating Cost Summary (millions of 1993 dollars). After Loudat, Zaiger, and Wiltshire (1994).

<u>Sector/Subsystem</u>	<u>(millions of \$) Annual Cost</u>	<u>% Distrib.</u>
Prospecting and Exploration	\$7.8	11.53%
CRC Subsystem	\$2.3	3.37%
Processing Subsystem	\$43.3	63.90%
Auxiliary Support Subsystem	\$5.9	8.67%
Marine Transport Subsystem	\$2.0	2.89%
Mining Support Subsystem	\$1.2	1.84%
Research and Development	\$0.4	0.64%
Cost of Sales	\$3.0	4.36%
Interest Expenses	\$1.9	2.80%
Total Operating Costs	\$42.80	100%
Dry Tons of Crust Processed	302,000	(per year)
Cost per Ton (in dollars)	\$224.50	

These are three economic viability measures: (1) pay back periods, (2) capital recovery rates and (3) internal rates of return of before and after tax profit streams. Mine site sensitivity analyses were done by altering base case scenario levels (i.e., changing cobalt grades and crust coverage). The base case scenario assumes crust has average Central Pacific regional metal grades (Chapter 1, Table 1.2) for the three key value metals (cobalt, nickel and manganese) and metal prices based on historical means averaged over more than 20 years (Chapter 1, Table 1.3). Base case scenario results are presented in Table 6.6. The ore value per ton is \$448.84 with revenue from metal sales of \$135.55 million per year. This base case scenario is used to calculate a minimum rate of return for the mining venture. However, a mine site most likely would be in only the highest grade areas. In addition, value metals would likely be sold at higher than the historic average prices of the base case scenario.

Table 6.6 Solution Mining Crust Per Ton Value (1993 dollars). Assumes 50% Crust Extraction Efficiency and 95% Metals Recovery from Lixiviant. After Loudat, Zaiger, and Wiltshire, 1994.

Metal Product	Recovery Per Ton of Ore Processed	Annual Metal Weight Recovered	Base Case Metal Price	Annual Revenue (mil. \$)	% of Total Revenues
Cathode Co (lbs)	0.83%	5,502,809	\$16.70	\$91.90	67.80%
Cathode Ni (lbs)	0.44%	2,909,531	\$4.01	\$11.67	8.61%
Mn (Metric tons)	23.77%	71,782	\$445.41	\$31.97	23.59%
Total Annual Revenue				\$135.55	(mil. \$)
Dry Tons of Crust Processed				302,000	(per year)
Processed Crust Ore Value				\$448.84	(per ton)

6.5 Analysis Results

Table 6.7 shows base case scenario results generated by the spreadsheet financial model. The returns of the solution mining venture's base case study shows good economic promise given the payback periods and the internal rate of return (IRR) which exceeds 30 percent. An economic study by Johnson and others (1987) concluded that an IRR of 30 percent or more is required in order for a mining company to start a high risk venture such as crust mining.

Mine site sensitivity analysis shows that the two most important economic variables are cobalt grade and cobalt price. Table 6.8 shows the impact of changing cobalt grades on the mining venture IRR. At a grade of 1.00 percent, the IRR is an attractive 37.2 percent. If a normal distribution about the mean 0.87 percent cobalt crust grade is assumed, 36 percent of crust in Middle Pacific crust permissive zones potentially have a cobalt grade of 1.00 percent or more. Table 6.9 shows the impact of alternate cobalt prices on the mining venture

Table 6.7 Solution Mining System Base Case Scenario Results. After Loudat, Zaiger, and Wiltshire (1994).

<u>Assessment Variables</u>	<u>Value</u>	<u>(mil. of \$)</u>
<i>Capital Expenditures</i>		
Total Fixed Capital Investment	\$129.7	
<i>Parent Capital Expenditures</i>		
Pre-Prod. + Parent Fixed Capital	\$124.5	
<u>Tax Savings</u>	<u>(\$52.2)</u>	
Net Parent Capital Funding	\$72.3	
<i>Pay Back Periods</i>	<i>Pre-Tax</i>	<i>Post-Tax</i>
On Fixed Capital	2.1	3.5
On Net Parent Capital Funding	1.2	1.9
<i>Real Rates of Return</i>	<i>Pre-Tax</i>	<i>Post-Tax</i>
Return on Fixed Capital	48.1%	29.0%
Return on Net Parent Capital	86.4%	52.0%
Internal Rate of Return (IRR)	29.8%	33.5%

Table 6.8 Impact of Changing Cobalt Grade on Solution Mining IRR. Other Variables at Base Case. After Loudat, Zaiger, and Wiltshire (1994).

<u>Co Grade</u>	<u>IRR</u>	<u>% Dif. from Base Case</u>	<u>Probability of Grade</u>
0.87%	33.5%	0.00%	--
1.00%	37.2%	11.13%	36.32%
1.25%	43.5%	29.79%	15.15%
1.50%	48.9%	45.82%	3.84%
2.00%	57.9%	72.69%	0.11%

Table 6.9 Impact of Changing Cobalt Price on Solution Mining IRR. All Other Variables at Base Case. After Loudat, Zaiger, and Wiltshire (1994).

Cobalt Market Value (\$/lb)	IRR	% Dif. from Base Case
\$16.70 (Base Case)	33.5%	0.00%
\$11.78 (20 yr Low)	23.4%	-30.19%
\$21.63 (20 yr High)	41.3%	23.31%
Break-Even = \$5.43/lb	0.0%	--
Current Price of \$18/lb	35.7%	6.65%

IRR. Over the range of prices shown, a 1.00 percent increase in price results in a 0.91 percent increase in the mine venture IRR, all other variables held constant. The solution mining venture break-even cobalt price is \$5.43 per pound.

Table 6.10 considers the selective mining scenario where high grade cobalt (1.25%) crust is targeted. Again, if a normal distribution is assumed, this grade level is expected to comprise 15 percent of crust in Middle Pacific crust permissive zones. As cobalt is chemically related to both nickel and manganese, 1.25 percent cobalt grade crusts also have similar enrichments in nickel and manganese (0.87% Ni and 30.2% Mn). Assuming historic average metal prices (much lower than current market price) this yields an IRR of 47.5 percent and very short pay back periods on capital. This selective mining scenario makes a solution mining system highly attractive.

Table 6.10 *Solution Mining System High Grade Selective Mining Scenario Results (1.25% Co, 0.87% Ni, 30.19% Mn, \$16.70/lb Co Market Value). After Loudat, Zaiger, and Wiltshire (1994).*

<u>Assessment Variables</u>	<u>Value</u>	<u>(mil. of \$)</u>
<i>Capital Expenditures</i>		
Total Fixed Capital Investment	\$129.7	
<i>Parent Capital Expenditures</i>		
Pre-Prod. + Parent Fixed Capital	\$124.5	
<u>Tax Savings</u>	<u>(\$52.2)</u>	
Net Parent Capital Funding	\$72.3	
<i>Pay Back Periods</i>	<i>Pre-Tax</i>	<i>Post-Tax</i>
On Fixed Capital	1.2	1.9
On Net Parent Capital Funding	0.6	1.1
<i>Real Rates of Return</i>	<i>Pre-Tax</i>	<i>Post-Tax</i>
Return on Fixed Capital	86.8%	52.1%
Return on Net Parent Capital	155.6%	93.5%
Internal Rate of Return (IRR)	43.0%	47.5%

CHAPTER 7

SUMMARY AND CONCLUSIONS

The University of Hawaii developed *in situ* crust solution mining system adapts terrestrial leach mining methods to the deep sea floor. The crux of the system is the “containment and regulation covers” (CRCs). CRCs deliver and confine lixiviant (recycling sulphurous/dithionate reductive leach solution) to the ore stratum at a crust mining site and retrieve pregnant leachate (metal containing solution) for processing onboard the mining/processing ship. The hydrometallurgical extraction is an adaptation of the U.S. Bureau of Mines process developed to recover cobalt from dilute copper leach solutions (Jeffers, 1985; Jeffers and Harvey, 1985; Bennett and Jeffers, 1988). This solution mining system is expected to cause much less environmental damage than that projected from crust mining by mechanical systems due to the elimination sediment plumes.

Many experiments using a refrigerated pressure bomb apparatus were completed to gain insight on characteristics of the sulphurous/dithionate reductive leach system at *in situ* conditions of seamount crust sites. A brief summary list follows:

1. Leach reaction rate (k) is fast despite low temperature. The reaction is essentially complete by five minutes.
2. Reaction rate (k) is pH dependant, as pH controls speciation of the SO_2 system.
3. Reaction rate (k) decreases with decreasing temperature when $\text{pH} = 1.0$. However, when $\text{pH} \geq 2.0$, k increases with decreasing temperature, probably due to a shift in the sulfurous acid system activity.

4. Reaction rate (k) increases with increasing pressure, except for Cu, probably due to an Eh dependant boundary shift in Cu soluble-solid equilibria.
5. Leach *surface product layer* formation is a problem as its buildup on crust creates resistance to the diffusive flux of lixiviant to unreacted crust minerals and dissolved products away from the crust.
6. The presence of oxygen negatively affects intact crust dissolution as free oxygen in the leach system contributes to *surface product layer* formation.
7. Leach *surface product layer* formation can be significantly mitigated by excluding free oxygen from the leach system. This can be accomplished by lixiviant deaeration.
8. Crust texture is a major factor affecting intact crust dissolution rate. Crust with botryoidal and porous structural textures achieved greater dissolution rates than crusts that have compact (massive) texture.
9. The lixiviant best suited for the *in situ* extraction of crust was determined to be a SO₂ saturated, anoxic seawater solution with pH \approx 1.0.
10. Using the “best suited” lixiviant, an extraction efficiency of 50% (an intact crust dissolution of \sim 1.25 cm thickness) is projected for an on site leaching time of 12 hours.

A preliminary economic assessment of the solution mining system was completed and compared with similar assessments of other ocean mining technologies. The innovative and low cost technology of solution mining favorably alters the economic viability of the crust mining scenario. A brief summary list follows:

1. The solution mining system-based ocean mining venture risks much less capital (\$145.7 million, total capital cost) in contrast with other potential crust mining systems, including the robotic miner--acid/hydrogen peroxide system (\$621.5 million) and the robotic miner--high temperature/pressure sulfuric acid system (\$884.6 million). In terms of *cost per ton of crust processing capacity*, the costs equate to \$482, \$665, and \$747, respectively.
2. The solution mining system post-tax pay back period on fixed capital is 3.5 years for the base case scenario and just 1.9 years for the high grade selective mining scenario.
3. The solution mining system break-even market price for cobalt is \$5.43 per pound. Historically, the 20-year low for cobalt was \$11.78 per pound. Thus even assuming a worst case scenario, the solution mining system-based ocean mining venture would still have a positive cash flow.
4. The solution mining system post-tax internal rate of return (IRR) is 33.5% for the base case scenario and 47.5% for the high grade selective mining scenario. These rates are well above the 30% IRR figure typically cited as the minimum rate demanded for high risk natural resources projects (Johnson et al., 1987).

Much additional research is required before a crust mining venture can become a reality. Needed research includes: further refinement of the leach method, scale model CRC testing and analysis, and validation of process flow rates. However, potential profitability seems likely based on preliminary economic assessments. Thus, development efforts to prove the viability of *in situ* solution crust mining at the pilot plant level seem highly justified.

APPENDIX: EXPERIMENTAL DATA: GROUND CRUST

Exp #	Leach Time (minutes)	pH	Temp (C)	P (atm)	N	r% Fe	r% Mn	r% Co	r% Ni	r% Cu	S.D. Fe	S.D. Mn	S.D. Co	S.D. Ni	S.D. Cu
1	5	1.0	0.1	1	3	96.22	98.95	98.18	93.08	94.12	5.31	5.82	4.55	2.37	5.88
2	5	2.0	0.1	1	3	20.99	78.29	83.27	63.80	45.75	0.76	2.37	2.78	0.99	1.13
3	5	3.0	0.1	1	3	5.40	45.92	45.00	27.61	1.58	0.43	2.90	2.00	1.48	2.37
4	5	1.0	5.0	1	4	86.51	99.52	96.95	92.40	91.88	2.61	0.62	0.37	1.53	3.42
5	5	2.0	5.0	1	3	17.14	79.93	81.90	64.39	28.08	1.13	5.10	4.28	3.66	1.59
6	5	2.0	5.0	100	3	19.87	78.57	83.05	70.06	38.98	1.32	4.52	7.22	4.42	1.69
7	5	2.0	5.0	200	3	17.55	76.75	81.17	60.48	10.96	0.15	1.90	1.35	0.10	4.32
8	5	1.0	15.0	1	6	94.01	99.97	99.10	96.04	93.51	1.11	1.33	1.97	2.57	9.23
9	5	2.0	15.0	1	6	14.13	72.04	70.96	57.46	24.58	0.81	0.50	1.31	1.52	2.78
10	5	3.0	15.0	1	6	2.11	49.32	42.90	32.60	3.79	0.15	0.58	1.00	0.58	3.67
11	5	5.0	15.0	1	6	1.51	47.00	37.41	28.78	6.23	0.06	1.97	0.93	1.04	2.59
12	5	1.0	15.0	100	3	92.82	99.99	99.36	92.79	33.28	1.50	1.37	0.27	0.17	10.35
13	5	2.0	15.0	100	3	12.92	74.50	73.11	59.00	0.68	0.38	2.55	2.27	1.34	1.17
14	5	1.0	15.0	200	3	91.33	95.40	99.65	93.70	54.13	1.33	0.55	0.46	0.45	0.23
15	5	2.0	15.0	200	3	21.60	88.42	84.34	71.13	16.83	0.07	0.10	0.01	0.55	5.39
16	10	1.0	10.0	1	4	94.37	99.98	99.99	96.21	99.99	0.47	0.82	0.77	1.40	1.97
17	15	1.0	0.1	1	3	95.94	99.99	98.15	94.18	93.61	7.89	7.44	5.19	2.46	5.86
18	15	2.0	0.1	1	3	22.98	84.04	88.01	68.74	37.14	1.36	3.27	1.81	0.89	2.82
19	15	3.0	0.1	1	3	5.82	56.76	51.66	36.25	1.58	0.29	3.45	2.36	1.87	1.24
20	15	1.0	5.0	1	3	83.47	99.99	97.74	93.35	95.31	4.69	2.42	1.65	4.23	3.08
21	15	2.0	5.0	1	3	17.93	79.06	80.21	64.83	21.09	1.09	4.35	3.67	4.24	0.11
22	15	3.0	5.0	1	3	3.12	61.84	50.00	40.91	4.75	0.20	2.36	2.45	3.16	0.68
23	15	5.0	5.0	1	3	1.90	53.47	43.41	35.28	3.62	0.11	3.27	2.50	1.98	1.47
24	15	1.0	5.0	100	3	98.64	99.99	98.37	91.12	98.69	6.95	5.81	4.31	1.38	9.82
25	15	2.0	5.0	100	3	23.99	87.30	87.73	72.83	41.29	1.82	6.37	5.00	5.43	2.83
26	15	3.0	5.0	100	6	3.26	61.48	51.52	41.44	6.10	0.15	2.29	1.48	1.00	0.45
27	15	5.0	5.0	100	6	2.26	57.33	46.09	37.76	4.58	0.12	2.83	1.71	1.48	1.92
28	15	1.0	5.0	200	3	92.17	98.12	99.99	94.87	51.75	1.33	1.09	0.69	0.45	4.13
29	15	2.0	5.0	200	6	22.41	85.99	89.11	73.06	11.86	1.99	2.59	3.32	2.04	8.74
30	15	3.0	5.0	200	6	3.12	62.87	52.47	43.24	6.04	0.72	2.52	2.00	1.69	7.38
31	15	5.0	5.0	200	6	1.48	57.20	47.65	39.39	3.36	1.51	3.77	2.56	5.00	3.12
32	15	1.0	15.0	1	6	91.97	98.22	99.53	95.60	91.66	1.38	1.18	1.23	0.82	2.34

Exp #	Leach Time (minutes)	pH	Temp (C)	P (atm)	N	r% Fe	r% Mn	r% Co	r% Ni	r% Cu	S.D. Fe	S.D. Mn	S.D. Co	S.D. Ni	S.D. Cu
33	15	2.0	15.0	1	6	14.44	78.58	73.06	62.70	20.20	3.91	3.52	4.18	4.50	8.09
34	15	3.0	15.0	1	6	1.53	59.54	42.78	40.21	5.16	0.17	0.88	0.86	0.58	3.94
35	15	5.0	15.0	1	6	1.30	57.42	36.25	36.54	8.34	0.17	0.82	0.82	0.41	2.22
36	15	1.0	15.0	100	6	93.74	99.55	99.99	95.25	41.78	1.32	1.65	1.47	1.10	11.27
37	15	2.0	15.0	100	6	11.47	81.51	77.28	64.87	1.17	4.23	4.18	2.55	3.09	2.04
38	15	3.0	15.0	100	6	1.74	66.31	45.89	45.07	0.39	0.26	2.39	2.07	1.20	0.80
39	15	5.0	15.0	100	6	1.24	60.13	39.39	39.90	0.00	0.22	0.23	1.64	1.14	0.00
40	15	1.0	15.0	200	6	90.47	97.69	99.20	91.79	39.24	3.64	2.60	1.46	2.23	14.25
41	15	2.0	15.0	200	3	13.16	78.07	72.65	62.55	2.37	0.10	0.28	0.91	0.64	0.23
42	15	3.0	15.0	200	3	1.79	66.44	46.27	45.53	0.98	0.04	1.27	0.91	0.35	1.50
43	15	5.0	15.0	200	3	1.13	62.75	41.43	42.49	0.60	0.04	0.55	0.71	0.01	1.05
44	15	0.5	10.0	1	5	84.71	93.25	90.97	86.13	90.88	4.71	4.48	3.44	4.32	2.42
45	15	1.0	10.0	1	5	82.92	98.49	96.02	90.11	94.48	2.70	3.73	2.60	2.29	4.96
46	15	1.5	10.0	1	3	71.04	77.92	78.36	73.39	82.20	6.83	7.81	5.90	5.55	7.01
47	5	1.0	25.0	1	3	92.18	98.32	99.99	95.98	91.72	0.13	1.79	0.54	0.15	2.87
48	30	1.0	0.1	1	3	98.21	99.99	99.26	94.66	90.27	4.64	5.45	3.03	0.05	8.82
49	30	2.0	0.1	1	3	25.75	89.49	90.00	74.51	31.22	1.13	4.37	2.23	1.88	4.07
50	30	1.0	5.0	1	3	88.74	99.99	98.57	93.85	96.59	4.12	2.37	1.17	3.02	2.90
51	30	2.0	5.0	1	3	15.69	85.49	82.27	68.18	15.27	0.56	3.27	2.73	1.38	2.38
52	30	1.0	5.0	100	4	92.39	99.30	100.00	92.66	42.95	3.51	2.74	2.46	2.55	9.60
53	30	2.0	5.0	100	4	22.46	90.13	90.80	74.60	1.66	0.62	1.32	1.19	0.69	3.32
54	30	1.0	5.0	200	4	92.77	99.99	98.91	93.00	30.75	4.05	2.59	1.75	0.87	9.72
55	30	2.0	5.0	200	3	14.77	86.52	85.00	68.64	0.00	0.68	4.10	4.09	2.33	0.00
56	30	1.0	15.0	1	6	94.07	99.06	98.73	94.97	95.50	1.84	1.10	2.89	3.36	7.17
57	30	2.0	15.0	1	6	16.41	84.71	76.90	69.83	21.20	5.56	2.47	5.20	3.78	10.71
58	30	3.0	15.0	1	6	1.65	66.59	39.75	46.42	5.46	0.24	1.09	0.54	1.10	4.45
59	30	5.0	15.0	1	6	1.13	63.25	31.90	41.31	5.30	0.31	0.68	0.53	0.10	2.11
60	30	1.0	15.0	100	3	90.17	99.99	97.77	92.60	35.70	1.83	3.91	1.37	2.22	11.98
61	30	2.0	15.0	100	3	8.80	86.82	76.21	71.25	0.00	0.15	3.18	1.14	1.88	0.00
62	30	1.0	15.0	200	3	90.55	99.99	94.08	90.50	33.40	1.00	0.28	3.17	1.97	11.75
63	30	2.0	15.0	200	3	25.76	67.48	69.39	58.89	21.27	0.12	0.36	0.26	0.40	2.83
64	30	3.0	15.0	200	3	11.89	61.23	62.45	49.93	11.25	0.17	0.46	0.26	0.25	0.40

APPENDIX: EXPERIMENTAL DATA; GROUND CRUST

REFERENCES

- Aplin, Andrew C.; Cronan, D.S. (1985): Ferromanganese oxide deposits from the Central Pacific Ocean, I. Encrustations from the Line Islands Archipelago. *Geochim. Cosmochim. Acta* v. 49, 427-436.
- Asai, S.; Negi, H.; Konishi, Y. (1986): Reductive Dissolution of Manganese Dioxide in Aqueous Sulfur Dioxide Solutions. *Canadian Journal of Chemical Engineering* v. 64, 237-242.
- Back, A.E.; Ravitz, S.F.; Tame, K.E. (1957): Formation of Dithionate and Sulfate in the Oxidation of Sulfur Dioxide by Manganese Dioxide and Air. (Bureau of Mines Report of Investigations, RI 4931) U.S. Dept. of the Interior, Washington, D.C. 14 pages.
- Basset, H.; Parker, W.G. (1951): The Oxidation of Sulfurous Acid. *Journal of the Chemistry Society, London*, 1540-1560.
- Bennett, P.G.; Jeffers, T.H. (1988): Recovery of Cobalt From Spent Copper Leach Solutions--Improved Elution and Impurity Removal Techniques, With Revised Process Economics. (Bureau of Mines Report of Investigations, RI 9190.) U.S. Dept. of the Interior, Washington, D.C. 9 pages.
- Boehlert, G.W.; Genin, A. (1987): A Review of the Effects of Seamounts on Biological Processes. In: *Seamounts, Islands and Atolls*. Geophysical Monograph No. 47. (Eds: Keating, B.; Fryer, P.; Batiza, R.; Boehlert, G.) American Geophysical Union, Washington, D.C., 319-334.
- Bradley, R.S.; Munro, D.C. (1965): *High Pressure Chemistry*. Pergamon Press Ltd., London. 186 pages.
- Brezonik, Patrick L. (1994): *Chemical Kinetics and Process Dynamics in Aquatic Systems*. Lewis Publishers, Boca Raton, FL. 754 pages.
- Brookins, Douglas G. (1988): *Eh-pH Diagrams for Geochemistry*. Springer-Verlag, New York. 176 pages.
- Burns, R.G.; Burns, V.M. (1977): Mineralogy. In: *Marine Manganese Deposits*. Elsevier Oceanography Series, Volume 15. (Ed: Glasby, G.P.) Elsevier Scientific Publishing Co., Amsterdam, 185-248.
- Carter, R.A. (1991): The Trend to SX-EW. *Engineering and Mining Journal* v. 192, no. 2, 16S-16U.

- Clark, A.L.; Johnson, C.J. (1986): Cobalt-Rich Manganese Crust Potential of the U.S. Trust and Affiliated Territories. In: Paper 5233 in Offshore Technology Conference. (Ed: Program Dept.) Offshore Technology Conference, Richardson, TX, 111-118.
- Cotton, F.A.; Wilkinson, G. (1980): *Advanced Inorganic Chemistry, A Comprehensive Text*. 4th edition. John Wiley & Sons, New York. 1,396 pages.
- Cotton, F.; Wilkinson, G.; Gaus, P. (1987): *Basic Inorganic Chemistry*. 2nd edition. John Wiley & Sons, New York. 708 pages.
- Cowen, James P.; DeCarlo, E.H.; McGee, D.L. (1993): Calcareous Nannofossil Biostratigraphic Dating of a Ferromanganese Crust from Schumann Seamount. *Marine Geology* v. 115, 289-306.
- Cowen, James P.; Li, Yuan Hui (1991): The Influence of a Changing Bacterial Community on Trace Metal Scavenging in a Deep-sea Particle Plume. *Journal of Marine Research* v. 49, no. 3, 517-542.
- Cowen, James P.; Massoth, G.J.; Feely, R.A. (1990): Scavenging Rates of Dissolved Manganese in a Hydrothermal Vent Plume. *Deep-Sea Research* v. 37, 1619-1637.
- CRC (1980): *Handbook of Chemistry and Physics*. 60th edition. (Series Eds: Weast, R.C.; Astle, M.J.) CRC Press, Inc., Boca Raton, FL. 2,450 pages.
- Cruickshank, Michael J.; Paul, R.C. (1986): Characterization of Seabed Rocks for Mine Planning in the EEZ. In: Paper 5236 in Offshore Technology Conference. (Ed: Program Dept.) Offshore Technol. Conf., Richardson, TX, 135-145.
- DeCarlo, Eric H. (1991): Paleooceanographic Implications of Rare Earth Element Variability within a Fe-Mn Crust from the Central Pacific Ocean. *Marine Geology* v. 98, 449-467.
- DeCarlo, Eric H.; McMurtry, G.M.; Kim, K.H. (1987): Geochemistry of Ferromanganese Crusts from the Hawaiian Archipelago--I. Northern Survey Areas. *Deep-Sea Research* v. 34, no. 3, 441-467.
- Dixit, S.G.; Raison, P.R. (1987): Effect of Oxygen on the Leaching of Manganese Dioxide by Aqueous Sulphur Dioxide Solution. *Indian Journal of Technology* v. 25, 517-519.
- Dobos, G. (1988): Studies on the Kinetics of Ion-exchange Leaching of the Hungarian Rhodocrosite Ore of Urkut Origin. *Reactive Polymers* v. 7, 277-288.

- Drago, Russell S. (1977): Principles of Chemistry with Practical Perspectives. 2nd edition. Allyn and Bacon, Inc., Boston. 848 pages.
- Dresler, W. (1984): Leaching of Manganese Dioxide in Nitrous Acid. Canadian Metallurgy Quarterly v. 23, 271-279.
- EIS (1990): *see* U.S. Dept. of the Interior, Minerals Management Service and the State of Hawaii Dept. of Business and Economic Development (1990).
- Faugeras, P.; Miquel, P.; Robaglia, M. (1977): Extraction of Metals from Sea Nodules. (to Commissariat a l'Energie Atomique) Application: Paris, France. U.S. Patent 4,029,733.
- Freeze, R.A.; Cherry, J.A. (1979): Groundwater. Prentice-Hall, Inc., Englewood Cliffs, New Jersey. 604 pages.
- Fuerstenau, D.W.; Han, K.N. (1977): Extractive Metallurgy. In: Marine Manganese Deposits. Elsevier Oceanography Series, Vol. 15. (Ed: Glasby, G.P.) Elsevier Scientific Publishing Co., New York, 357-390.
- Furrer, G.; Stumm, W. (1986): The Coordination Chemistry of Weathering: I. Dissolution Kinetics of $\delta\text{Al}_2\text{O}_3$ and BeO. Geochim. Cosmochim. Acta. v. 50, 1861-1869.
- Gimarc, B.M. (1979): Molecular Structure and Bonding. In: The Qualitative Molecular Orbital Approach. (Ed: Gimarc, B.M.) Academic Press, London, 153-169.
- Grigg, Richard W.; Malahoff, A.; Chave, E.H.; Landahl, J. (1987): Seamount Benthic Ecology and Potential Environmental Impact from Manganese Crust Mining in Hawaii. In: Seamounts, Islands, and Atolls. (Eds: Keating, B.H. et al.) (Geophysical Monograph, 43.) American Geophysical Union, Washington, D.C., 379-390.
- Gritton, K.S.; Jeffers, T.H. (1987): Numerical Prediction of Cobalt Sorption in a Continuous Ion-Exchange Column. (Bureau of Mines Report of Investigations, RI 9120.) U.S. Dept. of the Interior, Washington D.C. 13 pages.
- Halbach, Peter E.; Manheim, F.T. (1984): Potential of Cobalt and Other Metals in Ferromanganese Crusts on Seamounts of the Central Pacific Basin. Marine Mining v. 4, no. 4, 319-336.
- Halbach, Peter E.; Puteanus, D. (1985): Cobalt-Rich Ferromanganese Deposits within the Johnston Island EEZ: Environmental and Resource Data. Technical University of Clausthal, Internal Report., Clausthal-Zellerfeld, Germany.

- Halbach, Peter E.; Sattler, C. D.; Teichmann, F.; Wahsner, M. (1989): Cobalt-Rich and Platinum-Bearing Manganese Crust Deposits on Seamounts: Nature, Formation, and Metal Potential. *Marine Mining* v. 8, no. 1, 23-39.
- Halbach, Peter E.; Segl, M.; Puteanus, D.; Mangini, A. (1983): Co-fluxes and Growth Rates in Ferromanganese Deposits from Central Pacific Seamount Areas. *Nature* v. 304 (25 August), 716-719.
- Halkyard, J.E.; Felix, D. (1987): "Mining System". In: Mining Development Scenario for Cobalt-Rich Manganese Crusts in the Exclusive Economic Zones of the Hawaiian Archipelago and Johnston Island. (Ed: Marine Development Associates, Inc.) State of Hawaii Department of Planning and Economic Development, Honolulu, HI.
- Han, K.N. (1972): Geochemistry and Extraction of Metals from Ocean Floor Manganese Nodules, Ph.D. Dissertation. University of California, Berkeley. 212 pages.
- Han, K.N.; Fuerstenau, D.W. (1980): Extraction Behavior of Metal Elements from Deep-Sea Manganese Nodules in Reducing Media. *Marine Mining* v. 2, 155-169.
- Haynes, Benjamin W.; Law, S.L.; Barron, D.C.; Kramer, G.W.; Maeda, R.; Magyar, M.J. (1985): Pacific Manganese Nodules: Characterization and Processing. (Bureau of Mines, Bulletin 679.) U.S. Dept. of the Interior, Washington D.C. 44 pages.
- Heezen, Bruce C.; Fischer, A.G.; Boyce, R.E.; Bukry, D.; Douglas, R.G.; Garrison, R.F.; Kling, S.A.; Krasheninnikov, V.; Lisitzin, A.P.; Pimm, A.C. (1971): Site 44, Leg VI, Deep Sea Drilling Project. In: Initial Reports of the Deep Sea Drilling Project, Vol. 6. (Ed: Fischer, A.G. et al.) Government Printing Office, Washington, D.C., 17-39.
- Hein, James R.; Bohrsen, W.A.; Schulz, M.J.; Noble, M.; Clague, D.A. (1992): Variations in the Fine-scale Composition of a Central Pacific Ferromanganese Crust: Paleoceanographic Implications. *Paleoceanography* v. 7, 63-77.
- Hein, James R.; Kirschenbaum, H.; Schwab, W.C.; Usui, A.; Taggart, J.E.; Stewart, K.C.; Davis, A.S.; Terashima, S.; Quinterno, P.J.; Olson, R.L.; Pickthorn, L.G.; Schulz, M.S.; Morgan, C.L. (1990): Mineralogy and Geochemistry of Co-Rich Ferromanganese Crusts and Substrate Rocks from Karin Ridge and Johnston Island, Farnella Cruise F7-86-HW. USGS Open File Report 90-298. U.S. Geological Survey, Washington, D.C. 80 pages.
- Hein, James R.; Manheim, F.T.; Schwab, W.C. (1986): Cobalt-Rich Ferromanganese Crusts From the Central Pacific. In: Paper 5234 in Offshore Technology Conference. (Ed: Program Dept.) Offshore Technology Conference, Richardson, TX, 119-126.

- Hein, James R.; Manheim, F.T.; Schwab, W.C.; Davis, A.S. (1985): Ferromanganese Crusts from Necker Ridge, Horizon Guyot and S.P. Lee Gutot: Geological Considerations. *Marine Geology* v. 69, 25-54.
- Herring, A.P.; Ravitz, S.F. (1965): Rate of Dissolution of Manganese Dioxide in Sulfurous Acid. *SME Transactions* v. 232, 191-196.
- Higginson, W.C.E.; Marshall, J.W. (1957): Equivalence Changes in Oxidation-Reduction Reactions in Solution: Some Aspects of the Oxidation of Sulphurous Acid. *Journal of the Chemical Society of London*, February, 1957. 447-458.
- Hurlbut, Cornelius S. Jr.; Klein, C. (1977): *Manual of Mineralogy* (after James D. Dana). 19th edition. John Wiley & Sons, New York. 532 pages.
- Ingram, B.L.; Hein, J.R.; Farmer, G.L. (1990): Age Determinations and Growth Rates of Pacific Ferromanganese Deposits Using Strontium Isotopes. *Geochim. Cosmochim. Acta* v. 54, 1709-1721.
- Jeffers, T.H. (1985): Separation and Recovery of Cobalt from Copper Leach Solutions. *Journal of Metals*. v. 11, no. 1, 47-50.
- Jeffers, T.H.; Harvey, M.R. (1985): Cobalt Recovery from Copper Leach Solutions. (Bureau of Mines Report of Investigations, RI 8927.) U.S. Dept. of the Interior, Washington, D.C. 12 pages.
- Johnson, C.J. et al. (1987): Resource Assessment. In: *Mining Development Scenario for Cobalt-Rich Manganese Crusts in the Exclusive Economic Zones of the Hawaiian Archipelago and Johnston Island*. (Ed: Marine Development Associates, Inc.) State of Hawaii Department of Planning and Economic Development, Honolulu, Hawaii, 19-78.
- Johnson, J. (1992): New Frontiers for Cobalt. In: *Cobalt at the Crossroads*, Conference Proceedings, June 22-24, 1992, Washington, D.C. (Ed: Intertech Corporation), Portland, Maine.
- Jolly, W.L. (1984): Kinetics and Mechanisms of Reactions of Transition-metal Complexes. In: *Modern Inorganic Chemistry*. (Ed: Jolly, W.L.) McGraw-Hill, New York, 447-469.
- Jordan, C.E. (1988): Processing Technologies for Extracting Cobalt from Domestic Resources. (Bureau of Mines Information Circular, IC 9176.) U.S. Dept. of the Interior, Washington, D.C. 24 pages.
- Kane, W.S.; Cardwell, P.H. (1974 a): Method for Separating Metal Values from Ocean Floor Nodule Ore. U.S. Patent 3,810,827.

- Kane, W.S.; Cardwell, P.H. (1974 b): Mixed Ore Treatment of Ocean Floor Nodule Ore and Iron Sulfidic Land Based Ores. U.S. Patent 3,809,624.
- Kane, W.S.; Cardwell, P.H. (1975): Reduction Method for Separating Metal Values from Ocean Floor Nodule Ore. U.S. Patent 3,869,360.
- Khalafalla, Sanaa E.; Pahlman, J.E. (1981): Selective Extraction of Metals from Pacific Sea Nodules With Dissolved Sulfur Dioxide. (Bureau of Mines Report of Investigations, RI 8518.) U.S. Dept. of the Interior, Washington, D.C. 26 pages.
- Larson, D.A.; Tandanand, S.; Boucher, M.L.; Olson, M.S. (1987): Physical Properties and Mechanical Cutting Characteristics of Cobalt-Rich Manganese Crusts. (Bureau of Mines Report of Investigations, RI 9128.) U.S. Dept. of the Interior, Washington, D.C. 35 pages.
- Lee, Jong H. (1979): Chemical Analysis and Recovery of Metals from Ferromanganese Nodules by Sulfation. Ph.D. Dissertation, University of Hawaii, Honolulu. 163 pages.
- Lee, Jong H.; Gilje, J.; Zeitlin, H. (1978): Low-Temperature Interaction of Sulfur Dioxide with Pacific Ferromanganese Nodules. *Environmental Science & Technology* v. 12, no. 13, 1428-1431.
- Levenspiel, Octave (1972): *Chemical Reaction Engineering*. 2nd edition. John Wiley & Sons, New York. 578 pages.
- Lonsdale, Peter; Normark, W.R.; Newman, W.A. (1972): Sedimentation and Erosion on Horizon Guyot. *Geological Society of America Bulletin* v. 83, 289-316.
- Loudat, Thomas A.; Wiltshire, J.C.; Allen, J.P.; Hirt, W.C. (1994): The Economics of Mining Manganese Crust with Recovery of Platinum and Phosphorus. Report. State of Hawaii Department of Business and Economic Development, Honolulu, Hawaii. 65 pages.
- Loudat, Thomas A.; Zaiger, K.K.; Wiltshire, J.C. (1994): New Ocean Mining Technologies and their Impact on the Profitability of Mining Manganese Crusts. Report. State of Hawaii Department of Business and Economic Development, Honolulu, Hawaii. 40 p.
- Luther, George W. (1987): Pyrite Oxidation and Reduction: Molecular Orbital Theory Considerations. *Geochim. Cosmochim. Acta* v. 51, 3193-3199.
- Luther, George W. (1990): The Frontier-Molecular-Orbital Theory Approach in Geochemical Processes. In: *Aquatic Chemical Kinetics*. (Ed: Stumm, W.) Wiley Interscience, New York, 173-198.

- Malti, M.A.; Rophael, M.W.; Bhayat, I.I. (1981): The Kinetics of Pyrophosphate Leaching of Partially Reduced Manganese Dioxides. *Electrochim. Acta* v. 26, 239-243.
- Manheim, Frank T. (1986): Marine Cobalt Resources. *Science*. v. 232, 600-608.
- Manheim, Frank T. (1989): Introduction. In: U.S.G.S. Open File Report 89-020; Chemical Composition of Ferromanganese Crusts in the World Ocean: A Review and Comprehensive Database. (Eds: Manheim, F.T.; Lane-Bostwick, C.M.) U.S.G.S. Office of Energy and Marine Geology, Woods Hole, MA, 463 pages.
- Manheim, Frank T.; Lane-Bostwick, C.M. (Eds.) (1989): Chemical Composition of Ferromanganese Crusts in the World Ocean: A Review and Comprehensive Database. U.S.G.S. Open File Report 89-020; U.S.G.S. Office of Energy and Marine Geology, Woods Hole, MA, 463 pages.
- Manheim, Frank T.; Lane-Bostwick, C.M. (1988): Cobalt in Ferromanganese Crusts as a Monitor of Hydrothermal Discharge on the Pacific sea floor. *Nature* v. 335 (1 September 1988), 59-62.
- Masuda, Yoshio (1985): Continuous Line Bucket (CLB) Mining Systems. In: *Marine Mining: A New Beginning; State of Hawaii Marine Mining Program, Conference Proceedings July 18-21, 1982 Hilo, Hawaii*. (Ed: Humphrey, P.B.) State of Hawaii, Department of Planning & Economic Development, Honolulu, 61-71.
- Masuda, Yoshio (1991): Crust Mining Plans of the Japan Resources Association. *Marine Mining* v. 10, 95-101.
- Masuda, Yoshio; Cruickshank, M.J. (1991): Mechanical Design Developments for a CLB Mining System. In: *Ocean Technologies and Opportunities in the Pacific for the 90's. OCEANS 91 Proceedings, October 1-3, 1991, Honolulu, Hawaii, USA. Vol. 3.* (Ed: Oceanic Engineering Society) IEEE, Piscataway, NJ, 1583-1586.
- Masuda, Yoshio; Cruickshank, M.J.; Mero, J.L. (1971): Continuous Bucket Line Dredging at 12,000 Feet. In: *1971 Offshore Technology Conference Proceedings, Paper no. 1410* (Ed: OTC Staff) IEEE, Houston, TX.
- Matsuda, Yoshio; Cruickshank, M.J.; Abernathy, J.A. (1993): Design of a Turning CLB and Planning for a Small Scale Mining Test. In: *Recent Advances in Marine Science and Technology, 92.* (Ed: Saxena, N.) PACON International, Honolulu, HI, 395-403.
- Matsuda, Yoshio; Cruickshank, M.J.; Abernathy, J.A.; Winston, R. (1991): Feasibility Study of Crust Mining in the Republic of the Marshall Islands. In: *Ocean Technologies and Opportunities in the Pacific for the 90's. OCEANS 91 Proceedings, October 1-3, 1991,*

- Honolulu, Hawaii, USA. Vol. 3. (Ed: Oceanic Engineering Society) IEEE, Piscataway, NJ, 1475-1478.
- McMurtry, Gary M.; VonderHaar, D.L.; Eisenhauer, A.; Mahoney, J.J.; Yeh, H-W. (1994): Cenozoic Accumulation History of a Pacific Ferromanganese Crust. *Earth and Planetary Science Letters* v. 125, 105-118.
- Mero, J.L. (1962): Process for Separation of Nickel from Cobalt in Ocean Floor Manganiferous Ore Deposits. U.S. Patent 3,169,856.
- Miller, J.D.; Wan, R. (1983): Reaction Kinetics for the Leaching of Manganese Dioxide by Sulfur Dioxide. *Hydrometallurgy* v. 10, 219-242.
- Morgan, Charles L. (1989): The Primary Variables of Resource Assessment for Central Pacific Manganese Crust Deposits. In: *Proceedings, EEZ Resources: Technology Assessment Conference, January 22-26, 1989, Honolulu, HI USA.* (Ed: IOTC Staff) International Ocean Technology Congress, Honolulu, 5.69-5.75.
- Morgan, Charles L.; Mahan, R.O.; Malahoff, A.; Wiltshire, J.C. (1988): Microtopography of Cross Seamount. *Marine Mining* v. 7, 249-269.
- Murray, J.W.; Dillard, J.G. (1979): The Oxidation of Cobalt (II) Adsorbed on Manganese Dioxide. *Geochim. Cosmochim. Acta* v. 43, 781-787.
- Nasu, Keiji; Sasaki, T. (1973): Surveys of the Mid-Pacific Seamounts by the "RV KAIYO MARU". *Bulletin of the Japanese Society of Fisheries and Oceanography* v. 23, 56-70.
- Natland, J.H. (1976): Possible Volcanologic Explanations for the Origin of Flat-topped Seamounts and Ridges in the Line Islands and Mid-Pacific Mountains. In: *Initial Reports of the Deep Sea Drilling Project, Vol. 33.* (Ed: Aumento, F. et al.) U.S. Government Printing Office, Washington, D.C., 779-787.
- Pahlman, John E.; Khalafalla, S. E. (1988): Leaching of Domestic Manganese Ores with Dissolved SO₂. (Bureau of Mines Report of Investigations, RI 9150.) U.S. Dept. of the Interior, Washington, D.C., 15 pages.
- Petrie, Lloyd M. (1991): Lixiviant Selection for Manganese *In Situ* Leach Mining - A Geochemical Approach. Bureau of Mines Open File Report No. 6-91. U.S. Bureau of Mines, Twin Cities Research Center, Minneapolis, MN. 119 pages.
- Purser, G.H. (1989): The Significance of the Bond Angle in Sulfur Dioxide. *Journal of Chemistry Education* v. 66, 710-713.

- Ritchey, J.L. et al. (1986): Cobalt Rich Manganese Crust in the U.S. EEZ as a Potential Source of Cobalt, (Bureau of Mines Information Circular, IC 9067.) U.S. Dept. of the Interior, Washington, D.C. 10 pages.
- Ritchey, J.L. (1987): Assessment of Cobalt-Rich Manganese Crust Resources on Horizon and S.P.Lee Guyots, U.S. Exclusive Economic Zone. *Marine Mining* v. 6, 231-244.
- Roden, Gunnar I. (1987): Effect of Seamounts and Seamount Chains on Ocean Circulation and Thermohaline Structure. *Journal of Geophysical Research* v. 92, 335-354.
- Roden, Gunnar I.; Taft, B.A. (1985): Effect of the Emperor Seamounts on the Mesoscale Thermohaline Structure During the Summer of 1982. *Journal of Geophysical Research* v. 90, 839-855.
- Saini-Eidukat, B.; Marozas, D.C.; Blake, R.L.; Adamson, N.R. (1993): Implications of Rock Mineralogy and Texture on the Feasibility of *In Situ* Leach Mining of Mn-bearing Iron Formations of Central Minnesota, U.S.A. *Applied Geochemistry* v. 8, 37-49.
- Sasaki, T. (1986): Development and Present Status of Japanese Trawl Fisheries in the Vicinity of Seamounts. In: *Environment and Resources of Seamounts in the North Pacific*. NMFS Technical Report 43. (Eds: Uchida, R.N.; Hayasi, S.; Boehlert, G.W.) NOAA, U.S. Government Printing Office, Washington, D.C., 21-30.
- Schein, Daniel B. (1986): Separation of Metals from Ferromanganese Ores Via Sulfation, and Seawater Leaching of Trace Metals from Processed Ferromanganese Nodule Wastes. Ph.D. Dissertation, University of Hawaii, Honolulu, 139 pages.
- Segl, M.; Mangini, A.; Beer, J.; Bonani, G.; Suter, M.; Wölfli, W. (1989): Growth Rate Variations of Manganese Nodules and Crusts Induced by Paleooceanographic Events. *Paleoceanography* v. 4, no. 5, 511-530.
- Segl, M.; Mangini, A.; Bonani, G.; Hoffmann, H.J.; Nessi, M.; Suter, M.; Wölfli, W.; Friedrich, G.; Pluger, W.L.; Wiechowski, A.; Beer, J. (1984): ^{10}Be -dating of a Manganese Crust from Central North Pacific and Implications for Ocean Paleocirculation. *Nature* v. 309, 540-543.
- Shedd, Kim B. (1991): Cobalt. (Bureau of Mines, Minerals Yearbook 1989.) U.S. Dept. of the Interior, Washington, D.C. 11 pages.
- Spieß, F.N.; Mudie, J.D. (1970): Small-scale Topographic and Magnetic Features. In: *The Sea*, Vol. 4. (Ed: Maxwell, A.E.) Interscience, New York, 205-250.

- Stone, Alan T.; Morgan, J.J. (1984): Reduction and Dissolution of Manganese (III) and Manganese (IV) Oxides by Organics. 1. Reaction with Hydroquinone. *Environmental Science & Technology* v. 18, no. 6, 450-456.
- Stone, Alan T.; Morgan, J.J. (1987): Reductive Dissolution of Metal Oxides. In: *Aquatic Surface Chemistry*. (Ed: Stumm, W.) Wiley-Interscience, New York, 221-254.
- Stumm, Werner; Morgan, J.J. (1981): *Aquatic Chemistry, An Introduction Emphasizing Chemical Equilibria in Natural Waters*. 2nd ed. Wiley-Interscience, New York. 780 p.
- Stumm, Werner; Wieland, E. (1990): Dissolution of Oxide and Silicate Minerals: Rates Depend on Surface Speciation. In: *Aquatic Chemical Kinetics, Reaction Rates of Processes in Natural Waters*. (Ed: Stumm, W.) John Wiley & Sons, Inc., New York, 367-400.
- Uchida, R.N.; Hayasi, S.; Boehlert, G.W. (Eds.) (1986): *Environment and Resources of Seamounts in the North Pacific*. NOAA Technical Report, NMFS. U.S. Government Printing Office, Washington, D.C. 105 pages.
- Uchida, R.N.; Tagami, D.T. (1984): Groundfish Fisheries and Research in the Vicinity of Seamounts in the North Pacific Ocean. *Marine Fisheries Review* v. 46, 1-17.
- Usatenko, Y.I.; Ryl'kova, A.S. (1983): Dissolution Kinetics of Manganese Oxide Ores in an Acetic Acid Solution of Potassium Iodide. *Journal of Analytical Chemistry, U.S.S.R. (English version)* v. 38, 66-70.
- U.S. Bureau of Mines (1987): *Bureau of Mines Cost Estimating System Handbook*, (Bureau of Mines Information Circular, IC 9143) U.S. Dept. of the Interior, Washington, D.C. 34 pages.
- U.S. Department of Commerce (1993): *Statistical Abstract of the United States*. Bureau of the Census, Washington, D.C.
- U.S. Dept. of the Interior, Minerals Management Service and the State of Hawaii Dept. of Business and Economic Development (1990): *Final Environmental Impact Statement. Proposed Marine Mineral Lease Sale: Exclusive Economic Zone Adjacent to Hawaii and Johnston Island, EIS/EA MMS 90-029*. Vol. 1 & 2. U.S. Dept. of the Interior, Minerals Management Service and the State of Hawaii Dept. of Business and Economic Development, Washington, D.C.
- Van Hecke, M.C.; Bartlett, R.W. (1973): Kinetics of Sulfation of Atlantic Ocean Manganese Nodules. *Metallurgical Transactions*. v. 4, 941-947.

- VonderHaar, Denise L. (1990): A Stratigraphic Interpretation of Selected Fe-Mn Crusts from Schumann Seamount, Unpublished M.S. Thesis. University of Hawaii, Honolulu. 71 pages.
- Warren, I.H.; Devuyst, E.A. (1972): Leaching of Iron and Manganese with Ammonium Carbamate. Transactions of SME, AIME v. 252, 239-243.
- Welling, Conrad G. (1985): R.C.V. Air-Lift Mining; Text from the Film "Harvesting the Bounty of the Ocean." In: Marine Mining: A New Beginning. Conference Proceedings July 18-21, 1982, Hilo, Hawaii. (Ed: Humphrey, P.B.) State of Hawaii Dept. of Planning and Economic Development, Honolulu, HI, 82-92.
- Wen, Xi Yuan (1995): Geochemical Characteristics of Pacific Seamount Ferromanganese Crusts: Evidence for their Genesis. Unpublished M.S. Thesis. University of Hawaii, Honolulu. 131 pages.
- Werjefelt, Bertil; Yonover, R.; Henderson, M. (1989): An Innovative Seabed Mining System. Presented at: Marine Mining Technology for the 21st Century; Conference, 4-6 December 1989, Honolulu, Hawaii.
- Wilkinson, F. (1980): Chemical Kinetics and Reaction Mechanisms. Nostrand, New York. 335 pages.
- Wiltshire, John C. (1993): Manganese Crust Deposits in the Johnston Island EEZ as Potential Cobalt Resources. In: Proceedings of the 1993 PACON China Symposium, Estuarine and Coastal Processes Section, 14-18 June 1993, Beijing, China. (Ed: Pacific Science Congress) PACON International, Beijing, China, 159-168.
- Wyman, W.F.; Ravitz, S.F. (1947): Sulfur Dioxide Leaching Tests on Various Western Manganese Ores. (Bureau of Mines Report of Investigations, RI 4077.) U.S. Dept. of the Interior, Washington, D.C. 12 pages.
- Yamanaka, H. (1986): Oceanographic Studies of Seamounts. In: Environment and Resources of Seamounts in the North Pacific. NMFS Technical Report 43. (Eds: Uchida, R.N.; Hayasi, S.; Boehlert, G.W.) NOAA, U.S. Government Printing Office, Washington, D.C., 13-18.
- Zaiger, Kimo K. (1993): A Novel Method of Solution Recovery of Cobalt-Rich Ferromanganese Crusts from Seamounts. In: International Marine Minerals Society Newsletter v. 5, no. 1 (August 1993), 4.
- Zaiger, Kimo K. (1994): Potential Marine Mining by *In Situ* Leaching and Recovery of Metals from Cobalt-Rich Ferromanganese Ocean Crust. In: MTS 94 Conference

Proceedings, Challenges and Opportunities in the Marine Environment, September 7-9, 1994, Washington, D.C., Marine Technology Society, Washington, D.C., 226-232.

Zaiger, Kimo K. (1995): Submarine Solution Mining Containment and Regulation Cover and Method. (to University of Hawaii) U.S. Patent 5,431,483, issued 11 July 1995.

Zoltai, T.; Stout, J.H. (1984): Symmetry and Atomic Bonding. In: Mineralogy, Concepts and Principles. (Eds: Zoltai, T.; Stout, J.H.) MacMillian, London, 69-107.